2019

The why, when, and where of anabranching rivers in the arid Lake Eyre Basin

Sarah Victoria Eccleshall
University of Wollongong

University of Wollongong Australia

School of Earth and Environmental Sciences

Faculty of Science, Medicine and Health

The why, when, and where of anabranching rivers in the arid Lake Eyre Basin

Sarah Victoria Eccleshall

BSc (Hons.) University of Wales, Aberystwyth; MSc Stockholm University

This thesis is presented as a requirement for the conferral of the degree:

Doctor of Philosophy

of the

University of Wollongong

June 2019

Abstract

Multi-channel or anabranching planforms are a common river planform found in arid regions and nowhere is this more prevalent than in the 1.14 M km^2 endorheic Lake Eyre Basin (LEB) of arid Australia. Of the19 main rivers in this basin, 14 anabranch for large proportions of their length yet with different multi-channel planform styles occurring in different parts of the basin.

This thesis has three primary aims. The first is to constrain the timing for the onset of anabranching in the LEB whilst the second assesses the long-term sediment dynamics in such systems. The final aim investigates the characteristics of sandy ridge anabranching found in the NW of the LEB. The three aims provide an overarching objective, that of understanding the why, when and where of anabranching in the low-gradient arid LEB. The aims are addressed through primary and secondary data analysis including the use of terrestrial cosmogenic nuclide and optically stimulated luminescence dating to produced geochronological data from ~1 Ma years ago to the present.

Using a compilation of 94 luminescence ages of fluvial sediment from the Channel Country region of the LEB from MIS 5 to present data was plotted via a number of different methods, and compared to randomly generated data for a signal vs. noise comparison. This approach shows that a transition from laterally active, sandy bedload systems to muddy anabranching systems occurred after MIS 5. From MIS 5 to MIS 3 there was a tendency for meandering as a planform to decline and anabranching to increase. Between MIS 3 and the LGM the transition from a laterally active to anabranching planform progressed to completion. Independent palaeoclimatic data over the same period, but mostly collected from elsewhere in the basin, suggests that this planform metamorphosis from meandering to anabranching was climatically induced with an overall decline in river energy and often (but not everywhere) associated with a shift from more sandy to more mud dominated systems. However climate is not the sole control on channel planform as the lower reaches of Cooper Creek and the Diamantina River do not anabranch but remain largely single thread, even though they are under the same climatic regime. Here channel slope has

progressively increased due to the uplifting Innamincka and Gason domes and the lowering of base-level due to the decline in the water volume of Kati Thanda - Lake Eyre that was associated with increasing aridity.

Understanding long-term sediment dynamics is investigated here using cosmogenic radionuclides on bulk detrital sediment from the modern channel and from Quaternary outcrops. Concentrations of ^{10}Be in Cooper Creek vary little throughout the system implying a uniform exposure history. When used to calculate denudation they give rates of ~1.2 – 5.1 mm ka^{-1}, some of the lowest globally. For much of Cooper Creek the ratios of ^{10}Be/^{26}Al deviate from the steady state value of 6.7 implying burial is occurring throughout the system. The apparent burial duration of in-channel sediment in the Cooper Creek system varies from ~ 0.05 to ~1.2 Ma and of dune sediment from ~1.06 to ~1.29 Ma. Duration does not appear to have a direct correlation with distance downstream or with proportion of sediment cover in the upstream area but appears instead to be associated with accommodation space. Those locations with greatest potential accommodation, such as the subsiding Cooper-Wilson syncline, store sediment for the longest duration and those with little or no potential for storage, such as the narrow Innamincka Choke, show no conclusive deviation from the steady state erosion ratio. These results differ to other recently conducted research in the tectonically/isostatically different western LEB where duration is closely correlated to the distance downstream and the upstream sediment cover.

By forming sandy islands and ridges, the Marshall River on the Northern Plains exhibits a very different style of anabranching to that in the mud-dominated Channel Country. Single grain optically stimulated luminescence (OSL) dating has established that the depositional islands and ridges have formed over ~ 500 years. OSL ages of ~3000 years obtained from beneath the ridges suggests that these represent only the most recent ridges with previous ones having being eroded and replaced on a cyclical basis. It would appear that anabranching in this instance is a means by which to maintain equilibrium for sand transport in straight channels of low gradient where it is not possible to increase slope through straightening or down cutting.

This thesis concludes that anabranching in rivers in the LEB varies both temporally and spatially. It has been a means of maintaining equilibrium in response to

climatically-driven reductions in flow over the last glacial cycle. The mud-dominated systems in the east of the basin appear to have been progressively increasing their anabranching habit throughout much of the late Quaternary. The same may be true of the sandy systems in the north-west of the basin but the cyclical formation and destruction of their more erodible ridges and islands has left no evidence beyond ~500 years in age. The climate-induced metamorphosis from meandering to anabranching in the low-relief LEB appears to occur during glacial-interglacial cycles of great duration similar to global fluctuations in other fluvial systems, such as alternations in incision and deposition seen in high relief rivers. In contrast, cyclic island and ridge form anabranching can only be verified as occurring during the current depositional cycle of ~ 500 years. Flat arid landscapes, such as those investigated in this thesis, store sediment on route to their endorheic depocentres for 10^6 years and have adopted different anabranching styles to accommodate the late Quaternary history of diminishing flows over low gradients in different topographic and sedimentary settings.

Acknowledgements

Those to whom I offer thanks are numerous. There are so many people to whom I owe thanks, on many levels.

Firstly to my rabble of supervisors: John Jansen, Gerald Nanson, Tibi Codilean, Toshi Fujioka, Bert Roberts and particularly Tim Cohen who stepped is as my primary supervisor and saw this work come to fruition.

The University of Wollongong provided me with both tuition fee and living cost scholarships, without which I would never have had the opportunity to undertake this work.

Thanks must also go to Brent Peterson and Josef Stocker with limitless assistance in fieldwork and sample collection. To Nick Whitelaw for his assistance in the field, Bert Roberts, Zenobia Jacobs, and Terry Lachlan for their assistance in the UOW luminescence lab, and Steve Kotevski and Charles Mifsud for all the assistance at ANSTO.

All the PhD students, past and present, who have made this experience enjoyable should be reminded that the value of comradery cannot be overstated. I shall not list you all for fear of missing someone. Some of you deserve a special mention: Brent, Daniela, Deirdre, Martin, Nathan, Meagan, Maria.

I have been lucky enough to have some very special people in my life who have been so supportive of me (some of whom I have previously mentioned), some of you I've known a long time and others I have met more recently but you all have a special place in my heart: Rachel, Rachael, Jess, Deirdre, Brent, Nathan, Brendan, Rhi, Rob, Laura, Jessi, Heather - you've all been fantastic and I am so appreciative. Guinea Pig Rodeo, you have been my regular comic relief and never let me take anything too seriously – if in doubt it was probably Harold Holt, or Camembert. Sam, you appeared on the scene fairly late in the game, but I'd never have got this monster across that final line without you, thank you!

Lastly, and most definitely by no means least, I would never have made it this far without the support of my Mum and Dad, for everything you've done for me, I am eternally grateful.

Table of Contents

Part III

Appendices

List of Figures

4   Australia's arid zone and the Lake Eyre Basin

5   Isolating the onset of anabranching in Central Australia

6   Variation in downstream cosmogenic ^{26}Al and ^{10}Be ratios in a large, arid, endorheic drainage basin

7   Island dynamics in an arid zone anabranching river

8   Synthesis and discussion

B   Kernel density band width estimation

D   OSL dating of the Marshall River

E   Marshall River grainsize analysis

List of Tables

6 Variation in downstream cosmogenic ^{26}Al and ^{10}Be ratios in a large, arid, endorheic drainage basin

7 Island dynamics in an arid zone anabranching river

A   Fluvial data compilation

C   Cosmogenic nuclide extraction, measurements and calculations

D   OSL dating of the Marshall River

E   Marshall River grainsize analysis

List of Equations

D   OSL dating of the Marshall River

"In probably one sense only, rivers are like bananas...

...they are almost never straight"

G. Nanson

1 Introduction

1.1 Introduction

Globally, semi-arid, arid and hyper-arid zones make up 37.2% of the land area (Middleton and Thomas 1997) (Figure 1.1a). Comparatively, the dryland region in Australia covers ~70% of the continent (Middleton and Thomas 1997) (Figure 1.1b), making Australia the driest continent, excluding the polar regions, in terms of its mean annual precipitation and runoff (Finlayson and McMahon 1988).
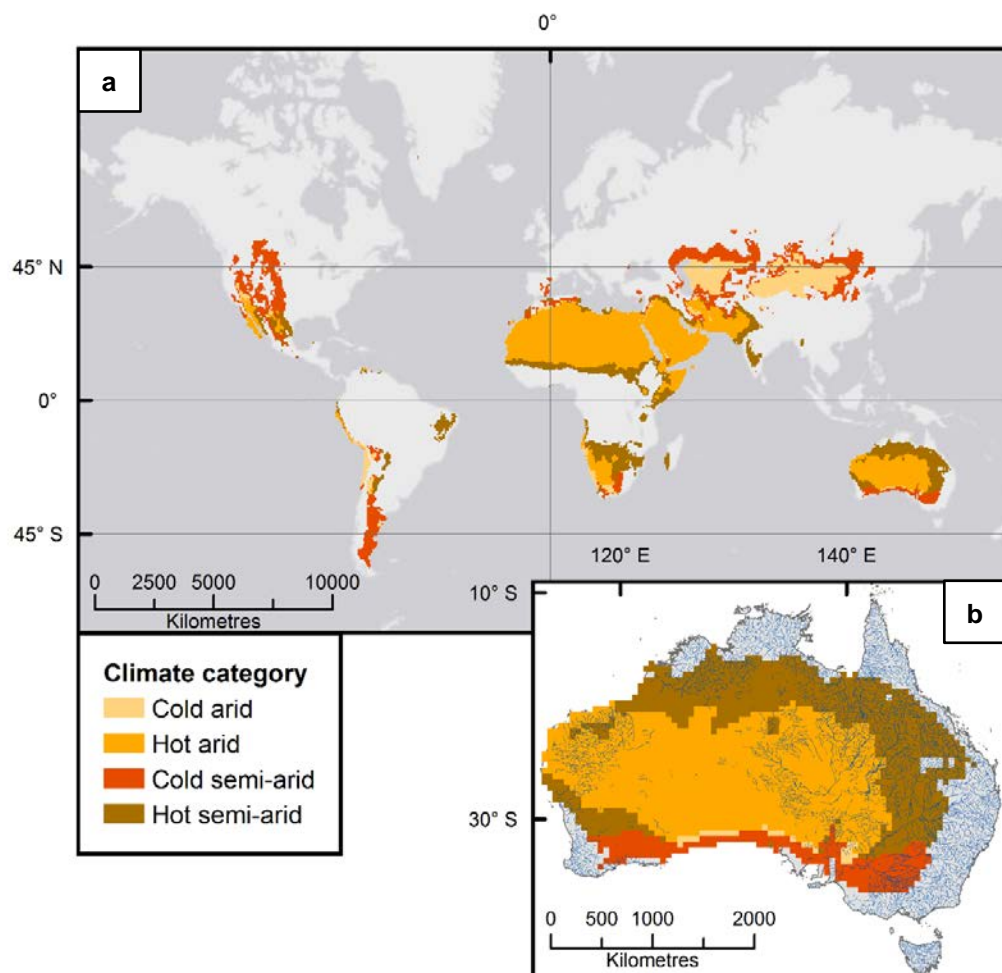
Figure 1.1 - Cold arid, hot arid, cold semi-arid and hot semi-arid climate zones globally (a) and in Australia with major non-perennial rivers in Australia marked (b). Climate zones are based on the updated Köppen-Geiger climate zones from Peel et al. (2007): Cold arid (BWk), hot arid (BWh), cold semi-arid (BSk) and hot semi-arid (BSh). Rivers are taken from the 1:250000 surface hydrology lines from the National Surface Hydrology Database (Crossman and Li 2015)

Australia supports a number of large rivers such as the Murray River and the tributaries of the Lake Eyre Basin (LEB) (Figure 1.1b), despite its aridity. Here aridity is defined by the low ratio of rainfall to potential evapotranspiration. The fluvial environments in dryland Australia are closely linked with the widespread aeolian deposits, often found close to the channel network and often derived from fluvial sediments (e.g. Mabbutt 1977; Tooth and Nanson 1995; Bullard and McTainsh 2003; Powell 2009; Jaeger at al. 2017; Al-Masrahy and Mountney 2015; Williams 2015; Yanes et al. 2019). The dryland rivers in Australia show the greatest hydrological variability (Bunn et al. 2006) of all global desert rivers. The mean coefficient of variation (ratio of standard deviation to mean) in annual flows is 1.27, considered to be high variance, compared to 1.25 in the Mediterranean and 1.14 for southern Africa (McMahon 1979; Finlayson and McMahon 1988).

Given the variability in hydrology in Australian drylands, it is not surprising that there is also variability in fluvial form with straight, meandering and anabranching planforms existing, however there appear to be no geomorphological features which are unique to dryland rivers, although waterholes in low gradient muddy systems are a possible exception (Nanson et al. 2002). Pivotal to this thesis is the notion that while dryland rivers show many of the same channel forms and geomorphological features as seen in humid and temperate rivers they cannot be defined by the same models. Additionally, models of rivers and river behaviour are infrequently derived from rivers with low gradients, so may not be applicable to the Australian dryland rivers that predominantly occur in low gradient environments. Anabranching rivers, rivers with multiple channels divided by islands at discharges up to bankfull (Nanson and Knighton 1996), are one of the most common dryland planforms and one of the least understood despite occurring in nearly all climatic settings. Furthermore, anabranching is considered to be the final end member mode of all very large alluvial rivers (Latrubesse 2008) with the world's five largest rivers anabranching for ~90% of their alluvial length (Jansen and Nanson 2004). Anabranching rivers are a diverse planform group and occur extensively in the Murray-Darling and Lake Eyre basins, and it is suggested that in Australia the climatic, hydrological and geomorphological conditions favour the development of this multiple channel planform (Nanson and Knighton 1996).

The prevalence of arid fluvial environments is not matched in abundance by research, with fluvial research tending to focus on humid and temperate areas, specifically those in the Northern Hemisphere. The lack of research is, in part, attributed to the remoteness of the areas and the lack of rainfall and runoff events, preventing the collection of consistent hydrological data (Reid and Frostick 1989) and also to the focus of previous research on landforms unique to dryland areas such as aeolian forms (Reid and Frostick 1989; Tooth 1997). Tooth (1997) emphasises that while the body of research on dryland fluvial systems is small, rivers are an important agent in shaping desert landscapes and, due to, commonly being unaffected by glaciation are home to long records of sediment dynamics.

Three key deficiencies in dryland fluvial research had been identified nearly 20 years ago by Tooth (2000a):

1) Limited study of modern characteristics
2) Limited understanding over Cenozoic timescales
3) Lack of integration between process-form studies and studies of long-term histories.

Tooth (2013) noted that these deficiencies are being addressed and that significant progress has been made in recent years. When analysing the number of publications with the keywords 'dryland' and 'fluvial' over the last 20 years, there has been a threefold increase in publications from 2010 to present compared to the preceding ten years and a more than twentyfold increase when compared to the period 1990-1999. Despite this, knowledge gaps do still remain.

One notable deficiency in the research is that, as is often the case, a geographical bias exists toward short, steep and tectonically active catchments, none of which are defining characteristics of dryland rivers on the Australian continent. This thesis addresses some of the deficiencies highlighted by Tooth (2000a; 2013), with a particular focus on dryland anabranching rivers and their short and long-term history, not purely for climate reconstruction, which is often the focus, but for greater understanding of dryland river behaviour, with a focus on Australia, as a low lying, low slope, and tectonically quiescent environment.

1.2   Thesis aims

This thesis addresses some of the research deficiencies above specifically relating to the LEB, but with the intention of being transferable to dryland rivers on a wider scale, specifically those in low slope, tectonically quiescent environments. The thesis will add to our understanding of the causes of planform change in arid zone rivers; the duration, mode, and potential of sediment storage in arid rivers; and the duration/longevity of the anabranching planform in arid environments. As such, the three aims are:

1. **To investigate the timing for the onset of anabranching in the arid zone using chronological, sedimentological and statistical techniques.**

   This aim addresses 'the history of anabranching rivers' throughout the late Quaternary in the Australian arid zone with a focus on the LEB, Australia's largest arid drainage basin. Understanding the causes and timing of anabranching is important for the wider understanding of the role that forcing factors, such as climate and tectonics, play in dictating the dominant channel morphology of the LEB arid-zone.

2. **To quantify sediment storage in a large anabranching system and establish the relevance of different storage zones in the system.**

   Long term storage in dryland systems is poorly understood and this research question addresses the longitudinal variation in sediment storage using terrestrial cosmogenic radionuclides. There are very few studies investigating downstream variation of sediment storage in dryland rivers and this aim adopts a whole-system approach looking at the interactions between proximal and distal parts of the system and the likely role of sediment sinks such as flood basins and dunefields.

3. **To constrain the age for the formation of anabranching islands/ridges and link this to concepts of equilibrium**

This aim examines the longevity or age of anabranching islands. While the sedimentary configuration and form of anabranching islands are generally well understood (e.g. Tooth and Nanson 2000a; Tooth and Nanson 1999), the age of such fluvial landforms is poorly constrained. By examining the age of different types of

islands will allow an assessment of the potential triggers for their formation. Identifying the age of the islands will be addressed by using single grain optically stimulated luminescence (OSL), targeting the base (onset of formation) and top of the islands.

1.3 Site Selection

The LEB (Chapter 2.5.1) is particularly well suited to the study of low slope, dryland rivers as it is the largest river basin in Australia and lies entirely within the arid and semi-arid zone occupying between 10% and 15% of the entire dryland region of Australia. Furthermore, the basin encompasses a range of conditions with a monsoon influenced region in the north-east and westerly influenced region elsewhere and anabranching rivers of various types and sizes. Importantly, the multi-channel river systems traverse Neogene basins and some of the largest Quaternary dunefields on Earth.

To approach the aims of this thesis different sites within the arid LEB were chosen. Cooper Creek is a large river which anabranches for much of its length, with a wide variety of planform and channel morphologies. It flows through a number a different arid environments in particular several large dunefields. Furthermore, from previous work, to be reviewed in later chapters, it is known to hold an extensive record of past fluvial systems. These aforementioned factors make it ideal to address the first and second aim. The third aim can be addressed using the Marshall River, a small river in the north-west of the LEB that is characterised by alternating single thread and anabranching reaches the causes of which have been previous investigated (Tooth and Nanson 2000a), but no chronology of its morphological features has been produced.

1.4 Thesis Organisation

The thesis consists of three parts, incorporating seven chapters.

Part I consists of this chapter, Chapter 2, and Chapter 3. This chapter introduces the purpose of the project, presents the aims and briefly introduces the study area. Chapter 2 introduces some important aspects of fluvial environments with a focus on anabranching rivers. It also introduces some of the characteristics of sedimentary forms and fluvial dynamics in drylands. Chapter 3 introduces the geochronological methods which are available for analysing deposition of sediments in fluvial

environments and explains the principles behind cosmogenic nuclide burial dating and optically stimulated luminescence which are used in this thesis.

Part II consists of chapters 4, 5, 6, and 7. Chapter 4 begins by introducing the study area and describing characteristics of the LEB pertinent to this thesis. Chapter 5, 6, and 7 each address an individual aim and show the results of the research. Chapter 5 addresses the origin of anabranching rivers in the LEB using statistical analysis of a dataset of previously obtained luminescence ages. Chapter 6 sets out to quantify the duration of sediment storage in Cooper Creek and how this relates to drainage basin morphology using cosmogenic nuclide burial dating. Chapter 7 investigates islands and rivers in a sandy anabranching river in the Northern Plains. This uses single grain optically stimulated luminescence.

Part III, consisting of Chapter 8, summarises the main findings of the results chapters and discusses how these relate to one another and to the LEB as a whole, then presents recommendations for future research that could further develop the findings of this thesis.

Chapter 2

---

2   Rivers and drylands

2.1   Introduction

Rivers are instrumental in shaping the Earth's surface through erosion, transportation and deposition of rock and sediment and are responsible for the majority of fluxes of water and sediment from land to the oceans (Milliman and Meade 1983). The aims of this thesis (Chapter 1 - 1.2) are diverse and cover a number of aspects of fluvial systems. This chapter outlines the key ideas of fluvial systems and drylands relevant to this thesis. Further details relevant to each individual aim will be addressed in the relevant results chapters (Chapters 5, 6, 7). The purpose of this chapter is to outline the major aspects of fluvial systems examining the different variables which control river morphology with specific reference to anabranching rivers and dryland regions. It will investigate the significance of sediment storage and transport in drylands, and the key modern and palaeo-features of the wider study area of the LEB.

2.2   River morphology and form

It is common practice for rivers to be classified according to their channel planform, which is an indicator of the boundary conditions of a river at catchment and channel scales. Long-standing convention was towards the classification of rivers into three channel patterns: straight, meandering and braided (Leopold and Wolman 1957). However, this restrictive definition has since been adapted to include the three original forms, and anastomosing channels, as 14 less distinct and therefore considerably more transitional patterns (Figure 2.1) (Schumm 1985), which are still commonly used, with additional subdivisions being applied to anastomosing rivers (Nanson and Knighton 1996). Planforms can be categorised by sediment load type with three categories: suspended load, mixed load, and bed load. These categories also reflect changes in relative stability, bed load/sediment load ratio, sediment load, and sediment size (Figure 2.1).
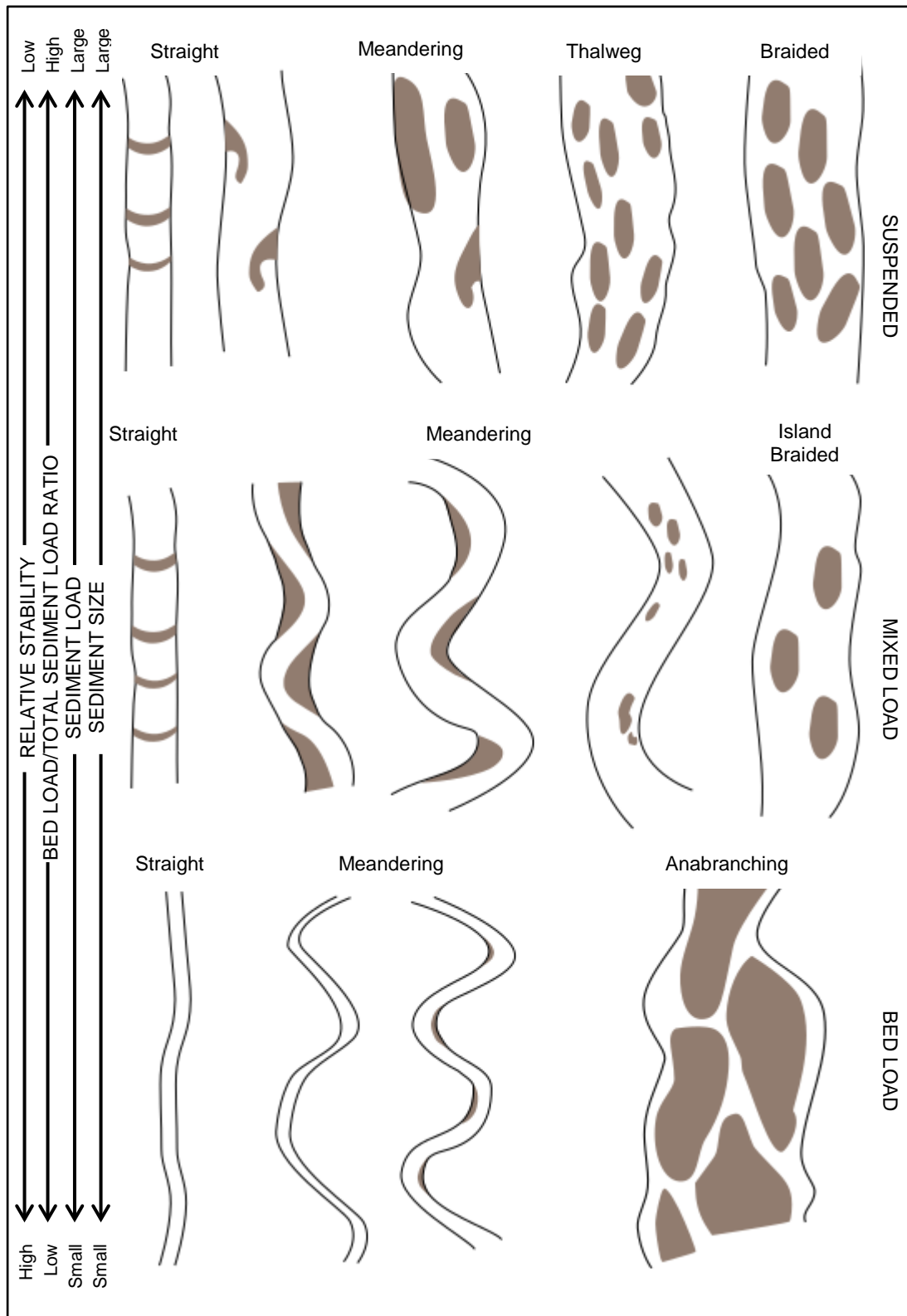
Figure 2.1 – Fourteen channel patterns as identified by Schumm (1981; 1985). The channel patterns are divided by sediment type with three categories: bed-load, mixed-load and suspended load. Anabranching channels, in the original categorisation of Schumm (1981; 1985), are defined as anastomosing. However, anastomosing is now considered to be only one type of the wider group of anabranching rivers (Nanson and Knighton 1996).

Rivers are dynamic in that they respond to forcing factors, which act in space and time, by adjusting their physical characteristics; which manifests as changes in morphology and planform. A fluvial system is the sum of a number of variables, which can be separated into internal and external forcing factors, the interactions of which dictate the pattern that rivers take and the landforms which are present. These forcing factors are numerous, controlling geometry, flow and sedimentary processes in river systems, and defining river type and form (Leopold and Wolman 1960; Leopold et al. 1964). The forcing factors act on timescales from less than a year (instantaneous or steady time) to tens to hundreds of years (short timescales), to thousands to tens of thousands of years (medium timescales) to timescales greater than 100 000 years (long or cyclic timescales) (Schumm and Lichty 1965). The most common timescales in fluvial environments are short to medium, also known as graded, timescales (Table 2.1).

Table 2.1 - Timescales of geological processes (after Schumm and Lichty 1965). Short to medium timescales, also known as graded timescales, are those which are most relevant in fluvial systems.

Timescale (years)	Timescale (qualitative)	
$<10^{-1}$	Instantaneous or steady time	
$10^1 - 10^2$	Short timescale	Graded timescales
$10^3 – 10^4$	Medium timescale	
$>10^5$	Long time or cyclic scale	

The two key external forcing factors which act in river systems are regional climate, and tectonics, including lithology and structure. These key external factors are independent of other characteristics of the river and its catchment, regardless of timescale, and influence the geology, climate, vegetation and topography of the catchment. In turn these catchment features affect the internal controls such as the supply of water and sediment which affect the characteristics of the river. The dependency of these other factors varies with the timescale of interest (Schumm and Lichty 1965) (Table 2.2).

Table 2.2 - Drainage basin variables and the timescales and dependency on which they act (after Schumm and Lichty 1965).

Drainage basin variable	Timescales – status of variables		
	Cyclic	**Graded**	**Steady**
Initial relief	Independent	Not relevant	Not relevant
Geology (lithology, structure)	Independent	Independent	Independent
Climate	Independent	Independent	Independent
Vegetation (type and density)	Dependent	Independent	Independent
Relief or volume of system above base level	Dependent	Independent	Independent
Hydrology (runoff and sediment yield)	Dependent	Independent	Independent
Drainage network morphology	Dependent	Dependent	Independent
Hillslope morphology	Dependent	Dependent	Independent
Hydrology (discharge of water and sediment)	Dependent	Dependent	Dependent

2.2.1 Equilibrium in rivers

One of the foci of this thesis pertains to understanding why certain planforms exist in preference to others. This can be explained by understanding the condition of equilibrium in rivers. As the forcing factors in a fluvial system are interconnected, a change in one variable will have an effect on other dependent variables in the system. Such a change can affect the stability of a system. Alluvial rivers tend to exhibit stability, such that when disturbed they temporarily enter a disequilibrium state and then, due to their ability to self-regulate, adjust their variables in order to expend surplus or conserve excess energy and to return to equilibrium (Nanson and Huang 2017). Equilibrium in a natural system holds an implication that there is a certain degree of 'dynamic balance or constancy between controlling and responding elements' (Howard 1982). Lane's equation (Lane 1955) (Equation 2.1) shows the relationship between discharge, slope, and bedload, which in a stable river are proportional to one another, e.g. if slope changes, in order to maintain stability the

other variables adjust thus remaining proportional and minimising the impact of the initial change.

$$QS \propto Q_s d_{50}$$

Equation 2.1 - Lane's equation for a channel instable channel. Where Q = discharge, S = channel slope, Q_s = bed material load, and d_{50} = median bed material size.

In addition to slope adjustment as a parameter (Mackin 1948), velocity, depth, width, channel roughness, and planform pattern can also adjust to maintain equilibrium and stability (Leopold and Bull 1979). In a scenario where the change in a particular variable reaches a threshold (e.g. cannot increase slope to maintain power when there has been a reduction in discharge) the system will adjust a range of variables (metamorphose) in an effort to achieve a new equilibrium and again become stable (Leopold and Bull 1979).

The concept of dynamic equilibrium in rivers is based on a river's potential to adjust to maintain a relatively stable form. The stable or relatively stable hydraulic geometry which river channels tend towards cannot be entirely explained by the basic flow relationships of continuity, resistance, and sediment transport (Huang et al. 2002). Under a set of defined conditions there are a number of possible geometries which can exist yet similar geometries tend to persist, indicating that there is an overriding factor controlling the geometry.

Different hypotheses have been proposed, often called extremal hypotheses; that require a maximum or minimum condition to be met. These hypotheses each represent a general principle in the fluvial system causing a preferred cross-section to be consistently created. Examples include:

- **Minimum energy dissipation rate**: a fluvial system is in equilibrium state when the rate of energy dissipation is at a minimum value. The minimum value is dependent on constraints of the system. When the energy dissipation rate is not at its minimum value the system will be in non-equilibrium and will adjust to reach a minimum value and regain equilibrium (e.g. Yang et al. 1981).

- **Minimum stream power:** the fluvial system is at equilibrium when the stream power per unit length of channel (ɣQS) is at a minimum for the imposed

discharge and sediment load. If the system is not in equilibrium width, depth, and slope will adjust so discharge can achieve a minimum power for those particular conditions (Chang 1980).

- **Minimum unit stream power:** for a system at equilibrium the unit stream power (ɣQS/w) will be at the minimum for the imposed discharge and sediment load. If the system is in non-equilibrium the channel will adjust velocity, slope, roughness, and geometry to achieve minimum unit stream power and thus equilibrium (Yang and Song 1979).

Nanson and Huang (2008) found fault with these extremal hypotheses because, while they are applicable to some extent in explaining the behaviour of alluvial rivers, they have each been arbitrarily adopted (assumed to be correct) and, therefore, there is no theoretical basis for selecting one hypothesis over any other. Consequently, the question can be posed as to why a river would maximise or minimise any particular condition? Huang and Nanson (2000) showed that the least action principle (LAP) provided a rational explanation for river channel adjustment. It does not maximise or minimise any particular condition in alluvial rivers, but shows that on average they maximise their overall efficiency by self-adjusting their hydraulic geometry. This operational efficiency is what leads to a highly consistent channel geometry globally (Huang and Nanson 2000; Nanson and Huang 2008). LAP shows that in order to reach maximal operational efficiency a system in motion must expend the least amount of energy for completion of an imposed task. In nature the LAP manifests as a system following the most 'economical path', which in rivers is interpreted as an adjustment towards conditions that minimize change and maximize operational efficiency (Huang and Nanson 2000; Huang et al. 2002). The LAP dictates that a river achieves stable hydraulic geometries that are precise for particular conditions because these are the most efficient for those conditions (Nanson and Huang 2008).

Three scenarios of energy in a fluvial system exist: (1) a system has excess energy, more than is needed to move given sediment and water; (2) a system has the exact amount of energy required; (3) a system has insufficient energy. A scenario where the exact amount of energy (slope and discharge) a river requires to move the load present is rare, but where this occurs these rivers are in stationary equilibrium. Below this threshold there is insufficient energy and above it there is excess (Nanson and Huang

2017). Energy can be expressed in terms of slope. For an optimally efficient channel, which meets the conditions of the LAP, the valley slope (S_v) will equal the minimum required equilibrium channel slope (S_{fmin}) and thus erosion or deposition will not occur and a straight channel will be maintained, this will be a stable, efficient river in stationary equilibrium. Under the LAP where S_v exceeds S_{fmin} excess energy is present, the river is above the threshold, and energy must be expended for equilibrium to be achieved (Figure 2.2; Table 2.3). In these rivers flow is driven by gravity and will achieve an equilibrium state by expending excess energy. This expenditure can be vertical through the formation of step pools which occurs in steep, constrained valleys. In more gently sloping valleys, where slope is not sufficient for step pools to form, systems expend excess energy through the reworking, widening, and forming in-channel bars such as in a braided system. In somewhat lower slope environments excess energy can be expended through lateral erosion by way of meandering. In very low-slope valleys where there is excess energy but where the banks are too resistant to allow meandering, anabranching rivers can form. When a single-thread channel changes to multiple channels this dramatically alters w/d ratios, which in turn alters the boundary resistance meaning no reduction in slope may be required to any reduce excess energy (Huang and Nanson 2007; Nanson and Huang 2008).

Where S_v is less than S_{fmin} a river is not in equilibrium. To achieve equilibrium, slope may be increased. In an environment where slope may not be increased an adjustment of the w/d ratio can lead to equilibrium providing the S_{fmin} is not greatly different to S_v. An example of this can occur in some anabranching rivers where the formation of depositional ridges and islands, which are stabilised by vegetation, reduces the w/d ratios and leads to dynamic equilibrium conditions. If S_v is less than S_{fmin}, unstable braided and wandering meandering forms will also result, due to aggradation. In rivers with a significant energy deficit, where the slope is too low for stabilisation to be achieved by adjustment of the w/d ratio, such systems are considered to be in non-equilibrium.

The measure of the efficiency of a river under stable equilibrium conditions is the *H* number. A river in stable equilibrium, at its most efficient, will have an *H* number (ratio between excess bed shear and width/depth ratio) close to 0.3. The individual anabranches are close to stationary equilibrium with average *H* numbers close to 0.3,

whereas if the islands are removed and the *H* number recalculated for a hypothetical single thread river, the *H* numbers average 0.5. An *H* number of 0.5 is close to the threshold at which rivers are no longer able to move sediment (Nanson and Huang 2017). This optimisation allows for sediment to be moved at relatively low discharges, whereas sediment in the single thread reaches are only moved during higher flows, infact requiring more than 50% more discharge than the anabranching reaches (Nanson and Huang 2017).

Much of the discussion above regarding equilibrium has related to anabranching rivers as it is these rivers that are of particular interest in this thesis.
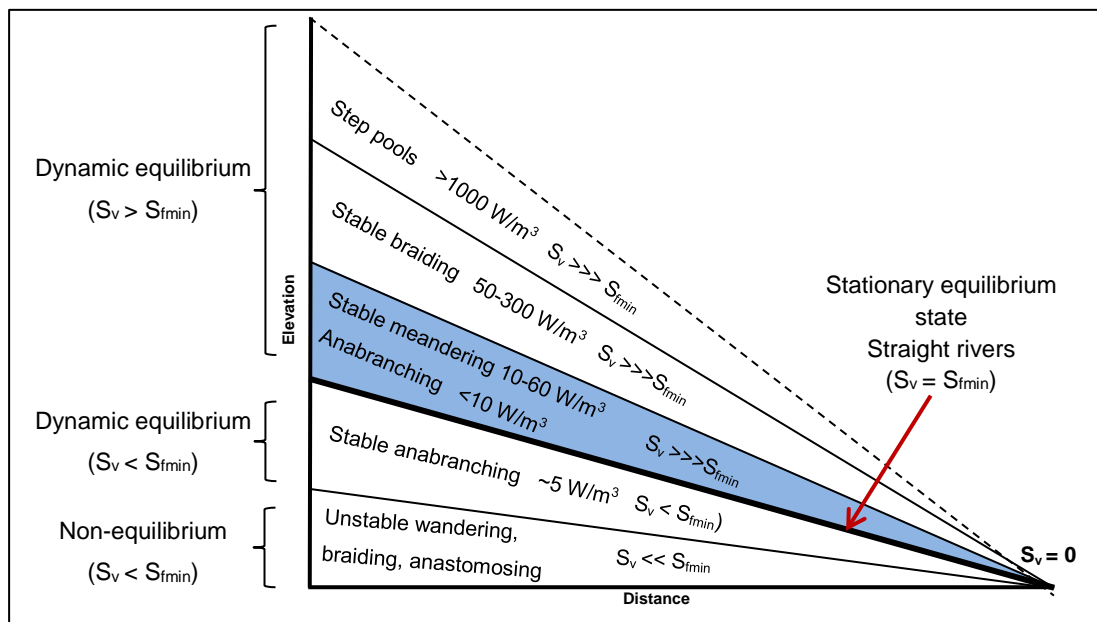
Figure 2.2 – River channel pattern is relation to slope. The lines are representative of steepening gradients, with S_v indicating valley slope and S_{fmin} indicating the minimum energy slope required to move an imposed discharge and sediment load (after Nanson and Huang 2008).

Table 2.3 - Equilibrium states and channel forms according to the relationship between valley slope (S_v) and minimum required slope (S_{fmin})(after Nanson and Huang 2008).

Relationship between S_v and S_{fmin}	Equilibrium state	Channel form and characteristics
$S_v >>> S_{fmin}$	Dynamic equilibrium	Vertically dominated energy expenditure – step–pool channels;
$S_v >>> S_{fmin}$	Dynamic equilibrium	Vertically and laterally mixed energy expenditure – stable braided channels
$S_v >>> S_{fmin}$	Dynamic equilibrium	(1) slope dominated energy expenditure – stable meandering rivers; (2) width/depth dominated energy expenditure – stable anabranching rivers
$S_v = S_{fmin}$	Stable equilibrium	Straight single-thread channels with a uniform boundary
$S_v < S_{fmin}$	Dynamic equilibrium	Stable anabranching channels with non-uniform boundaries confined by vegetation
$S_v <<< S_{fmin}$	Non-equilibrium	Aggrading braiding, meandering, anastomosing, and wandering unstable channels.

2.2.2 Form process relationships in anabranching rivers

Anabranching rivers, as a planform, are the focus of this thesis. Nanson and Knighton (1996) described anabranching rivers as *"a system of multiple channels characterized by vegetated or otherwise stable alluvial islands that divide flows at discharges up to nearly bankfull"* and this has become a widely accepted definition. Schumm (1968) first identified anastomosing as an independent form from braiding rivers, as only in Australia had these terms been previously applied with separate definitions. Braided rivers, in contrast, have multiple channels separated by bars which are submerged when the channel train is at bankfull. Nanson and Knighton (1996) were the first to clearly define anabranching rivers in terms of their geomorphology, sedimentology and process. When differentiating anabranching from braiding the independence in the actions of each anabranch is key. In braided rivers the braid bars are essentially bedforms that work together to alter the bed roughness of a large, wide, single channel at bankfull. In an anabranching river each anabranching has its own hydraulic characteristics at bankfull and can in its own right be meandering, straight, sinuous or braided (Nanson and Knighton 1996).

Anabranching rivers are found across the majority of climate zones and at most elevations, latitudes, and geological settings, so it is perhaps not surprising that they can take on a number of different forms, with the world's five largest rivers anabranch for up to 90% of their alluvial length (Jansen and Nanson 2004). Anabranching rivers also vary in size with respects to bankfull discharge, ranging from 34 $m^3.s^{-1}$ in the Mistaya (Smith 1986) to 160 000 $m^3.s^{-1}$ in the Amazon (Latrubesse 2008). Given the variety of settings in which anabranching rivers occur the causes of anabranching have been much debated and it has been identified that no singular cause exists (Nanson 2013). The main factors influencing rivers (Table 2.1) all play a role but the localized permutations of these can vary, so no single cause can be assigned.

Generally, though not exclusively, anabranching rivers have a low gradient relative to discharge and a high discharge relative to load. The ratio of suspended load to bedload is frequently high (Nanson and Knighton 1996). Many anabranching rivers are also characterised by erosion-resistant banks due to a combination of cohesive sediment and bank-reinforcing vegetation. Beyond this, there is not a singular group of characteristics which can be used to explain anabranching rivers. The variety of characteristics which anabranching rivers exhibit led Nanson and Knighton, (1996) to classify of six different types, based on bedload characteristics, the role of vegetation, floodplain characteristics, individual anabranch form and the mechanisms leading to anabranching (Figure 2.3, Table 2.4). Not all forms of anabranching are evident in the sedimentary record and for those that are, facies models are not well developed (Makaske 2001).
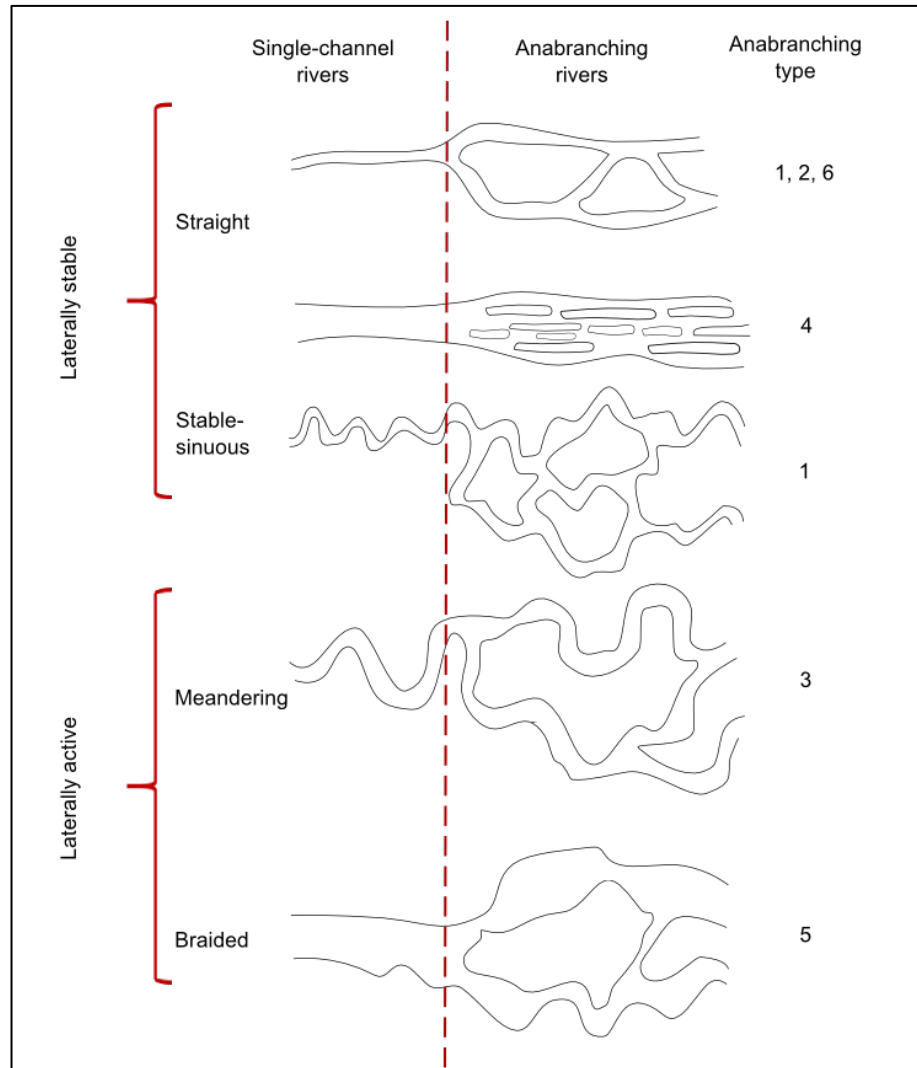
Figure 2.3 - Types of anabranching and the single channel forms from which they develop, divided by lateral stability or activity (after Nanson and Knighton 1996).

The six types of anabranching are designated type one to type six, with type one subdivided into 1a, 1b and 1c (Table 2.3) full descriptions of which can be found in Nanson and Knighton (1996) and Nanson (2013).

Table 2.4 – Type classifications of anabranching rivers, corresponding to the type numbers in Figure 2.3 (Nanson and Knighton 1996).

Type		Type description
1	Cohesive sediment (anastomosing)	a) Hyper-humid, organic
		b) Humid, organo-clastic
		c) Semi-arid, mud-dominated
2	Sand-dominated, island-forming	
3	Mixed load, laterally active	
4	Sand-dominated, ridge-forming	
5	Gravel-dominated, laterally active	
6	Gravel-dominated, stable	

A further important subdivision of anabranching rivers is equilibrium versus disequilibrium forms. Similarly to braiding and meandering channels, anabranching can represent a dynamic equilibrium form or an accreting form in disequilibrium (Huang and Nanson 2007). With regards to anabranching systems the least action principle explains how a slope-constrained river can reach dynamic equilibrium (e.g. Nanson and Knighton 1996; Nanson and Huang 1999; Tooth and Nanson 1999; 2000b).

The dynamic equilibrium mode anabranching systems form, without avulsion, by dividing the channel through the formation of ridges and islands as a means of changing the w/d ratios to alter transport efficiency. As will be shown in Chapter 7, this can result in stable long-lived anabranching systems. The least action principle for anabranching, as with any other river form, causes adjustment so the most efficient transport of sediment and water exists and that form will persist so long as the climatic and tectonic conditions dictate that it is the most efficient form (Nanson 2013). In the equilibrium mode of anabranching, vegetation plays a key role in stabilising the banks of channels and it acts as a point of inception for the formation of islands. The role of riparian vegetation has been addressed in a number of field studies in low gradient anabranching rivers Australia (Tooth and Nanson 1999; 2000a; Jansen and Nanson 2004; Huang and Nanson 2007). From this work it has been established that the ridges and islands, which form within anabranching channels, commonly rely on vegetation

for initiation, growth and long-term survival (Tooth and Nanson 1999; 2000a). If vegetation does not exist to stabilise the banks and islands the high flows during periods of flood would likely cause any anabranches that did form to degenerate and collapse (Nanson and Knighton 1996). This proposal for equilibrium form anabranching is supported by the work of Habeck-Fardy (2013) where it is shown that the *H* number, a measure of channel efficiency (Huang and Chang 2006), for single anabranch represents greater transport efficiency than the *H* number for the channel train with the islands and ridge removed. In conclusion, the dynamic equilibrium mode of anabranching can be considered a mechanism in which flow efficiency is enhanced to move bedload where gradients cannot be increased (Habeck-Fardy 2013).

In contrast to the dynamic equilibrium anabranching forms, a non-equilibrium anabranching form exists where sediment accretion is rapid due to the river being below the equilibrium threshold (Huang and Nanson 2017). In these cases the system is not stable, however a single channel system would be even more unstable (Huang and Nanson 2007). This type of anabranching has been commonly termed anastomosing (e.g. Makaske 2001) but will be referred to as 'type 1' anabranching (Nanson and Knighton 1996) within this thesis. As with all non-equilibrium systems (Figure 2.2) insufficient energy is available to meet sediment transport requirements. In order to achieve dynamic equilibrium in this scenario flow efficiency must be increased, or available energy must be increased (Jansen and Nanson 2004). Where a small adjustment is required flow efficiency will increase, however, if a large increase in available energy is required and adjustment via pattern, geometry, and bed configuration are inadequate to counter the insufficient energy, then aggradation will occur (Jansen and Nanson 2004). This aggradation often occurs in settings where tectonic and isostatic uplift can cause base-level rise causing and maintaining low gradients (Makaske 2001). Low gradients cause a decrease in discharge which can cause deposition of previously transportable load.

The floodplain accretion often results in frequent avulsions and slower abandonment of older channels (Smith et al. 1989; Makaske 2001). This is described in an evolutionary model by Smith et al. (1989) which describes anastomosis (type 1 anabranching) as a transitional state where there is a "quasi equilibrium" between avulsion and the rate of channel abandonment causing a constant number of channels

to remain active. A more efficient route can be established when, during flood, overbank flow takes a mechanically more advantageous route such as that with a steeper gradient, resulting in a new channel forming and the active channel being abandoned. These disequilibrium anabranching systems are intrinsically unstable as they cannot sufficiently adjust to maintain throughput of sediment quantities, however they will anabranch in this manner for extended timescales (Nanson 2013).

2.2.3 Anabranching in Australia

Anabranching is more prevalent in Australia than on any other continent, probably because of certain prevailing boundary conditions (Nanson 2013). Australia is the globe's lowest continent with mean elevation at ~340 m AHD, less than half that of the global continental average, with a number of large rivers declining in discharge downstream (Nanson 2013). The correlation between prevalence of anabranching in Australia and the low slope and declining discharge of Australian rivers supports the conclusion that rivers likely anabranch in order to maintain flow down valleys close to threshold values (Nanson 2013; Nanson and Huang 2018).

Within Australia, several different anabranching types are found, both in dynamic equilibrium and non-equilibrium. Many of the current definitions stem from work on anabranching in Australia. There is no singular type of anabranching rivers existing in Australia and in places they are superimposed upon other river forms. 'Type 1c', 'type 2', 'type 3', 'type 4' and 'type 6' (Figure 2.3; Table 2.4) all exist albeit usually in different regions.

'Type 1' anabranching rivers are a non-equilibrium form (Nanson 2013) and Cooper Creek and the Diamantina River, in semi-arid Central Australia (investigated in this thesis) are examples of subtype c (Nanson and Knighton 1996). Other examples of 'type 1' anabranching in Australia include the Lower Balonne River in southern Queensland (Kernich et al. 2009) and the Nogoa River in central Queensland (Finlayson and Brizga 1993). These are mud-dominated, low gradient systems with slowly accreting floodplains and channels, characterised by intermittent flow and minimal bedload transport. In comparison to other anabranching types, vegetation has a minimal control and due to the climatic conditions in which these systems occur is usually sparse (Nanson 2013; Nanson and Knighton 1996). Cooper Creek is one of the most studied anabranching rivers globally, anabranching reaches of Cooper Creek are

very low gradient and exist as part of an extensive floodplain, up to 60 km wide, extending upstream of an uplifting bedrock dome (Innamincka Dome) for hundreds of kilometres (Nanson et al. 2008; Jansen et al. 2013).

'Type 2' anabranching systems are also found in Australia, in the Northern Territory on Magela Creek, and on the Marshall River which is studied in this thesis (Chapter 7). Type 2 are considered to be dynamic equilibrium systems where anabranching increases transport efficiency in low-gradient rivers by changing w/d ratios (Jansen and Nanson 2004). In Magela Creek vegetation-stabilised sandy islands divide the channel train into multiple anabranches allowing for increased sediment conveyance when compare to a single channel with the same discharge (Jansen and Nanson 2004). The same is true in the Marshall River (Nanson and Huang 2017). Vegetation is key to the formation of a stable system as it allows for islands and banks to form in what would otherwise be non-cohesive alluvium (Tooth et al. 2008). The mechanism of anabranching here acts as a stabilising force to allow for excess sediment to be transported in a low slope environment, without the need to increase slope (Tooth and Nanson 2004).

'Type 3' anabranching rivers are likely to represent a non-equilibrium form with rivers such as the Thompson River, Victoria oscillating between energy states with short-lived anabranches formed during channel avulsions (Nanson and Knighton 1996). Type 3 anabranching rivers are defined by being laterally active (Nanson and Knighton 1996). Much of the Murray River and its tributaries, such as the Ovens River, feature type 3 anabranching. The Ovens River consists of a main channel with two active or developing anabranches, in addition to one failing and one abandoned anabranch (Judd et al. 2007). The channels formed due to the narrowing of existing channels through sediment deposition and the subsequent displacement of flow, which supports an interpretation of a non-equilibrium system (Judd et al. 2007).

'Type 4' anabranching, shares some similarities with type 2, the key difference being that the in channel islands found in 'type 2' have a much larger length to width ratio leading to them being defined as ridges (Tooth and Nanson 2004). There are several locations in Australia where type 4 anabranching exists, including the Durack River in the Kimberley region (Wende and Nanson 1998) and the Sandover-Bundey and Marshall Rivers of the Northern Plains. The Sandover-Bundy and the Marshall Rivers

on the Northern Plains have been extensively studied (e.g. Tooth 2000; Tooth and Nanson 2004; Habeck-Fardy 2013) and the Marshall River has been further investigated in Chapter 7 of this thesis. Studies of 'type 4' anabranching in Australia have focussed on the inception of islands, the role which vegetation plays in the persistence of anabranching and what the triggers of anabranching are, concluding that, as with 'type 2' anabranching vegetation has a stabilising effect and that ridge formation enables the movement of a coarse sediment load down a low gradient system, partially obstructed by within-channel trees (Tooth and Nanson 2004; Habeck-Fardy 2013).

Fowlers Creek drains the Barrier Range in western New South Wales. The upper reaches of the river is typical of a 'type 6' anabranching river, which are commonly found in small steep drainage basins with tree roots ensuring channel stability and anabranches formed by avulsion (Nanson and Knighton 1996), Fowlers Creek has gravel and sand beds which are host to *Eucalyptus camaldulensis* (River Red Gum) which through their location and contribution of woody debris through dropped limbs cause lea-side deposition of sediment and the formation of the islands which typify this anabranching pattern (Dunkerley 1992).

As described above, anabranching rivers are common throughout Australia, predominantly in the arid zone, nowhere more so than in the LEB and in Chapters 5, 6 and 7 of this thesis these are investigated on a localised and basin wide scale.

2.3 Drylands and their rivers

2.3.1 Drylands

Drylands are of scientific interest often due to their resource potential, growing human population, remoteness and delicate environmental state. As 38% of the global population live in dryland regions and 10-20% of these regions suffer from land degradation there is growing concern and demand for understanding of dryland regions (Reynolds et al. 2007). Aside from the human implications, dryland research is seen to have an impact on global science, with contributions to, amongst others, space science, early human anthropology and ecology, as well as expanding the bank of knowledge on deserts themselves (UNEP 2006).

Deserts and drylands, in this case used interchangeably, refer to hyper-arid, arid, semi-arid, and dry-humid areas, with rainfall <500 mm.a^{-1}. Dryland regions cover ~47% of the global land surface (Figure 1.1) (Middleton and Thomas 1997), with areas occurring on most continents and at varying elevations. Drylands are hydrologically diverse (Knighton and Nanson 1997) and are characterised by low, but highly variable, precipitation and, in non-polar regions, by high (yet variable) aridity with high evapotranspiration, and sporadic and highly adapted vegetation (Tooth 2013). The temporal and spatial variability of precipitation and aridity (Kingsford and Thompson 2006) leads to variable hydrology, ecology, sediment flux (McMahon et al. 1992) and extreme flow variability (Knighton and Nanson 2001). This variability leads to great diversity in their physical characteristics (Thoms et al. 2006), which is influenced by the climate, topography and vegetation of the systems.

With the exception of polar deserts, drylands are mostly confined to the tropics and sub-tropics and coincide with the major global endorheic basins due to low precipitation which prevents water levels from rising sufficiently to overcome geological obstacles or eroding channels to reach an ocean outlet (Hammer 1986). The latitudinal distribution is partly due to the distribution of Hadley Cells (Figure 2.4). The atmospheric circulation within Hadley Cells causes the tropics and subtropics to lie beneath stable, high-pressure zones meaning rainfall is rare, and where atmospheric subsidence occurs the moisture is evaporated as the air warms (Diaz and Bradley 2004). A further cause of aridity is continentality; the majority of water in the atmosphere is evaporated from the oceans, so, the proximity of land to the coast dictates the likelihood and quantity of moisture received (Gutierrez and Benito 2005). Aridity can then be maintained by the high albedo of the desert surface, which causes a temperature gradient at desert margins enhancing the effect of the distribution of Hadley Cells by causing the evaporation of moisture from descending warm air (Cooke et al. 1993). The local topography can also be a contributing factor to aridity with drylands often occurring on the lee side of mountain ranges to uplifting air and orographic rainfall, and upwelling of cold water creating advection fogs and enhancing atmospheric circulation (Houston and Hartley 2003; Laity 2008). An example of aridity attributed to topography is seen in the Atacama Desert, the formation of which is associated with the Miocene uplift of the Andes (e.g. Alpers and Brimhall 1988).

Rainfall in dryland regions, as with other regions, occurs due to monsoonal or tropical cyclonic depression, local convective thunderstorms (Figure 2.5) and rain-bearing low-pressure systems (Cooke et al. 1993; Tooth 1997), however when rainfall does occur, annual averages can be far exceeded in a rare single event (Pilgram et al. 1988). The variability of rainfall is not only temporal, but also spatial (Peel et al. 2001) with small, ~8 km (Morgan 1966), local convective thunderstorms accounting for much of this variability.
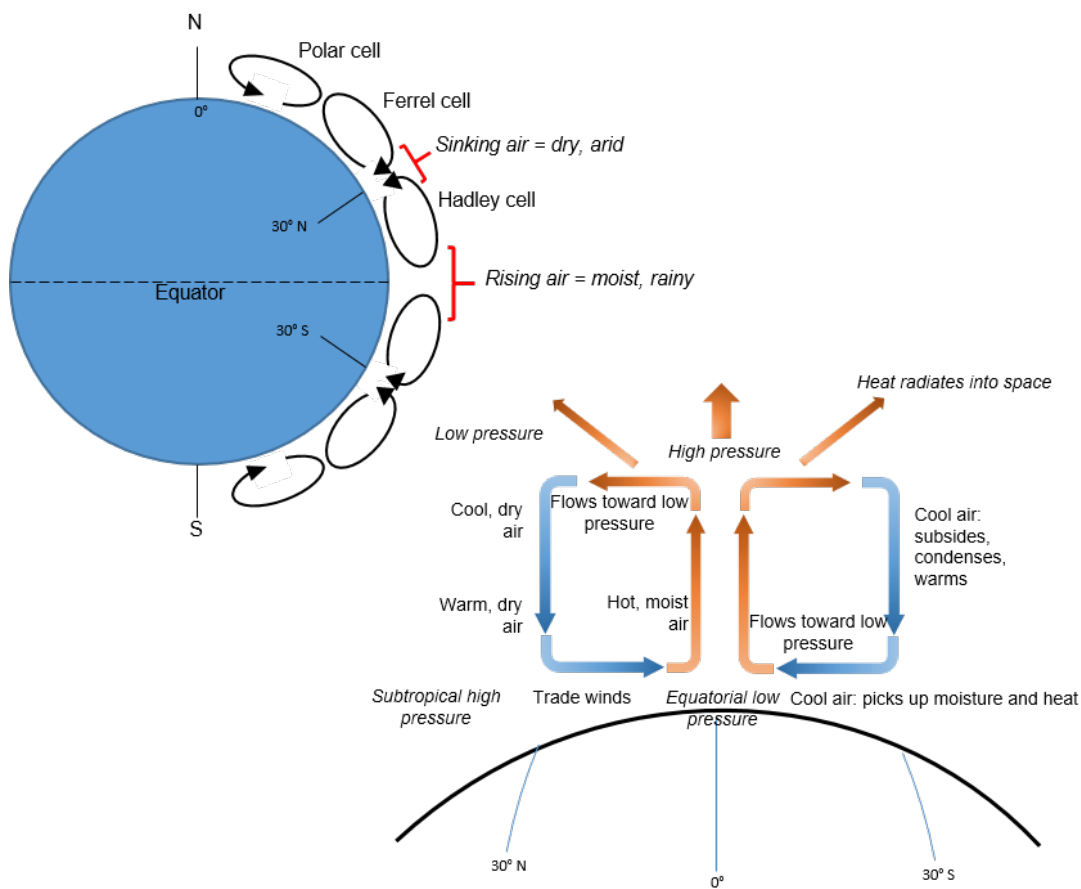
Figure 2.4 - Global distribution of atmospheric circulation cells and the movement of air within Hadley cells (after Kauffman and Cleveland 2008)

2.3.2   Rivers in drylands

Drylands support river systems which, despite infrequent flows, are pivotal in the shaping of landscapes (Tooth 2013). Understanding dryland rivers has, ultimately, relied on extrapolating from what is understood of rivers in the humid and temperate zones, yet those in drylands are significantly different to those in mesic regions (Graf

1988). This said, they possess very few completely unique landforms to set them apart (Nanson et al. 2002). The only landforms considered truly unique to dryland rivers are waterholes and floodouts (Kingsford and Thomspon 2006) and these are commonly found in low gradient dryland rivers, such as those in Africa and Australia (e.g. Nanson et al. 2002).

Allogenic rivers tend to be perennial, with 100% flow occupancy, whereas those that are endogenic are usually intermittent (50% flow occupancy) or ephemeral (0% flow occupancy) (Figure 2.5) (Tooth 2013). Hydrology in dryland systems is flood dominated, seen as four different types of floods: flash floods, single peak events, multiple peak events and seasonal floods (Graf 1988). Hydrographs in small basins are commonly steep as there is a short lag time between rainfall and discharge due to peak discharges for floods in dryland regions which are large when compared to similarly size humid or mesic basins (Graf 1988). The long-term hydrographs are identified by periods of severe flooding followed by prolonged periods of low or zero flow. Flash floods are usually associated with convectional thunderstorm precipitation and are found in basins or sub-basins of 100 km^2 or less. Single-peak floods often occur due to tropical storms and affect basins of several thousand km^2. Multiple-peak floods are produced when multiple rainfall events occur from a single storm that has stalled over a region (Graf 1988) (Figure 2.5). Seasonal floods often have multiple-peak hydrographs over a season and in dryland regions are often due to monsoonal rainfall (Graf 1988). In addition, these floods are also highly variable with a ratio of 1.5 between the 100 yr. flood recurrence interval and the mean annual flood (Q_{100}/Q), 1.5 times greater than other climatic regions (Finlayson and McMahon 1988). Such regimes are a function of high surface run-off, due to low soil infiltrability (Dunkerley 2011). The low absorption of rainfall results in the majority of run-off occurring as Hortonian overland flow (Figure 2.5), unlike humid zones where Hortonian overland flow is uncommon (Dunkerley 2011). The high run-off coefficient results from a number of characteristics of the desert ground surface. Organisms, such as algae, lichen, mosses, fungi, bacteria, and cyanobacteria, living in the active layer of desert soils form a crust by binding inorganic particles into a mucilaginous concretion, which prevents infiltration (Moore 1998).

Channels in dryland regions are characterised by intermittent flow and, due to low, yet variable, precipitation, are usually ephemeral. Those dryland rivers which do have perennial flow, often some similar characteristics to those in temperate regions (Knighton and Nanson 1997). The characteristic flow variations of arid rivers and the way this affects sediment transport influences channel morphology (Knighton and Nanson 1997). There is no one channel type or morphological feature that defines dryland rivers, but braided rivers are considered the most common channel type in drylands (Graff, 1988). However, there are few examples of extensive braided rivers described as occurring in arid regions of Australia, with braiding predominantly constrained to localised reaches (Nanson et al. 2002). However, single thread and anabranching rivers also widely occur reflecting different catchment characteristics such as slope, lithology, tectonics and vegetation.

FLOW OCCUPANCY

EPHEMERAL 0 — INTERMITTENT 50 — PERENNIAL 100%

Input
- Convective storms likely → **Variable combination of:** Convective storms + periodic incursions of moister air (often seasonal) → **Internally fed:** Predominantly springs / **Externally fed:** Wetter mountainous headwaters, snowmelt
- Highly localised → Larger supply area especially headwaters
- Extremely variable → Greater reliability

Throughput
- Hortonian overland flow dominant → Broader mix of surface and subsurface
- Rapid initiation of surface runoff → Longer response time
- Transmission losses largely through seepage → Transmission losses largely through evaporation (+artificial extraction)
- Flash Floods → Seasonal floods
- Single and multi-peaked floods

Output
- Sharply peaked hydrographs → Broader-based hydrographs
- Considerable variability → More (seasonally) dependable

Channels
- Poorly connected drainage network → Better integrated drainage network often of high density → Mostly dominated by a single large river
- High-magnitude floods as major control → More frequent discharges of greater significance in channel adjustment
- Transient behaviour dominant → Greater tendency for channels to equilibrate

Figure 2.5 - Diversity in dryland rivers' hydrology, drainage networks and channel characteristics (after Knighton and Nanson 1997).

2.3.3 Endorheic basins

Most sediment in the ocean is sourced from rivers (Phillips and Slattery 2006). However, not all basins drain to the ocean. Terminal drainage basins, endorheic and arheic, are estimated to cover ~25% of the continental area, excluding Greenland and Antarctica (Hostetler 1995), occuring mostly within the arid and semi-arid zone (Nichols 2007). Endorheic basins differ from externally draining basins as there is no marine outlet (Dorsaz et al. 2013), so sediment is not carried out of the system, therefore storage is a greater component of the system. Not only are endorheic basins commonly found in arid regions (Figure 2.6), they are also predominantly low altitude, low slope areas, as these characteristics allow for geomorphological or geological barriers to exist, preventing connection with the marine system, and can occur in areas of basin subsidence. In Australia, 64% of the land area does not drain into the sea and 21% is classed as endorheic (Hammer 1986).
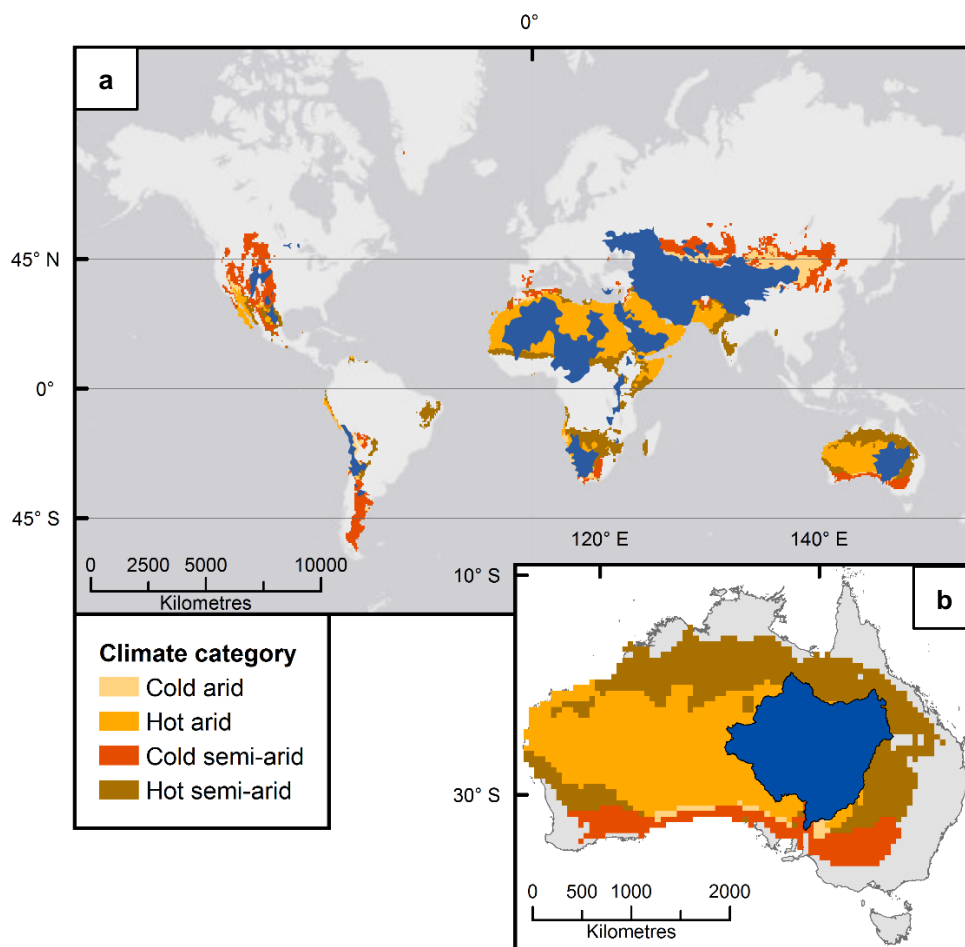
Figure 2.6 - (a) Major global endorheic basins (coloured blue) with Koppen-Geiger climate zones. The location of endorheic basins correspond closely to arid and semi-arid zones. (b) Koppen-Geiger climate zones and the LEB.

Endorheism is dictated by geography and climate, and requires a precipitation deficit relative to evaporation to prevent a sufficient depth of water pooling (usually as a lake) to overflow a topographic obstacle (Hammer 1986). The run-off within the endorheic basins of the world average 54.1 mm.yr^{-1}, whereas exorheic regions average 321.5 mm.a^{-1} (Meybeck et al. 2001). Endorheic drainage basins for the most part, culminate in lakes whether permanent, ephemeral, salt flats or alluvial plains. The dynamics of endorheic systems are driven in different ways to exorheic basins in particular in arid environments. This is due to the irregular magnitude and intensity of rainfall, high evaporation, pronounced orographic effects, low interception, geologically controlled infiltration and the role of groundwater (Laity 2008). The termini of endorheic basins are commonly saline and in basins where evaporation is the key form of water loss salinity is greatest.

2.4 Sediments: sources, sinks and sediment conveyor

In systems where flow is intermittent and where channels work to maximise flow efficiency, understanding sediment dynamics is important. The amount of sediment transported by rivers has long been underestimated. Current calculations show that they transport ~20 x 10^9 t.a^{-1} of particulate sediment to the ocean and an equal amount as solutes (Allen 2008). Sediment in the fluvial system is produced when rocks are weathered and the weathered material is transported throughout the system. Movement of sediment through river basins is dependent on watershed topography, climate, runoff, basin geology and human activities such as reservoir trapping and soil erosion (Syvitski and Milliman 2007). In a fluvial system there is a controlled volume of sediment that is inputted through erosion of hill slopes, channel perimeters and floodplains. In addition, sediment is contributed to the fluvial system from external sources such as ash and dust. The sediment transfer system has three spatial zones: denudation/erosion; transfer; and accumulation/deposition (Schumm 1977). The movement of sediment from source zones (usually the hillslopes in headwater areas, where sediment is eroded) through transfer zones (mid-catchment) to sinks, where sediment accumulates (such as, lowland plains, lakes or oceans), is termed the sediment conveyor (Schumm 1977; Fryirs 2013). The connectivity and efficacy of the conveyor can be measured by the sediment budget, which is the amount of sediment

moved from the headwaters to the mouth of the catchment, and is measured using Equation 2.2.

$$S_{in} - S_{out} \pm \Delta S_s = 0$$

Equation 2.2 - Sediment budget equation. S_{out} is sediment output, S_{in} is sediment input and ΔS_S is the change in sediment storage (after Bierman and Montgomery 2014)

The quantity of sediment within the sediment conveyor is calculated using the erosion rate of sediment from sediment storage; the amount of sediment stored throughout the system both via original deposition and redepositing of material; and the quantity of sediment which reaches the basin outlet. If the amount of sediment eroded (input) into the system exceeds that which reaches the outlet (output) then net deposition has occurred. If the output exceeds the input then net erosion has occurred. In the fluvial realm the connecting factor between storage zones is water (Thompson et al. 2016) and in most catchments sediment spends more time in storage than in transport (e.g. Otto et al. 2009). Sediment delivery to the sink is delayed by storage and intermittent remobilisation on variable timescales. Termed the 'sediment delivery problem' (Walling 1983), not all sediment eroded reaches the terminal sink in a catchment due to storage, which can be short lived and constantly reworked, or more permanent (Fryirs et al. 2007). Where sediment transport is rapid, direct measurements can be made, however where transport is intermittent and interrupted by periods of storage geochronological methods must be used, which are further discussed in Chapter 3.

The sediment conveyor behaves differently in different climatic and tectonic settings, which affect the relief and mode of sediment transport, controlling the effectiveness of the conveyor (Bishop 2007). In small high relief sediment routing systems (~10 - 15 km long) transfer zones are short and storage is negligible, however, in large continental systems (~100 - 1000 km long), of which the systems in this thesis are examples, transfer zones are long and sediment is stored either temporarily or, if subsidence promotes it, permanently (Romans et al. 2016). In tectonically active, humid and temperate environments, high discharge and rapid sediment transport result in short term shallow storage, with long term storage only occurring in deeper sediments, delivery of sediment to the terminal sink, in most cases the ocean, is high. In some humid and temperate environments, hillslopes tend to store little to no sediment as they are optimised for transport (Figure 2.7a) (Romans et al. 2016). In

tectonically quiescent, arid environments, shallow storage is extensive and storage in dunes and flood plains is long-term. Connectivity in these systems is generally low with sediment frequently stored at various points in the system (e.g. Struck et al. 2018a) (Figure 2.7). Delivery to the terminal sink is minimal due to intermittent flow, with the exception of high magnitude events, where high discharge results in efficient transfer of large volumes of sediment (Thompson et al. 2016). In the case of arid environments, the basin in which the sediment conveyor acts is often endorheic. The characteristics of the sediment conveyor in arid fluvial systems are discussed below.
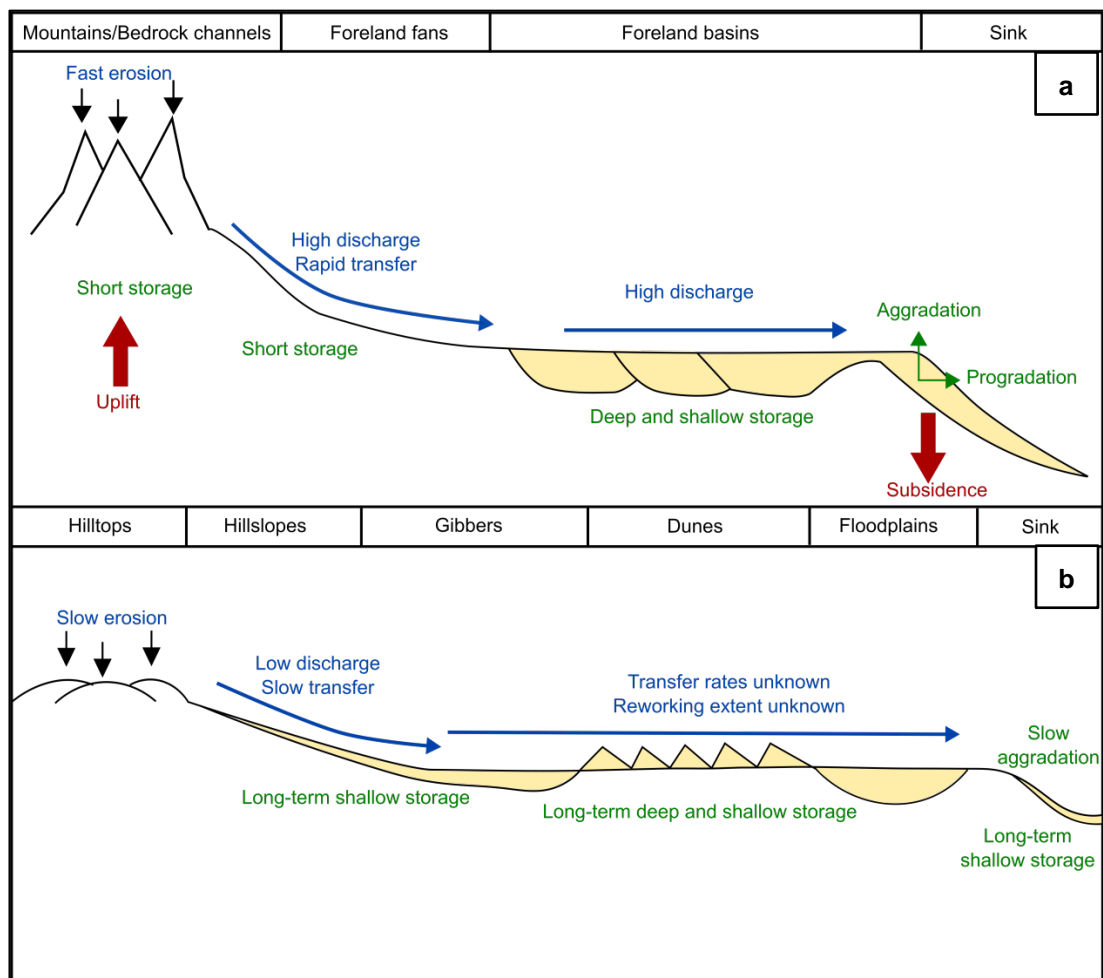
Figure 2.7- Sediment-routing systems in (a) an environment with active uplift, high seismicity and high precipitation events, such as is found in many temperate and humid regions (b) a tectonically quiescent environment with low seismicity and low precipitation such as is found in the arid zone in Central Australia (after Romans et al. 2016; Struck et al. 2018a). Yellow shading indicates sediment, green text relates to sediment deposition and storage, blue text relates to sediment transfer and discharge, red text relates to tectonic events.

2.4.1   Features of the dryland fluvial sediment conveyor

In the majority of dryland regions ~40% of the land area is bare bedrock with only a thin soil mantle (Bridge and Demicco 2008). The bedrock erodes by chemical and mechanical processes, at rates significantly slower than those in humid and temperate environments Sediment is eroded from bedrock in the headwaters by direct precipitation and overland flow and also by the channel in areas where bedrock is exposed at the surface. From the hillslopes, eroded sediment is input into the sediment routing system mainly through slow gravitational processes, such as soil creep. Once sediment is in the routing system it is more easily mobilised during flood events and is transported as both suspended load and bedload (Sharma and Murthy 1994; Red and Frostick 1989; Reid and Laronne 1995). The mobilisation of bedload is through scour of in channel materials which are then redeposited as the flood recedes (Leopold et al. 1966). This process of scour and fill is seen to its greatest extent in ephemeral rivers due to poor armouring of the channel bed that makes sediment more readily available (e.g. Laronne and Reid 1993).

Suspended load is frequently high in dryland rivers (Walling and Kleo 1979; Alexandrov et al. 2003) and has been shown to constitute 90% of total sediment loads (Powell et al. 1996). Suspended load is made available through the same mobilisation processes as bedload but also through mobilisation by overland flow and bank erosion. In contrast to temperate and humid rivers, transport is controlled more by changes in flow rather than in sediment availability (Reid and Frostick 1989), hence suspended sediment dynamics are distinctly different. Suspended sediment can frequently be transported in hyper-concentrations, <400 g.l^{-1}, in dryland rivers (e.g. Stoddart 1978; Walling 1981; Xu 1999; Cantalice et al. 2013) and these concentrations are less sensitive to changes in discharge and are commonly high, even at low flows (Frostick et al. 1983).

At points throughout the system both bedload and suspended load can be sequestered in sediment stores and sinks. In dryland, endorheic systems there are three key stores of sediment: fluvial landforms, dunes, and terminal storage points such as lakes, which are often saline playa lakes (Bullard and Livingstone 2002) (Figure 2.8). Storage in the arid zone conveyor is commonly long-term (e.g. Struck et al. 2018a). It is usually shallow in the lacustrine and hillslope realm and is deeper in floodplain zones where

accommodation space allows (e.g. Wright and Marriott 1993). Shallow storage also occurs in channels and sediment stores can be built on the surface in the form of aeolian dunes (Bullard and Livingstone 2002).

The fluvial store is made up of floodplains, channels and fans. As much as 20% of global deserts are composed of floodplains and alluvial fans associated with ephemeral rivers (Bridge and Demicco 2008). Floodplains are a key sediment storage point in alluvial systems, and are the most common landform in valley fills. The floodplain, defined at the alluvial surface next to the channel, is built of materials deposited by the river (Wolman and Leopold 1956; Tockner and Stanford 2002). Hydrologically, floodplains are defined as the surface that is inundated during a given return period (Ward 1978), so, by this definition, may be formed of bedrock instead of alluvium. In low energy systems, such as the ones in this thesis, floodplains are regions of net accumulation as opposed to high energy environments where floodplains store sediment for short time periods (Nanson and Croke 1992). They are built intermittently, with fine grained sediment transported as suspended load being deposited when flow exceeds bankfull. Floodplains in arid ephemeral dryland rivers are commonly of Class C from the Nanson and Croke (1992) three part floodplain classification system due to infrequent flows and low discharge. Class C floodplains are low-energy cohesive floodplains with specific stream power (ω) <10 W.m^{-2}. These can be further subdivided to give 13 distinct floodplain types. In low slope, arid environments floodplains are commonly low energy and cohesive, deposited by vertical accretion of overbank deposits and, in the case of association with anabranching rivers, by island deposition (Nanson and Croke 1992). Deposits are mostly fine grained forming horizontal beds with occasional lag deposits of more coarse material from splays or exceptional event flows (Graf 1988; Nanson and Croke 1992).

Coarser grained sediment is only mobilised during high magnitude events. During times of no or low flow, this sediment is stored in the channel and in alluvial fans. When sandy, or formed of mud pellets, this sediment is available for dune building and becomes sequestered, initially into source bordering dunes but can then be moved further afield and stored in desert dunefields and sandplains. The location of aeolian landforms is therefore strongly controlled by the availability of suitable sediment and

the potential for it to be mobilised often due to a lack of vegetation. Due to the proximity of aeolian and fluvial systems to one another, there is debate as to which dominates in any given environment (Bullard and McTainsh 2003). In arid areas aeolian and fluvial systems are cannot be considered independently as they either act together or act as a series of fluvial dominated or aeolian dominated units with fluctuating boundaries over time (Bullard and Livingstone 2002). In a combined fluvial-aeolian dryland system sediment is transferred between the domains from one store of sediment to another. The interactions that occur between fluvial and aeolian aspects of a system rely on the key variables of morphology, time, and the depth of the water table (Langford 1989). Just as sediment is entrained from the fluvial domain into dunes (Bullard and Livingstone 2002) (Figure 2.8), the reverse can happen. Dune material re-enters the fluvial system by transport associated with interdune flooding, migration of bedforms, the fluvial erosion of dune termini, and the rilling and sapping of dune slopes (Bullard and Livingstone 2002). Furthermore, distributary channels can extend into an aeolian system, enabling sediment exchange between the two systems with erosion occurring along the bases of the dunes or by sediment deposited in channels become mobilised by aeolian processes when flow ceases (Al-Masrahy and Mountney 2015).
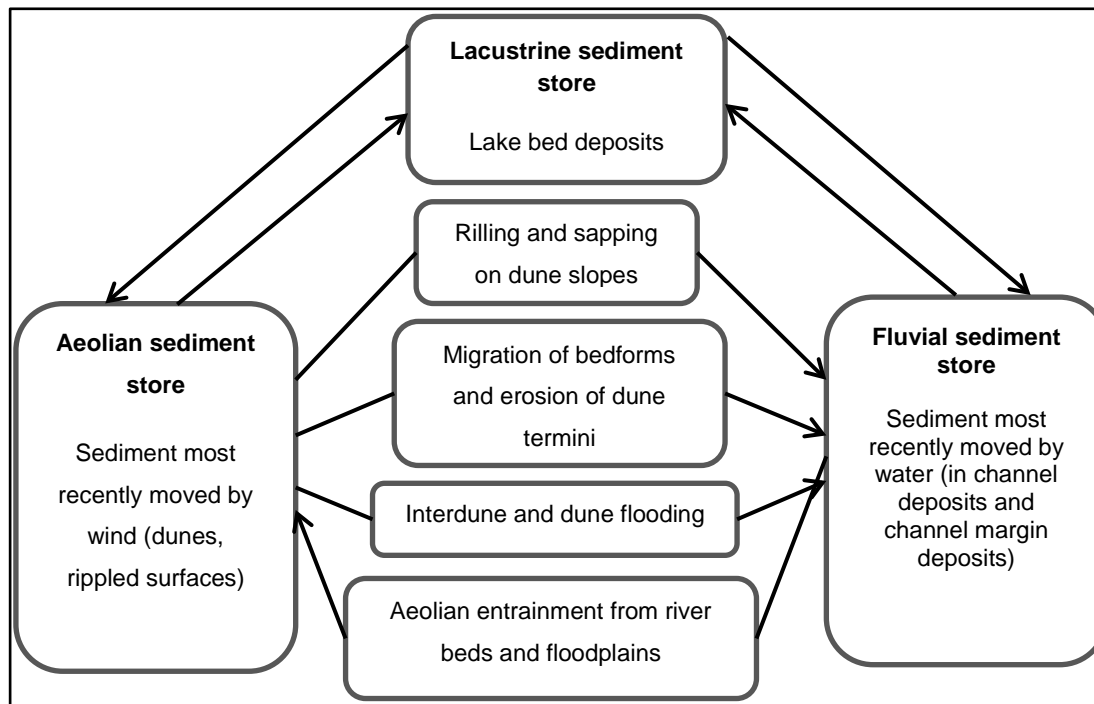
Figure 2.8 - Key links between the main sediment storage zones for sand-sized material in dryland system (after Bullard and Livingstone 2002).

Similarly dunes can interact with a lacustrine store. The latter is, for the most part, supplied from the fluvial store by the channel, however due to the dis-connectivity of the sediment conveyor because of ephemeral flow, lacustrine areas often receive minimal input. Sediment can also be received from the aeolian store, as wind-blown sediment, or by fluvial activity where sediment is eroded from the dunes by a channel and transported directly to the lacustrine store. Sediment is also lost from the lacustrine store, by deflation of surface sediment when lakes are periodically dry, and this can sequester sediment into lunettes and other dune systems.

Chapter 3

---

3 Quantifying geomorphology and geochronology in fluvial environments

3.1 Introduction

Working in dryland regions often poses problems due to size and remoteness. However, the remoteness of the majority of the LEB is advantageous in that many landforms remain undisturbed. To address the aims of this thesis (Chapter 1 - 1.2) two geochronological methods were used: optically stimulated luminescence dating (OSL), and terrestrial cosmogenic nuclide (TCN) analysis. This chapter address the choice of these methods and examines the theory behind them, their relevance in fluvial environments and how they are implemented, both in the field and in the laboratory.

3.2 Establish geochronology of fluvial landforms and events

Rivers are considered to be a highly important geomorphic agent playing a significant role in shaping the Earth's surface that we see today (e.g. Heerdegen 2001). Rivers are efficacious at adapting to environmental changes, and in doing so incorporate signals of geology, geomorphology, climate, hydrology, vegetation, and tectonics into their remnants (e.g. Mather et al. 2017). Fluvial deposits are archives of a basin's response to changes in climate, tectonics, and base level. Through dating these deposits, insight can be gained into both the distant and more recent geologic past. There are number of reasons why one may want to know the age of a fluvial deposit. This includes identifying the timing of progressive events such as changes in climate including precipitation and sea-level (Wallinga 2002) and sudden events such as floods, tectonic events, and landslides. Fluvial responses to climate change can be assessed by dating of samples and correlating times of peak deposition to known climate variations such as MIS, and can indicate patterns of long term fluvial variation.

In fluvial systems, here focussing on those in arid, low slope, endorheic environments, sediment is stored in a variety of landforms (Chapter 2.4). In order to use stored sediment as proxies for environmental change one must be able to extrapolate the conditions of deposition from the landform and also identify when they were deposited; either relative to landforms around them or with a numerical age for deposition. In fluvial environments there are a number of different techniques which can be used on different landforms extending over varied timescales. These methods can be used to quantify sediment storage, accretion, and the sequence of landform deposition (Rixhon et al. 2017).

There are a number of these geochronological methods which are commonly used in fluvial environments to establish age of deposition of landforms and sediments. These methods include: luminescence dating, radiocarbon dating, amino acid racemization, uranium series dating and cosmogenic nuclide burial dating. The methods each have their own limitations and requirements. Of these methods those which are most appropriate to answer the aims outlined in Chapter 1 are luminescence dating and cosmogenic nuclide burial dating. Radiocarbon dating can be excluded as in the arid environments in which this work is undertaken suitable organic material is rare in fluvial deposits, likewise suitable material, carbonate material such as shell, is rarely available for amino acid racemization (Walker 2005). Uranium series dating can also be excluded as the required material is also infrequently present in these deposits, specifically precipitated calcium carbonate (Walker 2005). Luminescence dating and cosmogenic nuclide burial dating both have a time span greater than 100 ka and require quartz bearing sediment which is abundant in these arid environments, where most sediment is sourced from sandstones and reworked from Cenozoic fluvial and aeolian deposits (Walker 2005). These methods are also complimentary (e.g. Guralnik et al. 2011; Luthgens et al. 2017) with luminescence recording a single, most recent event and cosmogenic nuclides being used to calculate a cumulative duration of burial, i.e. a summation of these single events .

3.3   Luminescence Dating – A synopsis

Luminescence dating is a class of techniques widely used in Quaternary science for geological and archaeological sites and is generally favoured for dating sediments in

palaeoclimate research. As a group of methods they have been developed since the middle of the 20th century (Daniels et al. 1953), initially with thermoluminescence which has been used as a tool for dating since the 1980s (Aitken and Mejdahl 1985). Luminescence dating will be used in addressing aims one and three (Chapters 5 and 7) and the following section explains the theory behind the method and how it can be applied to fluvial sediments from Central Australia. It also addresses the drawbacks and difficulties with the method and how these can be accounted for and where possible overcome.

3.3.1 The luminescence principle

Luminescence is light emitted from a substance. In the case of optically stimulated luminescence and thermoluminescence the luminescence in question is the light emitted from an irradiated substance through exposure to, respectively, light or heat. The intensity with which the substance luminesces is a function of irradiation dose, which is, in turn, a function of both time and the radioactive properties of the immediate surrounding environment (Mejdahl 1986).

Luminescence dating is used to establish time since last exposure to sunlight or elevated temperature, by means of a light and heat sensitive signal, in the form of an electron charge, in mineral grains (Wintle and Huntley 1980; Huntley et al. 1985; Aitken 1998). Energy is absorbed from a radiation source (in the surrounding environment) by a mineral. The environmental radiation is a result of alpha, beta and gamma radiation from the decay of naturally occurring ^{235}U, ^{238}U, ^{232}Th and their radioactive daughter isotopes, and ^{40}K. The radiation is absorbed and energy is stored within defects, known as traps, in the crystal lattice of the mineral electrons (Waddams 1958). The signal is removed, so–called resetting or zeroing, by exposure to sunlight or elevated temperature; then accumulates again during the subsequent period of non-exposure or normal environmental temperatures (Figure 3.1). The energy absorbed (J.Kg^{-1} = Gy) is the equivalent dose (D$_e$), which when divided by the rate of energy exposure (Gy.a^{-1}), known as the dose rate (D$_r$), gives time since resetting (Equation 3.1). The energy absorbed equates to electrons trapped in the minerals crystal lattice and the amount of electrons trapped is a function of time since zeroing and the number of electrons trapped per time interval, which is directly

related to dose rate (Aitken 1998). In short, the amount of radioactive energy imparted to a mineral during the time since last exposure or zeroing.

$$Luminescence\ Age\ (a) = \frac{D_e(Gy)}{D_r(Gy.a^{-1})}$$

Equation 3.1 - The luminescence age calculation. The luminescence age in years is calculated by dividing the measured dose in Gy (D_e) by the dose rate in Gy.a$^-$ (D_r).
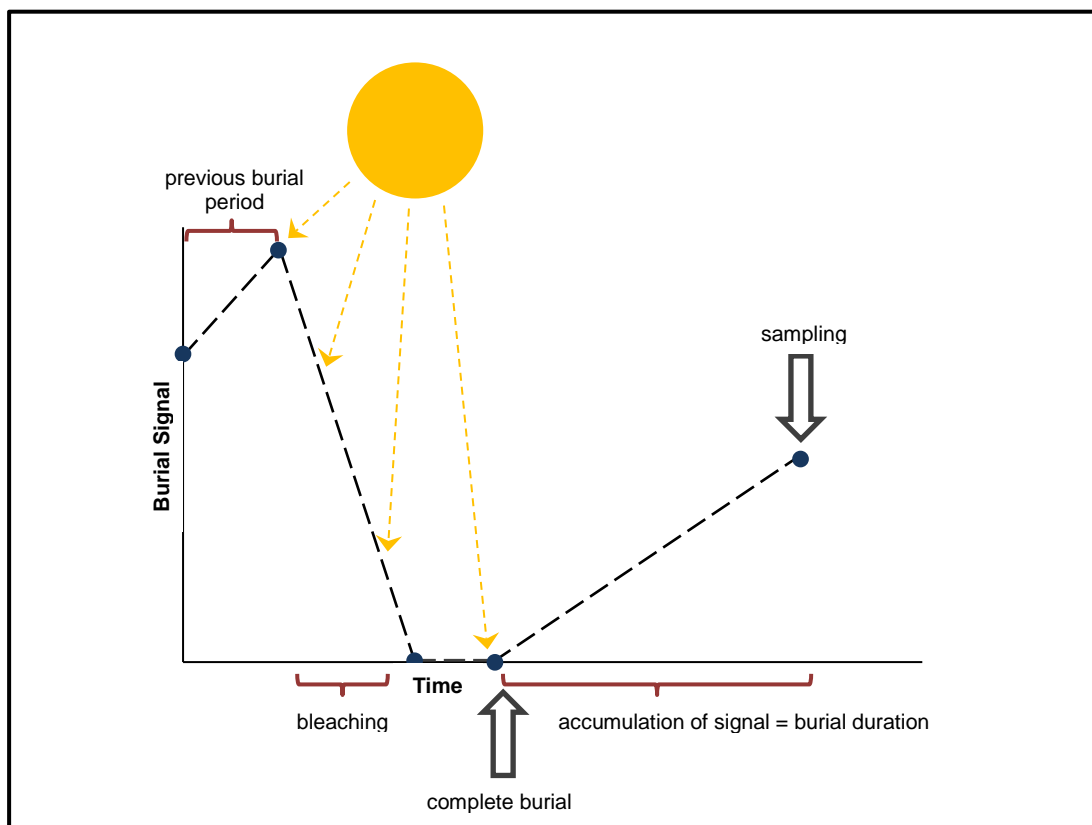
Figure 3.1 - Bleaching of sediment in the natural environment. Previous burial signal is removed (bleached) during sunlight exposure then accumulates once burial begins. The age measured is the time passed since complete burial, until sampling occurs.

3.3.2 Luminescence Materials

A number of different materials possess luminescence properties. For the most part, in Quaternary environments, luminescence dating is limited to quartz and feldspar (Duller 1996). This is due to their prevalence in geology, resistance to weathering and sensitivity to sunlight, furthermore, quartz and feldspar can be sufficiently bleached by sunlight, have a signal growth which can be mathematically defined and are stable over long periods of time.

Quartz is often the first choice for dating of sediments due to the fact that its luminescence properties are well known, it bleaches quickly compared to other materials (Figure 3.2), and furthermore, it does not suffer from anomalous fading, which is known to occur in feldspars in both thermoluminescence (Wintle 1973) and infrared stimulated luminescence dating (Spooner 1992; 1994). In addition, quartz is the most common rock forming mineral and is highly resistant to weathering, therefore is prevalent in many geological settings. Quartz has some limitations however; in rare cases (i.e. where mafic host rocks are dominant) quartz can be scarce. Also, there are settings where there are feldspar inclusions within the quartz resulting in a mixed dose signal were the quartz component cannot be isolated. It is possible for quartz to possess no luminescence signal or for the signal to be of insufficient quality for dating. Quartz also has a lower saturation dose than feldspar thus a reduced potential dating range (e.g. Chapot et al. 2012). Where quartz is not available or the dating range is too great for an age to be obtained, feldspar can be used (e.g. Buylaert et al. 2012; Li and Li 2012). Potassium rich feldspars are the most commonly used feldspars, although others do possess a luminescence signal. They have a bright luminescence signal and higher (than quartz) saturation dose implying a greater dating range. Also, there is less uncertainty from external dose as a substantial amount of dose comes from ^{40}K within the feldspar. Feldspar bleaches more slowly than quartz (Figure 3.2) so requires longer exposure to reset and a major problem can exist with anomalous fading (Wintle 1973) where part of the signal is lost over time.
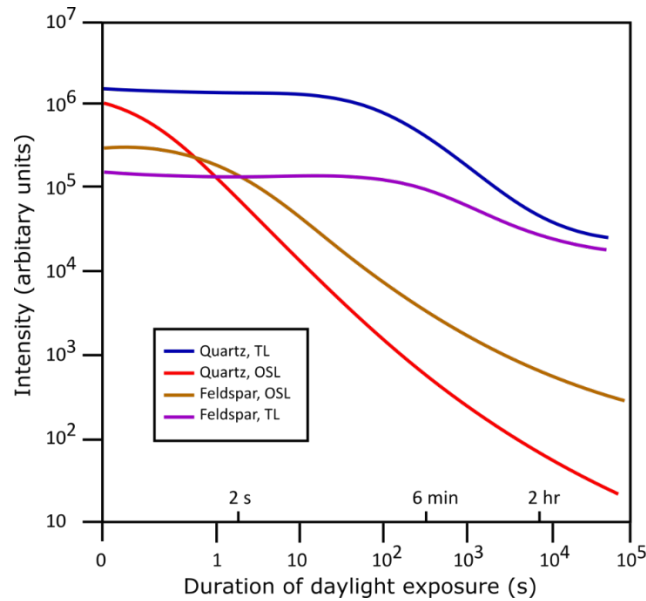
Figure 3.2 - Bleaching time of the thermally stimulated luminescence and optically stimulated luminescence signal from quartz and feldspar (after Godfrey-Smith et al. 1988)

3.3.3 Luminescence methods

Luminescence methods are broadly defined by the stimulation source. Primarily whether this stimulation from heat or light; thermoluminescence (TL) or optically stimulated luminescence (OSL). OSL is further subdivided into OSL and infrared stimulated luminescence (IRSL). OSL is typically used for quartz and IRSL for feldspar. From this point OSL and luminescence will refer to optically stimulated luminescence on quartz, unless otherwise stated. Thermoluminescence was initially developed as a dating tool for fired pottery (Aitken 1980) whereas the development of OSL occurred due to a need for a dating technique that could be used for sediments.

Luminescence can be conducted as either multi- or single grained measurements. Both of these methods have used the single aliquot regenerative dose (SAR) method (Figure 3.3) since the late 1990s, which applies measurements to aliquots (sub-samples) of an approximate known number of grains mounted onto metal discs. The SAR protocol is used in this thesis, using single grain measurements which differ in that measurements are made in individual grains rather than a collection of grains.

The SAR protocol, defined by Murray and Wintle (2000), is a regenerative dose approach, which allows for correction of sensitivity changes occurring during the measurement procedure. The protocol measures a signal (L_x) after each regenerative

dose and applies a test dose (remaining constant throughout) after each measurement including the natural and zero measurement (Figure 3.3)

The luminescence readout of each regenerative dose (and the natural dose), defined as Lx, is normalised by the test dose (Tx). Thus, the corrected signal is Lx/Tx. To implement the SAR protocol a minimum of three regenerative dose and zero point must be measured. The Lx/Tx values are plotted against the given regenerative dose to give a dose response curve. To find the palaeodose the natural signal is measured and a readout from the curve taken to give the equivalent dose (D_e) of the sample.

Single grain measurements, where the SAR protocol is applied in turn to individual grains from a sample, are the most effective and important for younger samples (less than a few thousand years) (Jain et al. 2004) as the residual luminescence signal contributes a larger portion of the measured D_e, thus producing a larger age overestimation than in older samples with higher burial doses where the effect is reduced. When using large aliquots the true burial age and any sign of partial bleaching is masked and in general the age will be an overestimation. Further reasons for using single grain measurements are discussed below.
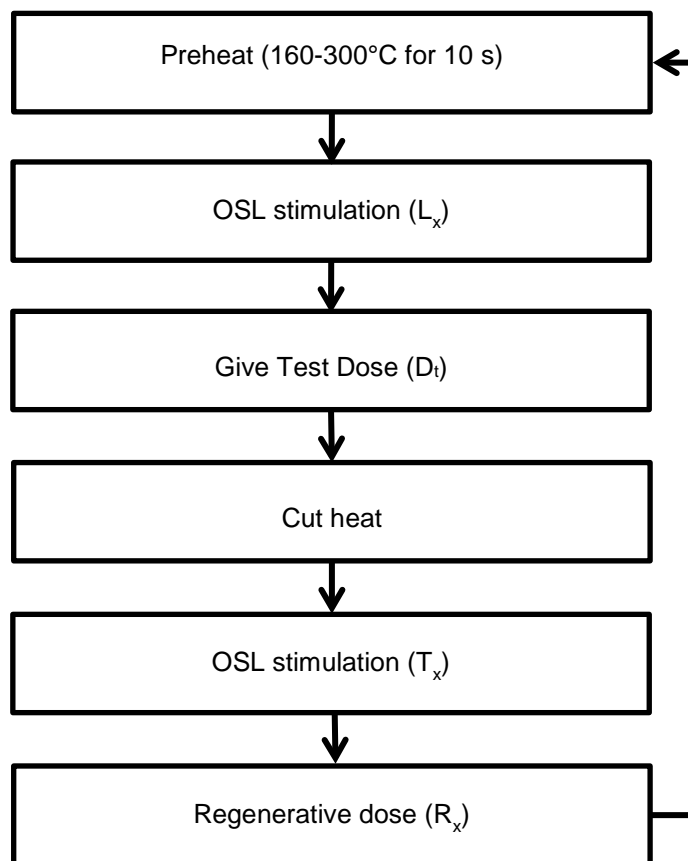
Figure 3.3 - Generalised SAR dose protocol (after Murray and Wintle 2000).

3.3.4 Models for D_e determination

In single grain measurements there is commonly a large distribution of D_e values, so a number of statistical methods have been developed to isolate the grains which are the most representative of the burial dose. The most appropriate method is sample dependent, depending on the dominant influences such as partial beaching, post depositional mixing or dose-rate heterogeneity (Bailey and Arnold 2006).

Galbraith et al. (1999) produced the two most commonly used age models in OSL dating, the central age model (CAM) and minimum age model (MAM). If the majority of grains are well bleached, the true D_e is represented by the lowest values in the dose distribution if the aliquots are small enough (Olley et al. 1999) and the CAM is most applicable. A true estimate is difficult if a large proportion of the grains are poorly bleached and there are a number of methods to establish a good estimate, including the MAM. Another method suggested is to use the lowest 5 – 10% of dose as these are most likely to represent the burial dose (Murray et al. 1995; Olley et al. 1998; 1999). An alternative method removes scatter from experimental

errors and uses the lower values, the so-called 'leading edge', of the distribution to estimate the D_e (Lepper et al. 2000). A method that can be applied to a small number of aliquots, when the preferred large dataset cannot be obtained, was devised by Fuchs and Lang (2001) which uses the arithmetic means of the two lowermost values and adds subsequent (numerically ordered) values until a standard deviation of 4% is exceeded. In this thesis both the CAM and MAM are used and described below. These two models are considered superior to other models, such as the leading edge model as they are well tested with samples of known age and have their basis in well-understood statistical principles. When choosing an age model, one must consider the distribution of the grains. The shape which a histogram summarising the measured aliquots takes is also an indicator of the bleaching characteristics of a sample. A well bleached sample will produce a tightly constrained symmetrical histogram with an approximate normal distribution, whereas poorly bleached sample show a wider spread, asymmetric histogram due to contamination from higher dose (incompletely bleached) grains.

3.3.4.1   CAM

The central age model (CAM) (Galbraith et al. 1999) is a calculation of a weighted mean. It is most commonly used for calculating the D_e of a well-bleached samples, where the D_e is truly representative of time since last exposure. In these samples, overdispersion, the variance in excess of what would be statistically expected, is usually 10 – 20% and the distribution of single grain measurements would be normally distributed.

3.3.4.2   MAM

The minimum age model (MAM) (Galbraith et al. 1999) is used where samples are incompletely or non-uniformly bleached, a typical distribution may include a mixture of grains that have different degrees of bleaching and, if a D_e were calculated using the CAM an overestimation would result. The presence of scatter in a measured sample is used as an indicator of partial bleaching, but the degree of scatter is dependent on the number of grains present and the ratio of poorly to well bleached grains. This mixture of bleaching results in a large overdispersion, and a distribution that is commonly left skewed, representing a truncated log-normal distribution with

the lower values, at the point of truncation, representing the most recent bleaching events, and the higher values have a residual unbleached signal (Galbraith et al. 1999).

3.3.5 Calculating environmental dose rate

Alpha and beta particles, and gamma and cosmic rays are the four forms of environmental radiation from the decay chains of ^{235}U, ^{238}U, ^{232}Th and their radioactive daughter isotopes, and ^{40}K. Alpha particles are short range particles that are emitted from uranium and thorium decay chains (Aitken 1985). Beta particles have a longer range (~2 mm) and are emitted from the U, Th, K and Rb decay. Gamma rays are longer range penetrating up to ~30 cm and are emitted from U, Th and K decay (Aitken 1985). Cosmic rays are charged, high-energy particles which penetrate long distances through the Earth's atmosphere from space (Prescott and Hutton 1994).

The majority of the environmental dose of a sample is from external radiation which comes from the surrounding sediment and cosmic rays (Aitken 1985). The effect of external alpha radiation can be removed by etching the sediment grains with hydrofluoric acid which removes the outer ~9 μm that the alpha particles affect. Beta particles and gamma rays from ^{235}U, ^{238}U, ^{232}Th and their radioactive daughter isotopes, and ^{40}K contribute the majority of external dose, while Rb is generally disregarded as its contribution is considered negligible (Warren 1978; Aitken 1976). The contribution from cosmic rays is variable as their intensity varies with latitude and altitude. The sampling depth and density of sediment overburden also attenuates cosmic rays, reducing their penetration with depth.

Internal dose also contributes to the overall dose rate. The alpha portion of the internal dose in quartz is low since there is minimal U, Th, or K in quartz (Aitken 1998) and cannot be measured, so 0.03 Gy.ka^{-1} is used (Bowler et al. 2003).

In the laboratory dose rate can be calculated from the measurement of the concentrations of radionuclides with methods such as with inductively coupled plasma mass spectrometry (ICP-MS), x-ray fluorescence (XRF) or neutron activation analysis (NAA), or by the counting of radioactive emissions through methods such as thick source alpha counting (TSAC), beta counting and high-resolution gamma

spectrometry (HRGS). Environmental dose rate can also be measured in the field through use of a portable gamma –spectrometer, which is preferable when sampling in pits or from exposures but is not easily applied when sampling through cores. Measuring dose rate in the field overcomes the problem of dose heterogeneity which occurs when sediments of different dose rates mix (Murray and Roberts 1997; Jacobs et al. 2008). Laboratory measurements assume dose homogeneity so can lead to either under or over estimation of dose. Aside from the problem of dose heterogeneity, problems can arise with disequilibrium in the radioactive decay chain.

Disequilibrium is when different parts of the decay chain show different activities due to some members of the decay chain becoming mobilised, being depleted, or being enriched. For example U is soluble in water so can move out of or into the sediment being sampled, therefore disequilibrium is most commonly found in sediments which are exposed to water, either at deposition or during burial.

3.3.6 Sources of error and considerations when OSL dating fluvial sediments

There is an abundance of studies using OSL to date fluvial samples ranging from floodplains, to terraces, to scroll bars and a number of other landforms (e.g. Rittenour et al. 2005; Cunningham et al. 2012; Gliganic et al. 2014; Sim et al. 2014; Gliganic et al. 2015). The aim of these studies is frequently to establish the sequence of deposition of landform and/or to understand changing river behaviour, often in relation to climatic or anthropogenic variation.

Dating of fluvial samples has long been problematic, with progress hampered by the lack of consistent dating (Cunningham and Wallinga 2012). Challenges are posed by the discontinuity of fluvial deposits and that they rarely possess the annual layering which is required for high precision techniques. It is often not possible to use other dating techniques, for examples radiocarbon dating, while offering the best precision, is of limited use in arid fluvial environments due to the frequent lack of organic carbon. OSL dating is usually possible, however, as the material required (most often quartz or feldspar) is commonly abundant in the fluvial environment, this, coupled with the long age range obtainable from OSL dating has meant that there are many proponents for its use as the standard method for dating fluvial deposits (Wallinga 2002; Rittenour 2008; Cunningham and Wallinga 2012).

There are a number of sources of error that can give inaccurate estimates of dose (D_e) when calculating ages aside from potential machine error. Discussed below are those sources of error which are commonly encountered in fluvial environments and must be taken into account when dating the sediments in this thesis.

Probably the most commonly encountered problem and source of error in OSL dating of fluvial sediments is due to partial/incomplete bleaching. Sediment is rarely uniformly bleached, but widespread partial bleaching commonly occurs in glacial and waterlain sediments and can result in an overestimation of age. Partial bleaching is more common in feldspars than quartz as feldspars require a longer exposure to sunlight for complete bleaching to occur, even in ideal conditions (Figure 3.2).

Attenuation of light by the water column results in limited solar resetting (e.g. Berger 1990), with the Beer-Lambert law stating that the intensity of light decreases exponentially with depth through absorption and scattering. The attenuation increases with the amount of dissolved solids as this increases the attenuation coefficient (e.g. Berger and Luternauer 1987).

The mode of sediment transport and distance which sediment is transported can also affect the bleaching of fluvial sediments. Shorter transport distances can give large age overestimates, due to the general overall bleaching of sediment in water the sediment is not exposed for sufficient time to completely bleach it. Relating to distance travelled is the scenario where sediment is inputted into the system during high discharge events, which is often poorly bleached due to rapid erosion, transport and deposition (Rittenour 2008). The environment from which the sediment enters the system also has an effect on bleaching. If sediment enters the channel from overbank or surface deposits it is likely to that a degree of bleaching has already occurred. If the sediment that enters the system is older, such as from river beds and banks it is likely to already be carrying a luminescence signal which can cause scatter by mixing with sediment at different stages of bleaching (Rittenour 2008). The proportion of completely bleached grains tends to increase with distance downstream (Gliganic et al. 2017).

It is highly unlikely that a partially bleached sample will show the same degree of partial bleaching for each grain (if this were the case it would be indistinguishable from a uniformly bleached sample). The distribution that usually occurs is that some

grains will be completely bleached and others will be incompletely bleached, with different amounts of bleaching having occurred (Olley et al. 1999). As the degree of solar resetting is variable there is greater scatter in the results than found in a uniformly and completely bleached sampled due to greater grain to grain variation.

In fluvial environments quartz is preferred to feldspar as it bleaches more rapidly and given the problems of incomplete bleaching in fluvial samples, a faster bleaching signal is preferred. In fluvial environments it has been show that coarser grains (90-200 μm) are generally better bleached than finer grains (4 -11 μm) (e.g. Olley et al. 1998; Wallinga 2002). This more complete bleaching can be due to a number of reasons. Coarser grains are transported more slowly than fine grains so, despite sunlight attenuation through the water column there is more time for bleaching to occur between initial erosion and final deposition (Rittenour 2008). Coarser grains are likely to experience multiple exposures to sunlight during transport such as deposition on sandbars (Rittenour 2008). Fine grains are generally more cohesive and can become pelletised and then transported as aggregates of grains so not all the cohered grains are exposed to sunlight (Lang 1994).

Given the scatter which occurs due to partial bleaching, it has been found that using large aliquots does not often yield useful results and can result in an age offset of several thousand years with a large error (Wallinga 2004). Additionally, it is not always possible to identify partial bleaching (Wallinga 2004). If one uses small aliquots the effect of averaging of grain to grain variations is reduced (Wallinga 2004). Single grain is the preferable, if more time consuming, method, as in single grain measurements grains that indicate that they are incompletely bleached can be excluded from age calculations and the population of grains showing the youngest age would be those completely bleached at deposition (Rittenour 2008; Olley et al. 1998). Furthermore, as different minerals and different signals within them bleach at different rates (Figure 3.2), quartz is preferred in fluvial environments as it bleaches more quickly.

In a given sample it can be possible to identify incomplete bleaching by plotting the D_e distribution of the grains, especially where single grains are used as the signal variation is not masked by averaging. The lowest grouping of values will represent those grains which were completely bleached prior to burial. In a sample with

incomplete bleaching a second grouping will exist grains with a higher D_e indicating there was residual luminescence a deposition that was no entirely reset (Murray et al. 1995). In the D_e estimate this can be accounted for by use of the minimum age model, as previously discussed.

D_e over and underestimation can also occur due to bioturbation. In dynamic environments younger grains can be moved down through the sediment by bioturbation (Bateman et al. 2003; Gliganic et al. 2017), this presents as a similar dose distribution to incompletely bleached sediments with the lowest D_e population representing the most recent burial event. A consideration must be made as to which population is representative of the event/stratigraphic layer in question. In this scenario the finite mixture model (Galbraith 2005) can be used to distinguish distinct populations within a distribution which are representative of different burial ages.

Further error can be integrated when adjusting environmental dose rate for water content as variations in water content can result in variations in energy absorption (Li et al. 2008). As water content can only be known for the time of sampling, an average based on current water content is used, which is not able to account for variations in moisture input over time from changes in environment.

Inhomogeneity of the dose rate can also affect the D_e estimation, as discussed above (Chapter 3 - 3.3.5) (e.g. Murray and Roberts 1997; Nathan et al. 2003; Jacobs et al. 2008). This is the biggest problem in quartz where the majority of dose is from the surrounding sediment; in feldspar a significant portion of the dose is internal so variations in external dose have a lesser impact. Calculations assume homogeneity of dose within the sediments, however due to natural variations of the different minerals within the sediments this is not the case. Radiation hotspots can occur which mean that some grains receive a greater dose than others due to closer proximity to a source of radiation (e.g. Jankowski and Jacobs 2018).

3.4 Terrestrial Cosmogenic Nuclides

The measurement of cosmogenic nuclides came to the forefront with pioneering studies on ^{3}He, ^{21}Ne, ^{22}Ne, ^{10}Be, ^{26}Al and ^{36}Cl (Craig and Poreda 1986; Klein et al. 1986; Kurz 1986a;b; Nishiizumi et al. 1986; Phillips et al. 1986; Marti and Craig 1987; Nishiizumi et al. 1987) in the mid – late 1980s. Since then methods have developed greatly and are used extensively in geomorphology and geochronology

(Dunai 2010). TCNs produced in the atmosphere by cosmic rays are used in a group of geochronological methods to establish burial, exposure and erosion on Quaternary timescales and beyond (Lal and Arnold 1985). TCNs will be used in addressing aim two and the following section explains the theory behind the method and how it can be applied to fluvial sediments from central Australia. It also addresses the drawbacks and difficulties with the method and how these can be accounted for and where possible overcome.

3.4.1 Cosmogenic Nuclides – Principles and Properties

Cosmogenic nuclides are isotopes of elements, rare on the Earth, that are produced by the interaction between cosmic rays and the nucleus of an atom. Some of these atoms are produced in the atmosphere, others are produced terrestrially in rocks and sediments in the ground, these terrestrially produced cosmogenic nuclides are used in cosmogenic nuclide dating. The processes by which cosmogenic nuclides are produced are cosmic ray spallation, thermal neutron capture and negative muon capture (Silberberg and Tsao 1990). Cosmic rays are charged, high-energy mostly atomic nuclei, but also electrons, positrons and other subatomic particles, from space that collide with the Earth (Gaisser 2016). When spallation occurs nucleons are released from the atomic nuclei which continue in motion to trigger spallation in other nuclei which produces a nuclear cascade in the atmosphere (Simpson and Fagot 1953; Gaisser 2016) (Figure 3.4). At the Earth's surface, more than 98% of the cosmogenically produced nuclides are produced by secondary particles such as muons and neutrons (Masarik and Beer 1999).

In the initial spallation reaction, high energy particles collide with the target nuclei (Figure 3.4; Table 3.1), releasing protons, neutrons and clusters, and resulting in a lighter nucleus (Silberberg and Tsao 1990). The released particles cause subsequent reactions and further spallation resulting in accelerated particles which collide with more nuclei producing a cascade of interactions that generate more particles and release high energy radiation. The reactions continue until the particles no longer have sufficient energy for further spallation to occur when the particles collide.

Cosmogenic nuclide production in sediment or rock decreases exponentially with depth, to zero production at ~30 m. Near the surface nuclide production is ~97.5% nucleons (Heisenger 1998), but with depth, muons dominate production (Granger

and Muzikar 2001). Production rates also decrease as atmospheric pressure increases at lower altitudes, and with decreasing latitude from 60° (Lal 1991). Further decreases occur if there is sheilding from surrounding areas of higher relief (Lal 1991). All of these factors can be incorporated into a number of models to create a shielding factor for a given sample, which is incorporated into subsequent calculations (Lal 1991; Dunne et al. 1999; Dunai 2000; Stone 2000; Desilets and Zreda 2003; Lifton et al. 2005; Desilets et al. 2006; Codilean 2006).
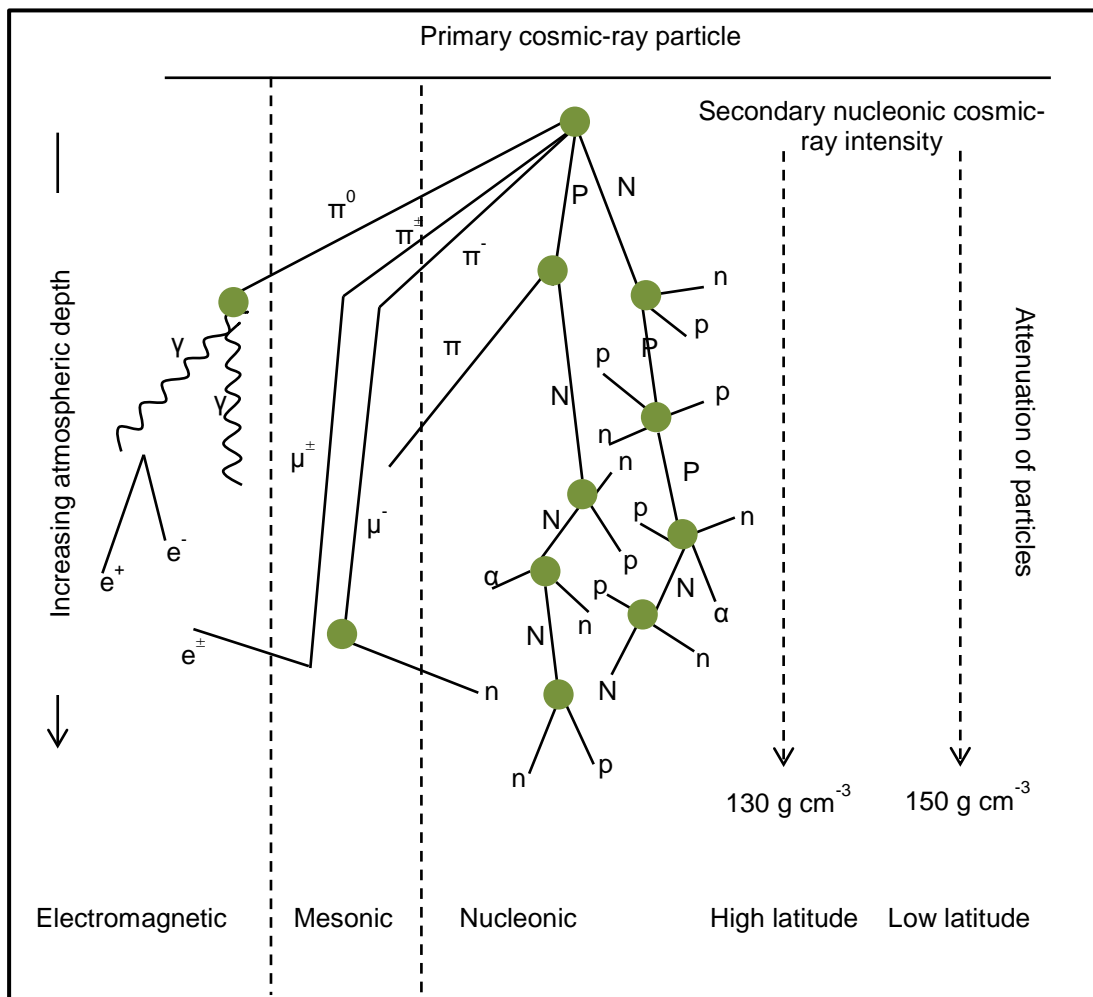
Figure 3.4 - The secondary cosmic ray cascade in the atmosphere and its intensity (after Simpson and Fagot 1953).

n = neutron, p = proton (capital letters for particles carrying the nuclear cascade),α = alpha particle, e⁻ = electron, e⁺ = positron, γ = gamma ray photon, π = pion and μ = muon

Table 3.1 - Cosmogenically produced isotopes, target elements and method by which they are produced (after Dunai 2010)

Isotope	Main target elements	Reactions
^{3}He	Numerous, includes Li	Spallation (100%) Thermal neutron capture (on Li via ^{3}H)
^{21}Ne	Mg, Al, Si	Spallation (>96.4%)
^{10}Be	O, Si	Spallation (96.4%) Muons (3.6%)
^{26}Al	Si	Spallation (95.4%) Muons (4.6%)
^{36}Cl	K, Ca, Cl, (Fe, Ti)	Spallation (95.4% from K, 86.6% from Ca; 100% from Fe, Ti) Thermal neutron capture (from Cl and K) Muons (4.6% from K; 13.4% from Ca)
^{14}C	O, Si	Spallation (82%) Muons (18%)

3.4.2 Cosmogenic materials and methods

As cosmogenic nuclides are not naturally occurring on Earth, it is possible to use the concentration of them as a chronometer to measure time that a rock or sediment has been exposed to cosmic rays during its lifetime. Not all cosmogenically produced nuclides are useful as chronometers, these nuclides must be:

i) naturally rare in the environment, ideally only produced by cosmic rays so it can be assumed that any measured is cosmogenically produced;

ii) stable or long-lived radioactive with a half-life that is greater than or equal to the time period of interest;

iii) able to have any meteoric or geological background easily resolved from the analysis;

iv) well understood in terms of production mechanisms and rates;

v) feasible to measure. The analytical effort should not outweigh the potential outcome; and

vi) produced and retained in commonly occurring minerals (Dunai 2010).

The six most common terrestrial, cosmogenically produce nuclides are ^{3}He, ^{21}Ne, ^{10}Be, ^{26}Al, ^{36}Cl and ^{14}C (Figure 3.5). These are produced at different rates which vary with location due to variations in topographic shielding, self-shielding and shielding

by over-burden. The most common target mineral is quartz, with ^{21}Ne, ^{10}Be, ^{26}Al, and ^{14}C all produced within it. Quartz is the most abundant rock forming mineral and is therefore found in the majority of environments ^{10}Be and ^{26}Al are the most commonly used nuclides in TCN dating. ^{3}He and ^{21}Ne are used in volcanic rocks where olivines and pyroxenes are commonly found, but quartz is rare. The nuclide used is also dependent on the dating range of interest, with ^{10}Be having the longest dating range of $10^2 - 10^7$ years (Figure 3.5b) adding to the frequency with which it is used. The dating range is dependent on the half-life of the nuclide (Figure 3.5c), in the case of radioactive nuclides, those minerals with a longer half-life having a greater dating range as they take longer to reach concentrations below detection.

There are five commonly used applications of TCNs (Dunai 2010): i) exposure dating; ii) erosion/denudation rate calculations; iii) burial duration dating; iv) uplift rates calculation; and v) soil dynamics. In fluvial systems those most widely used are erosion/denudation calculations, to calculate basin wide denudation rates and sediment sources (e.g. Wittmann and von Blanckenburg 2015; Dannhaus et al 2018), and burial duration dating, to quantify storage duration in fluvial systems (e.g. Ciampalini et al. 2015; Stor et al 2019). These applications are used in this thesis to assess erosion and burial within the arid zone sediment conveyor (Chapter 2 - 2.4). In the sediment conveyor in arid environments, burial dating can be applied to the two main storage points: dunes and floodplains (Chapter 2 - 2.4) to measure burial duration of sediment that is currently at the surface, and erosion rates can be measured as catchment averaged rates.
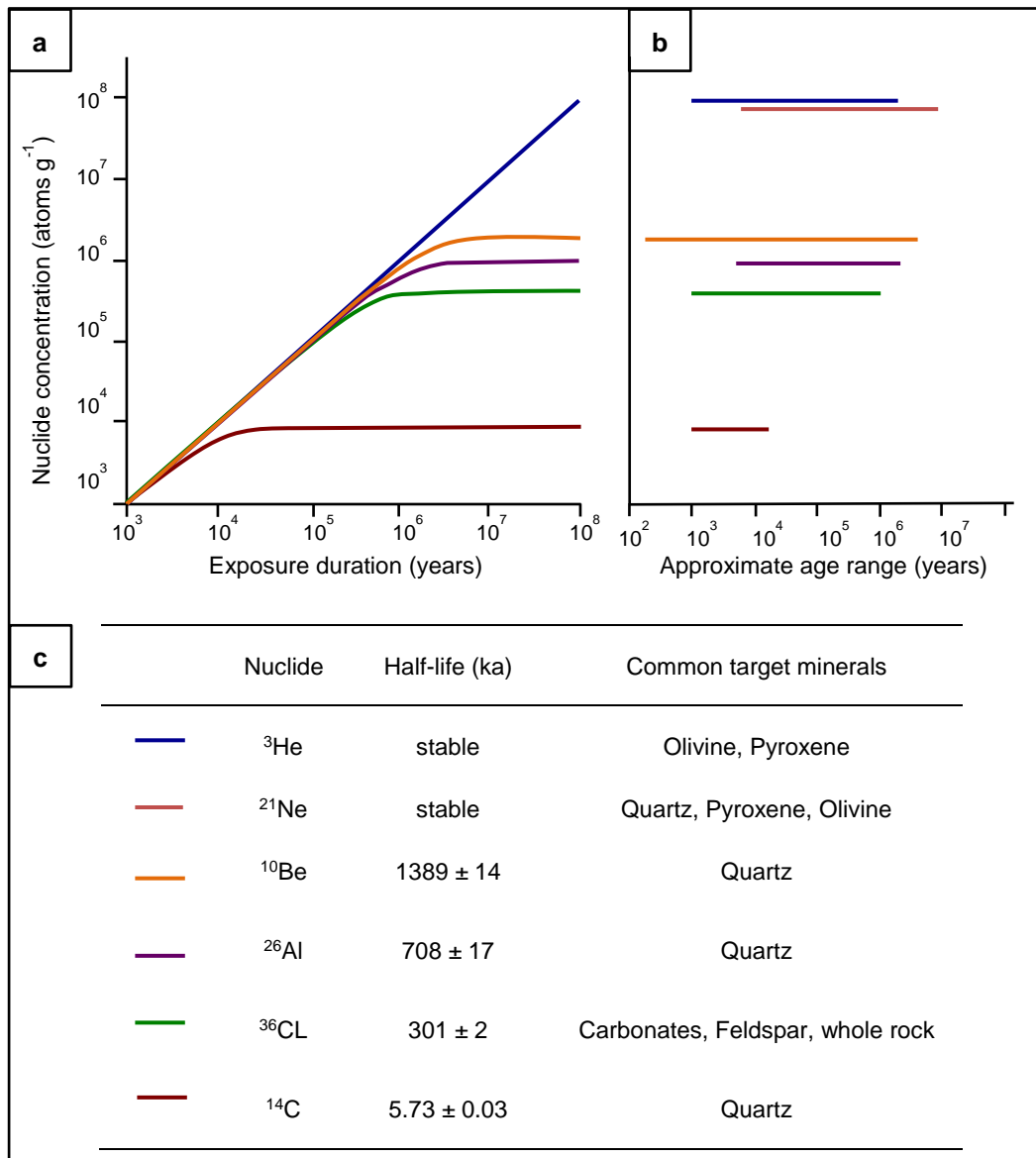
Figure 3.5 - The most common cosmogenically produced nuclides. (a) Concentration over time of the most commonly used cosmogenically produced nuclides assuming production rates of 1 at. g^{-1} yr^{-1} and no erosion; (b) Approximate age ranges of results obtainable from the most commonly used cosmogenically produced nuclides;(c) half-life in ka and common targets minerals for the most common cosmogenically produced nuclides corresponding to plots A and B (after Darvill 2013)

3.4.2.1 Denudation rates

The erosion rate is the rate at which grains are moved from a fully shielded position in bedrock to an unshielded position at the surface (Dunai 2010). The accumulation of a cosmogenic nuclide as the grain is transported to the surface is proportional to the time taken, therefore is proportional to the erosion rate (Granger and Muzikar 2001). The denudation rate is this erosion rate combined with the addition of chemical weathering. The calculation of bedrock denudation rates is on the earliest uses of TCN (e.g. Nishiizumi et al. 1986; Nishiizumi et al 1993; Bierman 1994) with ^{10}Be being the most commonly used nuclide (Dunai 2010). Calculation of the denudation rate assumes that the conditions are steady-state and the concentration of TCN remains constant over time, lying on the steady state erosion curve (Dunai 2010) (Figure 3.5a). Denudation rates for multiple grains can be combined to calculate catchment averaged denudation rates. This can be conducted by measuring concentrations within a bulk sample of stream sediment (Brown et al. 1995; Bierman and Steig 1996; Granger et al. 1996) and calculating the denudation rate of this bulk sample which is assumed to be representative of the entire upstream supply area of a sample. The capacity to calculate accurate catchment averaged denudation rates relies on the following five conditions (Dunai 2010):

(1) the erosion rate of the catchment area being constant over time;

(2) the mineral being measured being present in all lithologies, the more uniform the catchment lithology in type and grain size the more accurate the average;

(3) denudation must be primarily from surface erosion, not deep weathering;

(4) the erosion rate must be short when compared to the half-life of the nuclide being measured; and

(5) the transport time should be short, as in a fluvial system featuring long transport times the^{10}Be concentration can become altered and no longer be a true reflection of the erosion rate at the source.

3.4.2.2 Cosmogenic Burial Dating

To calculate burial ages there are several factors which must be known: That nuclides are produced within the mineral, that the sample has been shielded and the rate at which the nuclides are produced. Using TCN for burial dating is based on the

differential decay of two radioactive nuclides or the ratio in concentrations between one decaying and one stable nuclide. The most commonly used pairing is ^{26}Al/^{10}Be as they are both produced in quartz, the production rates are affected minimally by geographic location and production rate does not vary a large amount with depth in rock (Brown et al. 1992). The pre-burial ratio is usually well constrained and close to the ^{26}Al/^{10}Be surface spallation production ratio (Granger and Muzikar 2001; Balco and Rovey 2008) of 6.75 (Balco et al. 2008).

When the erosion rate is >10 m.Ma^{-1} then the initial ratio is relatively insensitive to erosion rate (Balco and Rovey 2008). The dating range for this method can extend to 5 Ma; a range not widely covered by other methods and is particularly useful as it extends beyond the dating range of OSL, radiocarbon, U-series and ESR (Walker 2005; Davis et al. 2011). The dating range is dictated by the half-life of ^{26}Al and the precision of the measurement techniques. The half-life of ^{10}Be is 1.36 ± 0.07 Ma and of ^{26}Al is 708 ± 17 ka (Nishiizumi et al. 2007). From this, and assuming an experimental uncertainty of 5% the uncertainty in burial ages in ~100 ka, giving a lower dating limit of ~100 ka (Granger and Muzikar 2001) the upper limit can be extended as far as 5 Ma as this is the point that ^{26}Al becomes depleted below detection limits. In samples with lower initial ^{26}Al the dating range can be significantly reduced due to a shorter time span being required for depletion below detection levels. The ratio of ^{26}Al/^{10}Be changes after burial following parallel to the radioactive decay lines in Figure 3.6 starting at the steady state erosion line, with the starting point on this line indicating erosion rate at source (Granger and Muzikar 2001).

Burial can be fast and complete, slow and/or incomplete, or complex. Fast and complete burial only occurs in specific cases such as sediment flushed into deep caves, under thick sediment sequences or under water. Shielding in excess of 30 m is required and the timespan which it takes to get to complete shielding must be much shorter than the subsequent burial period (Dehnert and Schluchter 2008; Dunai 2010).

In scenarios where burial is slow and/or incomplete, significant post burial production can occur due to interaction with muons (Granger and Muzikar 2001; Balco and Rovey 2008). Burial in these scenarios can be calculated through depth

profiles (Granger and Smith 2000; Wolokowinsky and Granger 2004) or through isolevel sampling of clasts in a single sedimentary layer (Balco and Rovey 2008), both of which require correction for post burial nuclide production.
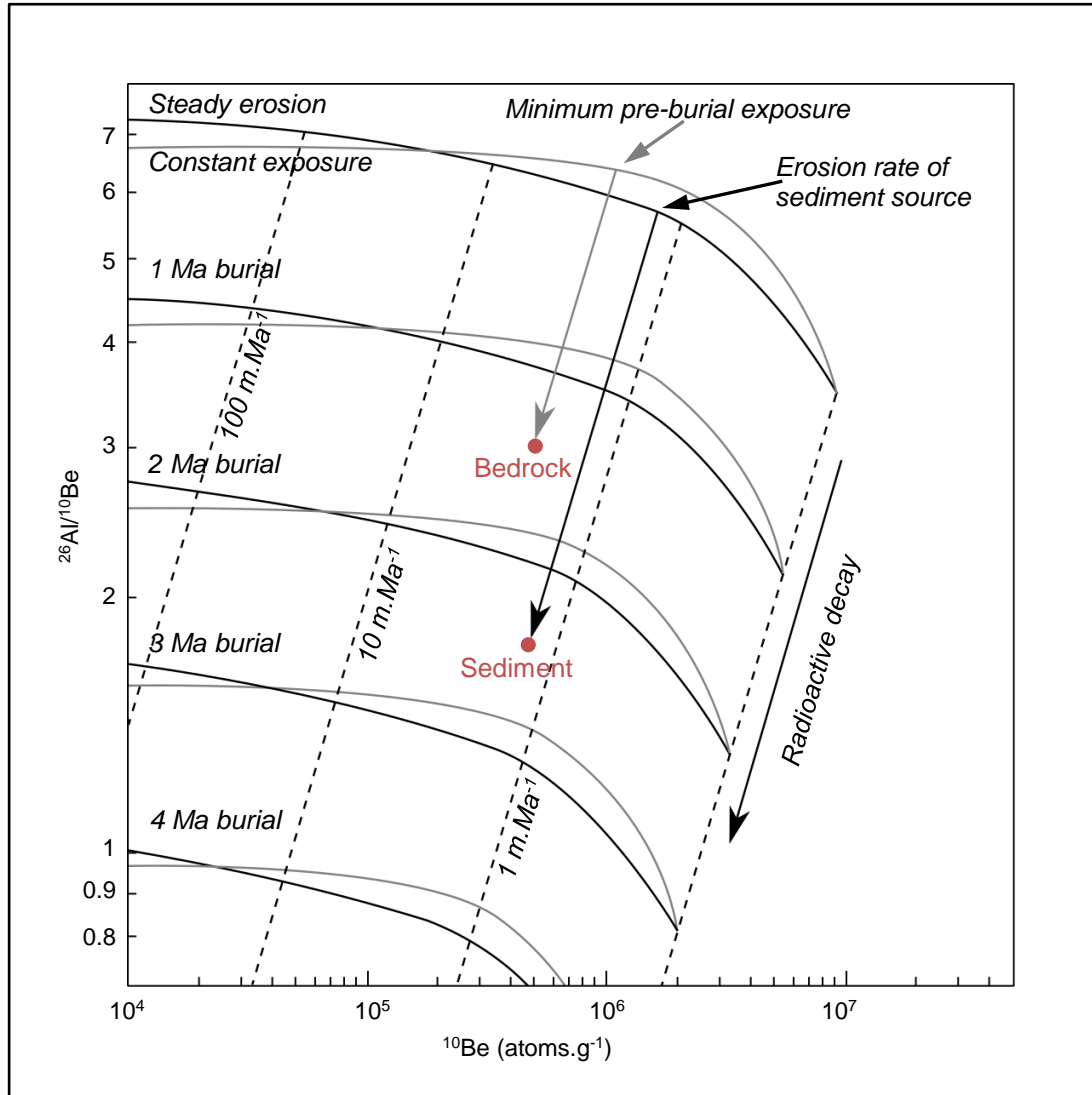
Figure 3.6 - Post-exposure burial dating diagram showing $^{26}Al/^{10}Be$ vs ^{10}Be concentration for different erosion rates and burial scenarios(after Granger and Muzikar 2001). Samples that have not been buried plot between the constant exposure and steady erosion line, in the erosion island. Once burial begins and the decrease in the ratio occurs, sediment with a simple complete burial history will follow the lines of radioactive decay down, respective of its erosion rate.

In environments associated with the sediment conveyor, complex burial scenarios in which sediment undergoes repeated periods of shallow burial and exposure during its time in the system, are common. In these scenarios any burial age obtained is a minimum burial duration, as the measured ratio of $^{26}Al/^{10}Be$ may have been adjusted during time at or close to the surface or in transport. Complex burial scenarios can

still be plotted on the burial dating diagram (Figure 3.6), however the trajectory will not directly follow the radioactive decay lines.

3.4.3 Using cosmogenic nuclides with fluvial sediments

Fluvial sediments can give insights into the history of a river and how the landscape has evolved. Sediment can be used as a means of ascertaining basin infill and channel incision in response to forcing factors; primarily, tectonics and climate (Granger and Muzikar 2001). However, burial dating and denudation rate calculation in fluvial environments has its own set of problems. Cosmogenic nuclides can accumulate during normal fluvial processes but the timescale of hillslope processes is generally longer than active bedload transport (Whipple and Tucker 2002). Sediment transported in water is considered to be shielded by the water so the sediment which is transported is not subject to significant nuclide accumulation (Wittmann and von Blanckenburg 2009). As previously mentioned, burial scenarios in fluvial environments are usually complex(e.g. Dunai 2010), so the burial age obtained is a minimum age, and it may be more suitable to consider the deviation of the ^{26}Al/^{10}Be from the production ratio, as an indication that burial may have occurred (Granger and Muzikar 2001). Denudation rate calculations also have problems due to catchment averaging (Granger 1996), particularly in the arid zone where sediment transport is frequently slow and often disconnected so the potential for sediment accumulation during transport is high (Wittman and von Blanckenburg 2016) thus yielding inaccurate denudation rates (Clapp et al. 2002).

There are a number of studies which use the ratio of ^{26}Al/^{10}Be to assess burial in fluvial systems and several of these are from arid, tectonically quiescent environments such as Central Australia (Clapp et al. 2000; Bierman and Caffee 2001; Bierman et al. 2005; Vermeesch et al. 2010; Davis et al. 2012; Struck et al. 2017). All of these except Clapp et al. (2000) show burial and reworking of existing sediment. In comparison, in tectonically active environments reworking is less common in both arid and non-arid climates.

3.5 Applicability and considerations

This chapter highlights the appropriateness of both cosmogenic nuclide burial dating and OSL in addressing the aims of this thesis, given the widespread usage of both

OSL and TCN dating in fluvial environments and that both have well developed methodologies.

In reference to the use of OSL, it can be concluded that when attempting to date fluvial deposits one should use the smallest aliquots possible and, where possible, coarse (sand-sized) grains. Single grain measurements are deemed the most appropriate for this thesis as they allow for isolation of different components of varying burial ages, so can help identify problems such as incomplete beaching and sediment mixing, which are common in fluvial deposits (Murray and Roberts 1997). Therefore, in this thesis (Chapter 7), single grain dating of sand sized quartz will be used, and all samples will be assessed for incomplete bleaching and the likely need to use the MAM. It should, however, be noted that the samples being dated in the thesis are from arid, low latitude environments where bleaching is usually more effective.

Cosmogenic nuclides will be used to calculate both burial ages and denudation rates for the fluvial systems in this thesis (Chapter 6). In doing so, it should be considered as to whether the denudation rates are a true representation of catchment wide source erosion rates, i.e. has the ^{10}Be concentration been altered during extended transport events. Also, it should be considered what it is that any burial age that is calculated truly represents, as burial at >30 m depth is unlikely to have been experienced by sediment at the surface in an arid, tectonically quiescent scenario, therefore burial should be treated as a minimum, cumulative age.

Chapter 4

4   Australia's arid zone and the Lake Eyre Basin

4.1   Introducing the Australian arid zone

Australia, since the breakup of Gondwana, has undergone minimal tectonic activity with only minor vertical movement and subsidence (Gurnis et al. 1998). This low tectonic activity has resulted in a relief unique to the Australian continent, with 60% lying below 300 m AHD. The Australian landscape has been shaped by endogenous tectonic and igneous activity, and exogenous weathering, erosion, depositional and diagenetic processes, but was minimally affected by Pleistocene ice ages, with no continental ice sheets, so a long-term sedimentation record exists. While dunes are the most dominant landform in Australia covering 40% of the continent and representing 40% of global dunefields (Wasson et al. 1988), much of arid Australia, the focus of this thesis, is dominated by landforms of fluvial origin (Warner 1988). Australia, at 10 to 40 °S, correlates with the location of the sub-tropical high pressure zone between the Hadley cells (Figure 2.5). Average precipitation is ~400 mm.a^{-1} and the average runoff ratio is 13% and potential evaporation is high (McMahon et al. 1992).
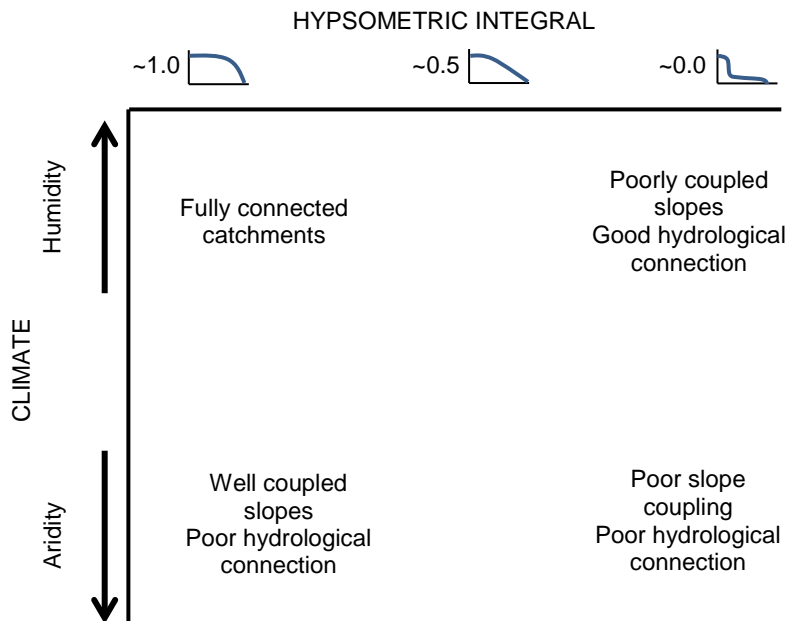
Figure 4.1 – The resultant degrees of slope coupling and hydrological connection with variation in climate and hypsometry (after Finlayson 2010).

The low overall relief, and high percentage of low elevation land, results in a low hypsometric integral (Finlayson 2010) (Figure 4.1). Only eastern, northern and southwestern coastal zones have rivers associated with significant runoff. All major drainage basins lie, at least partially, within the semi-arid or arid zone and are hydrologically defined by low levels of runoff, high inter-annual runoff variability and highly variable flood behaviour. Australian arid rivers, in general, have poor channel connectivity and poor slope coupling (Figure 4.1). However, on a local scale and in wetter parts of the continent they correspond to those on the upper left of Figure 4.1, with fully connected catchments. Slope-channel coupling and connectivity of channel networks then reduce with distance downstream (Finlayson 2010). Due to the poor hydrological connection associated with aridity, large areas of Australia are endorheic. The most notable of these endorheic areas is the LEB covering one seventh of the Australian continent, an area of $1.14 \times 10^6 \, km^2$.

4.2   The Lake Eyre Basin

The LEB is the focus of this thesis. It is ideal for the study of fluvial process and form as it has not been greatly affected by human interactions or modifications with no major flood or flow mitigations, channel redirections or man-made storage areas.

There is little filling and draining of wetlands and the aquatic systems are generally healthy. The only major human impact comes from grazing pressure close to waterholes (Lake Eyre Basin Scientific Advisory Panel 2008). A thorough review of the LEB exists (Habeck-Fardy and Nanson 2014) therefore the following outline of the location and characteristics of the LEB, the geology and tectonics of the region, and the Tertiary and Quaternary history and the modern climate and morphology, focusses on those aspects which are particularly relevant to the objectives of this thesis.

The LEB can be defined both hydrologically and geologically, so unless otherwise specified the use of LEB here refers to the hydrological basin (Figure 4.2). The basin itself extends from 19 °S to 32 °S, from the monsoonal tropics into the temperate zone, and is the largest endorheic basin in Australia.
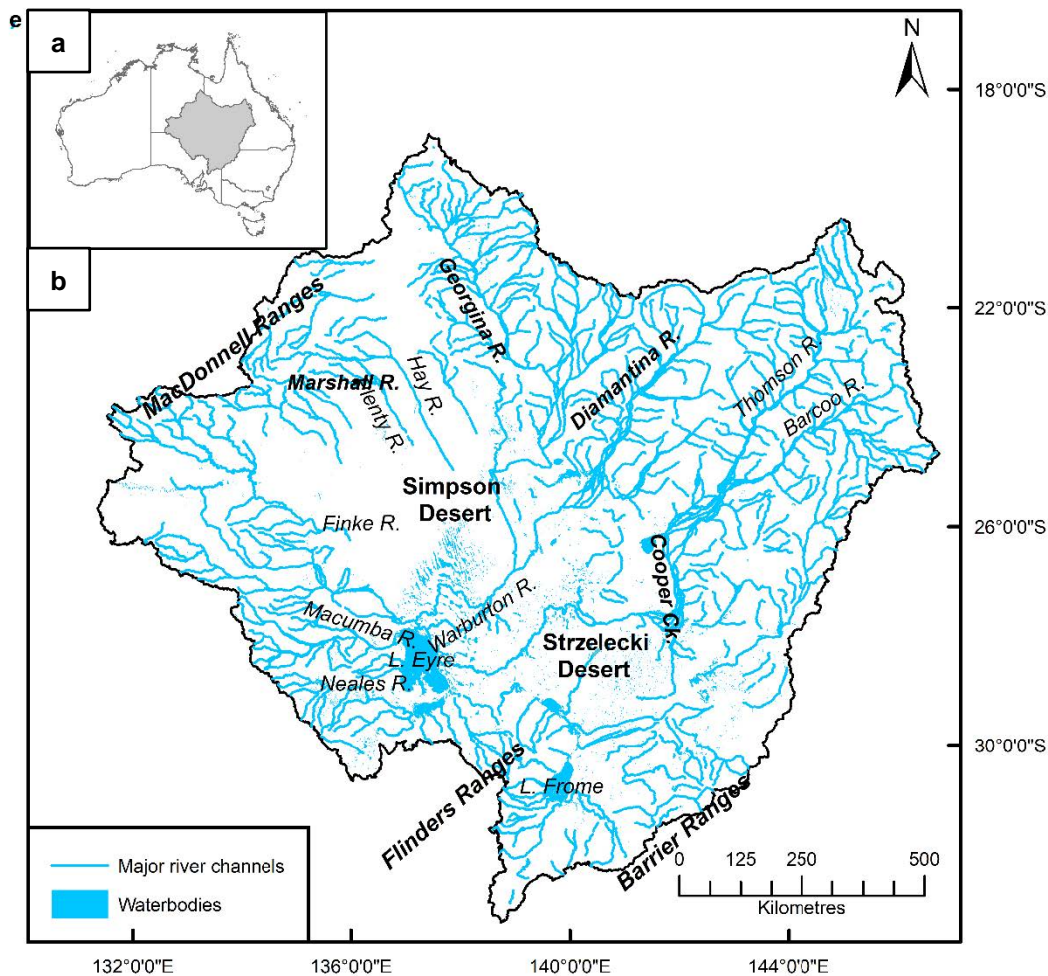
Figure 4.2 – An overview map of the LEB and its drainage system (a) with inset of the basin in Australia (b). The major river channels, waterbodies, and mountain ranges are labelled.

The basin is a shallow depression situated in an area of relatively consistent low relief, with the higher elevation of the MacDonnell Ranges at ~1500 m on the western periphery, and to the southwest the Flinders Ranges at ~1200 m (Figure 4.2). The remainder of the basin is predominantly low elevation with over 70% lying beneath 250 m AHD (Australian Height Datum) (Kotwicki 1986). The geomorphology is dominated by fluvial architecture and much of the LEB is occupied by the Simpson, Tirari and Strzelecki deserts, the dunefields of which have, to a degree, reorganised the drainage system during their development through redirection and obstruction. Elsewhere in the landscape is characterised by silcrete tablelands, gibber plains and rocky interfluves cutting through the large floodplains of ephemeral rivers. A number of these ephemeral rivers, rising at ~400 m AHD in the north and northeast, traverse the basin at a gradient of only 0.0002 m.m^{-1} and

feed the basin's namesake, Kati Thanda-Lake Eyre, a saline playa of ~9330 km^2 at -15 m AHD in the southwest of the basin.

4.2.1 Geology and tectonics

The geology of the LEB is dominated by Mesozoic and Cenozoic rocks with extensive overlying unconsolidated Tertiary and Quaternary sediments (Figure 4.3b). On the northern and southern peripheries Palaeozoic and Proterozoic rocks outcrop in an arc (Wasson 1983a) (Figure 4.3b). The geographically defined LEB is not, geologically, a single entity and it crosses into a number of geological provinces. The geological Lake Eyre depositional basin, has its depocentre at Kati Thanda-Lake Eyre (Alley 1998) and is dominantly made up of the Tirari and Callabonna sub-basins (Figure 4.4). The current basin is located within a series of older basins with three phases of deposition which record changes from wetter to the presently arid conditions. The deposition occurs from aeolian and fluvial activity, although current climate combined with low relief and a quiescent tectonic regime results in low depositional rates and the aforementioned low denudation rate (Jansen et al. 2013). The depositional and erosional activity has resulted in Quaternary deposits comprised of reworked alluvium and dune sand (Maroulis 2000). The dominant and consistent low relief indicates a subdued tectonic regime, further reinforced by low denudation rates calculated at <10 mm.ky^{-1} using cosmogenic methods (e.g. Heimsath et al. 2010; Fujioka and Chappell 2011). Given the low rates, sediment input into the system is also low and landscapes with extensive longevity exist (Quigley et al. 2010). While tectonic activity during the Neogene and Quaternary has been extensive in central Australia it has generally been of low magnitude but the relative flatness of the landscape means the subtle tectonic events that do occur can have a more noticeable effect than in areas with more variable elevation (Jansen et al. 2013). The main modern tectonics are the gradually uplifting Gason, Corryanna and Innamincka Domes (Figure 4.3c) which have had a distinct effect on the morphology of the low-gradient river systems including the formation of the extensive Cooper Creek floodplain (Jansen et al. 2013; Nanson et al. 2008) and the formation of swamps and lagoons in the lower Cooper Creek (Habeck-Fardy and Nanson 2014).
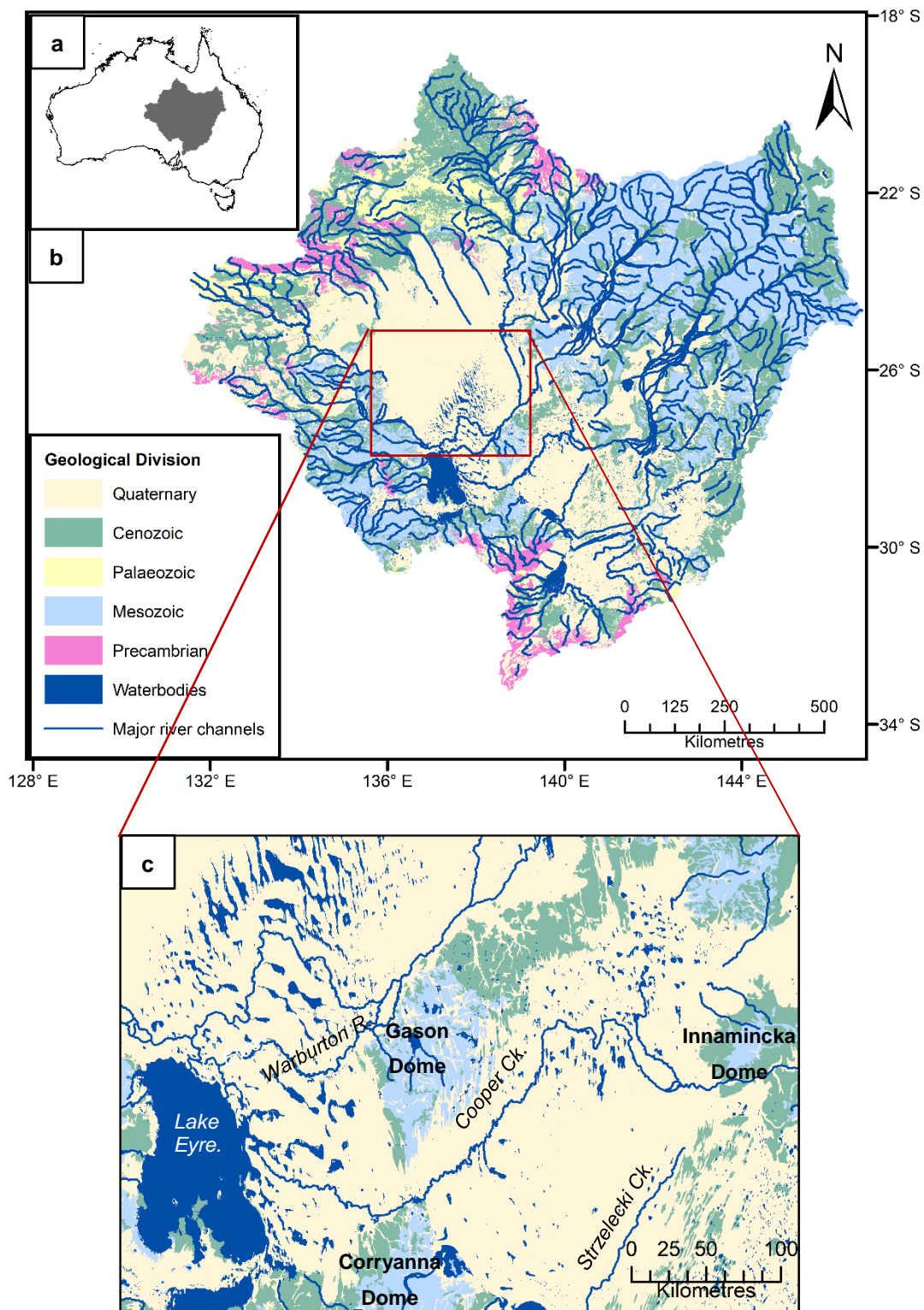
Figure 4.3 - Geological map of the LEB (a) The LEB in Australia; (b) Geology of the LEB divided into Precambrain, Mesozoic, Palaeozoic, Cenozoic (excluding Quaternary) and Quaternary rocks/sediment. Summarised from the 1:1 000 000 surface geology map of Australia (Raymond et al. 2012) (c)Magnified section of surface geology showing main tectonic features of Innamincka and Gason Domes.

4.2.2 Cenozoic History

The climate of Australia has been wetter, overall, in the past than today (Fujioka and Chappel 2010) and in Central Australia, including the LEB, there have been pronounced alternating periods of fluvial, lacustrine, and aeolian sedimentation. From the beginning of the tertiary the LEB has been progressively infilled with sediment. The geological record in the LEB is characterised by three main depositional phases (Kreig et al. 1990; Callen et al. 1995a; b): Phase one (P1), from the Late Palaeocene to the Middle Eocene; phase two (P2), from the late Oligocene to the Miocene; and phase three (P3) from the Pliocene to the Quaternary (Figure 4.4). The three phases of deposition record the change from wetter to the current arid conditions within the LEB (Alley 1998).

In Phase one (P1) the Eyre Formation and its equivalents were deposited, consisting mostly of sandstone, carbonaceous clastics and conglomerates. Phase one (P1) sedimentation deposits indicate warm and wet conditions with an environment dominated by active river systems, freshwater swamps and lagoons (Alley 1998). These conditions gave rise to tropical weathering with iron-rich weathering products, which are interpreted (Pillans 2005; Pain et al. 2012) to be the cause of the characteristic red colour of soils and sediments in the LEB.

Phase two (P2) followed with deposition of the Etadunna Formation and its correlatives, the Namba Formation, Doonbarra Formation and Cadelga Limestone, being deposits consisting of mostly clay fine sand and carbonate with some lesser conglomerates (Alley 1998) (Figure 4.4). These deposits represent a climate that was drier than P1, with the cessation of rainforest dominance (Hill 1994; White 1994). The conditions favoured lacustrine conditions, with shallow freshwater lakes, over the fluvial dominated conditions of P1. The continent wide drying was due to the northward drift of Australia which led to the development of circulation in the southern ocean and the growth of the Antarctic ice sheet (Fujioka and Chappell 2010), resulting in it entering the sub-tropical high pressure zone.

In phase 3 (P3) the Wipajiri, Tirari, Kutjitara, Katipiri, Eurinilla, Coomb Spring and Coonarbine Formations and the Simpson Sand consisting of sand and sandy clay were deposited in the centre of the basin and Willawortina Formation and mound springs on the basin peripheries (Alley 1998) (Figure 4.4). These sediments indicate

a further increase in aridity with this phase of deposition continuing through the Quaternary to present. P3 is well described as a number of these units are present at the surface. Arid conditions commenced about 2 - 4 Ma with stony deserts of the LEB forming at the start of the Quaternary (Fujioka et al. 2005). Following the Tertiary deposition of the Tirari Formation, the Kutjitara and Katipiri formations were deposited both of which record oscillating wet-dry conditions of rivers, which were a response to major climatic oscillations during the Pleistocene (Nanson et al. 1992).
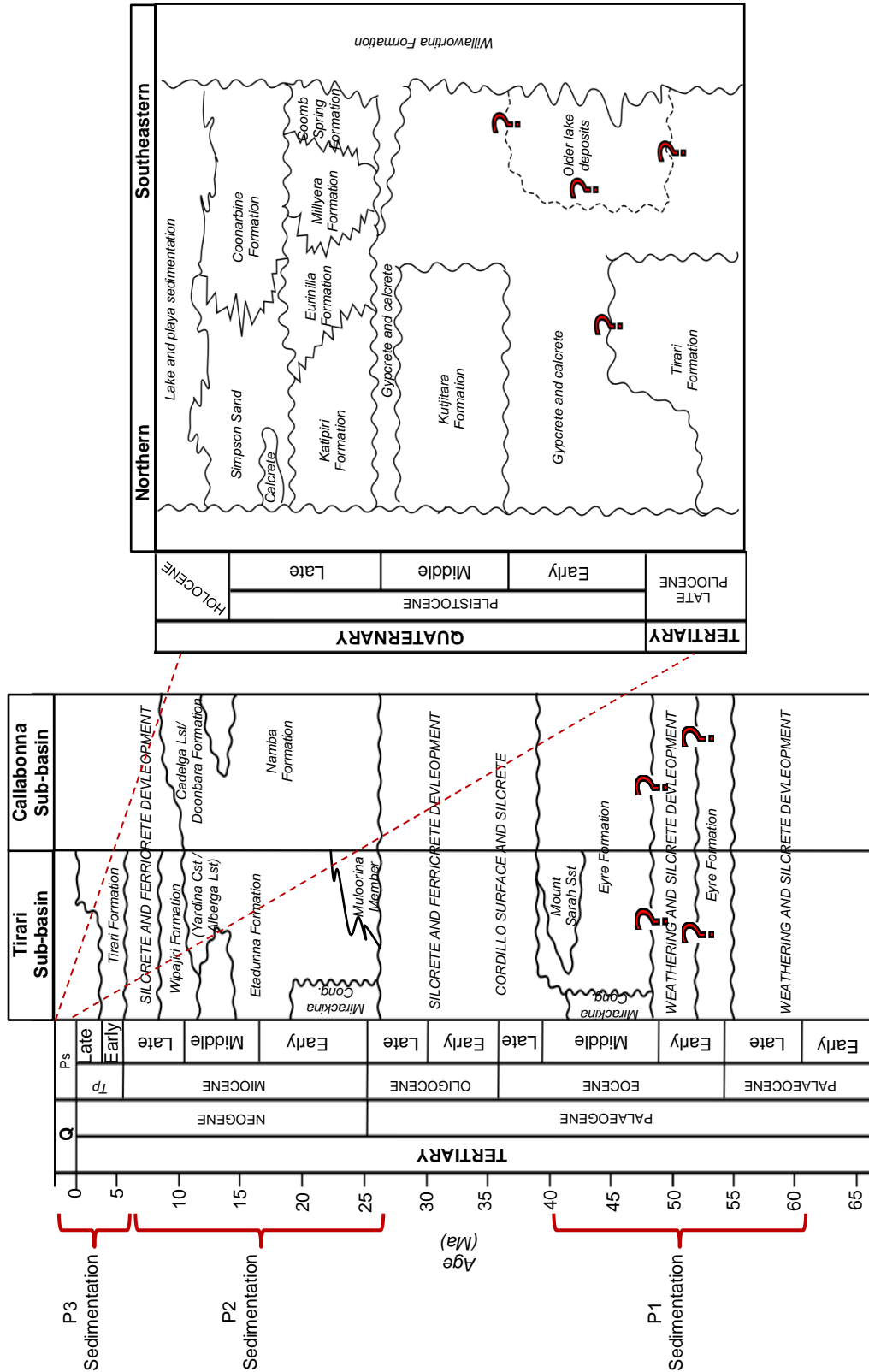
Figure 4.4 - Tertiary stratigraphic units in Tirari and Callabonna Sub-basins and Quaternary units from Northern and southeastern LEB (after Alley 1998) Q= Quaternary, Ps = Pleistocene, Tp = Pliocene

4.2.3 Late Pleistocene and Holocene palaeo-environments and climate changes

The landforms seen today in the LEB are, for the most part, the result of climatic variations through the Late Pleistocene (Alley 1998). The interior of Australia was not directly affected by glaciations so has a well preserved record of Quaternary changes in alluvial, lacustrine, and aeolian sedimentation, recording a response to glacial interglacial cycles, with extensive work conducted since the 1980s. During the late Quaternary, a continuing drying trend has been identified (e.g. Alley 1998; Nanson et al. 2008). In general, during interglacials, rainfall from outside of the basin caused fluvial activity to dominate, whereas during glacials the colder drier and windier conditions caused dune building to dominate (Alley 1998). The best records are found from MIS 7 to present which show cycles of wetting and drying in central Australia as a response to global climate oscillations (Nanson et al 1992; 2008) superimposed on a trend of gradually increasing aridity. These wetting and drying cycles are seen in the stratigraphic record in aeolian, fluvial and lacustrine systems. There is a correspondence between dune building periods, lake filling periods and enhanced fluvial activity, all of which were considered to reflect times where the climate was seasonally wet-dry. Rivers fluctuated between times of enhanced and reduced activity with source bordering dunes being fed when fluvial activity was more enhanced and seasonally wet and dry (e.g. Nanson et al. 1992; 2008; Croke et al. 1996; Hesse et al. 2004; Magee et al. 2004; Cohen et al. 2015).

Evidence of the basin's response to climatic changes is seen throughout the LEB, with the majority of evidence having been found in the eastern LEB in the deposits of Cooper Creek and the Diamantina River, and in Kati Thanda-Lake Eyre and Lake Frome (Figure 4.2). Evidence of fluvial response to climate change is also present in the Neales River in the western LEB (Croke et al. 1996;1998).

Enhanced fluvial activity is evident during MIS 5 (~120-80 ka), which is interpreted from coarser sand deposition, indicative of high discharge rivers (Nanson et al. 2008). The enhanced fluvial activity is also reflected in a lake high-stands at Kati Thanda-Lake Eyre and Lake Frome at ~128 – 110 ka and 100 – 85 ka (Magee et al. 2004). This is likely when the LEB was at its wettest with Kati Thanda-Lake Eyre at more than three times its current area with a depth of more than 25 m, resulting in it

merging with Lake Mega-Frome (Leon and Cohen 2012). The enhanced fluvial activity is further evidenced in source bordering dunes being built at ~120 – 100 ka and 85 ka – 80 ka, indicating that rivers were supplying material for dune building processes (Maroulis et al. 2007; Cohen at al. 2010).

A second period of heightened fluvial activity, although not as enhanced as MIS5, is identified at ~68 – 50 ka (Nanson et al. 2008) accompanied by heightened dune building (Cohen et al. 2010), the early part of which (68-60 ka) is also seen in elevated lake levels at Kati-Thanda-Lake Eyre (Magee et al. 2004), although more specifically constrained by Cohen et al. (2015) to 60 ± 2 ka at Kati Thanda-Lake Eyre and 68 ± 3 ka at Lake Frome. The last lake high-stands at Kati Thanda-Lake Eyre and Lake Frome were identified by Cohen et al. (2015) at 48 ± 2 ka and 48 ± 3 ka, this was the culmination of the mega-lake phase when Lake Mega-Frome last drained to Kati Thanda-Lake Eyre (Cohen et al. 2015), approximately coinciding with the culmination of that period of enhanced fluvial activity and the cessation of sand deposition in the eastern LEB (Nanson et al. 2008), an idea which will be explored in Chapter 5.

Since MIS 3 wetting and drying periods have continued (Fitzsimmons 2013), superimposed on a general drying trend with a renewal of fluvial activity at ~28 – 20 ka and ~12 – 4 ka (Fitzsimmons et al. 2013). Similarly, the Neales River showed intermittent fluvial activity from ~30 ka to the mid Holocene (Croke et al. 1996). There has however been no indication of extensive dune building since the LGM (Cohen et al. 2010) and the enhanced fluvial conditions are not comparable to those in MIS 5 – 3, with no return to the sand load rivers of this time which may be expected on the basis of the Holocene representing interglacial conditions (Nanson et al. 1992). These episodic wetter periods are also reflected in smaller lake high-stands in Lake Frome of decreasing magnitude from MIS 3 to the Late Holocene (Cohen et al. 2011).

4.2.4 Current environmental conditions

The LEB is made up of seven drainage basins with three main rivers: Cooper Creek, Diamantina River, and Georgina River (Figure 4.2) whose catchments drain 660 000 km^2, nearly 60%, of the LEB. All three of these main rivers originate in the relatively humid headwaters at mostly <400 m AHD. The remaining area is drained by four other catchments draining ~460 000 km^2 via nine different rivers (Habeck-Fardy and Nanson 2014). The cumulative distance of rivers in the LEB is ~8000 km. Of the total area only 68% contributes to water Kati Thanda-Lake Eyre, which is the terminus of the system.

Table 4.1 - The seven LEB drainage catchments, areas, primary rivers and length with catchment totals (after Habeck-Fardy and Nanson 2014).

Region	Catchment	Area (km^2)	Primary Rivers	Length (km)
Northeastern Rivers	Cooper Creek	300 000	Thomson River	450
			Barcoo River	400
			Cooper Creek	900
	Diamantina River	160 000	Diamantina River	729
			Warburton River	300
	Georgina River	200 000	Georgina River	1130
			Sandover River	300
			Burke River	200
			Hamilton River	180
			Eyre Creek	450
Desert Rivers	Todd River	60 000	Todd River	50
			Hale River	250
	Finke River	100 000	Finke River	730
			Macumba River	220
	Hay River	100 000	Hay River	200
			Marshall River	410
			Plenty River	430
Western Rivers	Lake Frome	200 000	Neales River	430
			Frome River	250
	Total catchment	*1 140 000*		*8009*

A number of different channel morphologies exist with the LEB, however the dominant channel planform is anabranching with several of the anabranching types described by Nanson and Knighton (1996) represented (Chapter 2 – 2.2.3). The rivers of the LEB are among the last of the world's unregulated large river systems and are amongst the most variable in the world (Knighton and Nanson 1994a; Puckeridge et al. 1998; Kington and Nanson 2001). They are characterised by catchments that lie almost entirely in the arid (and semi-arid) zone, low gradient rivers (rarely $>0.0002m.m^{-1}$), endorheic drainage, wide floodplains, large transmission losses, extremely high flow variability and steep flow duration curves (Costelloe et al. 2004). In fact, flow variability of LEB streams is about double the average variability found in river systems worldwide (McMahon et al. 2008a). In 1974 when a peak flood was recorded at Kati Thanda-Lake Eyre, the maximum recorded daily discharge was 25 000 m^3s^{-1} at Currareva and 5 800 m^3s^{-1} at Nappa Merrie (Knighton and Nanson 1994). Maroulis et al. (2007) note that not even the largest of floods reach much above the base of the sand dunes. Following this flood Tetzlaff and Bye (1978) estimated that 56 km^3 of water entered Kati Thanda-Lake Eyre from January 1974 to June 1976.

Long-term variability in arid zone rivers is not clearly understood, in part due to a dearth of hydrological data (McMahon 1979). In the LEB, there are 19 primary rivers (Table 4.1), however the 14 gauging stations present only record data on nine of these rivers mostly in the eastern and northern LEB, with the western LEB under represented with no streamflow data recorded for the Hay River and Lake Frome catchments. Of the 14 gauging stations present only five are used as Hydrological Reference Stations (Bureau of Meteorology 2015) (Table 4.2), designated with the purpose of identifying long term trends in flow variability. The sites where hydrological reference stations are situated are unaffected by human interference such as dams and irrigation, have 'high-quality' records, and have a minimum of 30 years of streamflow records (Turner et al. 2012). All of these records come from the Diamantina River and Cooper Creek catchments and there is no gauging station on any river as it enters Kati Thanda-Lake Eyre, again, highlighting the lack of data for the remainder of the basin.

Table 4.2: Flow data from Hydrological Reference Stations (HRS) in the LEB (Bureau of Meteorology 2017)

River	Site	Record Start End	Area (km^2)	Daily Min (cm^3)	Daily Max (cm^3)	Daily Mean (cm^3)	Annual Mean (cm^3)
Ranken River	Soudan Homestead	08-1965 03-2011	6390	0	289000	651	235 x 10^{12}
Hugh River	South Road Crossing	05-1972 12-2014	3324	0	165344	195	72.3 x 10^{12}
Diamantina River	Birdsville	10-1966 12-2014	119034	0	412082	3831	1432 x 10^{12}
Trephina Creek	Trephina Gorge	02-1973 12-2014	435	0	11494	22.9	8.54 x 10^{12}
Cooper Creek	Cullyamurra	02-1973 12-2014	232846	0	547748	4155	1517 x 10^{12}

4.2.5 Modern climate

The LEB lies entirely within the arid and semi-arid zones. The majority of the basin falls in the arid climate of BWh - hot desert with regions of BSh - hot steppe in the north and northeast and BSk - Cool Steppe (Köppen 1936) at the southern tip (McMahon et al. 2005) (Figure 2.6b).

Where rainfall does occur, it is, for the most part, orographic, influenced by moist tropical air passing over surrounding highlands in warmer months (Allan 1990). This results in the majority of rainfall falling in the northern and eastern areas of the basin as a function of subtropical high pressure ridge at the southern edge of the Hadley cell. This rainfall in the northern and eastern areas of the basin is summer dominant with weakly winter dominant rainfall occurring in the south (Gentilli 1986).

In summer, dry conditions prevail in the southern section and in the winter the north and northeast are dry with the southern part of the basin affected by northern limit of the westerly cold front (McMahon et al. 2008b). ENSO and other large scale ocean-atmosphere interactions also appear to strongly influence rainfall patterns (McMahon et al. 2008). The ENSO effects come in clusters in the LEB with a high rainfall year commonly followed by a second and likewise with low rainfall years (MacMahon et al. 2008). These weather patterns can be linked to occurrence interval of flood events

in the LEB (Pook et al. 2014). Rainfall and flooding are also affected by the monsoon, with tropical incursions during the summer months resulting in flow in the northeast of the basin, which can then propagate downstream (McMahon et al. 2008b).

The mean annual rainfall has the highest variability in Australia (Kotwicki 1986) and a high annual coefficient of variation is high (Knighton and Nanson 1994a) with ~700 mm.a^{-1} in the northeast (McMahon et al. 2008) and ~125 mm.a^{-1} near Kati Thanda-Lake Eyre with nearly half of the basin receiving average rainfall of 100-150 mm.a^{-1} (Kotwicki 1986). The flow of water only reaches Kati Thanda-Lake Eyre during very heavy rainfall events, where it can fill to a depth of several metres, occurring once every 5 – 10 yrs. during the last century.

Mean annual evaporation is 2400 mm in northeast to >3600 mm at Kati Thanda-Lake Eyre, with evaporation exceeding rainfall throughout the basin. Mean annual maximum temperature at Birdsville Airport (station 038026) in the centre of the basin for the period 2000 to 2018 is 40.5 °C in January and the mean minimum temperature 7.1 °C in July (Bureau of Meterology 2018).

Rainfall tends to be higher in the Cooper Creek catchment than in the Georgina River or Diamantina River catchments although the crystalline rocks in the latter two catchments and lower vegetation coverage mean that infiltration is minimal and run-off generally higher (Department of Sustainability, Environment, Water, Population and Communities 2011). The rivers of the LEB contribute water to Kati Thanda-Lake Eyre on different time intervals (Table 4.3) with Kati Thanda-Lake Eyre filling approximately once every ten years (Department of Sustainability, Environment, Water, Population and Communities 2011) with >200 mm of localized rain in a 72 hr period required for sufficiently large flows to connect the channels and floodplains in the dunefields (Larsen 2011).

Table 4.3 - Interval on which different rivers in the LEB contribute water to Kati-Thanda-Lake Eyre (Department of Sustainability, Environment, Water, Population and Communities 2011).

Contribution interval (years)	Rivers
~2	Diamantina River
~4	Macumba River, Neales River, Peake River
~6	Cooper Creek

The variability of flow in the LEB is greater than elsewhere in Australia and due to the higher than average inter-annual variability of rainfall, drought intensity is higher than expected for arid to semi-arid environments (McMahon et al. 2008b). Under current conditions only 68% of the basin contributes runoff to Kati Thanda-Lake Eyre, with many on the northwestern rivers ending in floodouts. Those which drain to Lake Frome, do not contribute surface water to Kati Thanda-Lake Eyre.

Chapter 5

---

5 Isolating the onset of anabranching in Central Australia

5.1 Introduction

Alluvial rivers adjust and change their form, including their cross-sectional geometry and planform (pattern), in response to changes in water and sediment input, the impact of riparian vegetation and the imposed gradient (e.g. a response to tectonism or valley obstructions). This chapter, through meta-analysis, investigates a widespread geomorphological change during the late Quaternary caused by metamorphosis from single-channel, laterally active, sandy bedload systems to the current mud-dominated anabranching network of channels seen in the Lake Eyre Basin (LEB), with a particular focus on the Channel Country area (Figure 5.1). Chapter 2 of this thesis describes the anabranching river form and the uncertainties that currently surround the causes behind it. Given the prevalence of anabranching in the LEB it is an ideal location for investigating the origins of anabranching on a wide scale.

Nanson et al. (1986) and Rust and Nanson (1986) recognised that, during the late Quaternary, Cooper Creek, the main river in the Channel Country, changed from a single-channel, laterally active, sandy bedload system to a mud-dominated, multi-channel system, although they were unable to establish if the changes were very gradual or relatively rapid, or with any degree of precision when this change occurred. This chapter aims to establish a bounding chronology for the most recent event in which the rivers in the Channel Country of the eastern LEB metamorphosed from single-channel, laterally active, sandy bedload systems to the laterally stable, mud-dominated anabranching systems of today. The approach uses a compilation of stratigraphic ages from throughout the LEB, principally from the reach of Cooper Creek that lies within the Channel Country, to identify a window in time in which this transition occurred and was completed. While there is sound evidence that the underlying sandy deposits in the stratigraphy were laid down by meandering channels (e.g. Nanson et al. 1986; Rust and Nanson 1986; Nanson et al. 2008), the overlying

muds are essentially massive and do not preserve a recognisable anabranching stratigraphy. The only channels present today within the surficial muds are of type 1 anabranching – muddy anastomosing (Nanson and Knighton 1996), creating a caveat to this research that presumes the transition from a sandy to muddy stratigraphy was accompanied by a coeval switch from a meandering to an anabranching channel pattern. The LEB, the Channel Country, and most specifically Cooper Creek have been widely investigated over the past three decades (e.g. Nanson et al. 1986; 2008) with much of the chronology established using luminescence dating; a summary of that research, as well as investigations within the LEB more generally, have been presented by Habeck-Fardy and Nanson (2014). The archives afforded by the alluvial deposits within the LEB drainage systems have made a significant contribution to understanding changes in Australian Quaternary climate and have been investigated with particular focus on the use of luminescence dating to identify increasing aridification by Nanson et al. (1992; 2008), Maroulis et al. (2007) and Cohen et al. (2011). However, the timing of any widespread fluvial metamorphosis from buried meandering to surficial anastomosing systems is yet to be addressed.

5.2   Study Area

The study region falls, almost entirely, within the Channel Country in the north east of the LEB (Figure 5.1). The Channel Country is morphologically designated as the region where the Diamantina River and Cooper Creek become anabranching. It is also an officially designated Interim Biogeographic Regionalisation for Australia (IBRA) bioregion. The Channel Country bioregion covers an area of 306 194 km^2 making it the second largest bio region in the LEB (Bastin and the ACRIS Management Committee 2008). As with the rest of the LEB, the Channel Country is characterised by an arid to semi-arid climate (e.g. McMahon et al. 2008b). Rainfall is minimal, with average rainfall ~168 mm.a^{-1}, and flow within the Channel Country rivers is commonly supplied from rainfall in the catchment sub-tropical headwaters, which can result in flooding in the absence of significant rainfall in the region (Bastin and the ACRIS Management Committee 2008).
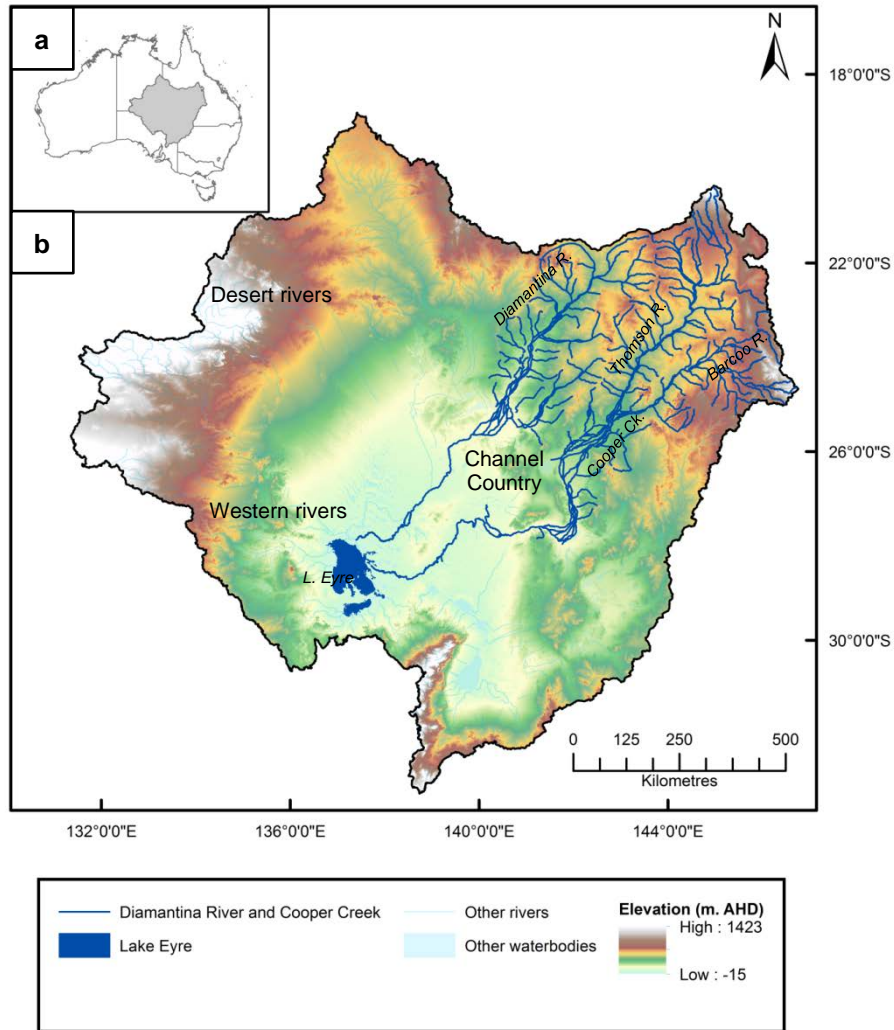
Figure 5.1 - Map showing the location of the LEB in Australia (a) and the location of the Channel Country (shaded area) within the LEB (b) with the major rivers and study sites that are discussed in this chapter.

The Diamantina River is fed by monsoonal rainfall in the semi-arid headwaters (Croke et al. 1999). Cooper Creek is fed by the Thomson and Barcoo Rivers which are, in turn, fed by monsoonal rainfall and also, in the case of the Barcoo River, easterly rain systems. More than 90% of the Channel Country lies below 500 m elevation and it is dominated by floodplains from 20 – 60 km wide consisting of grey clay alluvium (Figure 5.2a) which is deeply cracked (Maroulis and Nanson 1996) (Figure 5.2b) and characterised by gilgai hollows on the surface (Dawson and Ahern 1974). Vegetaion is sparse with trees, including *Acacia cambagei* (gidgee), *Eucalyptus camaldulensis* (River Red Gum) and *Eucalyptus coolabah* (Coolabah) lining the waterholes, which serve as drought refugia (Petit 2002) (Figure 5.2c;d). The floodplains are home to

sparse lower lying shrub vegetation (Figure 5.2e) such as *Astrebla spp.* (Mitchell grass) and *Spinifex spp.* (Bastin and the ACRIS Management Committee 2008), which are subject to grazing pressures leading to high levels of wind and water erosion and elevated atmospheric dust levels (McTainsh and Strong 2007; Bastin and the ACRIS Management Committee 2008).

The floodplains of the Channel Country consist of a complex network of anabranching channels 10 to 125 m in width with low W/D ratio that transport mud and minor sand (Fagan and Nanson 2004) (Figure 5.2f) and are supplied with runoff from headwaters in the north and northeast. As described by Knighton and Nanson (1994a), there is a well-integrated primary system of one to four channels, active at low to moderate flows on any section of floodplain, together with less frequently active secondary channels (continuous, but narrower than primary channels). In addition, tertiary channels (recognisable channel lines but not obviously connected in aerial view) exist which operate at higher flow levels. Surficial flood-channels on the alluvial surface have high width-depth ratios (~60) and are active at overbank stage when much or all of the floodplain is inundated. The flood-channels have the appearance of a "rather variable braided pattern" (Knighton and Nanson 1994b) with low sinuosity and low relief, mostly <1 m (Knighton and Nanson 1994b). The flood-channels are contemporaneous with the anabranching channels, in places cutting across them, following a preferential flow path (Knighton and Nanson 1994b).

Anabranching channel formation in the Channel Country is primarily by avulsion, without the formation of crevasse splays (Rust 1981). Waterholes are formed by local expansions within the anabranching channel network, the largest being on the primary system. These are commonly ~6 m deep at bankfull and scour into the underlying sand sheet which is generally capped with ~2-3 m of mud over most of the floodplain (Figure 5.2c;d). Splays, palaeo-channels and palaeo-source-bordering aeolian dunes characterise areas of the floodplain (Maroulis et al. 2007). The channels appear to be stable for extended periods, and no visible change is seen in aerial photographs after major flood events (Fagan 2001; Fagan and Nanson 2004).
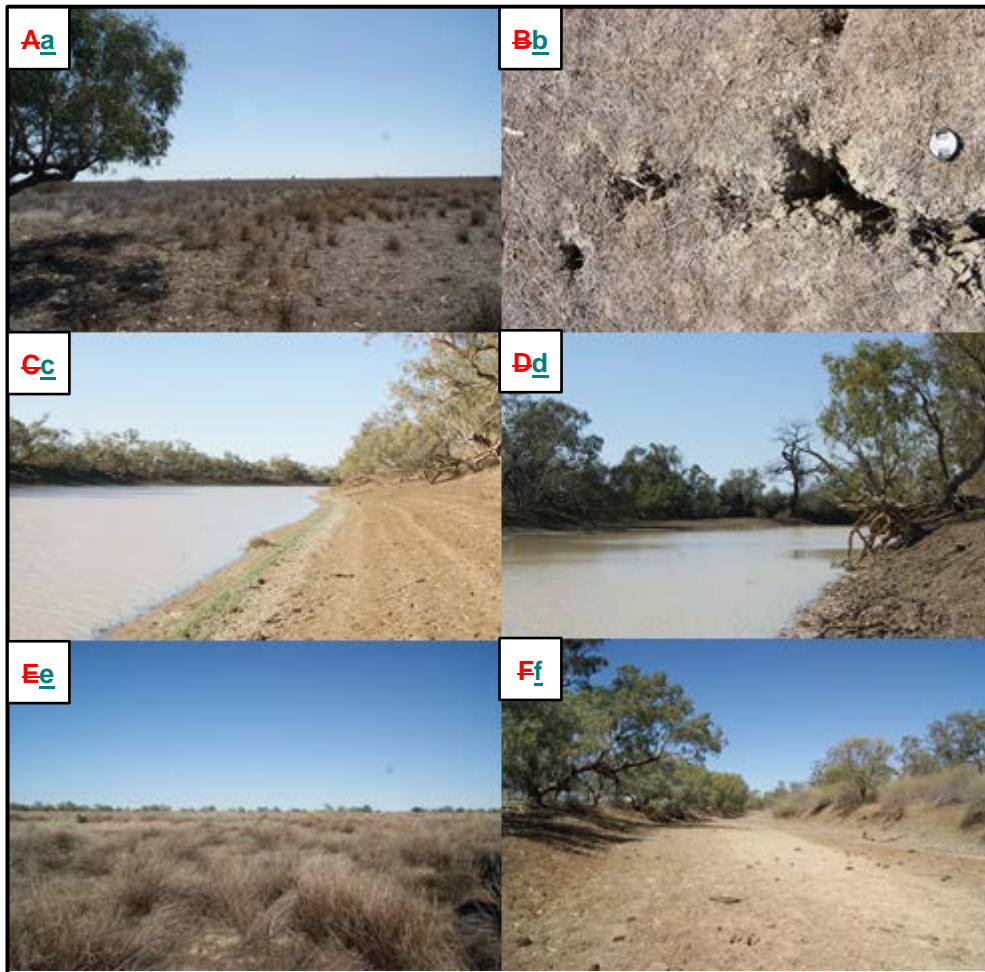
Figure 5.2 - Photos of features of the Channel Country fluvial systems. (a) The Cooper Creek floodplain with muddy sediment and sparse vegetation; (b) Cracks in the Cooper Creek floodplain surface; (c)Waterhole on the Cooper Creek system with vegetation lining the banks; (d) Waterhole on the Cooper Creek system with vegetation lining the banks; (e) Spinifex and Mitchell Grass growing in the Cooper Creek floodplain; (f) A primary channel on the Cooper Creek system with a low width/depth ratio and muddy sediment.

5.3 Approach

In the Channel Country, two key planforms (Figure 5.3) are identified as having existed; meandering (Figure 5.3a) and type 1 anabranching (Nanson and Knighton 1996) (Figure 5.3b). The former river planforms are interpreted from the sediments deposited (Figure 5.4) and have been widely dated (e.g. Maroulis et al. 2007) and investigated in detail starting with Rust and Nanson (1986) who first suggested that the underlying sands were representative of a former meandering system and raised the question as to the cause of the change in planform.
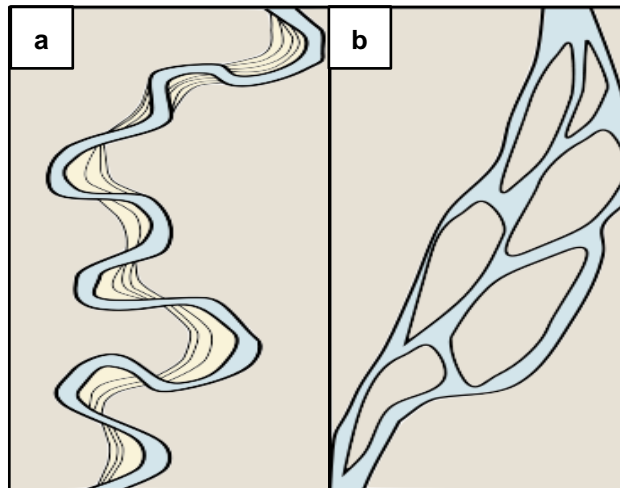
Figure 5.3 - Meandering (a) and 'type 1' anabranching (b) planforms. The meanders move laterally across the floodplain depositing point bars on the insides of bends as they move, resulting in a sand sheet being formed.

Sandy deposits found as sand sheets, showing, in places, planar cross stratification are evidence of a laterally migrating channel (Makaske 2001). These large scale, low angle cross-bedding are typical fining-upward point bar sequences dipping towards the channel (Figure 5.4a). Meanders migrate laterally by eroding the outer bank and depositing sediment on the inner bank as a series of ridges (Miall 1977). Such deposits build laterally in the direction of migration, forming point bar complexes. In a laterally active system where in-channel lateral erosion and accretion cause the channel to migrate across the floodplain a deposit forms which has greater width than the channel, but the thickness is equal to and representative of the channel depth (Makaske 2001). The sand sheets underlying the muddy floodplains of Cooper Creek have been interpreted to be deposited in such a fashion (Rust and Nanson 1986; Maroulis et al. 2007).

The more recent anabranching phase is recognised by stratigraphically uniform and structure-less mud deposits (Figure 5.4b). The lack of structures and depositional features is inferred to be a function of the grey clay vertisols, which due to their smectite rich composition undergo repeated swelling and shrinking (Rust 1981), resulting in a deeply cracked surface. In addition bioturbation contributes to the absence of depositional structures (Rust 1981). The muds are, for the most part uniform and massive in nature, with signs of extensive reworking close to where channels have been active. Evidence of active anabranching channels can be seen on the surface but are generally not distinguishable within the uniform muddy deposits in

the stratigraphic record. Coarser grained features may be present including crevasse splay and levee deposits, although these are uncommon in the LEB as overbank flooding is infrequent and the rivers lack a sandy bedload (Nanson and Knighton 1996). It should be noted that while much of the mud in the upper parts of the stratigraphy is indicative of the anabranching planform the mud deposited directly over the sand is likely to represent overbank and floodplain deposition as seen in Figure 5.4a.

Anabranching rivers in the Channel Country have been shown to be long-lived (e.g. Nanson et al. 1988) with a sedimentary record spanning thousands of years and slowly aggrading (e.g. Maroulis et al. 2007) producing a distinctive floodplain sediment configuration. The configuration of the sediments in these 'type 1' anabranching (Nanson and Knighton 1996) systems is less complex than those seen in humid and temperate environments, where anabranching rivers have been extensively studied and models of sediment configuration have been produced (Makaske 2001). The types of deposits seen in the sedimentary record are not unique to these kinds of anabranching systems and Gibling et al. (1998) note that because of their interconnectedness the preserved deposits and associated planform are not easy to document from the ancient record and they could easily be attributed to other kinds of fixed-channel facies models, rather than the anastomosing planform we currently see.
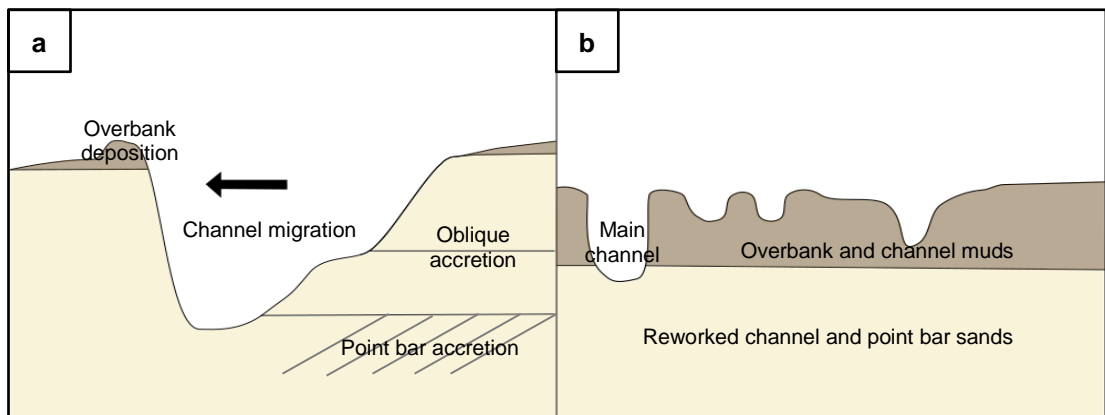
Figure 5.4 - Schematic of typical deposits of meandering and anabranching rivers. Meandering deposits (a) are usually sandy with deposition on one bank as point bars and erosion on the opposite bank, with muddy overbank deposits on both banks. Type 1 anabranching deposits (b) are heterogeneous and muddy, larger channels cut into underlying, older deposits.

The rivers being included in this work are those which are currently anabranching, underlain by sand deposits. These rivers have been widely investigated and given their current configuration and sedimentary deposits they are interpreted to have undergone

a transition from meandering (sand deposition) to anabranching (mud deposition) at least once during the latter part of the late Quaternary (Nanson et al. 1988).

5.3.1 Evidence of the transition

The Channel Country has an extensive record of Quaternary environmental change that can be seen in alluvial and aeolian sediments (e.g. Gibling et al. 1998; Maroulis et al. 2007; Nanson et al. 1988; 2008). The transition from meandering to anabranching is evident at a number of sites throughout the Channel Country. Figure 5.4 shows four sites within the Channel Country, from the existing literature, where the two types of deposit identified in Figure 5.4 are seen with anabranching systems replacing earlier, meandering systems and where the deposits have been extensively dated. All of the sites have the basic sedimentary configuration seen in Figure 5.4b; a mud sheet representing the current 'type 1' anabranching phase overlies a sand sheet (Knighton and Nanson 1994a; Nanson et al. 1986). The sandy deposit is variable with site-by-site variations in sedimentary structures and units, grain sizes and degrees of reworking (e.g. Maroulis 2000; Maroulis et al. 2007; Nanson et al. 2008). The majority of the sediments have been deposited by alluvial processes with some aeolian deposition.

5.3.1.1 *Chookoo sandhill complex*

The Chookoo sandhill complex (Figure 5.5a) is of interest as source bordering dunes are key in understanding the relationship between aeolian and fluvial systems and the chronology gives insight into changes in fluvial regimes over time (Maroulis et al. 2007). It also however shows the transition from a meandering system to a muddy anabranching system. The site (Figure 5.7; Table 5.1 (site #14)) is 3 km away from the main channel of Cooper Creek and is a 2250 m transect from north to south veering south east at 1450 m. The site consists of three source bordering dunes with muddy infill and channels between the dunes. Underlying the dunes are units of sand of various grain sizes from fine through to gravelly sand (Maroulis et al. 2007).

The underlying fluvial sand, indicating a meandering system is present from MIS 8 – MIS 3. Through this time, fluvial activity is interpreted to have decreased, as indicated by a decrease in grain size up unit. The source boarding dunes developed from material from the sandy channel in MIS 5 when fluvial activity was high. This aeolian deposit was most likely to have been reworked during MIS 3-1 as they were no longer being

supplied with fluvial bed material. No dune activity has been recorded during MIS 4 suggesting that material was not being supplied for dune building processes, but was largely confined to the channel as palaeochannels are present from this time at Chookoo and throughout Cooper Creek (Maroulis 2000; Coleman 2002; Maroulis et al. 2007). The infilling of the channel suggests that after 40 ka sand activity ceased as the floodplains and channels became inundated with mud, resulting in the anabranching system that is currently active (Maroulis et al. 2007; Nanson et al. 2008).

5.3.1.2   Mount Howitt

Mount Howitt (Figure 5.5b) is located on Cooper Creek (Figure 5.7; Table 5.1 (site #6)). and is a rare example which shows remnants of a meandering system preserved on the floodplain surface. In aerial photographs, but not on the ground, a relict meandering system is visible with scroll bars, cut-offs and meander loops (Rust and Nanson 1986). The surface planforms provide strong evidence of meandering channels with lateral migration. A 60 m long trench cut from west to east to a maximum depth of 7 m into one of these relict channels confirms the presence of the meandering system beneath the contemporary type 1 anabranching system (Maroulis 2000).

The trench shows sandy sediments at the base, dated using TL to late MIS 4, with a palaeo-cutbank to the east dated at MIS 5, indicating an active meandering channel cutting into and reworking an older deposit. Large channel migration ceased in late MIS 4 to early MIS 3. The channel likely maintained flow as a muddy channel until late MIS 3 when it began to infill (Maroulis 2000). The channel was then infilled with homogenous mud, as seen elsewhere in the Cooper Creek system, which was dated at the base of the deposit close to the contact with the sand deposit, at nearly 5 m depth, to late MIS 2. The mud infill is also dated at 2.5 m to late MIS 1 and close to modern 1m from the surface (Maroulis 2000).

5.3.1.3   Western River

The Western River section (Figure 5.5c) is a 1200 m section from south to north across the Western River, a tributary of the Diamantina River, at Winton (Figure 5.7; Table 5.1 (site #2)). The Western River site shows stratigraphy that differs from Cooper Creek, chiefly the interbedded sand and mud which underlays the uniform mud layer, which are not seen to the same extent in the Cooper Creek sedimentology. The mud

layer itself, while similar to that seen throughout the Channel Country, is thicker. The interbedded sand and mud is a minimum of 3 m thick, from the upper boundary to the extent of coring. The overlying mud sheet is a maximum of ~3.5 m, decreasing to 1.5 m at the base of the channels (Nanson et al. 1988).

The interbedded units indicate a period of alternating sand-load and mud-load rivers and have been dated using TL to MIS 3. The dominance of mud deposition after MIS 3 is interpreted as a decrease in fluvial activity, with a mud-load anastomosing system becoming dominant. The transition to this anastomosing planform is less abrupt than seen well elsewhere in the Channel Country with the transitional period of alternating sand and mud reflecting fluctuations in planform that not observed throughout the Cooper Creek stratigraphy (Nanson et al. 1988) and where it is seen it is to a lesser extent (e.g. Maroulis 2000).

The overlying mud sheet has been dated with TL to MIS 5 and MIS 2 at the extent of coring on the northern side of the transect and MIS 1 at ~2.5 and ~1 m depth on the south and north sides respectively (Nanson et al. 1988).

5.3.1.4 Shire Road

The Shire Road transect (Figure 5.5d) located on the Cooper Creek floodplain (Figure 5.6; Table 5.1 (site #15)) is 13.9 km wide with active waterholes and anastomosing channels throughout the floodplain, although the active channels are predominantly on the western side. At this location there is evidence of a sand unit to 36 m depth (the extent of coring) and this sand unit is variable in grain size and features occasional sub 1 m mud units. The overlying mud unit varies from ~5 m to ~1 m in thickness.

The Shire Road site (Maroulis 2000; Nanson et al. 2008) shows peak sand deposition and reworking of the whole floodplain in MIS 7 to MIS 6. After this time sand deposition was restricted to the western side of the floodplain indicating that fluvial activity had begun to decline to a point, shown by the 80 ka isochron, where only the western side of the flood plain was reworked, interpreted from the lack of induration of the sands and the thinner mud layer. Subsequent, but reduced, reworking occurred during MIS 3, until ~40 ka, when deposition and reworking reached 2- 3 km from the current channel. This progressive reduction in reworking post MIS 6 and 7 suggest a reduction in fluvial activity, but still with sufficient stream power to carry sand, with

overbank muds being deposited at the eastern side of the floodplain from MIS 5 to the Holocene (Nanson et al. 2008). Some alternating sand a mud deposition has been identified in the eastern floodplain (Maroulis 2000), although not to the extent seen in the Western River stratigraphy and the majority of structures in the deposition on the eastern side of the flood plain has been destroyed, likely due to the shrink swell nature of the muds (Rust 1981) and pedogenesis which has occurred due to less exposure to fluvial activity. After MIS 3 the reduction in stream power was sufficient to cause a shift to mud transport and deposition and likely coincides with a switch to the anabranching pattern seen today. A slight increase in stream power is likely to have occurred in the Holocene as is indicated by the reworking at the western side although this was not sufficient for a return to sand transport and deposition and a laterally active system (Nanson et al. 2008)

The four sites show the dominance of alluvial activity during MIS 5. The level of activity began to decline until MIS 3, by which point rivers were no longer powerful enough to transport sand and overall the sites indicate that by the end of MIS 3 sand deposition had ceased throughout the Channel Country. After MIS 3 mud systems appear to have dominated throughout the Channel Country. What remains unresolved, and is explored further in this chapter, is whether a compiled chronology can readily identify the timing of the shift in channel patterns.
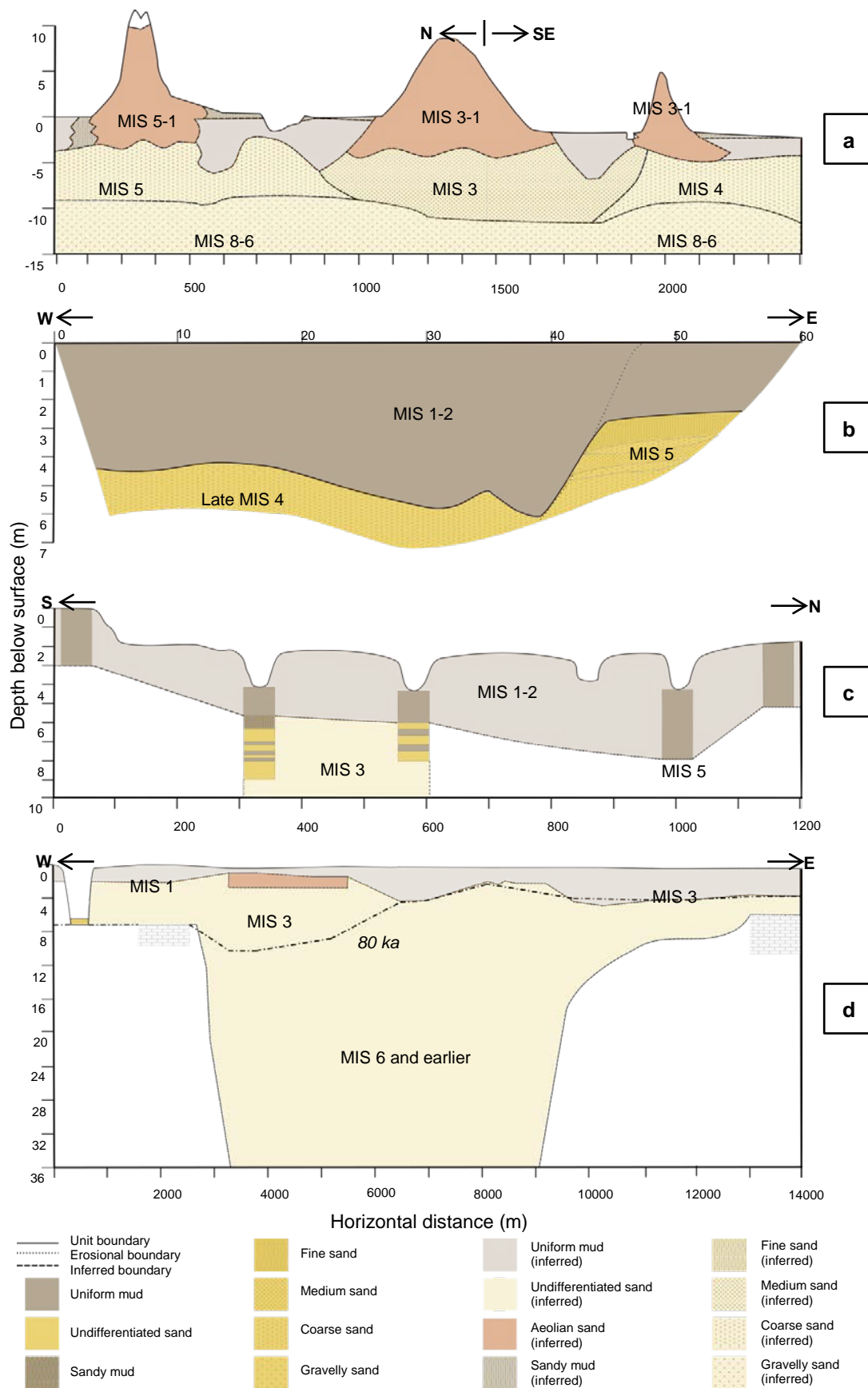
Figure 5.5 – Four sites in the Channel Country showing the transition from meandering to anabranching. (a) Chookoo Dune (after Maroulis et al. 2007), (b) Mount Howitt (after Maroulis 2000), (c) Western River at Winton (after Nanson et al. 1988), (d) Shire Road (after Nanson et al. 2008). (Correspond to Figure 5.6; Table 5.1 sites # 14, 6, 2, 15).

5.4 Data Selection

A compilation of 288 age estimates of fluvial sedimentary deposits were collated from previous work on 10 river systems in the LEB (Rust and Nanson 1986: Callen and Nanson 1992; Cohen et al. 2010; Larsen 2011; Coleman 2002; Bowman 2003; Maroulis 2000; Fagan 2001; Magee 1997; Tooth 1997; Nanson et al. 1988; 1991; 1992; 1995; 2008; Croke et al. 1996). The compilation consists of 242 TL age estimates and 46 OSL age estimates (33 multi-grain age estimates and 13 single grain age estimates).

In order to identify the transition from a meandering to anabranching system, it was first assumed that where the current planform is type 1 anabranching and a sand sheet is present lower down in the stratigraphy that all alluvial sand deposits in the stratigraphy represent meandering rivers and that all massive muds represent type 1 anabranching systems. This is in keeping with the caveat to this research that presumes the transition from a sandy to muddy stratigraphy was accompanied by a coeval switch from a meandering to an anabranching channel pattern. With this in mind the data set was refined as per Figure 5.6, first splitting the dataset into anabranching and non-anabranching river reaches as only those rivers which are currently anabranching can be assumed to have undergone the transition. The 121 age estimates from currently anabranching rivers were then refined by taking weighted means of those deposits in which there were multiple ages from the same stratigraphic unit and removing TL ages where there was also an OSL age for the same sample to minimise the bias of overrepresentation. Age estimates which did not have an error estimate or any depth data were also removed, as these parameters were required for meta-analysis. The remaining 109 age estimates were refined further with the next refinement restricting the sample group to those ages which were within two-sigma after the start of the MIS 5 (<130 ka). The remaining 94 samples were then split by deposit type into 47 meandering (Appendix A – Table A.1) and 47 anabranching (Appendix A – Table A.2) ages and are assessed as separate datasets. These remaining ages are from 17 sites within the Lake Eyre Basin (Figure 5.7; Table 5.2).
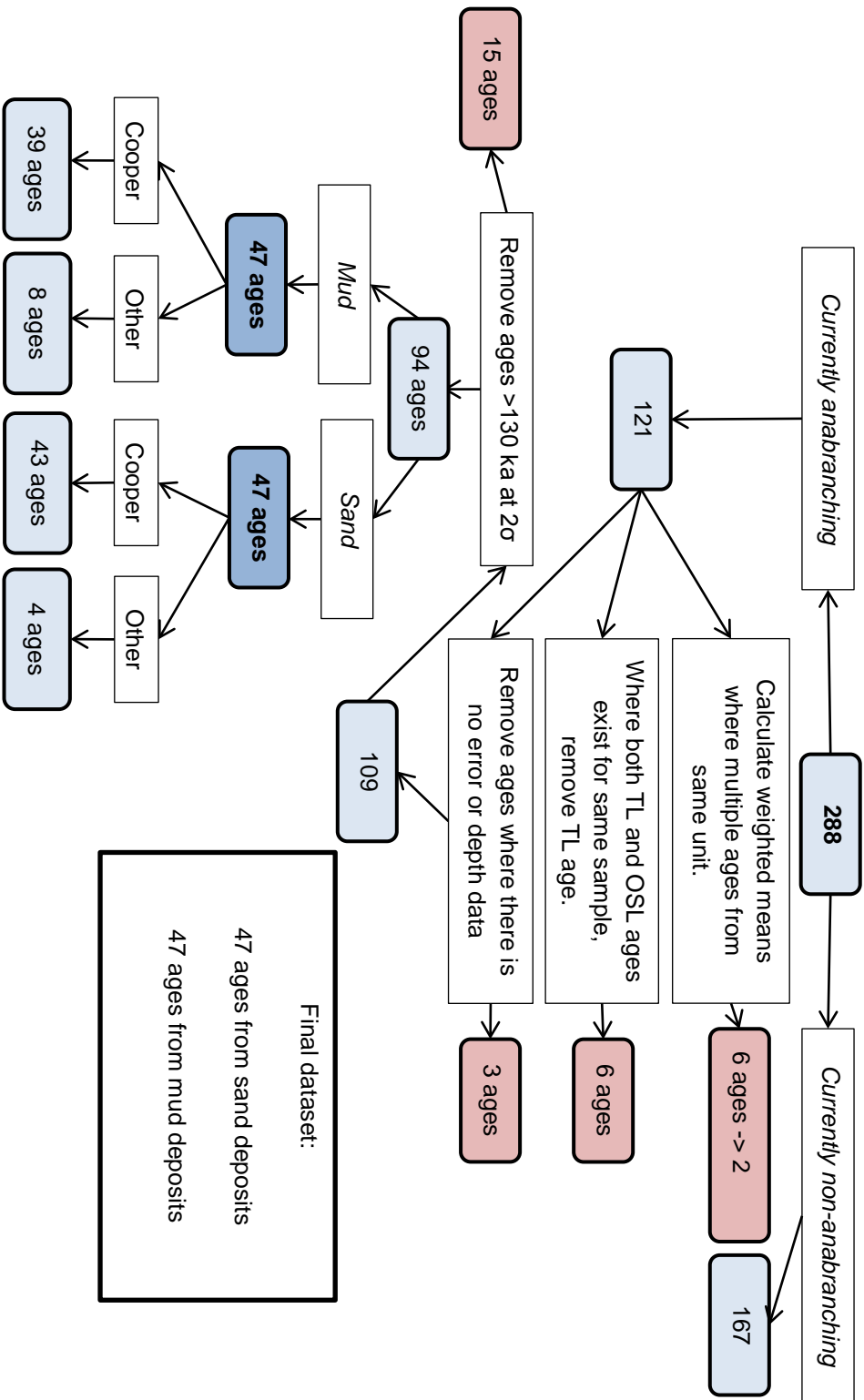
Figure 5.6 - Flow chart for selection of ages for analysis from initial 288 compiled ages

5.5   The age distribution

5.5.1   Spatial distribution of ages

The data selection, in section 5.4, gives a total of 94 ages from 17 sites throughout the LEB and the samples are refined to the Channel Country and its periphery. The Desert Rivers (Figure 5.1) were excluded as those reaches which do anabranch have not been widely studied, in general are sand dominated ridge or island forming anabranching (Nanson and Knighton 1996) rivers and do not have the muddy deposits identified as anabranching in the Channel Country, and no ages are published. The Western Rivers (Figure 5.1) are also excluded as they do not currently anabranch. By restricting the dataset to focus on the transition to anabranching from MIS 5 to present has given a bias to the dataset, mostly restricting the samples to the Channel Country and the immediate periphery. This results in samples from Cooper Creek and the Diamantina River and their respective headwater tributaries the Thomson River and the Western River (Table 5.2) (Figure 5.1). There are an equal number of sand and mud deposits, 47 of each deposit type. The majority of the samples are from the Cooper Creek floodplain, twelve of the 17 sites.
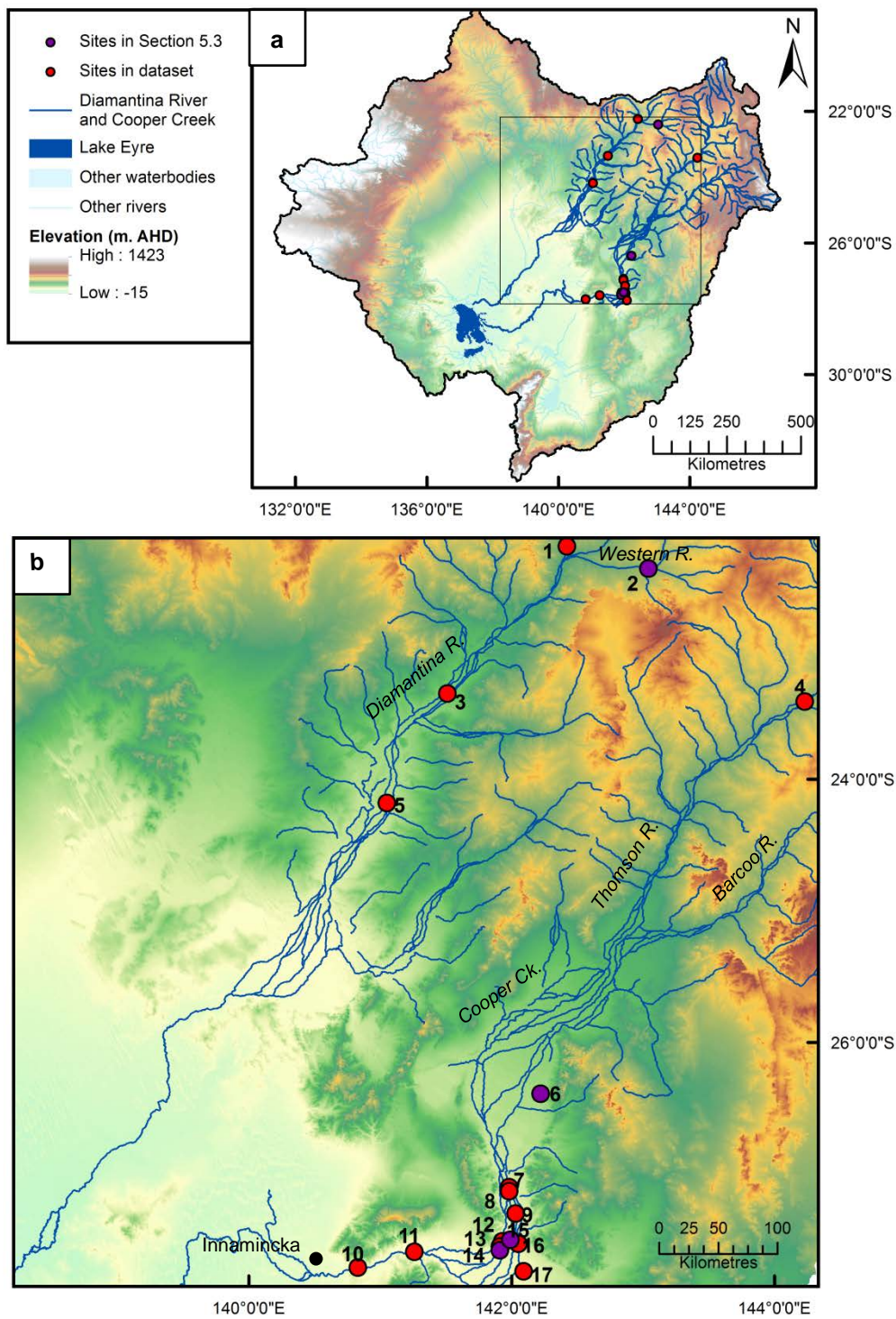
Figure 5.7 - (a) The Lake Eyre basin, showing the sites incorporated into the dataset (red), those also discussed as example sites in section 5.3.1 are marked in purple. (b) Rivers and sites incorporated into the dataset in this chapter. Numbers correspond to Table 5.1. Sites 2, 6, 14 and 15 marked in purple, correspond to those in section 5.3.1.

Table 5.1 - Sites incorporated into the dataset used in this chapter, after refinement per Figure 5.5. Numbers correspond to the points marked in Figure 5.6b. Sites 2, 6, 14 and 15 correspond to those in section 5.3.1.

Site #	River	Site	Latitude	Longitude
1	Diamantina River	Boulia Road Crossing	-22.23	142.42
2	Western River	Western River	-22.40	143.04
3	Diamantina River	Brighton Downs	-23.35	141.51
4	Thompson River	Longreach	-23.41	144.23
5	Diamantina River	Davenport Downs	-24.18	141.05
6	Cooper Creek	Mt Howitt	-26.39	142.22
7	Cooper Creek	South Narberry Waterhole	-27.10	141.98
8	Cooper Creek	Durham downs road	-27.13	141.98
9	Cooper Creek	Karmona	-27.30	142.03
10	Cooper Creek	Cullyamurra	-27.71	140.83
11	Cooper Creek	Maapoo Waterhole	-27.59	141.26
12	Cooper Creek	Levee A	-27.51	141.93
13	Cooper Creek	Goonbabina Waterhole	-27.55	141.91
14	Cooper Creek	Chookoo Sandhill Complex	-27.58	141.91
15	Cooper Creek	Shire Road	-27.50	141.99
16	Cooper Creek	Naccowlah	-27.53	142.05
17	Cooper Creek	Wilsons Swamp	-27.74	142.09

5.5.2 Methodological distribution and variation of ages

The majority of the samples are TL (88) ages and all of the six OSL ages are from anabranching deposits and are located on the Cooper Creek floodplain from 65 – 90 km upstream of the constriction at the Innamincka Dome at: Karmona, Cooper Levee A and Wilsons Swamp (Figure 5.1b).

The dataset is dominated by TL ages and one valid concern might be that the TL ages are susceptible to age overestimation due to incomplete bleaching of the slower bleaching TL signal (Chapter 3 – 3.2). In order to test the validity of TL ages Figure 5.8 compares TL and OSL ages from the same sample at 16 sites in the LEB (Fagan 2001; Cohen et al. 2010; May et al. 2015; Nanson et al. 2008).

Table 5.2 - Distribution of luminescence age estimates in the Channel Country, by deposit type and dating method.

River	# Sites	Total samples	# Sand	# Mud	# TL		# OSL	
					Sand	Mud	Sand	Mud
Total	17	94	47	47	47	41	0	6
Cooper Creek	12	78	41	37	41	31	0	6
Thomson River	1	4	2	2	2	2	0	0
Diamantina River	3	5	2	3	2	3	0	0
Western River	1	7	2	5	2	5	0	0
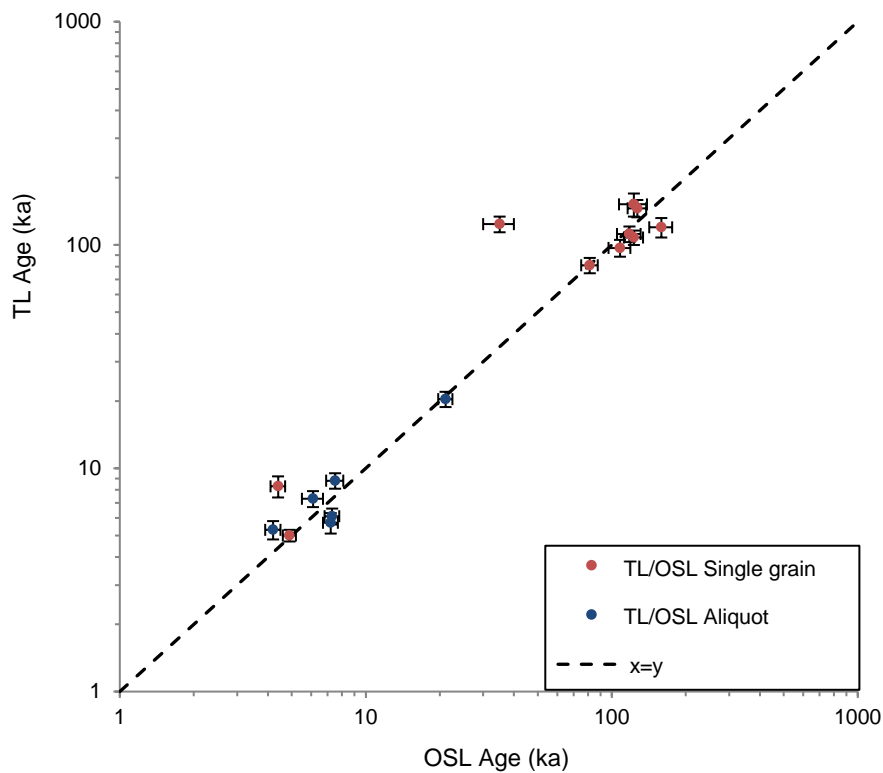
Figure 5.8 - Comparison of OSL ages (single grain and aliquot) with TL ages for the same samples from the LEB. Slight deviations from the line of equality (x=y) may be due to small intrinsic differences in luminescence characteristics or slight variations in dose rate that can occur even in sub-samples of the same sample.

Given the similarities between the age estimates when comparing OSL and TL in the LEB (Figure 5.7) the two methods are considered equally reliable and therefore merit combination into a single dataset. Generally, the older luminescence ages have larger

standard errors, however this does not mean they are necessarily less precise. Figure 5.9 compares the relative error of all samples to the age and their uncertainties. When comparing the uncertainty of the of TL ages to OSL ages there is similar precision with a mean relative error of 11.7% on TL ages and 7.6% on OSL ages and with no systemic differences. Both methods have similar minimum errors with 6.6% and 5.4% respectively. The maximum error is higher for TL with 49.1% compared to 9.8% for OSL although; given the small number of OSL ages in the data set, this is not necessarily representative.
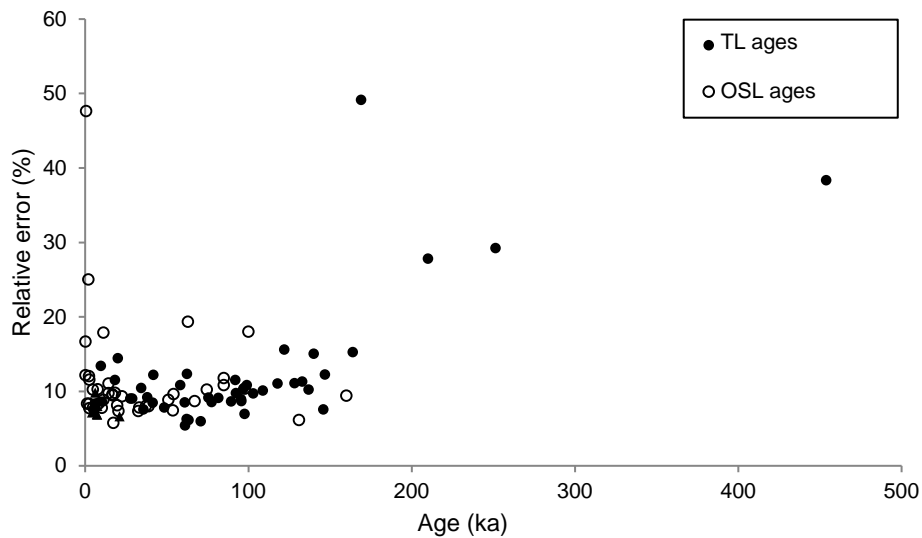
Figure 5.9 - Relative error against age for the TL ages and OSL ages in the dataset. The wider spread of errors in the younger samples is a function of the less precise estimates on young OSL samples.

5.5.3 Sampling depth bias

The ages compiled for this meta-analysis were not initially collected/sampled with the purpose of this analysis so there is some bias, not only to the sampling locations, but also the depth. Sampling is rarely at systematic depth intervals, although there are exceptions such as Chookoo Dune (Figure 5.5a) (Maroulis et al. 2007; Nanson et al. 2008). Sampling is frequently designed to pinpoint specific events or stratigraphic changes and the net effect is a strong depth bias. There is a general relationship between sample age and sample depth (Figure 5.10) and this sample depth bias likely indicates an over representation of young ages, particularly in the anabranching portion of the dataset. The sample depth is restricted, to a degree, by the capabilities of sampling equipment, with depths >10 m rarely being sampled, so the older end of the

dataset is most likely under-represented. The samples of sand deposits are, when compared to the mud deposits, from greater depths with no sample <1 m from the surface (Figure 5.11a). Anabranching deposits have a bias toward near surface deposits with nearly 50% of anabranching samples being from <2 m depth (Figure 5.11b).
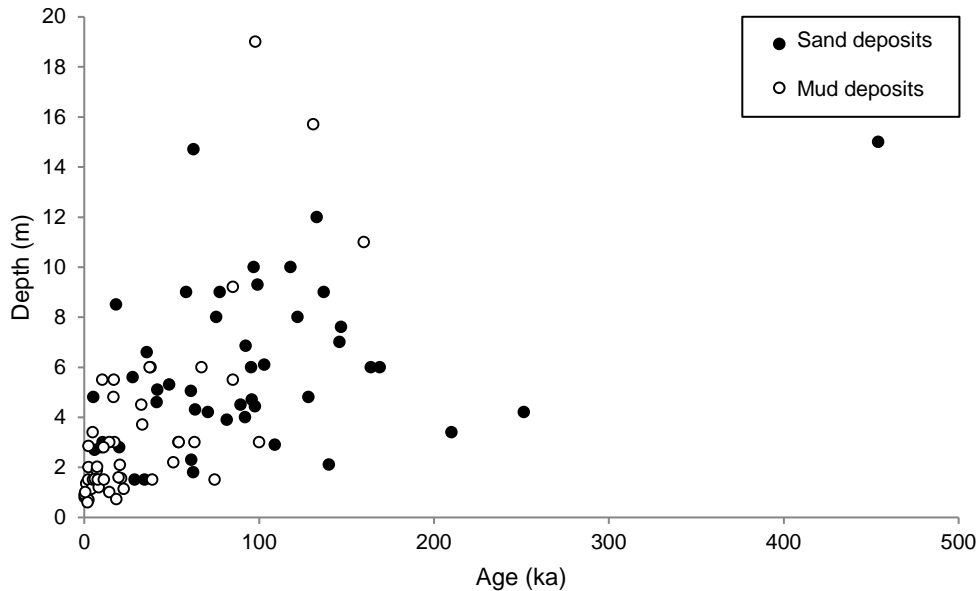
Figure 5.10 - Depth against age of all deposits in the dataset.
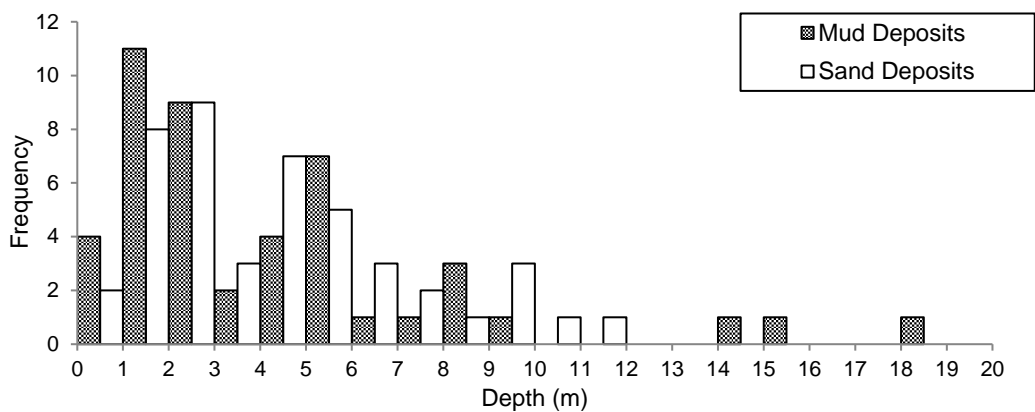
Figure 5.11 - Histograms, with 1 m bin widths, of sampling depths for sand deposits and mud deposits.

5.5.4 The Sadler effect

There is an inherent incompleteness to the sedimentary record due to preservation biases and the averaging of deposition, erosion and hiatus in calculating deposition rates over time. The Sadler effect (Sadler 1981; Schumer and Jerolmack 2009)

accounts for the variability in sediment accumulation rates and the apparent increase in accumulation rates with more recent time. The apparent increase is due to the stratigraphic record showing both periods of sedimentation, erosion and hiatuses so net deposition is inversely proportional to the time period over which it is measured (Sadler 1981). As the Sadler effect varies in different environments its numerical value is calculated using the deposition rates available for the study location.

The factor of the Sadler effect is calculated using the deposition rates calculated as an average rate given the depth from the surface, which is assumed to be zero age, of the sample and the age of the sample in mm.ka^{-1}. Deposition rates are plotted on a log-log graph (Figure 5.12). The Sadler effect which can be described by Equation 5.1, where *V* is apparent deposition rate, *t* is time, and *C* and Υ are constants. Υ is the gradient of the line obtained by log binning the deposition rates for each sample then regressing the mean deposition rate for each bin against the log age. For this dataset the equation of the line is y = -0.6527x + 1.998, giving Υ = -0.6527. This is consistent with previous calculations for the region, which give a value of Υ = -0.658 (Cohen et al. 2015).

$$V = C\, t^{-\gamma}$$

Equation 5.1 - Sadler effect equation (Sadler 1981) where V is apparent deposition rate, t is time, and C and Υ are constants.
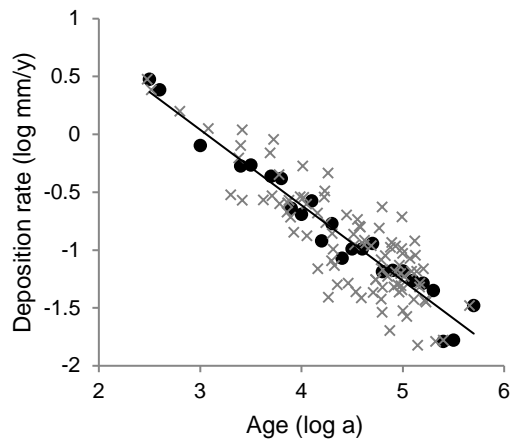
Figure 5.12 - Log deposition rate plotted against log age. Crosses indicate age and deposition rates of all data points, filled circles indicate averages for logged data binned at 0.1 width bins. Regression line is a linear fit through the binned data and has a gradient of -0.6527.

5.6   A meta-analysis of the meandering to anabranching transition

Presenting and analysing datasets such as the one in this research, in a way which allows for reliable interpretations to be made, is a problem which has been identified on a number of occasions (e.g. Thomas and Burrough 2012; Hesse 2014; Thomas and Bailey 2017). In this meta-analysis, the data are presented using histograms, probability density plots (PDP), kernel density estimates (KDE) and radial plots, which are then compared. On the recommendation of Galbraith and Roberts (2012) the KDEs are each accompanied by a plot showing the relative errors associated with each value.

Histograms showing the temporal abundance of sand and mud deposits are presented in Figure 5.13. Histograms are visually easy to interpret and universally used. Interpreting can however fall victim to bin width as the choice of bin width is arbitrary. Bin width choice is a balance between producing a histogram with a clear shape and limiting the resolution of the plot and thus masking some variations which can occur when bin widths are too large (Galbraith and Roberts 2012). Here 5 ka and 10 ka bin widths are used to test if bin width affects the data interpretation. A further flaw in histograms is that they do not incorporate the uncertainties on the values in the dataset treating all as if they had the same precision. The histogram approach was used by Nanson et al. (1992; 2008) with peaks identified in a dataset and correlated to climate events.

In the histograms of this data there is an increased frequency of sand deposits during MIS 5c at 90-100 ka and late MIS 4 at 60-70 ka; 95-100 ka and 60-65 ka, when plotted with 5 ka bin widths. Sand deposits are present throughout the age spectrum but are their lowest abundance from the start of MIS 3. Mud deposits are absent from the record prior to MIS 6 and sporadic prior to MIS 3 and there is an increased frequency through MIS 3 with peak deposition from 20 ka continuing during late MIS 2 and MIS 1. The similarity between the results from the plots of the different bin widths suggests the results are unlikely to be an artefact of bin width.
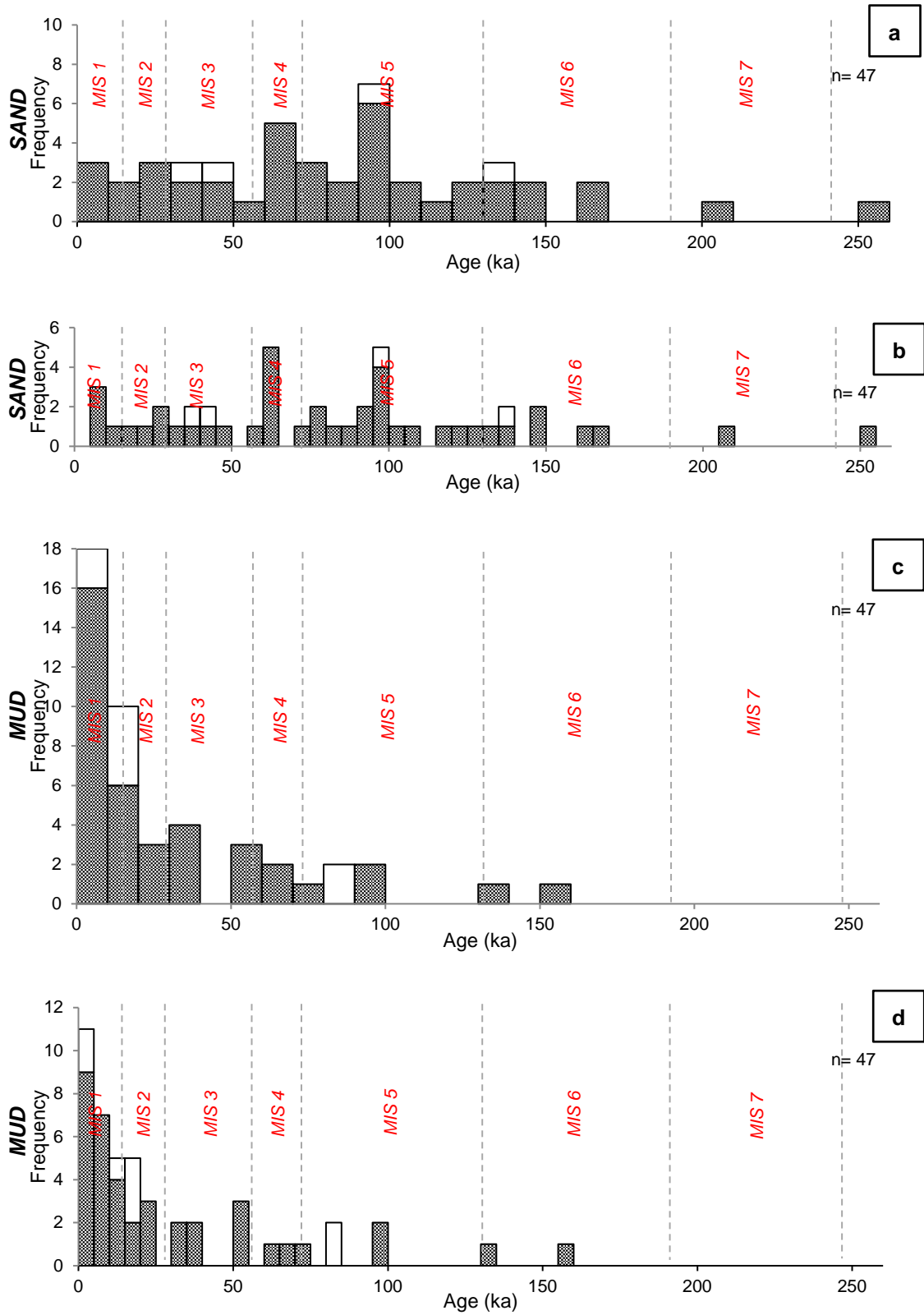
Figure 5.13 - Histograms of: (a) Sand deposits at 10 ka bin widths, (b) Sand deposits at 5 ka bin widths, (c) Mud deposits at 10 ka bin widths and (d) Mud deposits at 5 ka bin widths. Shaded region shows ages from Cooper Creek; unfilled region is ages from other rivers. Dashed lines indicate Marine isotope Stages from MIS 7 to present.

Probability density plots (PDP) are an alternative to histograms when displaying frequency data and have a hypothetical advantage as they incorporate the errors on each age estimate (Galbraith and Roberts 2012). The PDP calculates a 'Gaussian kernel' (Silverman 1986) for each incremental value with the age as the mean and the uncertainty in the age as the standard deviation. If the error is small the kernel is tall and narrow, if the error is large a wide shallow kernel is produced. The PDP is produced by summing the kernels at a series of fixed increments. PDPs have been widely used to display geochronological distributions with some success (e.g. Hesse 2014) and are often implemented due the incorporation of uncertainties when constructing the plots, thus the accounting for variations in precision. However, there are a number of problems associated with the displaying of geochronological distributions through PDPs. Due to the incorporation of error, the results of PDPs are noisy when the analytical precision is high, and oversmoothed when the analytical precision is low (Galbraith and Roberts 2012; Versmeech 2012). This can be easily confused with the taphonomic effect, where frequency of deposits decreases due to lack of preservation or destruction of older parts of the geological record (Surovell and Brantingham 2007; Surovell et al. 2009) or the Sadler effect, where a decrease in erosion or sedimentation rate through time occurs and which also describes the probability of an increase in sediment preservation over time (Sadler 1981; Schumer and Jerolmack 2009).

The PDPs (Figure 5.14) show a somewhat different shape to the histograms especially in the section of the curve representing the young ages. For both the sand and mud deposits the largest probabilities are in the youngest region of the plot, with mud deposits showing high probabilities from 10 ka to present and sand deposits showing slightly increase probabilities from 50 ka to present and then much greater probabilities from 10 ka to present, reflecting the absolute magnitude of the errors in young samples and the relative difference in errors size between young and old samples.
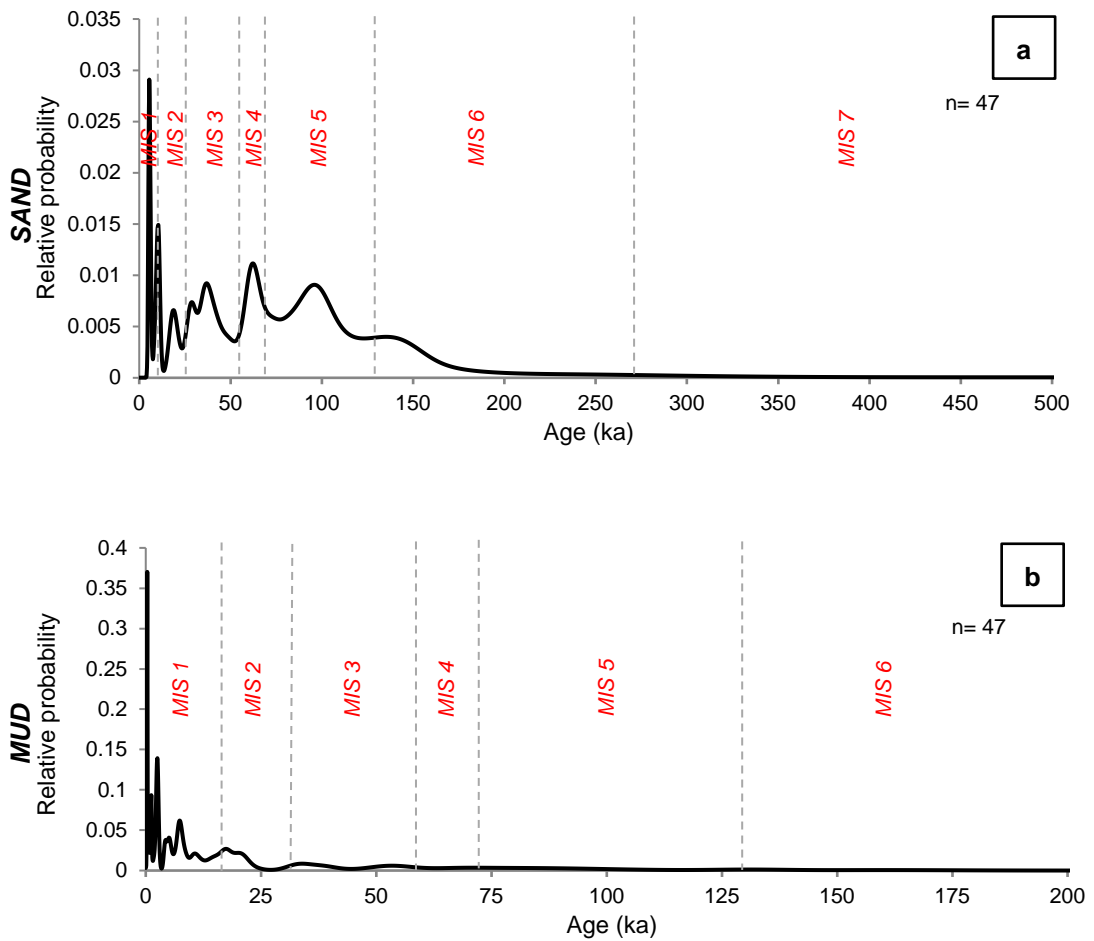
Figure 5.14 - Probability density plots (PDP) for sand deposits (a) and mud deposits (b). Dashed lines represent Marine Isotope Stages from MIS 7 to present.

A third method which can be used to present geochronological data as a continuous frequency distribution is kernel density estimates (KDE). A KDE takes, for each value, a kernel (usually Gaussian, but options also include: epanechnikov, rectangular, triangular, biweight, cosine and opticosine) of a pre-determined bandwidth and overlies them to form a single smoothed curve. The shape of the kernel dictates little in terms of the final kernel estimate, the smoothness of the resultant curve is mostly defined by the bandwidth (Hwang et al. 1994). Bandwidth choice is subjective. If a distribution is unimodal and smooth then *Silverman's rule of thumb* (Silverman 1986) (Equation 5.2) can be used to calculate bin width. However, in age distributions this often results in over smoothing (Galbraith and Roberts 2012).

$$h = \left(\frac{4\hat{\sigma}^5}{3n}\right)^{\frac{1}{5}} \approx 1.06\hat{\sigma}n^{\frac{-1}{5}}$$

Equation 5.2 - Silverman's rule of thumb for bandwidth (h) selection. Where n is the number of values in the distribution and $\hat{\sigma}$ is the standard deviation of the distribution (Silverman 1986).

Here the KDEs are displayed with a corresponding error plot as suggested by Galbraith and Roberts (2012), so relative errors can be associated with the values in the distribution.

Kernel density estimates were constructed using varying bandwidths and a bandwidth of ten was chosen for sand deposits and five for mud deposits as having the best degree of smoothing (Figure 5.15; Appendix B - Figure B.1) shows the comparison between bandwidths calculated using Silverman's rule (Silverman 1986) and bandwidths of 20, 15, 10 and 5. Bandwidths >10 for sand deposits and >5 for mud deposits resulted in over smoothing, as did use the bandwidths calculated using *Silverman's rule of thumb*. That the most appropriate bandwidth for anabranching deposits is smaller than that for sand deposits is attributed to the reduced range of values in the mud deposit distribution.

KDEs show elevated density in sand deposits from 180 ka to 140 ka with further increased density from 140 – 100 ka (MIS 5), where the highest density of 0.008 is reached. This persists until approximately 40 ka (late MIS 3) when, while sand deposits are still present, the density decreases continually to the present. The anabranching deposits show a low relative density until 25 ka (LGM) where there is a sharp increase to maximum density of 0.03 at 10 ka (Holocene).

Radial plots, while commonly used to display the dose of individual grains within single grains measurements from one luminescence sample, can also be used to display age distribution (e.g. Dibble et al. 2013). Radial plots plot the age on a curved y-axis (the radial axis) and the relative error and precision on the x-axis. The advantage of displaying distributions as radial plots is that the uncertainty on each measurement is also plotted allowing comparison of both the individual ages but also their errors as no smoothing or summarising of the data occurs. With a radial plot it is relatively easy to identify if points plot along any given line of interest (Galbraith and Roberts 2012). Figure 5.16 shows the sand and mud deposits displayed on radial plots. The sand deposit ages are most concentrated during MIS 5, with distribution through MIS 3-1,

being approximately uniform. The mud ages are mostly concentrated during MIS 2 and MIS 1 with a small number of uniformly distributed ages prior to MIS 2.
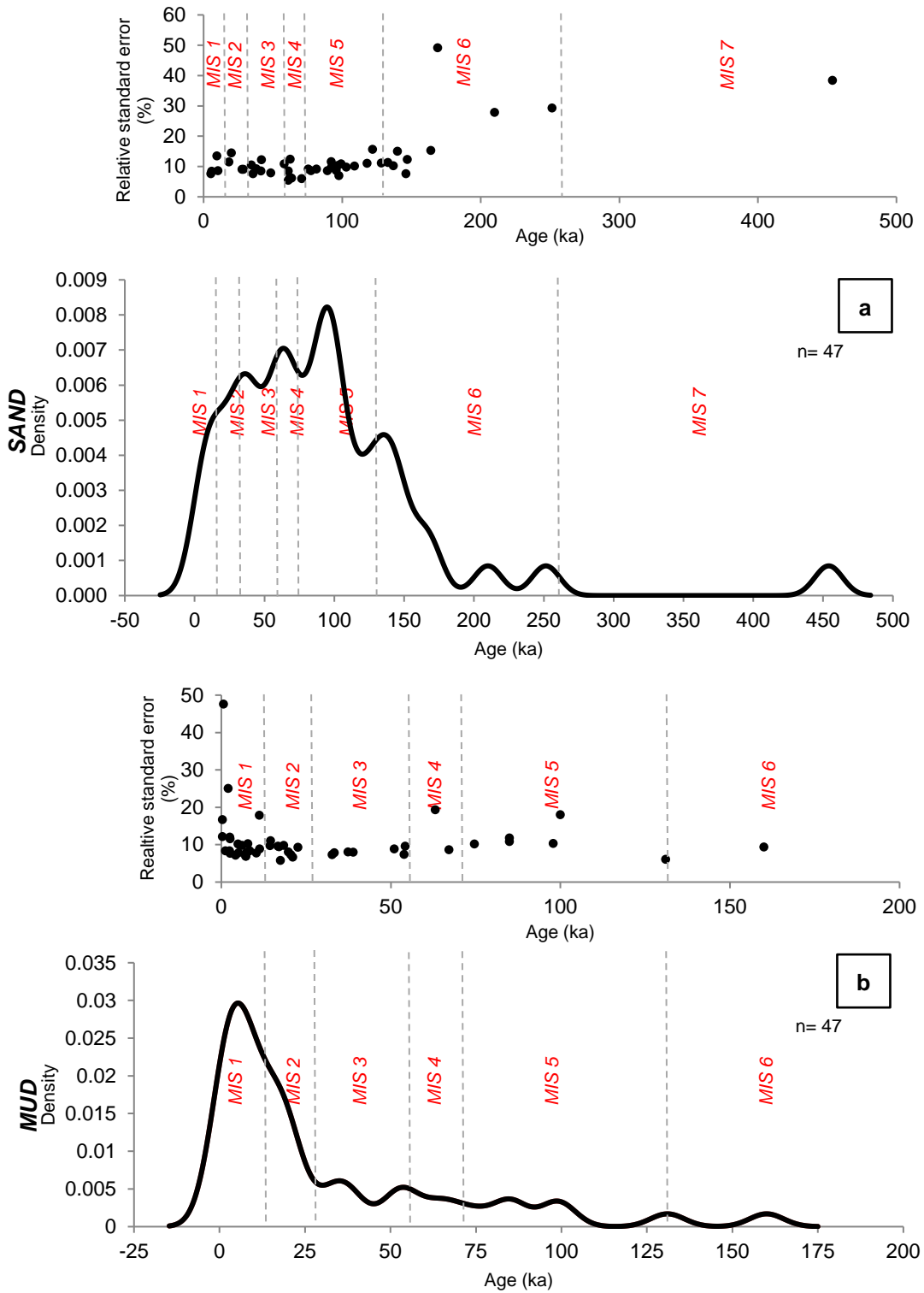
Figure 5.15 - KDE plots with accompanying error plots for sand deposits (a) and mud deposits (b).
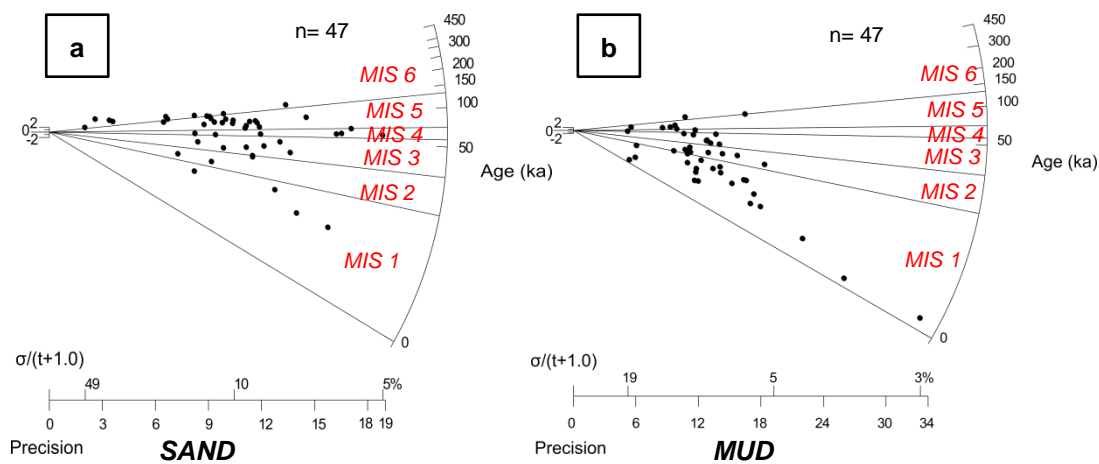
Figure 5.16 - Radial plots of (a) sand and (b) mud datasets. Lines represent Marine Isotope Stages from MIS 6 to present.

5.6.1 Signal versus noise

Given the relatively small amount of ages which meet the criteria to be included in the meta-analyses, there is a concern that the patterns seen in the observed record are indistinguishable from noise and cannot be interpreted as true observations in the dataset. In order to test this, artificial data sets were created using random numbers as a means of differentiating real fluvial regime change over noise. The technique presented below is used to identify whether the observed data are random or whether it stems from a normal distribution. The skew and kurtosis of this data (Appendix A - Table A.3) indicates that the observed data are not normally distributed. Identifying if the data are random is achieved through a simulation exercise creating synthetic datasets with the same maximum, minimum and number of values as the observed datasets using the generation of random numbers. The random numbers are derived using a pseudorandom number generator (PRNG) which despite producing numbers that are not truly random, generate a data set which meets the statistical criteria to pass as random. That is to say that the sequence can be generated by a polynomial-time algorithm but that no algorithm can predict the next value. The uniform random numbers are derived using the Mersenne Twister (MT) (Matsumoto and Nishimura 1998) which is considered superior to a number of other PRNGs, which can be defective and do not produce a high enough degree of randomness to pass the *Diehard Battery of Tests* (Marsaglia 1995). The MT has a periodicity of $2^{19937} - 1$; the number of cycles the generator can perform until a sequence repeats. High periodicity such as

this is essential to obtain numbers which can be considered to be as close as possible to being truly random.

Using the *runif* function in the base package in R two series of pseudo-datasets were generated. The pseudo-mud dataset was produced by 1000 generations of 47 values from 0.3 – 167 and the pseudo-sand dataset was produced by 1000 generations of 47 values from 5.3 – 454. These random number data sets of 47 values each are selected in a non-uniform manner from a uniform distribution that has the same maximum and minimum values as the observed dataset. KDEs were plotted as these present the data discretely (Figure 5.15) and show similar peaks in deposition as seen in histograms (Figure 5.13) and radial plots (Figure 5.16). PDPs were excluded as the low standard errors on the young ages appear to give a false representation of peaks in the distribution.

The observed sand dataset sits above the synthetic datasets from 100 ka until the present, with the peaks at ~100 ka, 60 ka and 40 ka all distinguishable and above the synthetic data (Figure 5.17a). The peaks at >100 ka are not, however, distinguishable from the synthetic data, likely due to the low sampling density at these older ages. The observed mud dataset sits above the synthetic data during the Holocene with twice the density of the synthetic dataset (Figure 5.17b). This is likely due to a combination of sample density and prevalence of anabranching deposition during the Holocene. No other mud peaks are distinguishable from the synthetic data.

Given the different plotting techniques and the use of the PRNG comparison overall peaks in the data can be identified at MIS 5 – 3 for sand deposits with something of a hiatus from late MIS 3 – 2 then mud deposition intensified from after the LGM to the present day.
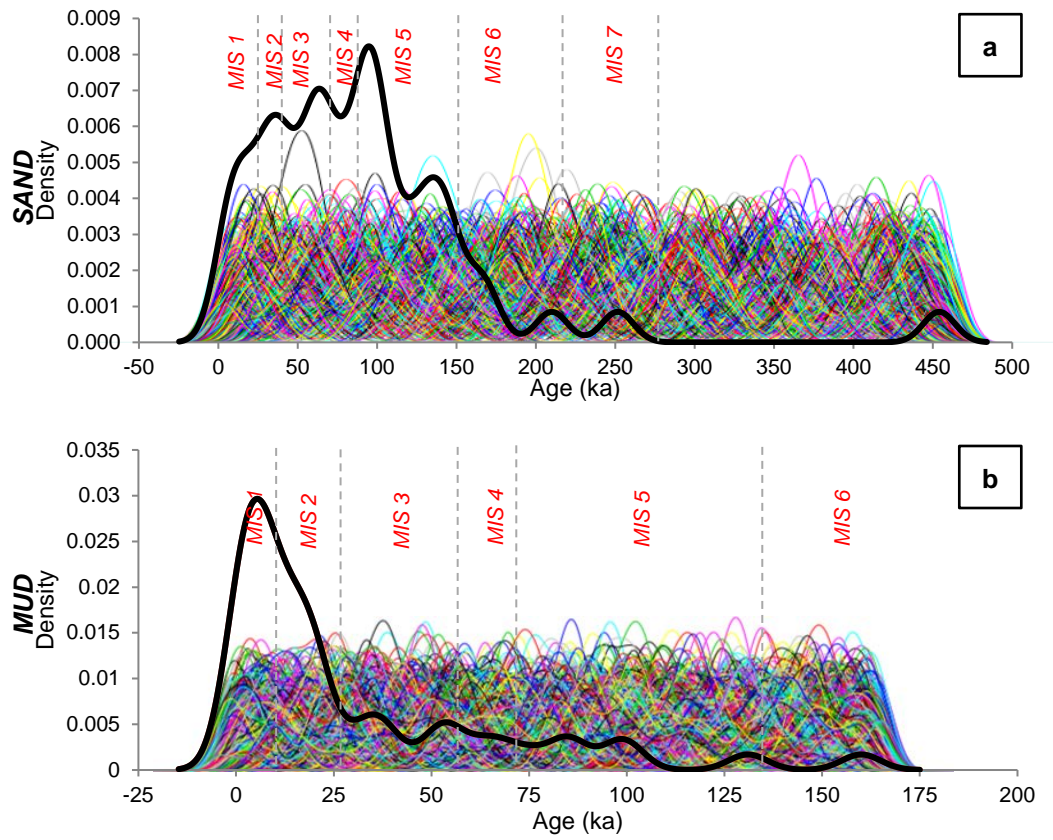
Figure 5.17 - Kernel density estimates of 1000 simulated random number datasets that follow the parameters of the observed (a) sand and (b) mud datasets and with the observed data overlaid (black line). Dashed lines indicate Marine isotope Stages from MIS 7 to present.

5.6.2   Interpreting the meta-analyses

The transition point at which the deposition type switched from sand to mud is defined at ~28 ka (Figure 5.18 and Figure 5.19). For mud deposits 66.0% of the deposits are younger than 28 ka and 34.0% are older indicating that the majority of mud deposition has occurred since 28 ka and that while mud deposition did occur prior to 28 ka it was not the prevalent deposition type. For the sand deposits 85.1% of the deposits were deposited prior to 28 ka. Only 14.9% have been deposited since 28 ka. The transition at 28 ka is interpreted as a completion in the transition from a meandering to an anabranching planform. Prior to this, where sand and mud deposits coexist, the presence of mud deposits initially represent overbank deposits and floodplains.
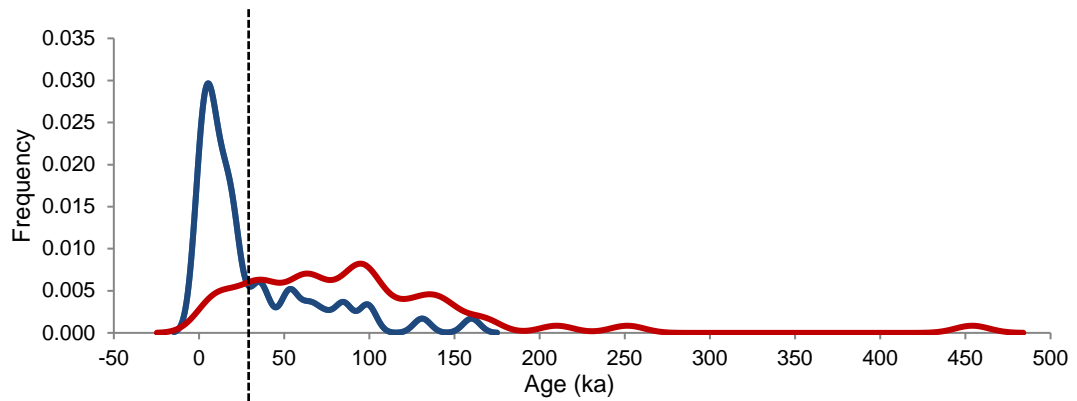
Figure 5.18 - Overlaid kernel density estimates for sand (red) and mud (blue) ages. The transition is identified as the switch in dominance of deposit type from sand to mud at ~28 ka and is shown by the dashed line.
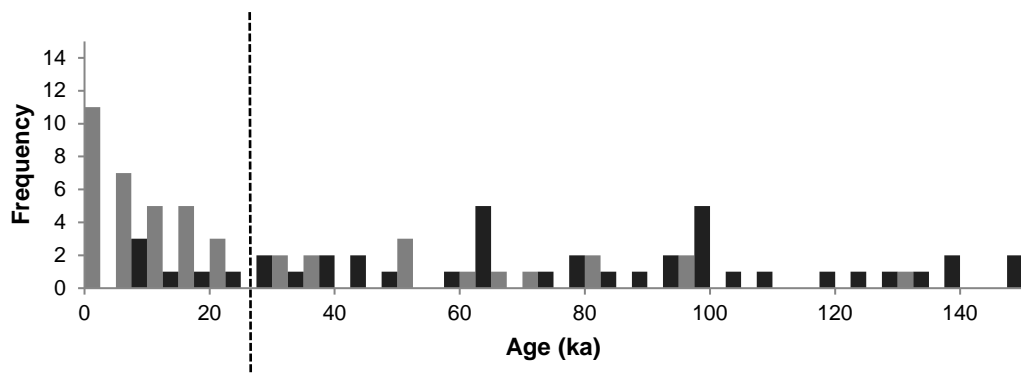
Figure 5.19- Overlaid histograms of mud (grey) and sand (black) deposits. The transition is the same as that from Figure 5.17, shown by the dashed line.

5.7   Discussion and synthesis

5.7.1   Appropriateness of the meta-analysis

When displaying ages distributions graphically, there are a number of options available. The work in this chapter supports the conclusion of Galbraith and Roberts (2012) that PDPs are not ideal for displaying geochronological distributions. In particular, because the incorporation of the standard errors into the distribution leads to an over-representation of young, more precise ages (Figure 5.14), as, with age, standard errors tend to increase. This flaw is perpetuated when generating random numbers and producing PDPs, as errors must also be produced and this is achieved through calculation of the average relative area for the dataset then using this value to create standard errors (e.g. Hesse 2014), therefore creating smaller errors on younger ages.

Histograms can be misleading due to the arbitrary attribution of bin width and the lack of consideration of error. An attempt was made to combat this in this chapter by using multiple bin widths (Figure 5.13). Despite this, histograms are widely favoured for displaying age distributions due to their ease of comprehension, by both experts and non-experts, and their ease of production. Furthermore histograms are not especially useful when verifying data interpretations as one is restricted to presenting a small number of replicates on a single plot.

From the work in this chapter it is apparent that KDEs should be the preferred method of presenting age distributions as they better present continuous data than histograms, provided a bandwidth comparison is conducted. KDEs also allow for large numbers of data sets to be displayed on a single plot, and do not require the propagation of artificial errors. While the error is not included, an accompanying plot of age against error enables understanding of the variation in uncertainties. Also, while bandwidth is arbitrary, as with histograms, it can be mathematically defined.

The shortcomings of these methods do not negate their usefulness, especially in the case of histograms and KDEs. A number of data compilations, including early iterations of this dataset have been analysed using histograms (Nanson et al. 2008), with conclusions being drawn that are consistent with interpretations from other sources, i.e. that enhanced frequency of deposits of certain ages, correspond to

enhanced deposition, and consistent with the conclusions drawn here. Work by Lewlin and Macklin (2003) assessed the frequency of alluvial units using histograms of radiocarbon ages, in which they caution as to over interpreting peaks in distributions, as current frequency does not necessarily reflect frequency at deposition.

KDEs pose similar problems with interpretation to histograms. Chiefly that interpretation of peaks in data cannot be isolated from incidental peaks. However, unlike with histograms, this can be combatted by isolation of the peaks as signals above background noise. KDEs also appear to be well suited to use in random number generation for the distinction of signal over noise. While the signal over noise method has not been further verified with additional datasets, it suggests that generating artificial datasets with the same parameters as the observed datasets are a useful method to distinguish which peaks in data are distinguishable from background noise. The removal of background or 'noise', which is, in effect, useless data that can be recreated by random number generation, allows for a certain confidence in the interpretation of the data.

5.7.2   The causes of the transition to anabranching

Anabranching is more widespread in Australia than elsewhere on the planet and is maintained for long periods of time (Nanson 2013). The sedimentary records through the Channel Country shows that the modern rivers have not always been the anabranching systems that they are today, as the record shows an underlying sand sheet deposited by meandering channels overlain by a homogenous mud deposit currently characterised by a anabranching channel network. This indicates planform metamorphosis from laterally active rivers with a sandy bedload to muddy anabranching channels. This transition would have been gradual and where the sand and mud deposits coexist in the dataset the mud likely represents overbank and floodplain deposits. Since MIS 5 the rivers became less competent and bedload was muddier, with flow cutting into the existing floodplain and mud infilling the existing channels culminating at 28 ka with the switch to the anabranching planform we see today.

Given the current prevalence of anabranching rivers in Australia, and the extent of evidence for a transition, it is likely that the transition was caused by a large scale forcing factor which resulted in a reduction in stream power; either climate and/or

tectonics and is discussed below. The indication is that the fluvial systems of the Channel Country were gradually reaching a threshold condition, where meandering systems were no longer stable, so a change in planform was initiated (Nanson and Huang 2008), initially by muddier bedload, then by anabranching channels which cut into the existing floodplain. A potential drop in stream power resulted in a system that was able to maintain an anabranching planform. The question is; what caused that reduction in stream power? Increasing aridity has been identified in the LEB from prior to MIS 5 to present, with superimposed wetting and drying oscillations (e.g. Nanson et al. 1992). This increase in aridity would result in a decrease in stream power, which will be discussed further in Chapter 8 of this thesis. An alternative scenario exists that the loss of stream power, which initiated the transition to anabranching, may have been caused by a reduction in slope. Uplift is occurring at Innamincka and has been since the mid-late Miocene, currently at a rate of ~17–65 mm.ka^{-1} (Jansen et al. 2013). Uplift is reducing the slope upstream of Innamincka Dome, due to subsidence and trapping of sediment. Subsidence is also occurring on the western side of the floodplain resulting in the dominant channel occurring on this western side (Maroulis 2000).

While it is likely that the tectonic setting is contributing, in part to the location and extent of the Cooper Creek floodplain and the current fluvial planform the data shows too close a link with climate fluctuations to not be interpreted as the main forcing factor. This is supported by numerous previous studies which have identified the link between anabranching in the LEB and climate (e.g. Nanson et al 1992; 2008; Cohen et al. 2015).

5.8   Limitations and further research

Currently we lack a second dataset with which to run the 'geochronology signal vs. noise program'. Ideally the approach should be trialled with other datasets to establish a runnable program by which to generate noise and run the dataset comparison. Furthermore, there is the potentially unresolvable limitation that without knowledge of variables of the palaeo-river system it is difficult to understand the dynamics of the underlying system represented by the sand sheet and how it changed over time. While we know that the sediment load size and the river planform has changed we have no further reconstruction of the behaviour of these rivers. Without any parameters beyond sediment size we have insufficient variables for hydraulic or geometric calculations.

5.9   Chapter summary

Meandering systems dominated in the LEB prior to MIS 5c, after which meandering systems began to decline, based on dated stratigraphic abundance, reaching a low point at ~60 ka. From 25 ka – 60 ka few ages are present for either mud or sand deposits indicating a period of reduced deposition, or possibly increased erosion, with a combination of the two being likely. Aridity in the LEB occurred during the MIS 3 and into MIS 2 with maximum aridity at ˜25 ka. After 25 ka, the frequency of mud deposits increases, interpreted as the completion of the transition to anabranching. The anabranching planform has persisted until present, despite an increase in aridity during the early to mid-Holocene. This persistence indicates that anabranching within a mud dominated system is now the stable fluvial form in the majority of the LEB. Given the correlation between marine isotope stages and changes in deposition, climate is likely to be the key driver of anabranching continent wide, coupled with low relief and low sediment supply making the persistence of anabranching an indirect effect of the lack of long term tectonic activity in the basin. Localised topography and tectonism do, however, have an effect on individual reaches of channel, as seen in the downstream sections Cooper Creek.

Chapter 6

---

6 Variation in downstream cosmogenic ^{26}Al and ^{10}Be ratios in a large, arid, endorheic drainage basin

6.1 Introduction

Low, flat terrain covers ~90% of Earth's land surface and is thought to account for roughly half of the global sediment flux (Willenbring et al. 2013). In areas of high slope sediment transport is controlled by hillslope and sediment is transferred from source to sink, or a series of sinks, in a relatively rapid manner with limited storage. In areas of low slope the controls on production, transport, and storage are not as well understood (Chapter 2 - 2.4). Combining this with the fact that 37.2% of the globe is in the hyper-arid, arid, and semi-arid zones (Middleton and Thomas 1997), and rivers in these regions are less well understood than in temperate regions (Tooth 2000; Tooth 2013) (Chapter1 - 1.1) adding to the understanding low slope arid fluvial environments is important.

Fluvial systems are a key geomorphic agent in the redistribution of sediment from an erosional source to an ultimate depositional sink (Allen 2008). In a fluvial system there are a number of points at which sediment can be input into the system and stored for different durations. Quantifying sediment storage duration can give insights into transport rates and the efficiency of the sediment conveyor in a system, which in arid environments often has a low level of connectivity (Chapter 2 - 2.4) (e.g. Fryirs et al. 2007). In an arid low-slope fluvial system sediment is produced slowly with denudation rates frequently less than 10 m.Ma^{-1} (e.g. Bierman and Caffee 2002; Heimsath et al. 2010; Struck et al. 2018a). Movement of sediment is episodic, due to the nature of precipitation and fluvial regimes in ephemeral rivers, leading to prolonged storage periods with probable hiatuses in sediment movement (Fryirs et al. 2007). Therefore the measurement of these extended burial durations is often in excess of tens of thousands of years (e.g. Maroulis et al. 2007; Nanson et al. 2008) (Chapter 5). This negates the use of direct measurements such as can be used where transport is rapid and burial is short-term (<0.01 ka), over longer timescales geochronological

methods can be used (Chapter 3 - 3.1). Sediment burial duration is frequently quantified through luminescence dating, however this only gives a burial age for the time since most recent exposure to sunlight. Terrestrial cosmogenic nuclides can be used to calculate burial duration and denudation rate as further explained in Chapter 3 of this thesis. Terrestrial cosmogenic nuclides are produced in the upper few metres of the earth's surface by interaction of cosmic rays with minerals in sediment and rock (Gosse and Phillips 2001). A single nuclide, in this case ^{10}Be, can be used to calculate rates of denudation and when a pair of nuclides, with known rates of production and decay, are measured, such as ^{10}Be and ^{26}Al, the ratio of their concentrations can initially be used to establish if sediment has undergone a complex transport history, which is indicated by deviation from the steady state erosion island. This ratio can then be used calculate a minimal cumulative burial duration on timescales of $\sim 10^5 - 10^6$ years (Lal 1991; Granger et al. 1996).

This chapter continues from the work in Chapter 5, where it was established that buried sediment in the Channel Country displays a transition from large, laterally active, meandering sand-load rivers, to 'type 1' anabranching (Nanson and Knighton 1996) systems starting at MIS 5 and continuing, until a complete transition by the LGM. This chapter looks beyond the most recent burial event represented in the ages in Chapter 5 and aims to identify if significant burial is occurring in Cooper Creek representing the cumulative duration of multiple burial events, over time periods $> 10^5$ years and how this relates to the geomorphology of the system. Cosmogenically produced ^{10}Be and ^{26}Al are measured from detritals throughout Cooper Creek and used to trace potentially complex sediment transport histories by identifying ^{26}Al/^{10}Be ratios which deviate from the production ratio, and to establish if these measured ratios can be used to imply burial within the system. Given the prevalence of low slope arid regions in Australia questions are posed here regarding potentially prolonged storage, over hundreds of thousand years, of sediments in a fluvial system in a low slope environment in the arid zone and how different parts of the system interact with one another.

6.2   Cooper Creek and its sediment sinks

To summarise from Chapters 4 and 5, Cooper Creek dominates the eastern half of the LEB (Figure 6.1a) and is the most widely investigated of all the arid zone rivers in Australia (Nanson et al. 2008). Draining 350 000 km^2 of intracratonic drylands, it

flows 1600 km from northern Queensland to the continental depocentre at Kati Thanda-Lake Eyre (. Cooper Creek stems from two headwater rivers: the Thomson River and the Barcoo River, draining 94 930 km^2 and 53 242 km^2 respectively (Habeck-Fardy and Nanson 2014).and characterised by alternating anabranching and braided floodplain channels with occasional single channel reaches (Nanson et al. 1986).
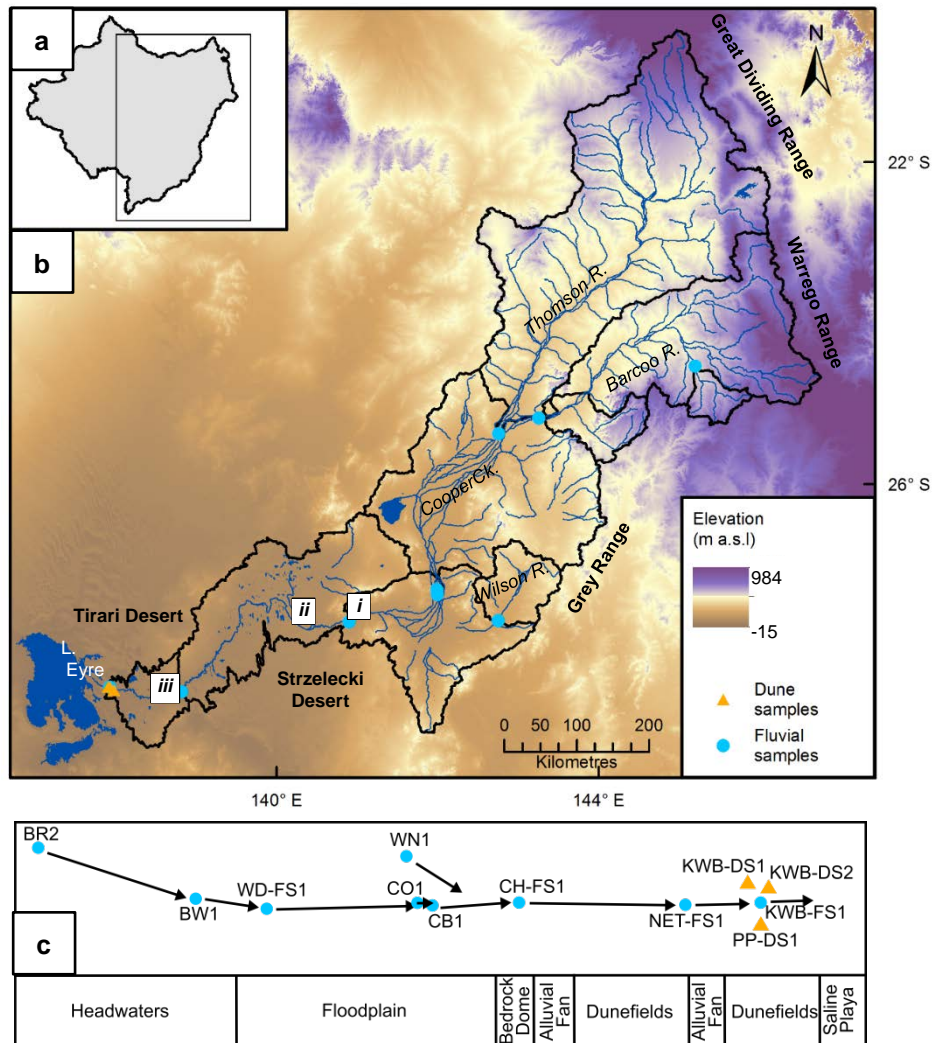
Figure 6.1- (a) The study site within the LEB (b) The Cooper Creek catchment area with fluvial sediment (blue circles) and source bordering dune samples (orange triangles). Upstream watershed areas are shown as a series of basins nested within that of the most downstream watershed (bold black lines)locations marked (i) Innamincka dome; (ii) Cooper Fan (iii) Gason dome (c) Schematic flow relationship between each of the samples

Cooper Creek and its headwaters consist of a range of geomorphological features which are key to understanding its sediment dynamics. The Thomson River originates in the north western Great Dividing Range, and converges with the Barcoo River (Figure 6.2a), rising in the Warrego Range, to become Cooper Creek, flowing through

a large floodplain 8 - 60 km wide with 'type 1' anabranching channels, defined as muddy anastomosing (Nanson and Knighton 1996) (Figure 6.2b). Cooper Creek then becomes a single thread channel cutting through the uplifting bedrock Innamincka Dome (Figure 6.2c) which rises ~250 m above the floodplain surface (Jansen et al. 2013). After flowing through this constriction the flow forms an alluvial fan (figure 6.2d) with a slope of 0.00027 m.m^{-1}, steeper than the surrounding plains (Wasson 1983; Callen and Bradford 1992), and forms a distributary channel which, downstream, becomes sinuous, winding through the dunefields of the Tirari and Strzelecki Deserts (Figure 6.2e) and culminating at Kati Thanda-Lake Eyre (Figure 6.2f).

Figure 6.4 –Sampling locations along Cooper Creek (a) The Barcoo River, in a single channel reach, (b) The Cooper Creek floodplain, (c) Cooper Creek cutting a bedrock channel at the Choke near Innamincka (d) The Cooper Creek alluvial fan and longitudinal dunes (e) Cooper Creek and its source bordering dunes near Kutjitara West Bluff (f) Kati Thanda-Lake Eyre. (c, d and e reproduced

Heimsath et al. 2010; Struck et al. 2018a), compared to global values off up to 6000 mm.ka^{-1}. When compared to similar low slope environments (< 200m.km) that have

average rates of ~45 mm.ka^{-1} (Willenbring et al. 2013) denudation rates in the LEB are substantially lower. This slow erosion is a function of low relief, tectonic quiescence and arid climate which in turn limit sediment transport creating ideal scenarios for burial within the system (Willenbring et al. 2013). Given the morphology of the system there are a number of points where sediment can be stored on varying timescales. The storage points within Cooper Creek are typical of many low slope arid environments: floodplains/alluvium, dunefields and lakes (Figure 6.3a). Evidence of sediment storage in the Cooper Creek system for extended periods is seen through dating of sediments using OSL (see Chapter 5 of this thesis). In the Cooper Creek system storage in the floodplain is well documented, with burial durations from luminescence exceeding 200 ka in the upper 10 m of the Cooper Creek floodplain. There is evidence that extensive burial is concentrated directly upstream and directly downstream of the uplifting Innamincka Dome (Figure 6.4; 6.5) with burial in the upper 4 m for as long as 200 ka (Figure 6a;b). Deeper burial (4-10 m) shows this same burial pattern with some burial ages exceeding 200 ka (Figure 6.5). The Innamincka Dome is uplifting at 17.4 ± 6.5 mm.ka^{-1} (Jansen et al. 2013) and, directly upstream of the dome, aggradation, where subsidence associated with the Cooper-Wilson synclinal depression, creates accommodation space is 48 mm.ka^{-1} (Jansen et al. 2013) storing an estimated 660 - 990 km^2 of sediment (Figure 6.3b). Downstream of the dome sediment is also accumulating on the Cooper Fan, a alluvial fan of ~ 30 x 22 km with at least 5 m of accumulated sediment consisting of fine alluvial sand overlain by alluvial silty sand (Wasson 1983; Cohen et al. 2010).

Kati Thanda-Lake Eyre is, globally, the fifth largest terminal lake, with a total area of ~ 9300 km^2 (Habeck-Fardy and Nanson 2014). Modern sedimentation is occurring in three settings: (1) north saline playa; (2) a terminal salina environment in the south end, where evaporation of brines leaves salt crust overlying gypseous sediments; and (3) a saline flocculation environment (Dulhunty 1982). However, despite this modern sedimentation there is a paucity of post Miocene sediments in Kati Thanda-Lake Eyre (Magee et al. 1995) (Figure 6.3c). There are currently two large dune fields proximal to Cooper Creek (Figure 6.1b). The dunefields are the Tirari Desert (~70 000 km^2) directly to the east of Kati Thanda-Lake Eyre, and of which the Cooper Fan is part, and further east to the south of the Cooper Creek channel the Strzelecki Desert (~100 000 km^2) (Hesse 2011). Mapping of the dunes by Hesse (2010; 2011) indicates that

the dominant control on the distribution of dunes is wind directional variability and that the morphology of the dunes within the LEB is highly variable. The dune sands are pale-coloured close to fluvial and lacustrine forms, becoming red brown to orange as they become more distal and as the sediment source changes from fluvial or lacustrine sediments to locally weathered bedrock (Wasson 1983a:b).
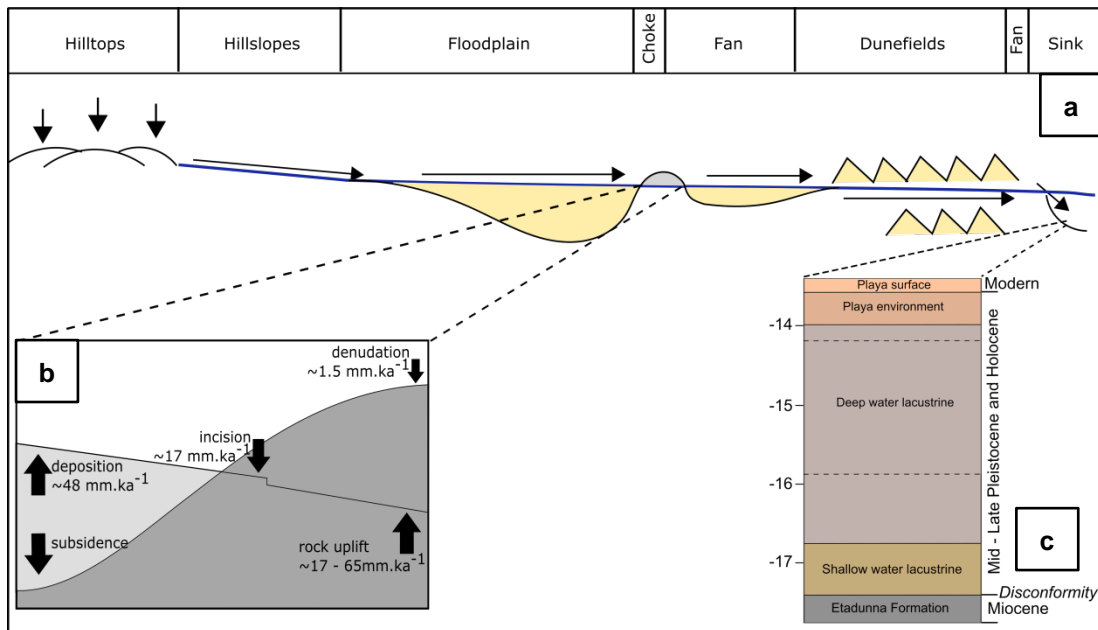
Figure 6.7 - (a) Schematic scenario of Cooper Creek showing movement of sediment from the headwaters and potential sediment stores in the system (yellow shading) (b) Cooper Creek across the Cooper-Wilson synclinal depression to Innamincka Dome showing basin subsidence and deposition rate upstream of the dome, incision rate at the dome, and denudation rate and rock uplift downstream of the dome (after Jansen et al. 2013) (c) Representative stratigraphic sequence from core LEWP1 at Williams Point at the south of Lake Eyre North showing the depositional environments represented in the ~ 4 m of sediment deposited post Miocene (after Fu et al. 2017).

6.2.1 Hypothesis

Given the paucity of post-Miocene deposition at Kati Thanda-ake Eyre two conflicting hypotheses have been proposed: post-depositional deflation to surrounding dunefields (Magee et al. 2004) versus storage of fluvial sediments en route (Jansen et al. 2013). Much of the subsurface sediment at Kati Thanda-Lake Eyre has not been dated however Magee et al. (2004), identified just 4 m of sediment from MIS 5, although further work by Fu et al. (2017) identifies sediments as MIS 7 – MIS 5. Jansen et al. (2013) propose that the reason for such short sequences of sediments is that the sediments do not reach Kati Thanda-Lake Eyre due to being sequestered on route. This hypothesis is also proposed here due to the known presence of long buried sediment in the upper few metres of the floodplain (Figure 6.4; 6.5) and as the morphology of

the system presents multiple opportunities for sediment storage, particularly with regards to the tectonic basin structure with the Cooper-Wilson syncline creating ~660 - 990 km^3 of potential sediment storage, vastly overshadowing the 16 - 40 km^2 at Kati Thanda-Lake Eyre (Jansen et al. 2013).

This work will test the hypothesis that in Cooper Creek, sediments are stored and reworked multiple times along the channel, which may be recorded as reduced ^{26}Al/^{10}Be ratios in detritals (Chapter 3 – 3.4.2; 3.4.3). The ratio of ^{26}Al/^{10}Be has been used to identify a complex exposure history such as one including burial, where a lower offset in ^{26}Al/^{10}Be ratio from the expected production-rate ratio of 6.75 (Balco et al. 2008) can be converted to a burial age A system without significant burial is deemed unlikely due to the previous dating evidence (Figure 6.4; 6.5), which also points towards burial in the floodplains, rather than the larger dunefield areas as proposed by Magee et al. (2004).
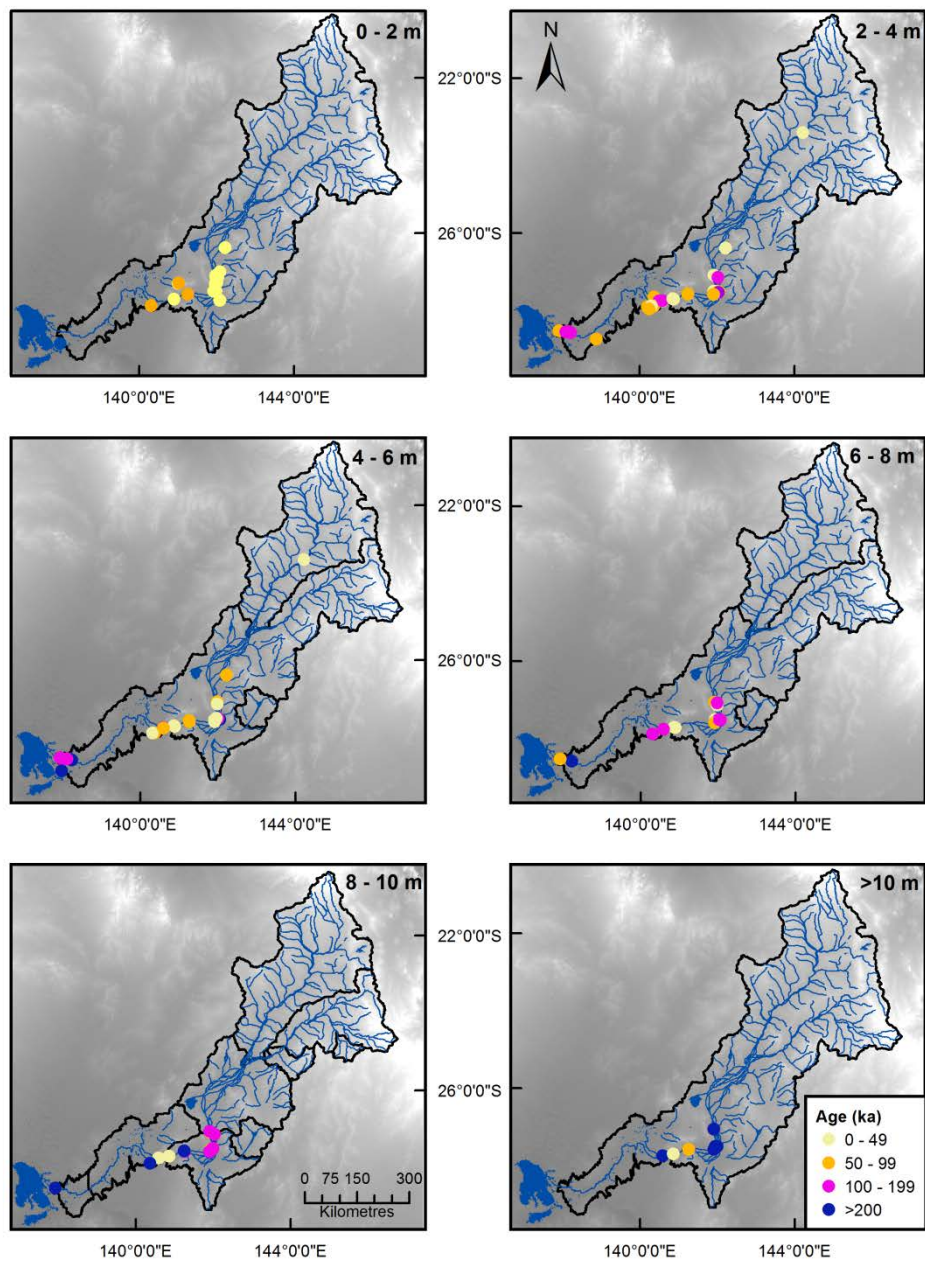
Figure 6.8 - Sediment samples from Cooper Creek dated using luminescence dating plotted at 0 - 49, 50 - 99 , 100 - 199 and >200 ka at 2m depth increments.
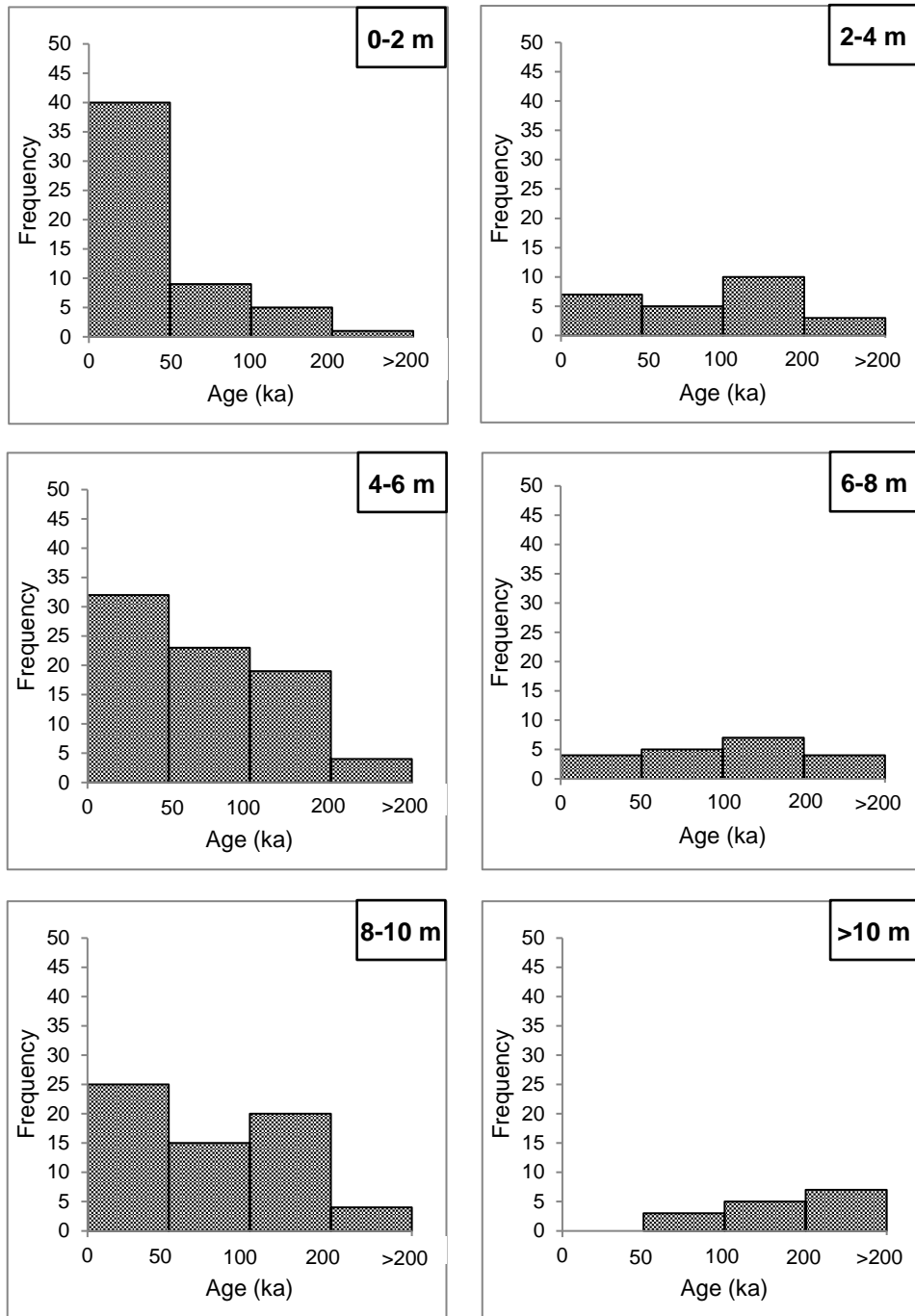
Figure 6.9 - Corresponding histogram for each map in Figure 6.4 showing the frequency of samples of 0 - 49, 50 - 99, 100 - 199 and >200 ka at 2 m depth increments.

6.3 Methods

6.3.1 Sample selection

Nine detrital samples (Table 6.1) were collected along the full length of Cooper Creek, plus three surface samples from source bordering dunes in the lower reaches (Table 6.1) (Figure 6.1b). The study reach covers the entirety of Cooper Creek. Samples were taken to represent all aspects of the system. Two samples (BR2, BW1) were taken from the Barcoo River, from alluvial channels. Three samples (WDFS1, CO1 and CB1) were taken to represent the anabranching reaches Cooper Creek where it flows through the floodplain. To the east of Cooper Creek is the Wilson River (WN1) originating in the Grey Range and flowing for 220 km until it meets with Cooper Creek, with a hydrological connection existing at times of high flow. Downstream of the connection between Cooper Creek and the Wilson River the channel is constrained through the Choke, where a fourth sample (CHFS1) was collected. The channel then crosses the Cooper Fan, which is populated by the linear and source bordering dunes of the Strezelecki desert (Cohen et al. 2010). As the river become sinuous flowing towards Kati Thanda-Lake Eyre, two further samples were taken from the channel, one upstream (NETFS1) and one downstream (KWBFS1) of the Gason–Cooryanna Domes, which the channel crosses albeit with a less distinct change in morphology than that seen at Innamincka. At Kutjitara West Bluff two source bordering dune samples (KWBDS1; DS2) were taken to accompany the channel samples KWBFS1, with a further source bordering dune sample being collect at Pink Pool (PPDS1) ~10 km upstream of Kutjitara West Bluff.

Table 6.1 - Sample site details. Altitude, longitude and latitude are from field measurements with a hand held GPS.

Sample	River system	Location	Altitude m.a.s.l	Latitude Longitude	Material	Part of system
BR2	Barcoo-Cooper	Ravensbourne Creek	255	-24.5362, 145.1987	River sand	Headwater -alluvial channel
BW1	Barcoo-Cooper	Welford	149	-25.1813, 143.2562	River sand	Headwater -alluvial channel
WD-FS1	Cooper	Windorah	129	-25.3763, 142.7587	River sand	Floodplain – anabranching channel
CO1	Cooper	Okotoko anabranch	82	-27.3086, 141.9888	River sand	Floodplain – anabranching channel
CB1	Cooper	Bogaller waterhole	81	-27.3713, 141.9962	River sand	Floodplain– anabranching channel
WN1	Wilson-Cooper	Nockatunga	105	-27.6963, 142.7537	River sand	Ancillary Basin
CH-FS1	Cooper	Cullyamurra water hole - choke	54	-27.7112, 140.9012	River sand	Bedrock confinement
NETFS1	Cooper	North Etadunna - Wet Crossing	19	-28.5814, 138.8163	River sand	Alluvial channel
PPDS1	Tirari - Cooper	Pink Pool	15	-28.5612, 137.9713	Dune sand	Source bordering dunes
KWBFS1	Cooper	Kutjitara West Bluff	13	-28.5237, 137.9238	River sand	Alluvial channel
KWBDS1	Tirari - Cooper	Kutjitara West Bluff	15	-28.5212, 137.9013	Dune sand	Source bordering dunes
KWBDS2	Tirari - Cooper	Kutjitara West Bluff	15	-28.5212, 137.9238	Dune sand	Source bordering dunes

6.3.2   Catchment analysis

The watershed areas upstream of each fluvial sample were analysed for slope, elevation and mean relief using one arc-second digital elevation data from the Shuttle Radar Topographic Mission (SRTM). The mean local relief was taken for each watershed as the mean of the relief in a 2.5 km radius of each pixel. Surface geology was analysed using a digital 1:1 million surface geology map of Australia (Raymond et al. 2012). The surface geology was first classed as bedrock, unconsolidated sediment and anthropogenic deposits. Sediment was divided into seven classes: colluvium, alluvium, black soil plain, dunes, ferruginous duricrust, lake deposits, lunette dunes, and sand plains. Sand plains are separated from other surface deposits as undifferentiated Cenozoic sand deposits, with no distinction by origin (Raymond et al. 2012). The area of each of these surface geologies was then expressed as a percentage of the total watershed area.

6.3.3   Sample preparation, measurement, and calculation

All 12 samples were prepared to extract Be and Al from purified quartz in the 250-500μm grain size fraction at the University of Wollongong at the Australian Nuclear Science and Technology Organisation (ANSTO) the full method for which is outlined in Appendix C. Standard methods of HF/HNO3 (Kohl and Nishiizumi 1992), hot phosphoric acid (Mifsud et al. 2013), and ion chromatography (Child et al. 2000) were used to extract Be and Al, a ^{9}Be carrier, at 1090 ± 15 ug.g^{-1} or 1128 ± 22 ug.g^{-1}, was added to all samples for ^{10}Be measurement. The ratios of ^{10}Be/^{9}Be and ^{26}Al/^{27}Al were measured on the ANTARES Accelerator Mass Spectrometers (AMS) (Fink and Smith 2007) and normalised to standard KN-5-2 (Be) (Nishiizumi et al. 2007), and KN-4-2 (Al) (Nishiizumi 2004). The uncertainties on the concentrations of ^{26}Al and ^{10}Be were calculated in quadrature using uncertainties in Table 6.2.

Table 6.2 - Intrinsic uncertainties used in calculating uncertainties on ^{10}Be and ^{26}Al concentrations.

Nuclide measured	AMS uncertainty (%)	Beryllium spike uncertainty (%)	ICP-OES uncertainty (%)
26Al	3	n/a	4
10Be	2	1	n/a

Burial durations were calculated using CosmoCalc 3.0 (Vermeesch 2007). The calculations use the scaling of Dunai (2000) and the exponentials of Schaller et al. (2002). The basins and long profiles were extracted from the 30m SRTM digital elevation model.

The calculations assume a half-life of ^{10}Be of 1.387 ± 0.012 Ma (Chmeleff et al. 2010; Korschinek et al. 2010) and a half-life for ^{26}Al of 0.705 ± 0.024 Ma (Norris et al. 1983). With total production rates of 4.68 for ^{10}Be and 31.9 for ^{26}Al respectively. This is explained in more detail in Appendix C – C.2.

6.4   Results

6.4.1   Catchment characteristics

Mean catchment slope ranges from $\leq 0.5 - 0.8\ °$ (Table 6.3) with a gradual decrease in slope with distance downstream (Figure 6.6). The Barcoo and Wilson Rivers are the steepest tributary catchments (Figure 6.6), whereas the slope of the Thomson is similar to that of Cooper Creek itself. The total relief of the system increases downstream with increasing catchment size from 220 m to 823 m (Table 6.3), however the mean catchment relief decreases due to the increasing proportion of low relief areas with increasing catchment areas.

Table 6.3 - Catchment characteristics of catchment area upstream of each sample

Sample	Distance from source[a,b]	Catchment size	Elevation[a]			Slope[a]			Total relief[a]	Average local relief[a,d]
	(km)	10^3 km^2	Min (m)	Max (m)	Mean[c] (m)	Min (°)	Max (°)	Mean (°)	(m)	(m)
BR2	93	3.52	251	471	329 ± 40	1.56×10^{-3}	10.72	0.76	220	44.08
BW1	388	54.80	142	720	310 ± 90	2.17×10^{-5}	18.63	0.80	578	39.90
WDFS1	458	151.37	125	816	278 ± 84	2.17×10^{-5}	19.51	0.57	740	28.09
CO1	708	201.39	74	816	247 ± 93	2.17×10^{-5}	19.51	0.57	742	32.48
CB1	716	201.40	74	816	247 ± 93	4.23×10^{-4}	7.60	0.48	184	32.47
WN1	738	8.4079	96	279	155 ± 29	4.38×10^{-6}	19.51	0.58	767	26.73
CHFS1	846	234.83	48	816	229 ± 98	2.17×10^{-5}	19.51	0.59	691	32.67
NETFS1	1221	243.07	3	816	222 ± 102	9.23×10^{-7}	19.51	0.58	813	31.74
PPDS1	1331	n/a	n/a	n/a	n/a	n/a	n/a	n/a	n/a	n/a
KWBFS1	1347	245.64	-8	816	220 ± 104	9.23×10^{-7}	19.51	0.58	823	31.57
KWBDS1	1347	n/a	n/a	n/a	n/a	n/a	n/a	n/a	n/a	n/a
KWBDS2	1347	n/a	n/a	n/a	n/a	n/a	n/a	n/a	n/a	n/a

a) Based on 1 arc-second SRTM data; b) Flow distance from start point of river to sampling point; c) Uncertainties taken as one standard deviation; d) Catchment average relief calculated as an average of the relief from a 2.5 km radius around every pixel in each catchment.
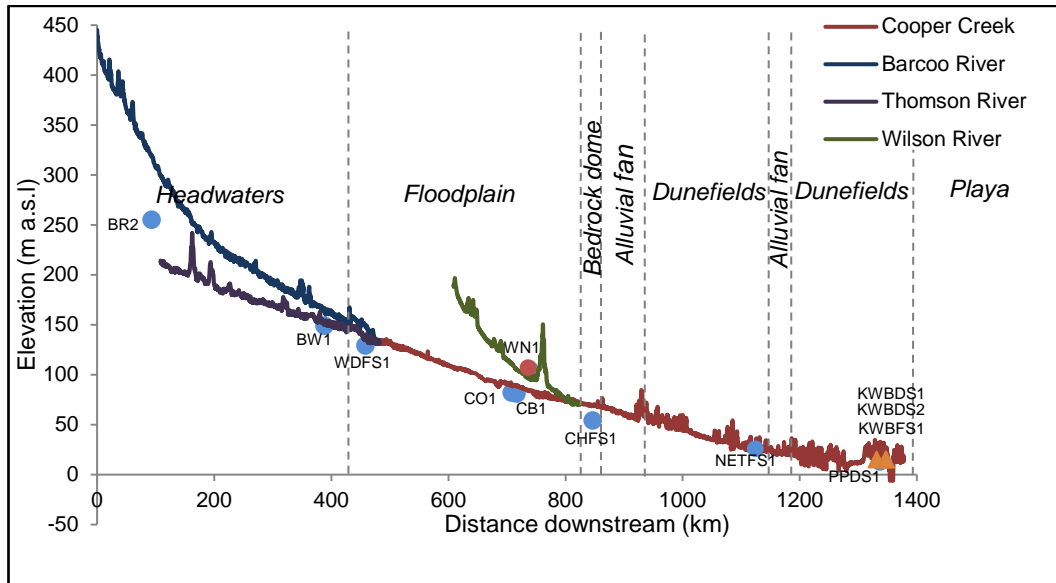
Figure 6.10 - Long profiles of the Barcoo River, Thomson River, Wilson River and Cooper Creek with sample locations marked (Fluvial samples = blue circles (WN1 = red circle), dune samples=orange triangles) and morphology sections of the reach defined. Where elevations do not exactly match between sample locations and long profile this is largely due to the averaging of the channel train into a single line, and the precision of handheld GPS measurements. Long profiles were extracted from the 1 arc-second SRTM digital elevation model.

The Barcoo River catchment has the highest proportion of bedrock (Figure 6.7) at ~86 % and ~68 % of surface geology as bedrock for BR2 and BW1 respectively. Moving downstream the amount of bedrock decreases to ~48 % at its lowest proportion with the exception of the Wilson River catchment which has ~35 % exposed bedrock. Colluvium and lacustrine deposits are also proportionally minimal with less than 0.1 % throughout. Alluvium increases downstream from 0.61% in the headwaters to 21.65 % in the most downstream watershed. A similar pattern is seen in dune sediment with an increase from 0 to ~7 % downstream. The proportion of sand plains remains approximately constant throughout, notably there is ~13 – 22 % sand plain cover in the Barcoo River headwaters (Table 6.4).
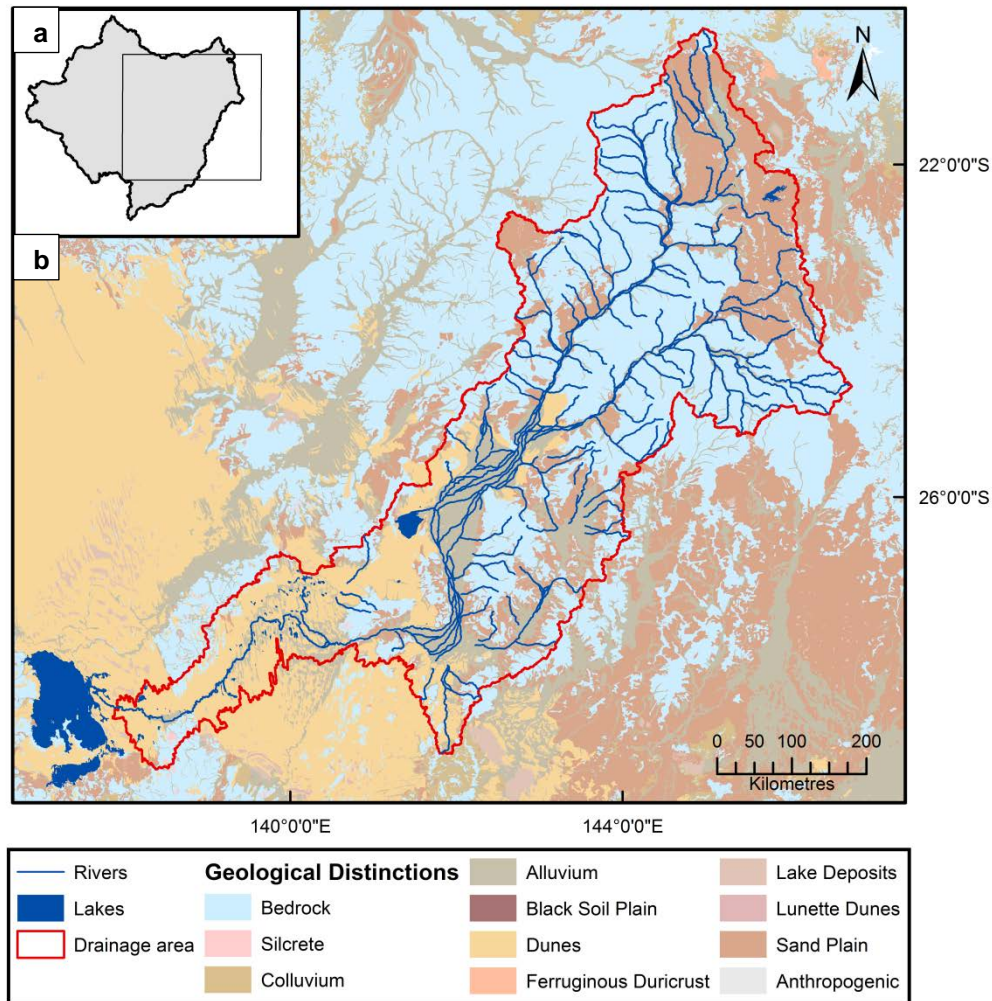
Figure 6.11 – (a) The study are in the LEB. (b) Surface geology of the study area with study drainage area marked in red. Surface bedrock is grouped as a single unit with the exception of silcrete for the purpose of mapping however for the calculation of percentage cover; all bedrock is treated as a single unit. Sediment cover is differentiated into colluvium, alluvium, black soil plains, dunes, ferruginous dunes and anthropogenic sediments. While all these divisions appear in the mapping area only colluvium, alluvium, dunes, lake deposits and sand plains are present in the study area. Mapping units are taken from the 1:1 million scale geology map of Australia (Raymond et al. 2012).

Table 6.4 - Surface geology of sample catchments with proportions of bedrock, silcrete colluvium, alluvium, dunes, lacustrine sediments and sand plains from the 1:1 million scale geology map of Australia (Raymond et al. 2012)

Sample	Bedrock	Colluvium	Alluvium	Dunes	Lacustrine sediments	Sand plains
	(%)	(%)	(%)	(%)	(%)	(%)
BR2	86.07	0.00	0.61	0.00	0.00	13.32
BW1	67.79	0.00	10.54	0.00	0.00	21.67
WDFS1	60.65	0.01	12.60	0.70	0.02	26.01
CO1	53.77	0.01	19.61	2.64	0.02	23.95
CB1	53.76	0.01	19.62	2.64	0.02	23.95
WN1	34.78	0.00	28.30	0.00	0.00	36.91
CHFS1	50.32	0.08	21.07	4.72	0.01	23.79
NETFS1	48.74	0.08	21.61	6.53	0.06	22.98
KWBFS1	48.50	0.08	21.65	6.93	0.06	22.65

6.4.2 ^{10}Be abundances

The ^{10}Be abundances within the Cooper Creek system vary little with abundances of ~ 0.42 to 0.53 x 10^6 atoms.g^{-1} in fluvial samples (Table 6.5; Figure 6.8), the exception being the Wilson River tributary catchment (WN1) which has a ^{10}Be abundance of ~1.4 x 10^6 atoms.g^{-1} (Figure 6.8). The source bordering dunes range from 0.52 to 0.57 x 10^6 atoms.g^{-1} (Table 6.5; Figure 6.8). The ^{26}Al abundances range from ~1.6 – 5.1 x 10^6 atoms.g^{-1} in the fluvial samples and 1.7 – 2.0 x 10^6 atoms.g^{-1} in the source bordering dunes (Table 6.5).

6.4.3 Apparent burial durations

The ^{26}Al/^{10}Be ratios range from 3.59 ± 0.34 to 6.66 ± 0.48 for the fluvial samples (Table 6.5). The dune samples generally have lower, and less deviated, ratios ranging from 3.40 ± 0.26 to 3.84 ± 0.41 (Table 6.5). The majority of the ratios deviate from the steady-state erosion ratio, as absolute values, and therefore are inferred to have undergone a minimum of one period of burial (Figure 6.8; 6.9). However within one-sigma samples CHFS1, NETFS1 and WDFS1 intersect with the steady-state erosion ratio so it is not distinguishable from a simple exposure model (Figure 6.8).

When converting $^{26}Al/^{10}Be$ ratios to burial ages values that deviate from the steady-state erosion curve (Figure 6.8; 6.9) are assumed to have undergone a minimum of one episode of burial and exposure, however this burial cannot be isolated from variable rate exhumation (Gosse and Philips 2001). Therefore, while deviations from the steady-state curve are presented as burial ages, these are simply the measure of distance of data from the steady-state erosion island and do not necessary indicate actual burial durations.

The apparent burial ages in fluvial samples vary, as absolute values, from ~ 0.05 (CHFS1) to 1.20 Ma (CB1) (Table 6.6) Apparent burial in the dunes are consistent at one-sigma and the absolute values range from ~ 1.06 (PPDS1) to ~ 1.29 Ma (KWBDS1). At one-sigma the minimum values still show substantial apparent burial.
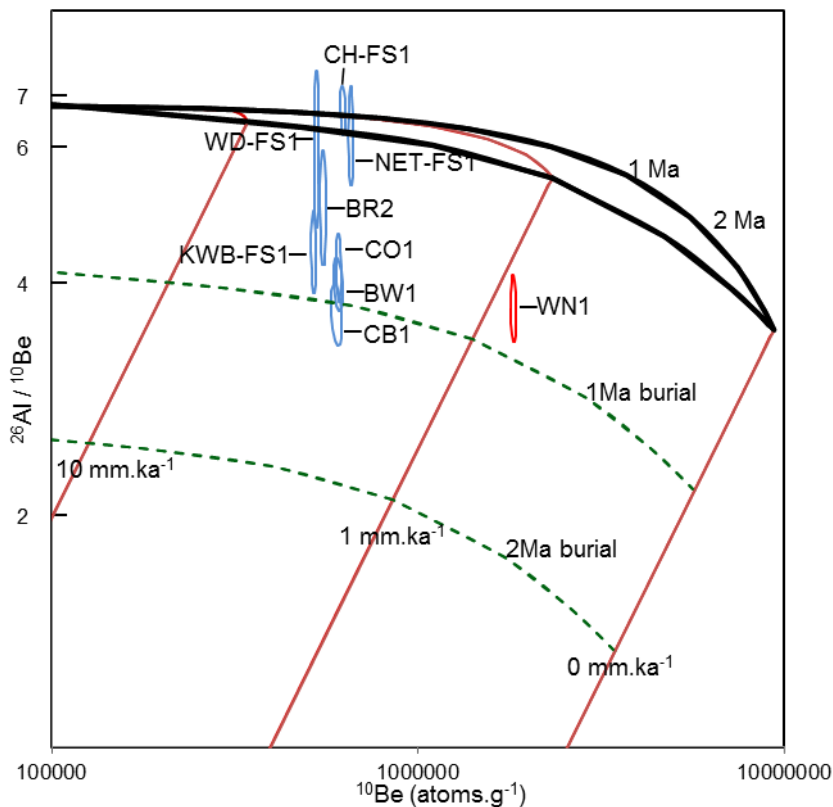
Figure 6.12 - Two nuclide logarithmic plot of $^{26}Al/^{10}Be$ ratios (normalised to sea-level high latitude) in the Barcoo River and Cooper Creek (Blue) and the Wilson River (Red). The region between the black lines indicates a history of simple exposure/erosion with samples to the left of this region indicating a history which includes burial.
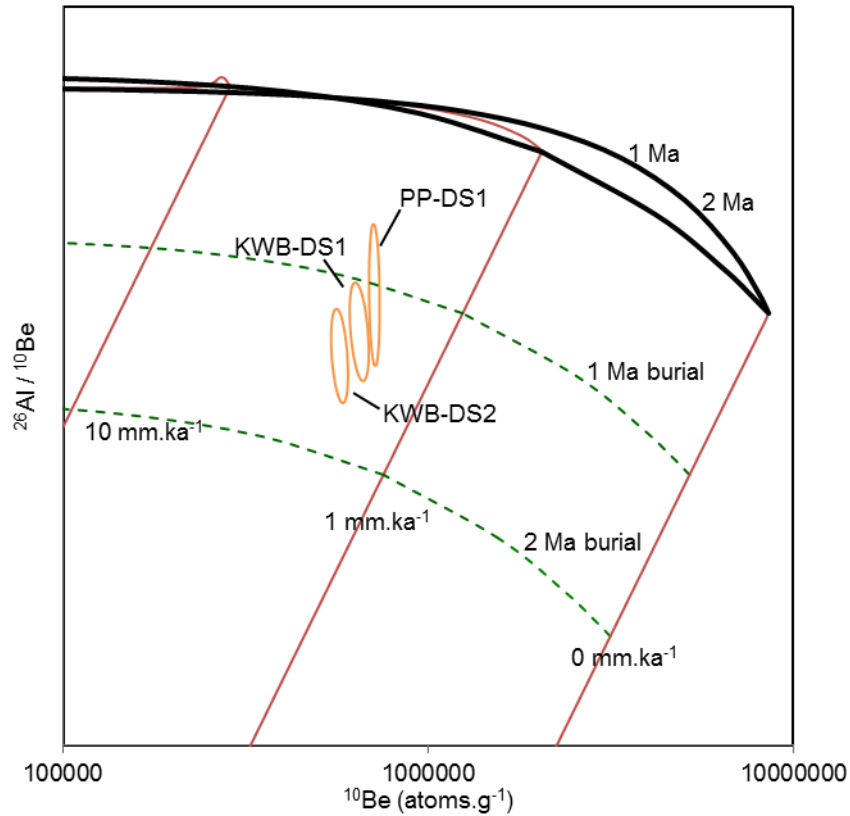
Figure 6.13 - Two nuclide logarithmic plot of ^{26}Al/^{10}Be ratios (normalised to sea-level high latitude) in the Tirari dunes bordering Cooper Creek at Kutjitara West Bluff (KWBDS1, KWBDS2) and Pink Pool (PPDS1). The region between the black lines indicates a history of simple exposure/erosion with samples to the left of this region indicating a history which includes burial.

Table 6.5- Cosmogenic nuclide measurement data

Sample	AMS ID	Production scaling factor[a]	Sample Mass (g)	10Be/9Be ratio (10^-15)[b,c,d]	9Be carrier mass[e]	10Be 10^6 at.g^-1	26Al/27Al ratio (10^-15)[d,f,i]	27Al icp conc µg.g^-1	26Al 10^6 at.g^-1	Ratio
BR2	A2592/B5745	0.80	40.243	837.56 ± 16.71	0.316[1]	0.48 ± 0.010	861.29 ± 141.86	124.72	2.25 ± 0.40	4.68 ± 0.84
BW1	A2710/B6017	0.86	39.57	924.00 ± 16.07	0.297[2]	0.52 ± 0.017	348.01 ± 19.24	264.57	2.06 ± 0.15	3.93 ± 0.31
WDFS1	A2597/B5757	0.79	40.163	767.54 ± 11.01	0.311[1]	0.43 ± 0.006	905.88 ± 211.15	126.81	2.39 ± 0.61	5.52 ± 1.42
CO1	A2591/B5744	0.79	40.436	873.33 ± 13.03	0.315[1]	0.50 ± 0.007	638.12 ± 57.48	145.27	1.86 ± 0.23	3.76 ± 0.48
CB1	A2709/B6016	0.78	42.91	939.35 ± 23.63	0.298[2]	0.49± 0.018	407.01 ± 29.35	194.69	1.77 ± 0.16	3.60 ± 0.34
WN1	A2598/B5751	0.82	30.262	1878.50 ± 31.83	0.315[1]	1.42 ± 0.024	1819.84 ± 159.76	129.98	5.09 ± 0.52	3.57 ± 0.38
CHFS1	A2593/B5746	0.80	40.373	887.90 ± 15.14	0.318[1]	0.51 ± 0.006	1509.24 ± 75.62	100.69	3.25 ± 0.23	6.39 ± 0.49
NETFS1	A2595/B5748	0.84	40.014	927.17 ± 14.06	0.316[1]	0.53 ± 0.008	910.73 ± 130.32	162.16	3.04 ± 0.50	5.70 ± 0.94
PP-DS1	A2596/B5749	0.79	40.778	1013.60 ± 17.07	0.313[1]	0.57 ± 0.010	745.37 ± 68.81	130.52	1.90 ± 0.23	3.36 ± 0.41
KWBFS1	A2594/B5747	0.79	41.296	760.37 ± 12.59	0.314[1]	0.42 ± 0.006	741.70 ± 83.58	111.14	1.62 ± 0.22	3.84 ± 0.52
KWBDS1	A2711/B6018	0.79	40.71	723.20 ± 14.66	0.388[2]	0.52 ± 0.018	502.11 ± 22.29	157.86	1.77 ± 0.12	3.41 ± 0.25
KWBDS2	A2712/B6019	0.79	43.09	670.14 ± 18.70	0.465[2]	0.55 ± 0.022	513.99 ± 24.43	171.45	1.97 ± 0.14	3.61 ± 0.28

[a] combined atmospheric pressure/latitude scaling factor using the time-independent scaling of Dunai (2000); [b] normalised to standard KN-5-2 (Nishiizumi et al. 2007); [c] corrected for blank of 9.58 ± 2.06 x10^-15; [d] uncertainties at 1-σ; [e] 9Be carrier solution concentrations of 1) 1090 ± 15 mg.g^-1 2) 1128 ± 22 mg.g^-1; [f] 26Al/27Al normalised to SRM KN-4-2 at a ratio of 30 960 a 10^-15 (Nishiizumi 2004); [i] corrected for blank

Table 6.6 - Basin-wide erosion rates, erosion rates adjusted for burial and apparent burial ages.

Sample	Surface erosion rate (mm. ka^{-1})[b, c]	Surface erosion rate corrected for burial (mm.ka^{-1})[c, d]	Apparent burial age (ka)[c, e]
BR2	4.81 ± 0.11	3.38 ± 6.31	617.32 ± 1499.11
BW1	4.34 ± 0.14	2.38±1.55	1032.31 ± 499.93
WD-FS1	5.00 ± 0.08	4.22 ±12.98	297.55 ± 2524.30
CO1	4.31 ± 0.07	2.49 ± 2.34	939.77 ± 718.08
CB1	4.39 ± 0.17	2.17 ± 1.53	1203.67 ± 531.61
WN1	1.16 ± 0.03	0.65 ± 0.60	819.84 ± 471.08
CHFS1	4.15 ± 0.08	4.03 ±4.12	50.59 ± 837.48
NETFS1	3.92 ± 0.07	3.52 ± 7.16	186.76 ± 1633.23
PPDS1 [a]	3.66 ± 0.07	1.95 ± 1.73	1064.21 ± 646.06
KWBFS1	5.14 ± 0.10	3.08 ±3.62	885.35 ± 927.28
KWBDS1[a]	4.09 ± 0.14	1.91 ± 0.98	1287.08 ± 379.09
KWBDS2[a]	3.87 ± 0.16	1.93 ±1.09	1169.65 ± 415.7

[a] dune sample; [b] calculated using the single-nuclide-erosion tool of CosmoCalc 3.0 (Vermeesch 2007), from ^{10}Be concentrations. Uses scaling of Dunai (2000) and production mechanisms based on Schaller (2002); [c] uncertainties at 1-sigma; [d] calculated using the burial-erosion tool of CosmoCalc 3.0 (Vermeesch 2007), from ^{10}Be and ^{26}Al concentrations. This calculation does no account for any post-burial exposure events, assuming one erosion event followed by one burial event; [e] calculated using the burial-erosion tool of CosmoCalc 3.0 (Vermeesch 2007), from ^{10}Be concentrations. The calculation adjusts the surface erosion rate to account for alteration in abundances due to burial.

6.5   Discussion

6.5.1 ^{10}Be abundances

The abundances of ^{10}Be does not vary with downstream distance (Figure 6.10) and, in fluvial samples, appear to be independent of the increase in sediment cover and basin size, and the decrease in relief with distance downstream (Figure 6.11) implying a uniform exposure history.
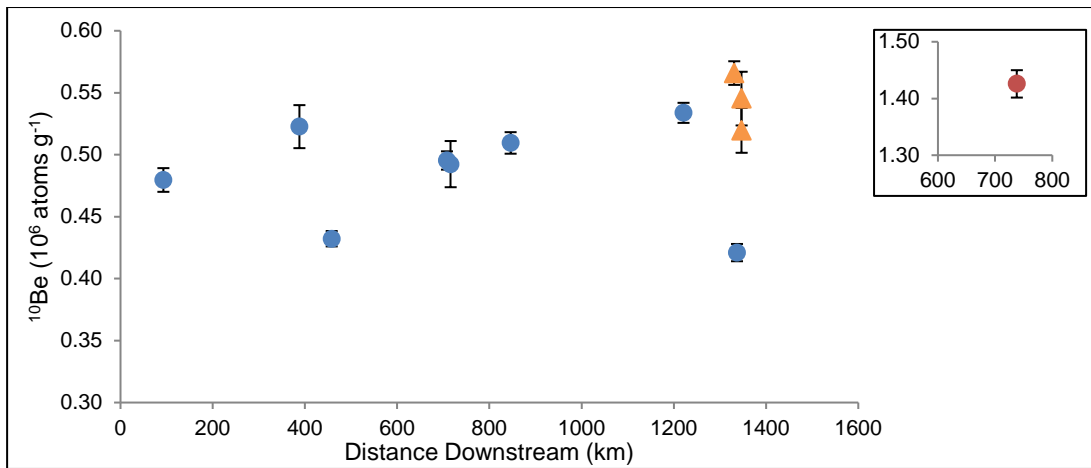
Figure 6.14 - ^{10}Be concentrations with distance downstream from the source of the Barcoo River. Showing fluvial samples from the Barcoo River and Cooper Creek (blue circles), the Wilson River (red circles) is inset, and Tirari source bordering dunes (orange triangles).
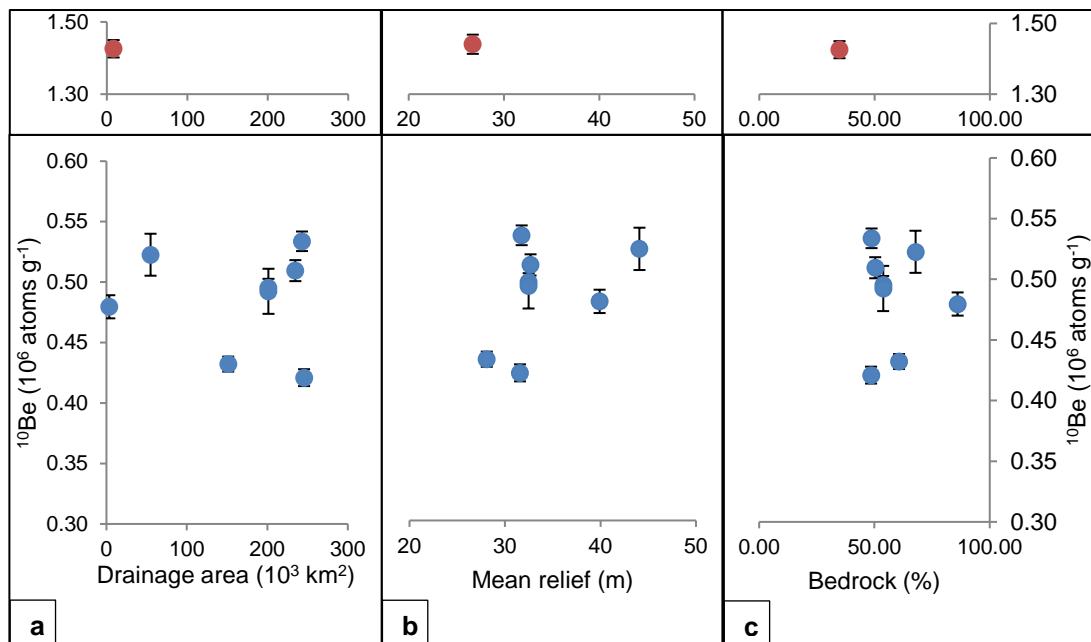
Figure 6.15 - ^{10}Be concentrations of fluvial samples compared to (a) variation in drainage area; (b) mean relief; and (c) proportion of bedrock cover. Blue circles represent the Barcoo River and Cooper Creek. The Wilson River (red circles) is inset, to allow for a sufficiently large scale to show error bars.

6.5.2 Source to sink burial signal in Cooper Creek

Cooper Creek and its headwater compose a system which is over 1000 km in length, up to 60 km wide and drains over 300 000 km^2 with a number of potential sources and storages of sediment. The potential for reworking of sediment to give an inherited burial signal is recognised in fluvial systems (e.g. Kober et al. 2009; Hidy et al. 2014; Bierman et al. 2005; Wittmann et al. 2011). Given that the ratios and apparent burial ages indicate that in parts of the Cooper Creek system there is deviation from the steady-state erosion curve and that apparent burial of up to ~1.2 Ma is occurring this is likely the case in the Cooper Creek system also. However, there is not a simple negative relationship between the nuclide ratio and the distance downstream as would be seen if there was constant, consistent reworking and transport of sediment. As with the ^{10}Be abundances there is no apparent relationship between ^{26}Al/^{10}Be ratio and the increase in sediment cover and basin size, or the decrease in relief with distance downstream (Figure 6.12; 6.13). A number of the samples overlap at one-sigma, which could be interpreted as a minimal headwater burial signal that is transmitted downstream with no additional burial. However, the correlation between reduced nuclide ratios and the large storage points along the channel leads to a two part system being proposed, with the major storage zones separated by the uplifting Innamincka Dome.
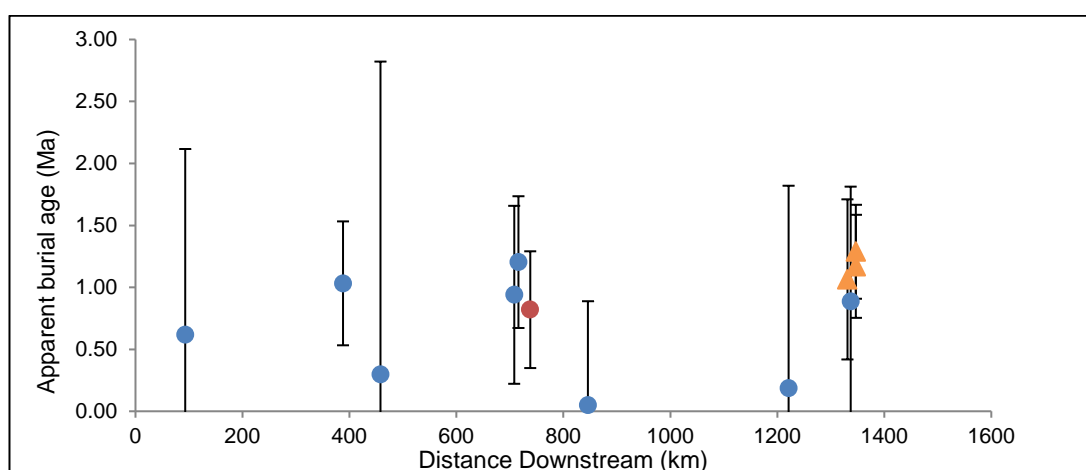
Figure 6.16 - Apparent burial age with distance downstream. Showing fluvial samples from the Barcoo River and Cooper Creek (blue circles), the Wilson River (red circles), and Tirari source bordering dunes (orange triangles). Large uncertainties are an artefact of the burial-erosion model resulting from the requirement to solve for time and erosion simultaneously (Vermeesch 2007).
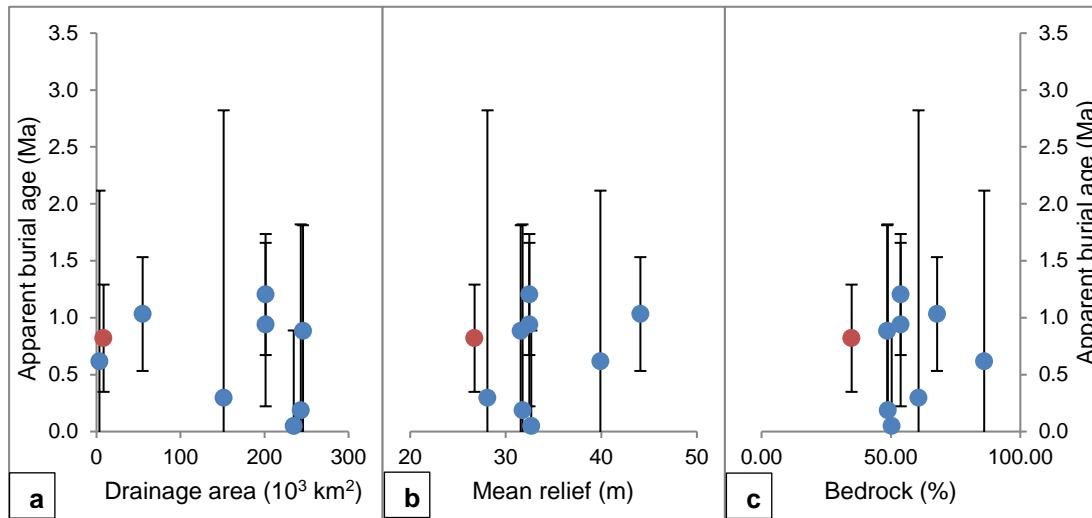
Figure 6.17 - Apparent burial ages of fluvial samples plotted against (a)drainage area; (b)mean catchment relief; and (c) proportion of bedrock cover for the Barcoo River and Cooper Creek (blue circles) and the Wilson River (red circles).

In the two part interpretation of the apparent burial ages, the upstream section of the Cooper Creek system spans from the Thomson River and the Barcoo River through the floodplain of the Cooper Creek to the bedrock constriction of the Choke (CHFS1). Within this section are five samples (BR2, BW1, WD-FS1, CO1, CB1) (Figure 6.1c).

The Barcoo River headwaters have the highest mean elevation and slope, and high average local relief (Table 6.3). The ^{26}Al/^{10}Be ratio of BR2 (5.0 ± 0.9) from Ravensbourne Creek, a tributary of the Barcoo River, is only slightly lower than the nominal production rate ratio sitting close to the steady-state erosion curve at one-sigma. The modelled ages intersect with the constant exposure ratio at one-sigma (Figure 6.8). Given the high proportion of exposed bedrock and low proportion of sediment cover (Table 6.4) it is likely that burial, if present is of minimal duration, and/or at shallow depths. The upstream catchment of BW1 incorporates the majority of the Barcoo River catchment and features an increased proportion of sediment compared to exposed bedrock at the surface relative to the upstream sample (Table 6.4). The sample exhibits a complex exposure history as shown in ratio ~3.9, equivalent to apparent burial age of ~1 Ma, which is similar to many of downstream data. Therefore it is likely that a burial signal in this upstream area is being transmitted downstream. The Barcoo River then converges with the Thomson River to form

Cooper Creek. The most upstream sample (WDFS1) marks the start of the floodplain and shows a small increase in proportion of sediment relative bedrock (Table 6.4). The ^{26}Al/^{10}Be ratio of WDFS1 is close to the steady-state erosion curve and intersects at one-sigma (Table 6.5). The apparent burial duration also overlaps substantially, given the large uncertainties, with constant exposure (Figure 6.8). The watershed of WDSF1 incorporates the entire upstream area of both the Thomson and Barcoo River, therefore any cosmogenic signal measured will combine both catchment signals. Any interpretation is not conclusive from the WD-FS1 sample due to large analytical errors.

Samples CO1 and CB1 are from near the centre of the floodplain zone. Both samples show clear deviation from the steady-state erosion curve. Both samples are fed by an upstream area with ~ 50% surface cover (e.g., alluvium, sand plains, dunes), ~20% of which is alluvium. Here it is likely that sediment is stored for extended period, as the floodplain is only active during flood events so sediment is transported infrequently. This is reflected in apparent burial ages of ~ 0.9 – 1.2 Ma (Table 6.6). This is supported by a number of luminescence ages which show a single burial event of up to 200 ka in the upper 4 m of sediment in the region directly upstream of Innamincka dome. Thermoluminescence (TL) ages from the oldest buried sediment in the LEB, at the Shire Road (~20 km downstream of CB1), of ~700 ka at 17 m depth, indicate the potential for extended burial in the system (Maroulis et al. 2007). The Shire Road is ~140 km upstream of the Choke at Innamincka, aggradation in this upstream area, where subsidence associated with the Cooper-Wilson synclinal depression is creating accommodation space, is 48 mm.ka^{-1} (Jansen et al. 2013). It is likely, therefore that large volumes of sediment are being stored in this depression before being moved further downstream.

The downstream section starts from the Choke (sample CH-FS1) (Figure 6.1c) where the channel of Cooper Creek flows through the uplifting Innamincka Dome, which is uplifting at 17 - 65 mm.ka^{-1} (Jansen et al. 2013). The channel is an approximately 30 m wide mixed bedrock-alluvial channel, constrained by a bedrock gorge with the channel incising into the uplifting anticlinal dome at a rate of 17 mm.ka^{-1}. The morphology and ^{26}Al/^{10}Be ratio, which is consistent with continuous exposure (Table 6.5; 6.6) imply that, unlike other sample sites along Cooper Creek, little deposition is occurring, but erosion of fresh material is. Due to the uplifting dome slope is decreased

upstream which, combined with subsidence of the Cooper-Wilson synclinal depression, results in the trapping of large quantities of sediment.

After flowing through the Choke, Cooper Creek flows into the Cooper Fan and from then continues as a single channel cutting through the dune fields of the Tirari and Strzelecki Deserts. Sample NETFS1 was taken at North Etadunna, at the Cooper Wet Crossing (Figure 6.1c). This sample has a $^{26}Al/^{10}Be$ ratio intersecting with the steady-state erosion curve at one-sigma, indicating a simple exposure history. Surprisingly, the ratio of this sample is not distinguishable from that of the Choke. Given that alluvial fans are considered to have high storage potential, similar to floodplains, and the Cooper Fan should be no exception given the presence of long term burial in the dunes. This is verified by thermoluminescence ages from interdune samples at Gidgealpa (Cohen et al. 2010) which show a single burial event ranging from ~ 192 to 288 ka (Cohen et al. 2010) (Table 6.7). The ratio of cosmogenic $^{26}Al/^{10}Be$ from the same samples (T. Fujioka 2018, pers. comm, 11 March) indicate apparent burial durations range from ~1.3 to 1.8 Ma (Table 6.7; Figure 6.14). These dunes are considered to have formed during times of high sediment supply from the palaeo-Cooper with periods of mobilisation during times of low sediment supply (Cohen et al. 2010), and the thermoluminescence ages represent the most recent period of stabilisation. Furthermore the distributary network of channels which occupies the Cooper Fan and runs between these dunes would likely be mobilising material and supplying it further downstream, therefore the implied constant exposure interpreted from the intersection of sample NETFS1 with the steady-state erosion curve appears to be anomalous. Alternatively, sediment in the Cooper fan may be undergoing minimal remobilisation under the current regime and the minimal apparent burial signal seen in NETFS1 is from sediment supplied at the Choke.

Table 6.7 - Thermoluminescence ages from Gidgealpa dune transect samples (Cohen et al. 2010) and cosmogenic erosion and apparent burial ages from the same samples (T. Fujioka 2018, pers comm. 11 March)

Sample	Site[a]	Location	TL age (ka)[b]	^{10}Be[c]	^{26}Al/^{10}Be[c]	Surface erosion rate (mm. ka^{-1})[d]	Surface erosion rate corrected for burial (mm.ka^{-1})[e]	Apparent burial age (ka)[f]
GGPDS1	Gidgealpa	East inter-dune at 8m	192 ± 12	0.50 ± 0.01	3.06 ± 0.23	0.54 ± 0.02	0.22 ± 0.11	1551.91 ± 378.85
GGPDS2	Gidgealpa	West inter-dune at 4m	228 ± 13	0.52 ± 0.01	3.04 ± 0.25	0.51 ± 0.02	0.21 ± 0.11	1553.98 ± 399.92
GGPDS3	Gidgealpa	West swale at 2m	239 ± 17	0.56 ± 0.01	3.51 ± 0.28	0.48 ± 0.01	0.23 ± 0.13	1274.11 ± 451.83
GGPDS4	Gidgealpa	East swale at 2m	c.245 ± 13	0.57 ± 0.02	3.18 ± 0.22	0.47 ± 0.01	0.20 ± 0.09	1448.80 ± 346.95
GGPDS5	Gidgealpa	East swale at 4m	c.288 ± 17	0.36 ± 0.01	2.74 ± 0.23	0.77 ± 0.03	0.27 ± 0.13	1821.93 ± 389.05

[a] location of transect at 27.87899 ° S 140.311 °E; [b] thermoluminescence ages from Cohen et al. (2010); [c] ^{10}Be and ^{26}Al concentrations; [d] calculated using erosion tool in Cosmocalc v3.0 (Versmeech 2007) using scaling factor of 1; [e] calculated using the burial-erosion tool of CosmoCalc 3.0 (Vermeesch 2007), from ^{10}Be and ^{26}Al concentrations. This calculation does no account for any post-burial exposure events, assuming one erosion event followed by one burial event. Uses scaling factor of 1.; [f] calculated using the burial-erosion tool of CosmoCalc 3.0 (Vermeesch 2007), from ^{10}Be concentrations. The calculation adjusts the surface erosion rate to account for alteration in abundances due to burial. Uses scaling factor of 1.
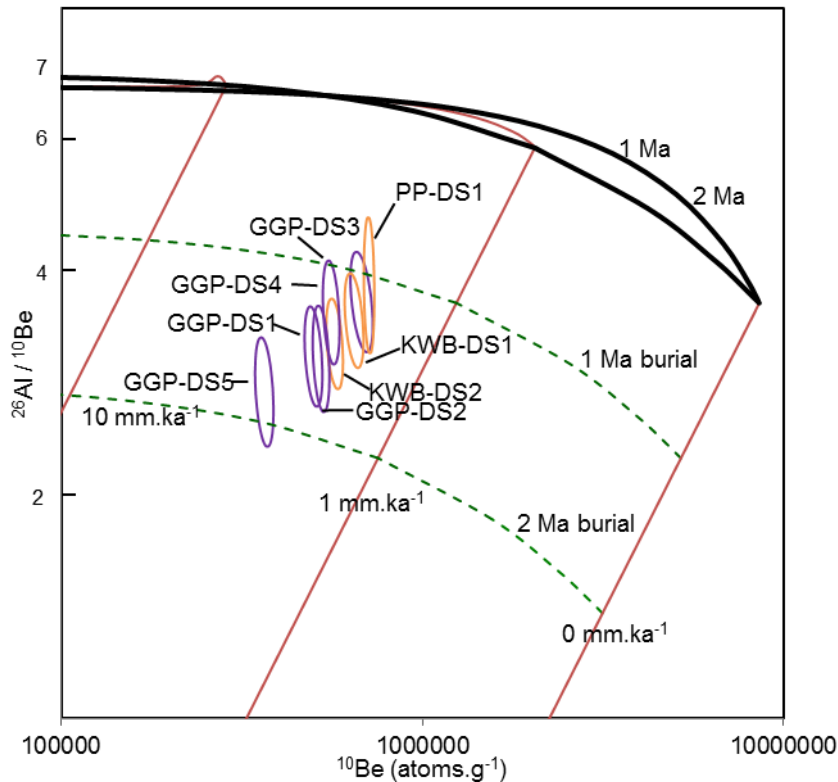
Figure 6.18 - Two nuclide logarithmic plot of $^{26}Al/^{10}Be$ ratios (normalised to sea-level high latitude) in the Tirari dunes bordering Cooper Creek at Kutjitara West Bluff (KWBDS1, KWBDS2) and Pink Pool (PPDS1) and the dunes at Gidgealpa , part of the Strzelecki dunefield on the Cooper Fan. The region between the black lines indicates a history of simple exposure/erosion with samples to the left of this region indicating a history which includes burial.

In the lowermost reaches of the channel, close to Kati Thanda-Lake Eyre, lower $^{26}Al/^{10}Be$ ratios (3.4 - 3.8) are observed, relative to further upstream in the lower section of Cooper Creek, in both the source bordering dunes (PPDS1, KWBDS1, KWBDS2) (Figure 6.8) and the channel (KWBFS1) (Table 6.5; Figure 6.9). The calculated apparent burial ages are ~1.1 to 1.3 Ma (Figure 6.12, Table 6.6) similar to data at Gidgeapla (Figure 6.14; Table 6.7). Optically stimulated luminescence ages from the main exposed section at Kutjitara West Bluff present a single burial event ranging from ~75 – 225 ka (Magee 1997). The channel cuts through these sediments allowing for mobilisation of sediment into the channel which, at times of reduced flow then becomes available for aeolian mobilisation and built into dunes. Similar nuclide data, in both concentrations and ratios, between these downstream samples (i.e., KWB-FS1, PP-DS1, KWBDS1 and KWBDS2) supports the notion of the locally interactive processes between fluvial and aeolian systems.

6.5.3   Wilson River

The Wilson River catchment is a tributary of Cooper Creek, but as it is only connected during times of elevated flow little sediment moves from its catchment into the main Cooper Creek channel. The concentration of ^{10}Be (Table 6.5) is approximately twice that of the rest of the Cooper Creek system, however the apparent burial age of ~800 ka is similar to the apparent burial ages from the floodplain zone and the channel at Kutjitara West Bluff (Table 6.6). The burial signal is likely due to characteristics which are preferential to extended burial, the Wilson River follows the line of the Wilson Syncline so accommodation space is created. There is also, the highest proportion of sediment cover in the whole of the Cooper Creek system (Table 6.4) and the lowest average relief (Table 6.3) and in addition, due to the ephemeral nature of the catchment, the sediment can remain in the same location for extended periods and not moving into the main Cooper Creek channel.

6.5.4   Denudation rates

The ^{10}Be abundances are consistent throughout the system, implying that the time sediment spends in transit is insufficient for the ^{10}Be concentration to become altered. Using ^{10}Be to calculate denudation rates assumes the average concentration is representative and that the erosion rate has been constant over time, either of which can results in an under or over estimation in the calculated value (Beirman and Steig 1996).

Catchment averaged denudation rates, uncorrected for burial, are slow, and consistent between samples, ranging from ~3.9 (NETFS1) to ~5.1 mm.ka^{-1} (KWBFS1) in fluvial samples, with the exception of WN1 which has a much lower rate of ~1.2 mm.ka^{-1} (Table 6.6). By correcting the denudation rates to account for burial of the samples, and the decrease in ^{10}Be that accompanies this, slightly slower rates from ~ 2.2 (CB1) to 4.2 mm.ka^{-1} (WDFS1) are calculated (Table 6.6). After correction WN1 remains low in comparison to the other fluvial samples at ~0.7 mm.ka^{-1}. The denudation rates for the dune samples are reduced to ~1.9 to 2.0 mm.ka^{-1} (Table 6.6).

An assumption is made that the denudation rates calculated for sediment in the channel and dunes are an accurate depiction of the denudation rates at the source, and that catchment averages are a true representation implying a homogenous sediment that is

sourced by uniform erosion. Assuming this is the case denudation rates in the Cooper Creek system are, globally, some of the lowest, lower than values of other regions with slopes <200m.m^{-1} (Willenbring et al. 2013) (Figure 6.15). There does not appear to be any downstream or locational trend to the concentrations and the similarity between the concentrations regardless of the location, with the exception of WN1, indicating that they are all likely from a similar source.
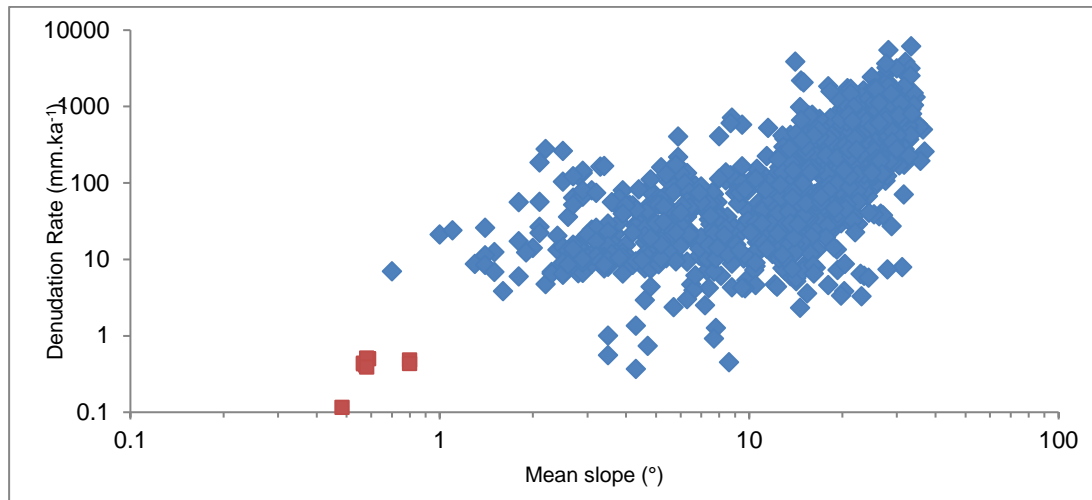
Figure 6.19 - Catchment averaged denudation rates from cosmogenic ^{10}Be against catchment slope. Dataset includes the global compilation of fluvial sediment ^{10}Be denudation rates (blue diamonds) from Willenbring et al. (2013) and the fluvial samples from this study (red squares). Slope is in degrees, from the 90m (3 arc-second) SRTM digital elevation model.

6.5.5 Comparison to other LEB rivers

Recent work in the LEB, using cosmogenic nuclide burial dating has focussed on the western LEB and includes the catchments of the Neales, Finke, and Macumba Rivers (Struck et al. 2018a; b). The eastern and western LEB have similar climates, and the rivers are all ephemeral in nature. The three catchments of the western LEB,the Macumba River, Finke River and Neales River differ in morphology and geology to the eastern LEB. The Finke River catchment's average local relief is more than twice that of Cooper Creek, however the Macumba and Neales River catchments have similar average local relief. In the Finke River catchment, the proportion of bedrock in the headwaters is higher, whereas in the Macumba and Neales River catchments the proportion of bedrock is less but the proportion that is silcrete is higher. In the Macumba and Neales River catchments there is also a greater proportion of both colluvium and gibber cover than in the Cooper Creek catchment (Struck et al. 2018a).

The presence of larger areas of silcrete and gibber cover result in a greater proportion of erosion resistant material in the supply area.

^{10}Be concentrations in the western river sediments are more varied than in the east. In the Finke River catchment the ^{10}Be concentrations are similar to Cooper Creek ranging from ~ 0.3 to 0.6 x 10^6 at.g^{-1} but lead to slightly higher catchment averaged denudation rates corrected for burial (~3.6 – 7.0 mm.ka^{-1}) (Figure 6.16a) . However, in the Neales and Macumba River catchments the ^{10}Be are generally higher, although variation is great, and give mostly lower catchment average denudation rates (~0.3 – 2.6 mm.ka$^{-1)}$ with one higher value (8.13 mm.ka^{-1}) (Figure 6.16b;c) (Struck et al. 2018a). The lower denudation rates can be attributed to the higher proportion of silcrete bedrock which is more resistant to erosion, which is not present in the eastern catchments.

In the western LEB throughput of sediment acts in an approximately linear fashion with an increase in apparent burial with downstream distance, increasing sediment cover, and decreasing basin average basin relief (Struck et al. 2018a). The apparent burial durations are similar to Cooper Creek, however Struck et al. (2018a) conclude that in the western LEB the catchments show burial signals that deviate further from the steady state erosion curve as one moves downstream with cumulative minimal burials of ~0.4 – 0.8 Ma (Figure 6.16 a;b;c). The only deviance from the correlation being where tributary inputs dilute the burial signal, as occurs in the Neales River system where tributaries from the Peak and Denison Ranges meet the main channel. The downstream increase in burial can also for all catchments, generally be correlated with a downstream increase in sediment cover and it is concluded that this is due to the combination of sediment from storages along the channel in dunes, fans, desert pavements, floodplains and palaeo-alluvial plains (Struck et al. 2018a).
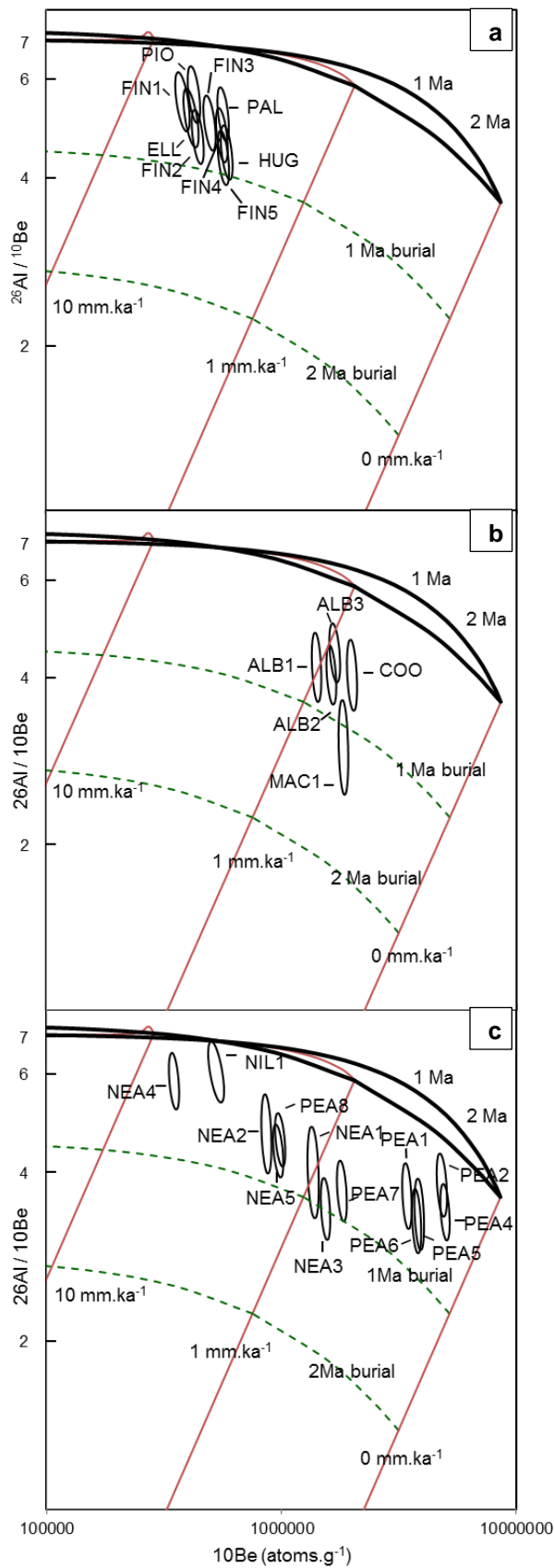
Figure 6.20 - Two nuclide logarithmic plot of $^{26}Al/^{10}Be$ ratios (normalised to sea-level high latitude) of fluvial samples from Struck et al. (2018a). (a) the Finke River catchment, (b) the Macumba River catchment, (v) the Neales River catchment.

The approximately linear increase in burial in the western rivers can be attributed to the lack of large sediment sinks within the system. Burial is generally shallow and either in the channel or in regions proximal too it. Cooper Creek watersheds are larger in comparison, and due to the presence of synclinal structures and the Cooper Fan there is greater potential for large quantities of sediment to be stored at depth. Furthermore, there is a greater availability of distal sediment and/or potential for distal storage as a result of the Tirari and Strzelecki dunefields. Apparent burial in the Cooper Creek system appears to be dictated by the morphology of the system but burial patterns elsewhere in the LEB are not controlled in the same way.

6.6 Limitations and further research

In Chapter 6 a limitation of the cosmogenic nuclide dating of Cooper Creek, is that the dynamics of the burial cannot be identified from the burial signal and that our understanding of the sediment conveyor between the Choke and Etadunna (wet-crossing) is restricted by the lack of samples. For further research, the burial durations in the lower Cooper Creek should be more closely investigated with particular reference to the burial on the Cooper Fan.

6.7 Chapter summary

The concentrations, denudation rates and apparent burial ages have been calculated for nine in-channel and three source bordering dune samples from Cooper Creek in the eastern LEB, from the headwaters in the Barcoo River to ~30 km upstream of the terminal sink at Kati Thanda-Lake Eyre. These samples have been compared to the Neales, Finke and Macumba River catchments in the western LEB and further dune samples from Gidgealpa on the Cooper Fan. The main findings of this chapter are:

1) ^{10}Be abundances are independent of the decrease in the proportion of bedrock downstream and remain unchanged throughout the system in both fluvial and dune samples, with the exception of the Wilson River, therefore a uniform exposure history is implied.

2) The Wilson River flows off the Grey Range has an elevated ^{10}Be abundance when compared to the rest of the catchment. This elevated abundance does not, however, alter the downstream signal as the Wilson catchment has very low erosion rates, ~75% less than the rest of the upstream area and is also

infrequently connected to the main Cooper Creek channel, both factors limiting long-term sediment supply.

3) Denudation rates are similar throughout the system ranging from ~1 - 5 mm.ka^{-1} which fall to the lower end of the range of global denudation rates of <0.5 to >6000 mm.ka-1 (Willenbring et al. 2013).

4) There is overlap between ^{26}Al/ ^{10}Be ratios and their inferred burial signal due, in part to large uncertainties on some samples. However, the areas of prolonged apparent burial duration coincide with the major sediment sinks within the system, which leads to the proposition of a two-part system which is divided by the uplifting Innamincka dome. The availability of accommodation space is the driver behind the variation in apparent burial duration and the cause of the differing burial trend seen in the eastern and western LEB.

Chapter 7

---

7   Island dynamics in an arid zone anabranching river

7.1   Introduction

Straight rivers, those with a single channel with a sinuosity of less than one (Leopold et al. 1964), are considered to be the optimum stationary equilibrium state of rivers (Huang et al. 2004; Nanson and Huang 2008) (Chapter 2 – Figure 2.3), however they are rarely achievable and relatively uncommon in un-engineered rivers for distances exceeding ten times the channel width (Leopold and Wolman 1957). Their rarity is due to the fact that straight rivers, through the least action principle (LAP) (Chapter 2 - 2.2.1) will commonly adjust to other planforms, through adjustment of channel slope, cross-sectional morphology, planform and boundary roughness to limit instability in order to dissipate excess energy or, conversely, to increase stream power for sediment transport.

This chapter, through single grain optically stimulated luminescence dating of sediments from fluvial islands, investigates anabranching as a means by which straight rivers adjust their form in order to increase stream power where an increase in slope is not possible, using the Marshall River on the Northern Plains in the north western LEB (Figure 7.1a). The Marshall River (Figure 7.1b;c), which lies approximately 250 km north-north-east of Alice Springs in central Australia is anabranching but, in contrast to the work in Chapters 5 and 6 of this thesis, is sand-dominated rather than carrying the muddy sediments currently seen in the Channel Country rivers.

In systems where stream power is insufficient to transport the sediment load present, a river can steepen the gradient, either through straightening the channel or by down cutting. The Marshall River is already straight and the channel bed is close to bedrock so steepening by downcutting cannot occur (Tooth and Nanson 2004). Therefore, in order to adjust stream power and transport sediment more efficiently, anabranching occurs (Tooth and Nanson 2004). The Marshall River currently anabranches but it is not known for how long it has done so or if a planform change, such as that seen in the eastern LEB and discussed in Chapter 5 of this thesis, occurred. Tooth (1999), Tooth

and Nanson (2000a), Tooth and Nanson (2004) and Habeck-Fardy (2013) have assessed the hydrological characteristics of the Marshall River and attributed its current planform to islands forming around in-channel trees which grow in greater abundance at particular locations in the trunk channel due the input of water at those locations from tributaries rising on the northern periphery of the drainage basin. There is sound evidence that anabranching in the Marshall is a means by which a dynamic equilibrium is maintained (Tooth and Nanson 2000b; Tooth and Nanson 2004). This chapter aims to build on previous work, primarily that of Tooth and Nanson (2004), and establish a chronology for the island building in the Marshall River and relate this to the ridge-formation processes and sedimentology.

7.2   Study Area

The Marshall River traverses the south-east of the Northern Plains of central Australia in the 'Alice Springs region' (Stewart and Perry 1962), to the north of a belt of ranges, consisting of the Macdonnell, Strangeways, and Harts Ranges, running in a westerly direction across the region (Figure 7.1b;c) The Marshall River rises to the north of the central ranges in the Dulcie and Mopunga Ranges, consisting of Palaeozoic crystalline rocks and sedimentary rocks overlain by Cenozoic sedimentary rocks (Freeman 1986) (Figure 7.2). The river flows for 430 km, eastwards from these ranges, draining a catchment of ~3520 km^2. In the middle reaches the Marshall River is joined to the Plenty River by a 'linking anabranch' (Figure 7.1c) after which the rivers diverge (Tooth and Nanson 2000a). The Marshall River continues to flow eastwards where it joins Arthur Creek and becomes the Hay River (Figure 7.1c), which then turns to the south and forms a floodout in the linear dunes of the Simpson Desert (Tooth and Nanson 1999; Tooth and Nanson 2004).
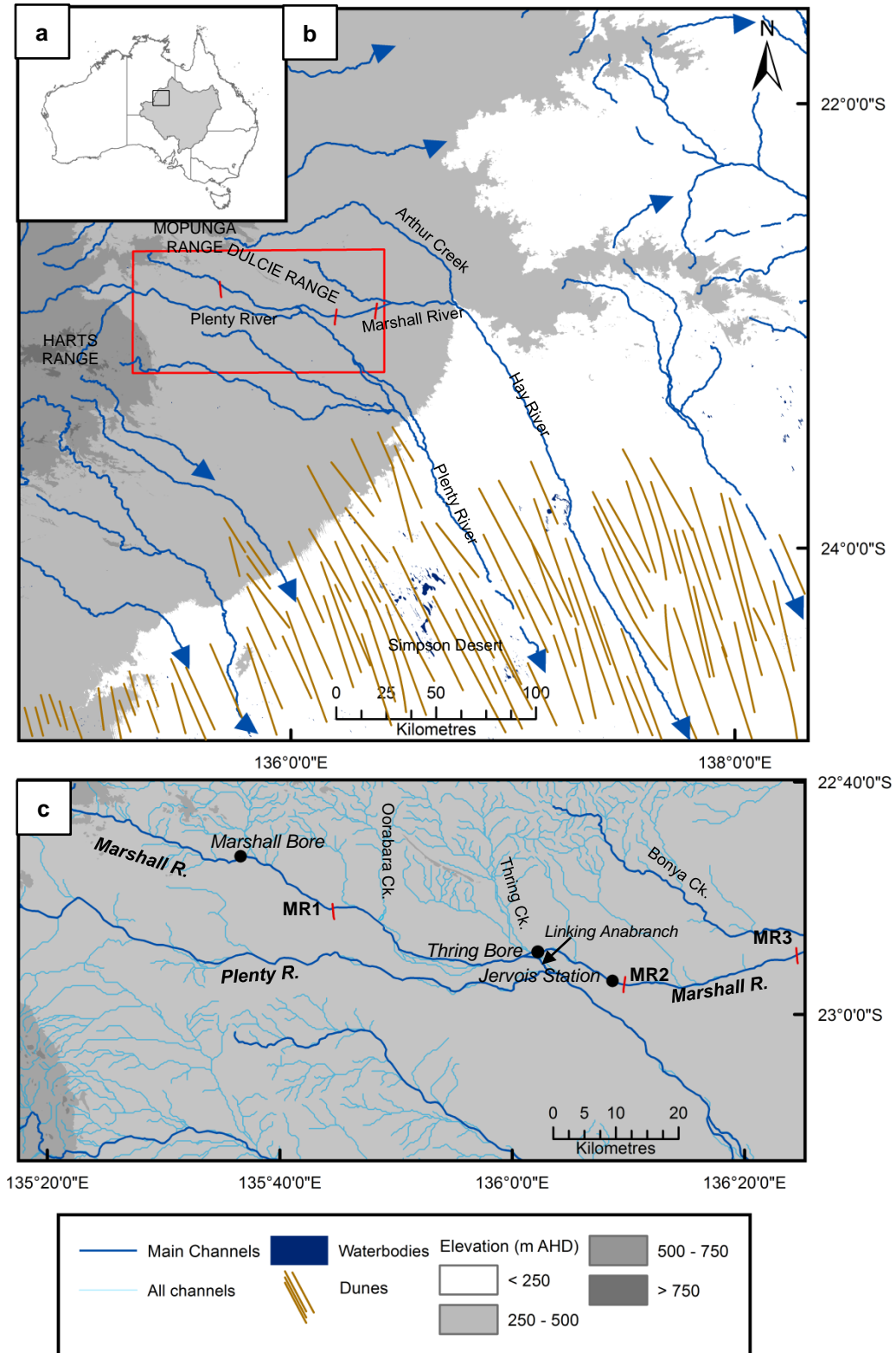
Figure 7.1 - (a) Australia with the LEB and the wider study region in the black rectangle. Cross sections discussed in the chapter are denoted by red lines; (b)The study region with the major channels, waterbodies, and dunefields marked. The red rectangle indicates the main study region for this chapter. (c) Main study area for this chapter, with major rivers and landmarks labelled. Sections discussed in this chapter are labelled MR1, MR2 and MR3.
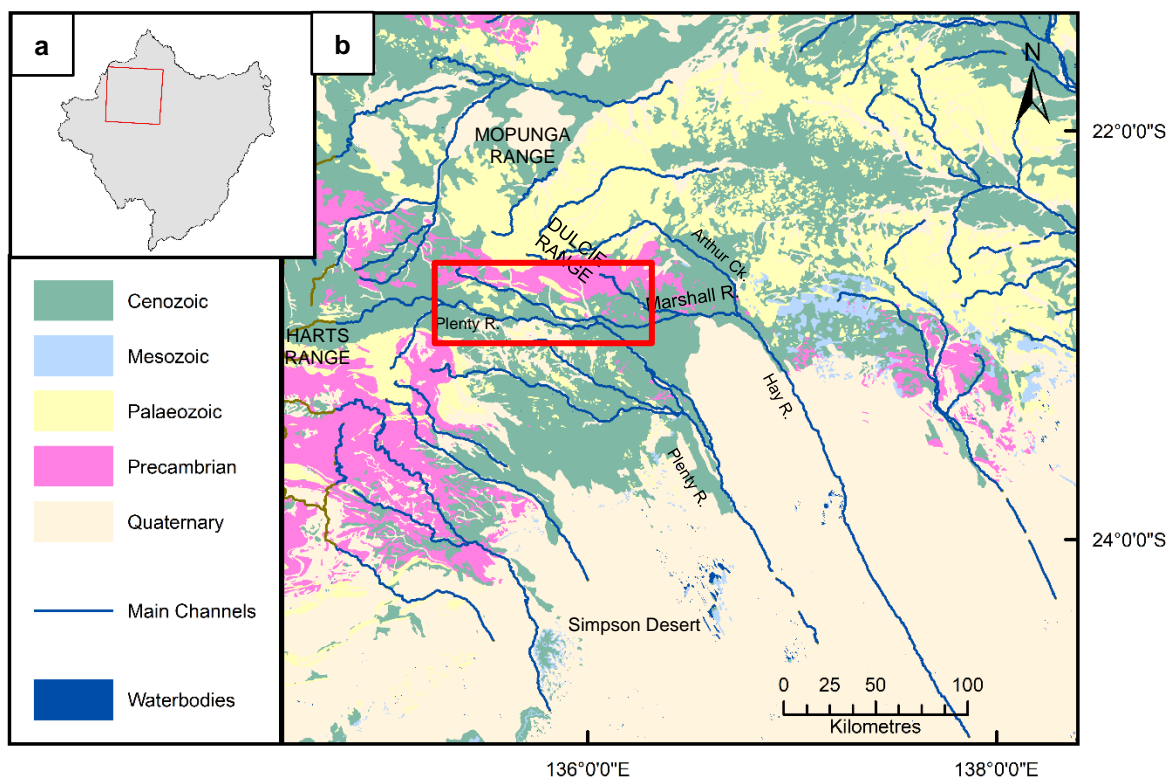
Figure 7.3 - (a) Australia with the wider study region marked in red rectangle; (b) lithostratigraphy, summarised by time period, of the study region, taken from the digitised 1:1 M scale geological map of Australia (Raymond et al. 2012).The red rectangle denotes the key study are for this chapter.

7.2.1 Climate and hydrology

The Marshall River is ephemeral, dry for much of the year, and rarely flows for its full length, which is due to low rainfall on the Northern Plains of ~300 mm.a^{-1} and pan evaporation which exceeds this by an order of magnitude at ~3000mm.a^{-1} (Tooth and Nanson 1999).

There are no rated gauging stations on the Marshall River and only limited stage heights are available at Marshall Bore (Figure 7.1c), which show that sub-bankfull flows occur in most years but overbank flows are infrequent (Tooth and Nanson 2000a). There is a 51 year rainfall record for Jervois Station (Figure 7.1c) located in the centre of the anabranching reach of the Marshall River. The average monthly rainfall from 1966 – 2018 (Bureau of Meteorology 2018) shows rainfall is highest during summer with ~40 – 60 mm per month falling during December, January and February. From April to October average rainfall does not exceed 20 mm per month (Figure 7.3). Southward incursions of moist tropical air or the easterly passage of

frontal weather systems cause occasional heavy rainfall (>100 mm.d^{-1}) and the daily, monthly and annual recurrence intervals for rainfall events from 10 mm to 150 mm (Table 7.1) show that in the 51 year record at Jervois station no daily rainfall maximum has exceeded 130 mm. Furthermore, a 100 mm.d^{-1} event associated with regionally widespread flooding is only likely to occur once in every 17.3 years. The intensity-frequency-duration (IFD) plot for Jervois Station (Figure 7.4) shows that rainfall over predicted 100 year period does not exceed an intensity of 200 mm.hr^{-1} even for short intervals of less than five minutes and that over a 72 hour time scale rainfall intensity does not exceed 5 mm.h^{-1} (Bureau of Meteorology 2016). In addition, anecdotal evidence from local landowners indicates that the channels are dry almost all year and that flood waves move slowly downstream with flow persisting at a point for a number of days or possibly weeks during high flow events (Tooth and Nanson 2004). Asynchronous tributary flow is seen throughout the Northern Plains (Tooth and Nanson 1999) and in the Marshall River localised rainfall in tributary catchments results in flows in the trunk channel for short distances downstream of the tributary junctions, whereas upstream reaches remain dry (Tooth and Nanson 2000). This rainfall, when sufficient to produce bank full flow, results in discharges (Q) that vary between channels from 2 to 1000 m^{3}s^{-1} (Habeck-Fardy 2013).
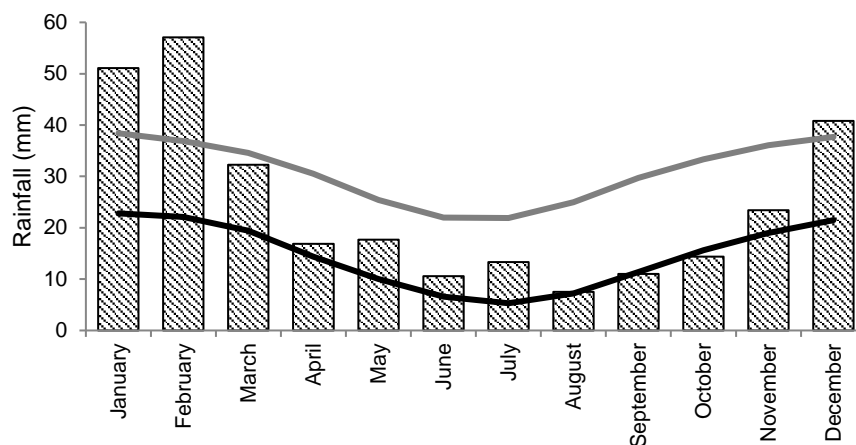
Figure 7.4 – Recent climate data for the study area showing mean monthly (bars),mean minimum (black line) and mean maximum rainfall (grey line) at Jervois Station from 1966 – 2018 (Bureau of Meteorology 2018).
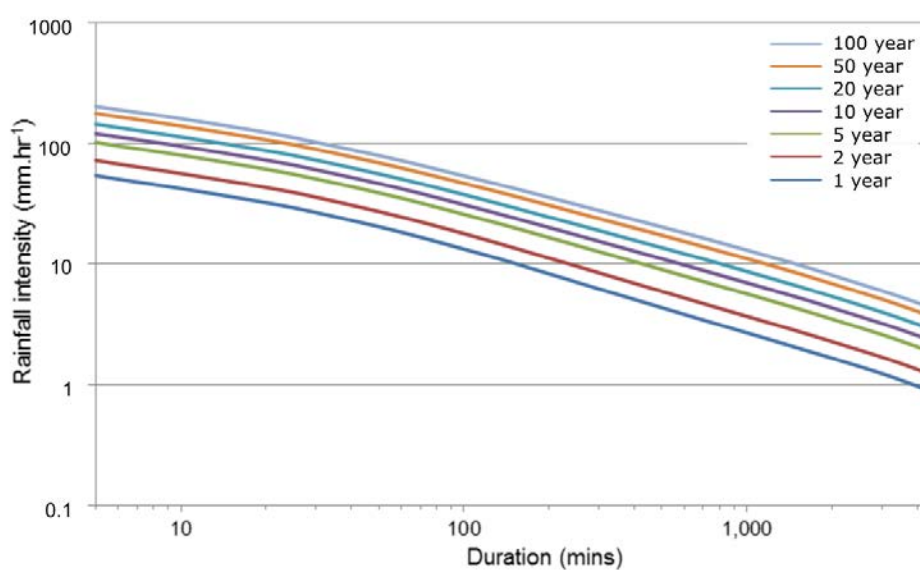
Figure 7.7 - Intensity - Frequency - Duration plot showing the 1 - 100 year frequency of rainfall intensity for event durations from five minutes to 72 hours(Bureau of Meteorology 2016).

Table 7.2 - Table of daily and annual rainfall recurrence intervals from Jervois Station using daily rainfall records from 1966 - 2018 (Bureau of Meteorology 2018)

Rainfall (mm.hr^{-1})	Number of days where maximum event exceeded	Recurrence interval	Number of years where maximum event exceeded	Recurrence interval
>5	715	26.04	51	1.00
>10	406	45.87	51	1.00
>20	196	95.01	47	1.10
>30	105	177.34	42	1.20
>40	68	273.84	33	1.60
>50	46	404.80	27	1.90
>60	29	642.10	19	2.72
>70	20	931.05	14	3.70
>80	12	1551.75	8	6.50
>90	5	3724.20	5	10.40
>100	3	6207.00	3	17.30
>110	1	18621.00	1	52.00
>120	1	18621.00	1	52.00
>130	1	18621.00	1	52.00
>140	0	0.00	0	0.00
>150	0	0.00	0	0.00

7.2.2 Channel pattern and geometry

For its entire length the Marshall River is classified as a straight river and it alternates between single thread and anabranching with strongly anabranching reaches alternating with shorter reaches where large islands are absent and ridges are juvenile, poorly developed, or absent. The upper Marshall River is laterally stable with single thread, low sinuosity (P≤1.15) (Tooth and Nanson 2004) rocky channels transporting sand and gravel bedload (Tooth and Nanson 1999). In the middle reaches the rocky channels merge into larger channels flowing west to east through a wide valley of low relief plains bordered by low ranges of crystalline and sedimentary rocks and isolated mesas with caps of Tertiary limestone (Mabbutt 1965; 1967; Freeman 1986; Tooth and Nanson 1999) (Figure 7.2). The channel is bordered by narrow floodplains which are rarely more than 50 m wide, confined by bedrock outcrops and indurated alluvial terraces or aeolian sand deposits (Tooth and Nanson 2004).

The middle reaches of the Marshall River mostly anabranches with a number of channels divided by both narrow ridges and broad islands. These two types of island indicate two types of anabranching: 'type 2' – sand dominated island forming and 'type 4' – sand dominated ridge forming (Nanson and Knighton 1996). These forms coexist in places where the channel train is subdivided around large 'type 2' islands with the individual channels then featuring 'type 4' ridges. The middle reaches of the Marshall River are joined by large tributaries, namely Oorabara Creek, Thring Creek, Bonya Creek, and Arthur Creek (Figure 7.1c), which rise in the ranges that flank the northern edge of the catchment and input coarser gravelly sediment. The trunk stream has a low slope (0.0011 – 0.0015 m.m^{-1}) and carries a coarse sand bedload with occasional gravels. Once the Marshall River joins with Arthur Creek they become the Hay River and continue to anabranch until they dissipate as floodouts in the dunefields of the Simpson Desert (Tooth and Nanson 1999).

In reaches with 'type 2' anabranching, broad alluvial islands up to ~600 m wide are flanked with low sinuosity channels (*P* = ~1.03 – 1.12). In reaches with type 4 anabranching, closely spaced low sinuosity channels are separated by narrow ridges up to 10 m wide aligned with the average flow direction within the main channel train.

The number of anabranches at any given point within the channel train varies from two to eight and bankfull cross sectional areas of the individual anabranches varies

from <10m^2 - ~200 m^2 with well-vegetated, well-defined, steep (>40°) banks (Tooth and Nanson 2004). Anabranching reaches appear to be stable on a decadal scale with few detectable changes in aerial photographs even after large flood events (Tooth and Nanson 1999). Aerial photographs from 1950 – 1980 show no substantial change in anabranching reaches, however, the in-channel changes are likely too subtle to be detected in aerial imagery (Tooth and Nanson 2004) and long term changes or stability have not yet been quantified. Further evidence for channel relative-stability are the mature trees (discussed below) that line many channel banks and ridge-form islands.

The individual anabranching channels vary in morphology with width/depth (W/D) ratios from 10 to 200, although where anabranching is well developed w/d ratios are more consistent, from 20 – 40 (Tooth and Nanson 1999). The channels are dominated by a sandy bedload with a mean grain size of 1.3 mm, the coarseness of which is attributed to the coarse grained source rocks both in direct source area and the source area of the tributaries (Tooth and Nanson 2004). Channel beds are mostly planar with only occasional dunes.

7.2.3 Islands and ridges

Tooth and Nanson (1999) differentiate between ridges (Type 4) and islands (Type 2) in an arbitrary manner by the length to width ratio. Islands have a length to width ratio less than 10 and ridges have a length to width ratio greater than 10. Islands can be a number of shapes, commonly streamlined with some slightly irregular forms The construction method can be defined as either depositional or erosional. Those which are formed by in situ depositional processes consist of a finer grained outer layer from silty sand to mud that encases a core of coarser sand to gravel material (Tooth and Nanson 2000a). The top of the sand and gravel core is generally slightly elevated above the channel bed and is overlain by finer grained units varying in number, texture and thickness dipping at 30 – 60º down from the centre (Tooth and Nanson 2000a). The boundaries between these units are indistinct and sedimentary structures within the islands are rare but but trough cross-beds or opposed planar cross-beds with forests are seen (Tooth and Nanson 2000a).

The erosional islands/ridges occur less frequently and are caused by cutting of the floodplain, with further depositional forms in the excavated channels (Tooth and Nanson 2000a).

7.2.4 Vegetation

Large trees (mostly *Eucalyptus* spp.), shrubs (e.g. *Acacia* spp. and *Melaleuca* spp.) and perennial grasses (e.g. *Eulalia fulva* and *Bothriochloa ewartiana*) populate the upper and middle reaches of the Marshall River with well vegetated near channel margins and the channel-back lines. The channel beds and larger 'type 2' islands are also populated by mature *Eucalyptus camaldulensis* (river red gum) where they are able to access moisture and reach maturity (Tooth and Nanson 2004). The 'type 4' ridges are more commonly populated by *Melaleuca glomerata* (white tea-tree) which, along with perennial grasses, are essential for the stabilisation and maintenance of the islands.

Ridges and islands are relatively densely vegetated with large trees, shrubs and swards of grass (>1 tree per 100 m^2). In-channel density is <1 tree per 1000m^2 (Habeck-Fardy 2013).

7.3 Samples site selection

The study reach covers ~70 km; 40km upstream and 30 km downstream of Jervois Station (Figure 7.1c). Three cross sections were chosen using the work of Tooth and Nanson (2004) and Habeck-Fardy (2013) as a guide. These sections show the variety of island/ridge types within the study reach. MR1 corresponds to M1b (Tooth and Nanson 2004) representing 'type 2' anabranching (Nanson and Knighton 1996), MR2 is located between M5 (Tooth and Nanson 2000) and M5u (Habeck-Fardy 2013) and represents a mix of 'type 2' and 'type 4' anabranching (Nanson and Knighton 1996). MR3 represents 'type 4' anabranching (Nanson and Knighton 1996). The sampling sites are summarised in Figure 7.5 and Table 7.2.
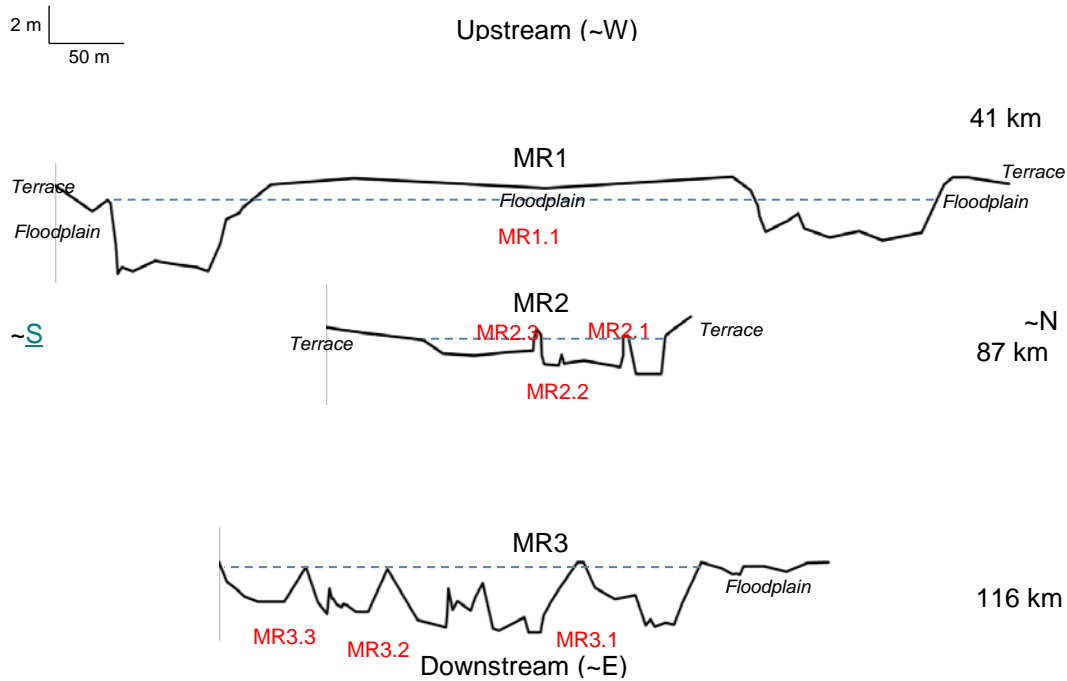
Figure 7.9 – Cross-sections of the Marshall River surveyed. Scale applies to cross-sections only. Downstream distance is not to scale. Dashed line indicate bankfull level of whole channel-train. Location of cross sections marked in Figure 7.1c.

Table 7.4- Location of drilled ridges and islands from three cross sections of the Marshall River.

Site	Coordinates	Ridge/island width at base (m)	Ridge/Island length (m)[1]	Length/Width ratio	Island/Ridge (I/R)[2]
MR1.1	22° 50' 58.9" S 135° 45' 56.4" E	1001.20	8000.00	7.99	I
MR2.1[3]	22° 57' 26.1" S 136° 09' 18.7" E	9.96	278.31	27.94	R
MR2.2	22° 57' 28.0 "S 136° 09'17.7" E	2.32	175.11	75.48	R
MR2.3	22° 57' 23.1" S 136° 09' 3.7" E	6.64	133.65	20.13	R
MR3.1	22° 54' 20.8" S 136° 25' 56.5" E	13.01	65.20	5.01	I
MR3.2	22° 54' 21.8" S 136° 25' 56.7" E	23.01	95.67	4.16	I
MR3.3	22° 54' 22.3" S 136° 25' 56.9" E	12.30	420.01	34.15	R

[1]*Distinction between island and ridge is based on Tooth and Nanson (1999) ratios <10 denoting an island and ratios >10 denoting a ridge;.*[2]*This island width is for the main part of the island seen in Figure 7.5 not including the stepped section to the right side as this is interpreted as a second island which has joined together*

M1 is ~41.4 km downstream of the start of the Marshall River and features two main channels divided by a substantial island (Figure 7.1; Figure 7.5; Figure 7.6 b;c)). The transect is 650 m wide. The island is approximately 1 km wide and 8 km long with its surface about 3.5m above the channel bed. It is populated with a mature population of trees and grasses in the form of a savannah. *Triodia spp.* and *Pletrachne spp.* are the dominant grasses and the trees are mostly *Eucalyptus camaldulensis* and *Acacia spp.* One hole was drilled at 195 m from the RH side of the Island.

Cross section MR2 is ~87 km downstream of the start of the river, located downstream of the linking anabranch between the Marshall and Plenty Rivers, and features three ridges along with other smaller bed features and juvenile islands (Figure 7.1; Figure 7.5). The section is ~210 km wide. The ridges are defined as such due to having a length/width ratio of more than ten, ranging from 20 to 75. The ridges range from 2 to 10 m wide and 134 to 278 m long. The ridges are well populated by grasses and gumtrees. The left anabranch is lower than the others increasing in height left to right. The central ridge, MR2.2 (Figure 7.6 d;e), is smaller and more immature than the others with minimal vegetation.

Cross section MR3 is located between M5 and M5u (Habeck-Fardy 2013) (Figure 7.1; Figure 7.5). It is located ~116 km downstream of the start of the river and features three large ridges/islands, ranging from 12 to 23 m in width and 65 to 420 m in length, and a number of smaller ridges (<1 m wide). The transect is ~410 m wide. The right-most feature (facing downstream) is MR3.1, with MR3.2 (Figure 7.6 f;g), and MR3.3 from right to left. MR3.1 and MR3.2 are defined as islands with length/width ratios of 5 and 4 respectively. MR3.3 is defined as a ridge with length/width ratio of 34. Both the ridges and islands are populated by savannah type vegetation with the dominant tree species being *Melaleuca glomerata.* On their section M5u, which is morphologically similar to MR3, Habeck-Farby (2013) conducted a point centred quarter stem density and concluded ~20 stem/ 100 m^2 which is considered sufficiently dense to affect channel density and act as a barrier to flow (Habeck-Fardy 2013).
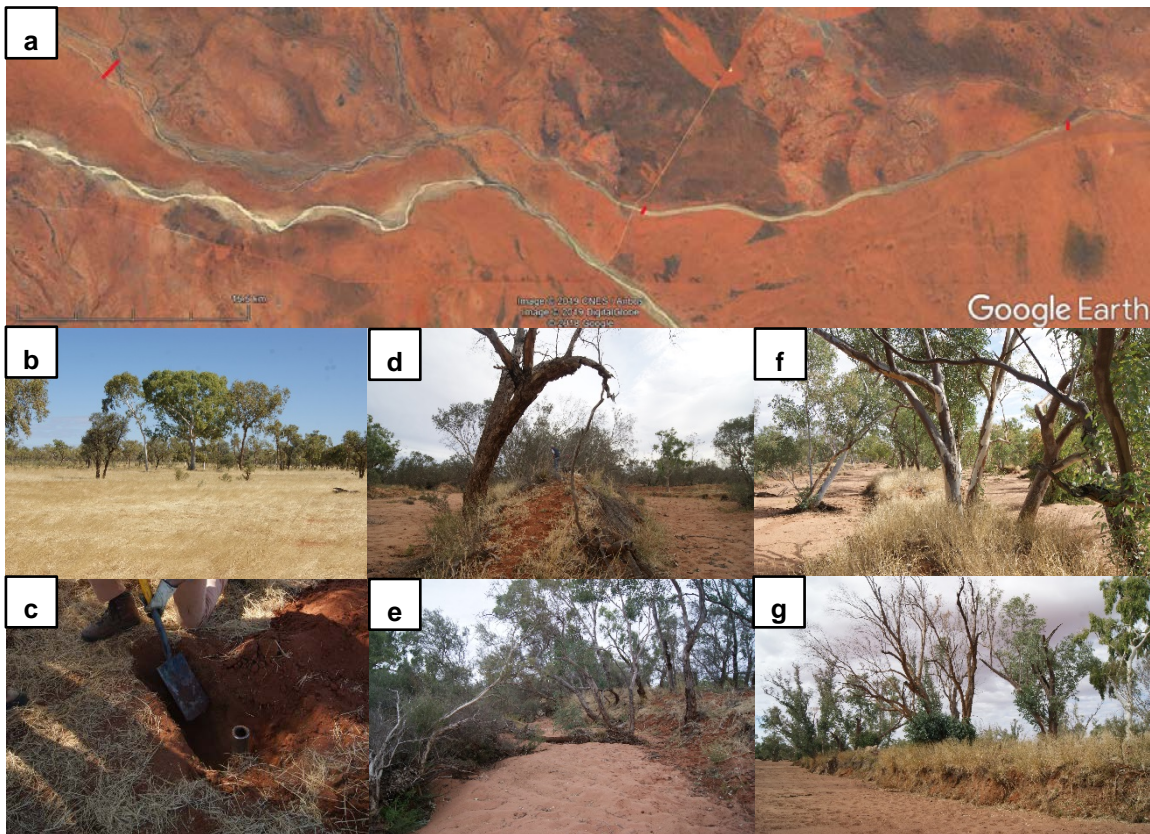
Figure 7.6 - Photos of sampling locations. a) Google earth image showing location of cross-sections. Red lines showing cross sectionc correlate to Figure 7.1; b) MR1- Island surface; c) MR1 - sediment; d) MR2.2 – island looking downstream; e) MR2.2 – looking along island in downstream direction; f) MR3.2 – looking downstream from island surface; g) MR3.2 – looking along island in downstream direction.

7.4 Methods

7.4.1 Sample collection

In the Marshall River 14 OSL samples were taken from a total of seven islands and ridges in core-holes drilled along the three transects, MR1, MR2 and MR3 (Figure 7.5). One additional sample (MR-SS-1) was taken from the channel bed surface to act as a modern analogue to test for any likely residual luminescence within the core-hole samples at the time of their deposition.

Samples were collected using a Cobra percussion auger with black PVC light-safe liners inside the core barrel to prevent sunlight exposure. Cores were packed and sealed to prevent light exposure and mixing of sediments in transit. The channel surface sample was collected at night from approximately 5 cm below the channel surface as this is representative material in transport as suspended or bedload under current flow conditions) and was sealed in light-safe black PVC.

Cores were drilled at the approximate apex of the islands to the depth where the island intersects with the original channel bed. These cores were split under subdued red light conditions and were subsampled at 10 cm intervals for grain size analysis. Two OSL samples were taken from each core; one at ~50 - 60 cm depth and one close to the base of the core, where a change to a coarser grainsize was visually identified that is likely to represent the channel bed prior to island formation at that point. For each sample an accompanying dosimetry and water-content sample was taken. The sampling strategy was designed to identify: 1) If there was a difference in the age of the islands downstream; 2) If there was a difference in the age of islands from laterally across the channel; 3) To establish a basal age for the islands; 4) To identify if there is a significant age difference between the narrow ridges and the more three dimensional islands.

Table 7.5 - OSL samples and their cores, with sampling depths and location in the core.

OSL code	Section	Island name	Depth (m)	Location in core[1]
MR-SS-1	MR3	Channel	0	Surface
MR1676	MR3	3.1	60	Top
MR1682	MR3	3.1	320	Bottom
MR1683	MR3	3.2	60	Top
MR1748	MR3	3.2	345	Bottom
MR1686	MR3	3.3	60	Top
MR1750	MR3	3.3	280	Bottom
MR1751	MR2	2.1	55	Top
MR1753	MR2	2.1	155	Bottom
MR1754	MR2	2.2	60	Top
MR1756	MR2	2.2	160	Bottom
MR1757	MR2	2.3	50	Top
MR1759	MR2	2.3	160	Bottom
MR1741	MR1	1.1	55	Top
MR1744	MR1	1.1	164	Bottom

[1]*Samples taken from the top are close to the top of the island, those taken from the bottom are close to the interface between island/ridge deposit and original channel bed.*

7.4.2 OSL Chronology

7.4.2.1 Sample preparation and measurement

OSL samples were prepared for single grain analysis of 180- 212 μm quartz using the standard quartz extraction and purification method of Wintle (1997) the chemistry and methodology of which is detailed in Appendix D – D.2. The samples were sieved to extract the 180-212 μm fraction, which was then immersed in 10% HCl to remove carbonates. There was no evidence of reaction for any sample, so the samples were assumed to contain minimum carbonate. The samples were cleaned and immersed in 10% H_2O_2 for 24 hrs to remove organics and cleaned. This step was repeated three times due to the large amount of organics, especially in the uppermost samples, likely due to the sample site being located on cattle grazing land and the presence of small

roots from lower plant species. The samples were then re-sieved at 180 and 212 μm to remove any smaller grains that had been disaggregated during the sample preparation, this was followed by density separation with sodium polytungstate (SPT) to isolate the quartz grains; first at 2.7 g cm^{-3}, to remove heavy minerals which constituted approximately 5 – 10% of the sample then at 2.62 g.cm^{-3} to remove feldspars. Feldspar content was minimal. The samples were then etched with 40% HF for 40 minutes to remove the outer, alpha irradiated layer, and to remove any feldspars that had not been removed by density separation and sieved again at 180-212 μm to remove grains reduced in size by etching.

Single grains of the samples were then measured using a Risø TL/OSL reader fitted with a U-340 filter to measure ultra-violet light emitted from quartz. Measurements use the single aliquot regenerative (SAR) dose protocol (Murray and Wintle 2000) on single grains.

7.4.2.2   Dosimetry

Samples for dosimetry measurements were dried, and crushed to a fine powder using a Tema disc mill to give a homogenised sample. Water content, at time of sampling, was measured by weighing the sample before and after drying using Equation 7.1.

$$M_n = ((W_w - W_d)/W_w) \times 100$$

Equation 7.1 - Equation to calculate water content of a sample where M_n = moisture content (%) of sample; W_W = wet weight of the sample; W_d = weight of the sample after drying.

Environmental dosimetry was measured using inductively coupled plasma mass spectrometry and inductively coupled plasma optical emission spectrometry (ICP-MS/OES); Geiger-Mueller beta counting and thick source alpha counting (GMBC and TSAC); x-ray fluorescence (XRF); and high resolution gamma spectrometry (HRGS). The values obtained by these methods were converted to dose rates using the conversion factors of Guérin et al. (2011). The cosmic dose rate contribution for each sample was determined as per Prescott and Hutton (1994) and β-attenuation factors were taken from Mejdahl (1979).

7.4.2.3   Grainsize analysis

Grainsize samples were taken from all cores at 10 cm intervals and measured by laser diffraction using a Malvern Mastersizer 2000, which outputs the percentage of clay,

silt, and sand, the sorting and the mean grainsize amongst other variables, for the <1.5 mm grainsize fraction. The >1.5 mm fraction, where present, was weighed and calculated as a percentage weight proportion of the whole.

7.5   Results

7.5.1   Island and ridge forms

The following section draws upon planform observations supplemented with some field observations. Islands and ridges in the Marshall River tend to have streamlined forms with long axes parallel to the direction of flow and are typically elongate in shape or lemniscate tapering downstream. Island and ridge form anabranching can co-exist. Ridges can occur within the channels that are divided by islands. The ridges and islands vary in size but the majority are, in planform, either downstream lachrymiform (tear-drop) (Figure 7.7c) or elliptical in shape, streamlined to the direction of flow (Wyrick and Klingeman 2011) (Figure 7.7e). Islands and ridges tend towards a narrow flow-aligned, streamline shape in order to minimise drag. Some larger lenticular islands are also present, which although wider are also streamlined (Figure 7.7a; d). The islands (L/W ratio <10) and ridges (L/W ratio >10) can be either erosional or depositional. Those which are excised are predominantly islands and can be several hundreds of metres to several kilometres in length (Figure 7.7a). They are mostly lenticular in shape, although some tend towards a more elliptical geometry. These erosional islands are formed by erosion of the existing flood plains either through avulsion of a channel or from rapid incision by flood channels into the sediment (Osterkamp 1998). In general erosional islands are larger than depositional islands and ridges, erosional ridges not appearing to exist. Two modes of excisional island are seen: (1) where the avulsion is essentially permanent and the channel path is changed or the secondary channel is subsequently abandoned and conditions return to unilateral flow leaving a hemispherical form (Figure 7.7b), and (2) where channel avulsion is temporary and the original channel is reoccupied in subsequent flows to give bilateral flow (Figure 7.7a).

Depositional islands and ridges tend towards a more elliptical shape once established, although some remain lenticular. Juvenile islands/ridges are commonly lachrymiform, a shape which Tooth (1997) attributes to the formation in current shadows, where

sediment is deposited on the lee side of an obstacle where current velocity is reduced. In the Marshall River this is commonly on the downstream side of in-channel trees (Figure 7.8). In-channel trees are substantial obstacles and it appears that they may be an inception point for the islands. This has been described in other similar rivers on the Northern Plains such as the Sandover-Bundy River (Tooth 1997) and is a similar process to that described by Morón et al. (2017) on the Neales River whereby the inception of anabranching islands is controlled by the presence of sandbars. Once the islands are initiated their growth depends on colonisation by vegetation, preventing scour. In terms of the interaction with flood flow it is likely that some islands form in favourable positions so are more long-lived. Bedform formation in straight rivers has commonly been attributed to helical secondary flow (HSF) (e.g. Allen 1982; Nezu et al. 1985) and this theoretically could be extrapolated to island formation processes (Tooth 1997), however in the case of the Marshall River it is excluded as a primary formation process as the process would result in a regularity which is not seen here in terms of spacing and height (Tooth 1997). Furthermore the infrequent and irregular flows would not be conducive to island formation by HSF (Tooth 1997).
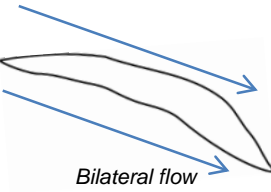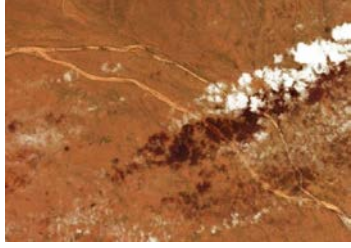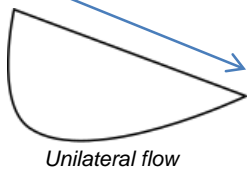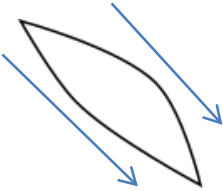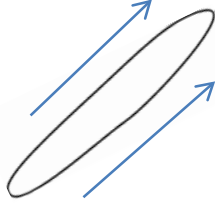
Formation type	Shape[1]	Examples[2]

Figure 7.7 - The types of islands and ridges seen on the Marshall River. For both excisional and depositional formation, the shapes of the islands seen on the Marshall River are shown in outline and with an example from aerial footage. [1] Shapes taken from definitions in Wyrick and Klingeman (2011), with the exception of lachrymiform which is described by Wyrick and Klingeman (2011) as lemniscate. Arrows show direction of flow. [2] Aerial images from DigitalGlobe (2017).

Direction of flow ⟶   **1 m**
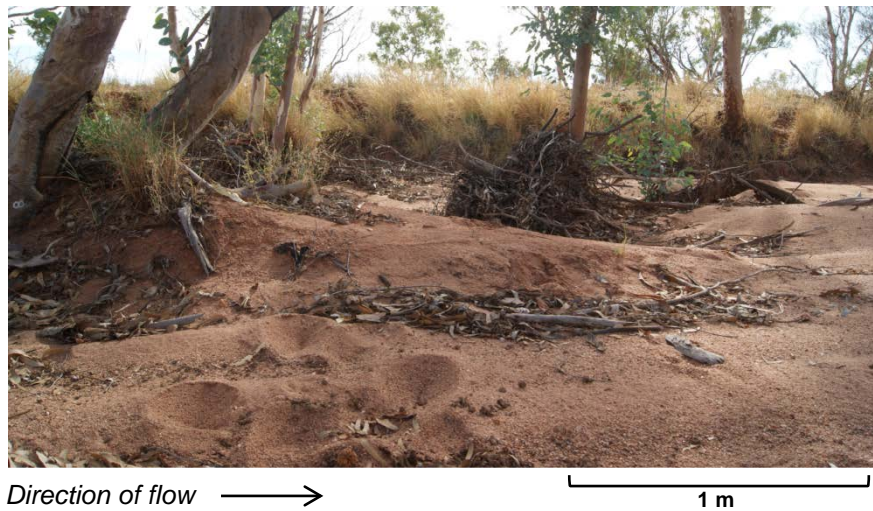
Figure 7.8 - Formation of a downstream lachrymiform island, in a current shadow on the ley side of an in-channel tree

7.5.2 Sedimentary composition

The general sedimentology of the islands and ridges in the Marshall River varies from coarse sand to silt. There is little distinctive stratigraphy in the cores or in eroded banks and no evidence of erosional boundaries within the stratigraphy. The boundaries are indistinct and organic material is common throughout. All cores from depositional islands and ridges show a degree of coarsening towards the base of the core (Appendix E – Figure E.2 b-g). The basal layer of coarser sand, where reached, is likely representative of the channel bed prior to island formation. In places this is below the level of the current channel bed, suggesting that in some places there has been subsequent channel-bed accretion after the islands or ridges have formed.

Island MR1.1 (Appendix E – Figure E.2a) is interpreted as an excisional or floodplain island initially due to its larger size as observed by Tooth and Nanson (2000). The sediments were also typical of floodplain deposits with a finer grain size and greater compaction than seen in the other islands and ridges. Furthermore the vegetation is more mature than on the other ridges and islands, suggesting greater longevity. The island also shows no evidence of current shadow deposition as a formation process. The surface is also not domed towards a ridge form along its length as is the case for depositional islands and ridges (Figure 7.5), but slightly concave similar to the surface morphology of a floodbasin created by low levees at its margins. Table 7.4 presents the mean grainsize of MR1 which ranges from 95-33 μm. The percentage of clay in

MR1.1 ranges from 2- 6% and silt from 23.0- 63%. Sand proportions range from 32-75% with sand dominating in the upper 1.4 m of the core and silt becoming dominant below this.

The depositional islands and ridges are generally coarser than the excisional island with mean grainsizes varying from 42- 792 μm, however there is no distinct grainsize difference between the depositional forms. All depositional islands and ridges have low proportions of clay ranging from 0-5% and silt from 3-49%. Sand is consistently the dominant grainsize making up 46-97% of the sedimentology. The mean grainsizes are generally higher from the bases of the cores (Appendix E – Figure E.2 b-g; Table E.1 b-g). Sorting, expressed as standard deviation of the grain size, is generally consistent for the excisional island with values from 1-2 μm. For depositional islands the range is greater from 0-2 μm.

Table 7.6- Summary of grainsize distributions: Means, minimums, and maximums of grainsize contributions from clay, silt and sand, mean grainsize and sorting for each core.

Core (n=# samples)	Clay (%)			Silt (%)			Sand (%)			Mean grainsize (µm)			Sorting (ø)		
	Mean	Min	Max	Mean	Min	Max	Mean	Min	Max	Mean	Min	Max	Mean	Min	Max
MR1.1 (n=28)	4.20	1.67	6.47	42.06	22.96	62.93	53.74	32.00	74.52	56.62	33.18	95.17	1.86	1.33	2.34
MR2.1 (n=17)	1.73	0.00	4.62	25.56	12.04	48.92	72.71	46.46	86.54	100.17	42.22	186.29	1.33	0.69	2.19
MR2.2 (n=16)	1.28	0.00	3.12	22.48	10.58	41.51	76.24	55.37	89.42	112.33	62.48	175.54	1.41	0.93	2.04
MR2.3 (n=17)	0.95	0.00	3.03	19.45	6.85	31.78	79.60	65.19	93.15	124.48	80.55	175.38	1.35	0.87	2.01
MR3.1 (n=35)	1.71	1.55	5.36	25.37	8.16	44.46	72.92	50.19	91.20	105.46	43.24	340.50	1.07	0.16	2.21
MR3.2 (n=36)	0.12	0.00	0.37	17.09	3.23	27.70	82.18	70.72	96.77	157.48	85.52	415.33	1.25	0.72	2.00
MR3.3 (n=30)	0.75	0.00	2.99	16.07	4.29	39.90	83.17	57.10	95.48	193.88	69.63	792.25	1.24	0.86	1.97

7.5.3 Island chronology

7.5.3.1 Dose recovery tests

Dose recovery tests are described in detail in Appendix D – D.4. The dose recovery tests were conducted at four different preheat/cutheat combinations on one sample using a single aliquot regenerative dose protocol (Murray and Wintle 2000) on single grains, with bleaching by exposure to sunlight for 48 hours prior to measurement. The sample was irradiated for 100 s at ~0.073 Gy.s^{-1} to give a dose of ~7.3 Gy. Five discs were measured for each of four different temperature combinations, each using a 160°C cutheat (PH2) and preheat (PH1) of 180 °C, 200 °C, 220 °C and 240 °C. For each of four temperature combination five discs (500 grains) were measured (except 180 °C/160 °C where four discs (400 grains) were measured). A weighted mean was calculated using the central age model (Galbraith 1999) and this value calculated as a ratio to the given dose (Table 7.5).

Table 7.7 - Results of dose recovery tests at four different preheat-cutheat combinations. Measured dose is presented in βs as a weight mean calculated using the central age model (Galbraith et al. 1999)

PH1	PH2	Number grains		Given Dose (βs)	Measured Dose (βs) (CAM)	Measured to given ratio	OD%
		Measured	Accepted				
180	160	400	114	7.3	7.26 ± 0.07	0.99 ± 0.02	4.99 ± 0.99
200	160	500	117	7.3	6.47 ± 0.11	0.89 ± 0.02	14.63 ± 1.52
220	160	500	68	7.3	6.49 ± 0.15	0.89 ± 0.03	13.43 ± 2.11
240	160	500	116	7.3	6.35 ± 0.12	0.87 ± 0.02	15.84 ± 1.56

The temperature combination of 180 °C/160 °C gives the highest proportion of accepted grains and has dose recovery closest to unity (Figure 7.9) and with the lowest standard error. The overdispersion is also lowest for this temperature combination indicating the least scatter in the results.
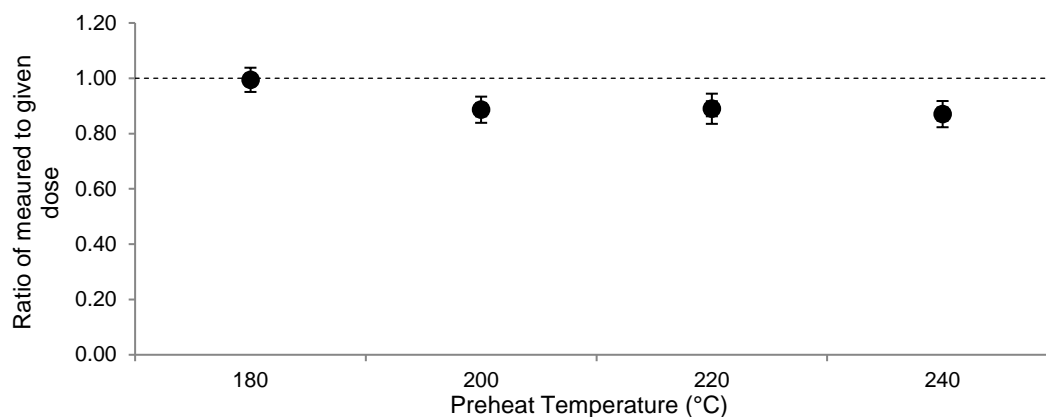
Figure 7.9- Results of dose recovery test. The ratio of measured to given dose is plotted for each preheat-cutheat temperature combination. Errors are displayed at one and two sigma, although those at one sigma are masked by the data points.

7.5.3.2   OSL Characteristics

Twelve rejection criteria were applied sequentially to the samples (Appendix D – Table D.3). A total of 13 200 grains were measured with 1821 (13.8%) passing all the rejection criteria and being used in the De determination. For each sample 7.5 – 22.5% of the total measured grains were accepted. The majority of grains which failed the rejection criteria did so due to signal related criteria, with between 291 and 856 grains for each sample failing, equating to a minimum of 50% of grains for all samples (Appendix D – Table D.4). A small number of grains, <70 for any sample, then failed based on the recycling ratio between the first and fifth regenerative doses, with grains rejected if recycling ratio did not give unity at 2-sigma. Even smaller numbers, <20 grains for all samples (except MR1750 where 76 grains failed), failed with the recycling ratio between the sixth and fifth regenerative doses not being within 10% of unity, thus indicating the presence of an infrared signal, inferring feldspar contamination. Of the remaining grains between 24 and 138 grains failed as the figure of merit, a test of goodness of fit, was not sufficient to satisfy the model used to fit the growth curve. The remaining rejection criteria, 7 – 12 (Appendix D - Table D.3), failed only a small number of grains, mostly <12 grains with the exception of MR 1750 and MR1744 where 22 and 24 grains failed to calculate an estimate of the dose.

As reflected by the large number of grains which failed the rejection criteria for signal related criteria, grains were generally dim. Grains had a weakly sensitive luminescence signal showed as decay curves with a slower than expected decay and a noisy background signal (Figure 7.9 a,b,d), although there were occasional brighter grains

with better defined decay curves (Figure 7.9 c) (Appendix D - D.5.2.1 addresses this in detail). The majority of grains, when assessing either all the grains or just the accepted grains have background correct sensitivities in cts.Gy^{-1} of <100 (Appendix D – Table D.5; Table D.6). The variation in brightness can be seen by the number of counts and how well distinguished the decay curve of the natural dose is relative to the test dose on the natural (Figure 7.9). There appears to be no relationship between sensitivity variation and depth, deposit type or distance downstream.

A full description of the characteristics of grains and analysis of OSL, including a description of the rejection criteria is presented in Appendix D.
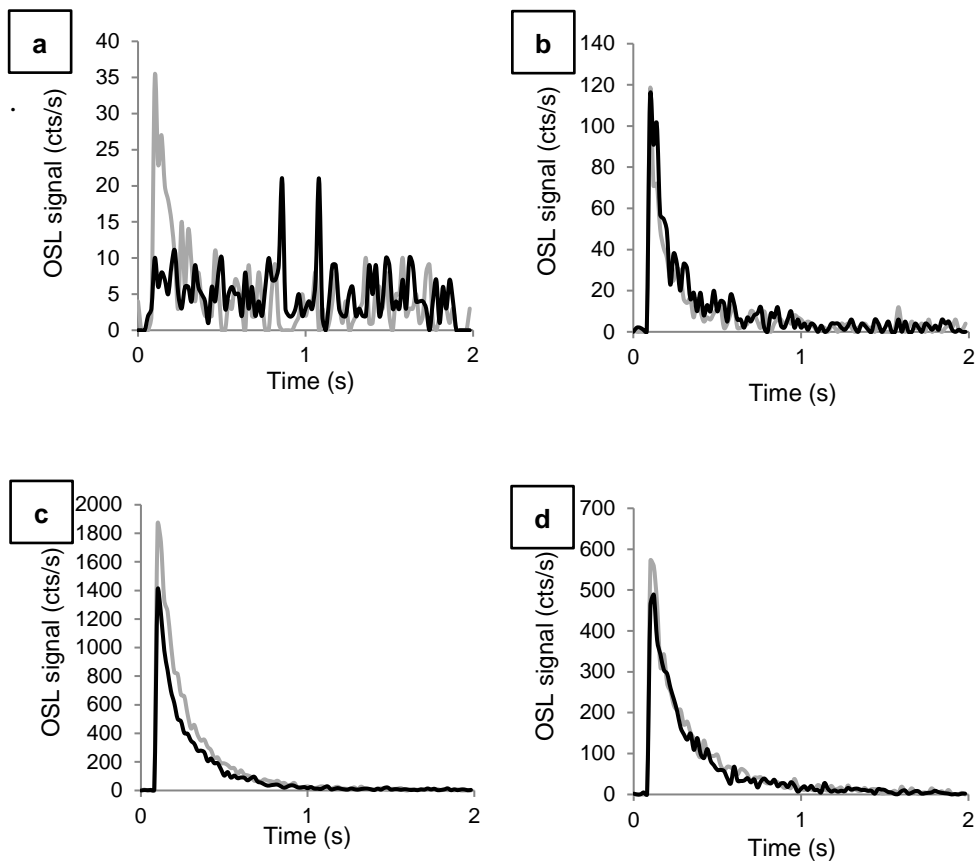
Figure 7.10 - Examples of decay curves of natural signal (grey) and test dose signal on the natural (black) for four grains from(a) MR1683; (b) MR1748 (c) MR1756 (d) MR1741

The shape of the decay curves is also affected by the size of the fast component within a luminescence measurement (Smith and Rhodes 1994; Bailey et al. 1997) A small fast component will give a slow decaying curve (Figure 7.10 a,b,d) and a large fast

component will have a faster decay curve (Figure 7.10 c). The fast component is highly variable but the majority of samples have a small fast component, with only samples MR1686 and MR1682 having more than 25% of grains with a fast ratio greater than 20.

7.5.3.3   Dosimetry

Measurement using HRGS showed no evidence of disequilibrium in the uranium or thorium decay chains (Appendix D – Table D.9; D.10; D.12). Given the lack of disequilibrium and that the different dosimetry methods give results within one sigma of unity (Appendix D – Figure D.9; D.10) TSAC and GMBC were chosen to use in the age calculations. The samples showed an average dry beta dose rate of 2.45 Gy.ka^{-1} and an average dry gamma dose rate of 1.58 Gy.ka^{-1}, equating to an average total dose rate of 3.78 Gy.ka^{-1} (Table 7.6).

Water content at time of sampling was measure at between 0.66-6.51% (Table D.11), 4% $\pm$2% was used to represent the long term average given the ephemeral nature of the river and infrequent flows.

Cosmic dose rates show minor variation (Table 7.6), from 0.16 $\pm$ 0.02-0.21 $\pm$ 0.03 Gy.ka^{-1}. This limited variation is due to the consistent elevation and minimal variation in depth of the samples.

Table 7.8 Elemental concentrations, total dry beta and gamma dose, cosmic dose rate, water content and total dose rate for all OSL samples.

OSL code	Site	Depth	Uranium	Thorium	Potassium	Beta	Gamma	Cosmic	Water	Total
		m	ppm	ppm	%	Gy.ka⁻¹	Gy.ka⁻¹	Gy.ka⁻¹	%	Gy.ka⁻¹
MR1676	MR3.1	0.60	3.45 ± 0.17	10.31 ± 1.42	1.60 ± 0.08	1.27 ± 0.07	1.27 ± 0.07	0.21 ± 0.03	4 ± 2	3.12 ± 0.25
MR 1682	MR3.1	3.20	2.73 ± 0.20	19.26 ± 1.89	0.72 ± 0.08	1.69 ± 0.10	1.69 ± 0.10	0.16 ± 0.02	4 ± 2	3.76 ± 0.30
MR 1683	MR3.2	0.60	3.40 ± 0.13	7.20 ± 1.02	1.04 ± 0.06	0.98 ± 0.05	0.98 ± 0.05	0.21 ± 0.03	4 ± 2	2.82 ± 0.22
MR 1748	MR3.2	3.45	3.37 ± 0.20	15.37 ± 1.78	0.70 ± 0.08	1.77 ± 0.09	1.77 ± 0.09	0.16 ± 0.02	4 ± 2	4.33 ± 0.35
MR 1686	MR3.3	0.60	3.46 ± 0.18	10.67 ± 1.46	0.90 ± 0.07	1.30 ± 0.08	1.30 ± 0.08	0.21 ± 0.03	4 ± 2	3.18 ± 0.25
MR 1750	MR3.3	2.80	2.51 ± 0.18	13.55 ± 1.65	0.91 ± 0.07	1.73 ± 0.09	1.73 ± 0.09	0.17 ± 0.03	4 ± 2	4.53 ± 0.37
MR 1751	MR2.1	0.55	3.65 ± 0.17	10.05 ± 1.39	0.89 ± 0.07	1.26 ± 0.07	1.26 ± 0.07	0.21 ± 0.03	4 ± 2	3.04 ± 0.24
MR 1753	MR2.1	1.55	3.10 ± 0.16	12.60 ± 1.39	0.90 ± 0.07	1.36 ± 0.07	1.36 ± 0.07	0.19 ± 0.03	4 ± 2	3.21 ± 0.25
MR 1754	MR2.2	0.60	3.30 ± 0.19	12.88 ± 1.66	0.84 ± 0.08	1.47 ± 0.09	1.47 ± 0.09	0.19 ± 0.03	4 ± 2	3.57 ± 0.29
MR 1756	MR2.2	1.60	4.98 ± 0.30	20.05 ± 2.44	0.23 ± 0.11	2.18 ± 0.13	2.18 ± 0.13	0.17 ± 0.03	4 ± 2	5.02 ± 0.41
MR 1757	MR2.3	0.5	0.56 ± 0.26	28.96 ± 2.49	0.73 ± 0.10	2.22 ± 0.13	2.22 ± 0.13	0.19 ± 0.03	4 ± 2	5.05 ± 0.41
MR 1759	MR2.3	1.60	5.29 ± 0.32	22.27 ± 2.65	0.11 ± 0.11	2.24 ± 0.14	2.24 ± 0.14	0.19 ± 0.03	4 ± 2	4.95 ± 0.41
MR 1741	MR1.1	0.45	2.61 ± 0.28	13.78 ± 2.50	0.94 ± 0.11	1.39 ± 0.13	1.39 ± 0.13	0.19 ± 0.03	4 ± 2	3.31 ± 0.28
MR 1744	MR1.1	1.64	2.64 ± 0.17	11.20 ± 1.51	1.03 ± 0.07	1.25 ± 0.08	1.25 ± 0.08	0.17 ± 0.03	4 ± 2	3.04 ± 0.25

7.5.3.4   Age determination

There is a measurable signal present in the modern channel sample (MR-SS-1), representing a residual non-bleached component in the sample of ~0.4 Gy. All the samples have higher overdispersion than would be expected, assuming a normal distribution (Table 7.7) (Figure 7.11) varying from 51.59 ± 3.43 to $313.62 \pm 83.43\%$. Galbraith et al. (1999) and Arnold and Roberts (2009) respectively suggest maximum values of 20% and $13 \pm 0.7\%$ overdispersion to indicate a homogeneously bleached sample. Higher overdispersion is therefore often taken as an indicator of a sample which has been heterogeneously bleached or dosed, or contains multiple dose populations, either discrete or continuous.

Age models were chosen by assessing the distribution through radial plots (Figure 7.11 a; b; Figure 7.12 a;b) and histograms (Figure 7.11 c; Figure 7.12c). The radial plots use a linear De scale (rather than the more usual logarithmic scale) due to the prevalence of low De grains and use absolute standard errors on the x-axis (rather than the more usual relative standard errors on the x-axis) as the relative standard errors are often large due to being "relative to something small" (Galbraith and Roberts 2012).

The three parameter minimum age model (MAM-3) (Galbraith et al. 1999), notably the unlogged version of this model (Arnold et al. 2009) was applied to all samples. The application of the unlogged age model is necessary with very young ages (therefore low De values) as, where grains intersect with zero, log values cannot be taken. The model was tested with user defined overdispersion values of 10, 15 and 20% and it was found that 20% gave the most samples where it was possible to calculate the De and also gave the highest *p* values (Table 7.8). The *p* value is the proportion of grains which are included in the MAM-3 De, the maximum possible being 1.00. Where it was not possible to calculate a De using MAM-3 the central age model (CAM) (Galbraith et al. 1999) is used, again unlogged (Table 7.8). The majority of sample age calculations use the MAM-3, with five using the CAM. Those samples with ages calculated using MAM-3 are, with the exception of MR1748 and MR1753, from the upper part of the cores so are those mostly likely to have been affected by bioturbation and the infiltration of younger grains. None of the samples with ages calculated using CAM are from the upper part of the core.
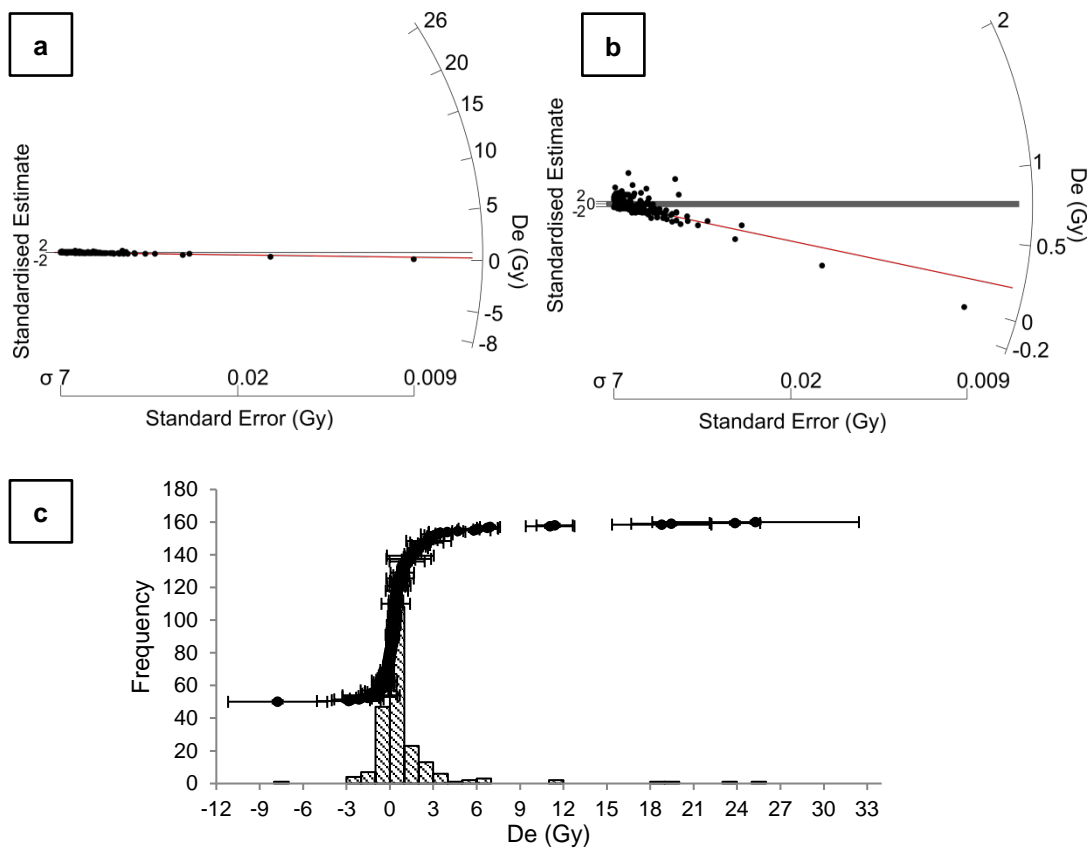
Figure 7.11- An example of a sample distribution where the minimum age model is used (MR1683, upper sample from core MR3.2) from the Marshall River displayed as (a)a radial plot with linear y-axes, and standard error on x-axes; (b)a radial plot zoomed in to show z-axes; (c) a histogram with 1 Gy bin widths and ranked plot of ages. Grey shaded areas on radial plots show the central age model (Galbraith et al. 1999) estimates of burial dose with 2-sigma errors. Red line on radial plot shows unlogged 3-parameter minimum age model (Arnold et al. 2009) estimate of burial dose.
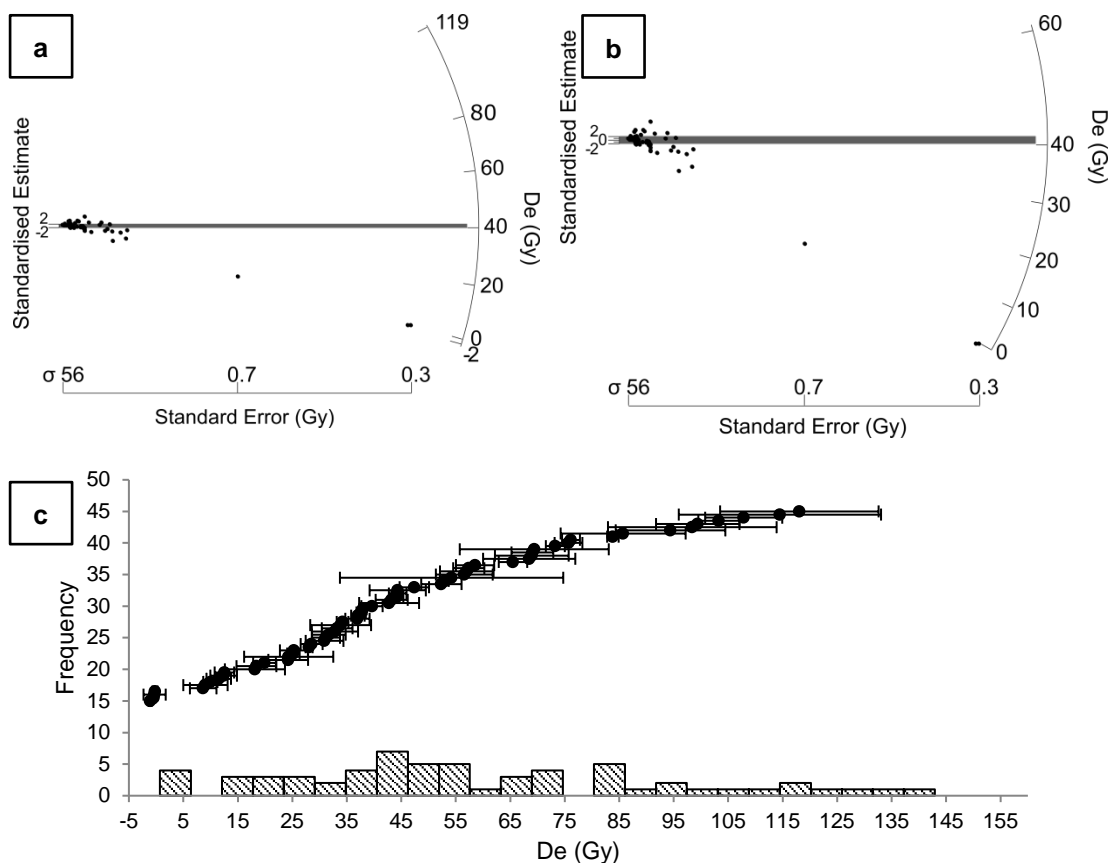
Figure 7.12 - An example of a sample distribution where the central age model is used (MR1744) from the Marshall River displayed as (a)a radial plot with linear y-axes, and standard error on x-axes; (b)a radial plot zoomed in to show z-axes; (c) a histogram with 1 Gy bin widths and ranked plot of ages. Grey shaded areas on radial plots show the central age model (Galbraith et al. 1999) estimates of burial dose with 2-sigma errors.

Table 7.9 - Estimates of De and burial age for all samples using the 3 parameter minimum age model where possible and the central age model (Galbraith et al.1999) With overdispersion from the CAM and skew from Bailey and Arnold (2006). For dosimetry values used in age calculations see Appendix D – Table D.12

OSL code	Depth	MAM - 3		CAM		OD	Skew	n	Total Dose rate
	m	Gy	ka	Gy	ka	%			Gy/ka
MR-SS-1	surface	-	-	0.41 ± 0.13	-	382.10 ± 126.30	66.92 ± 0.20	147	-
MR1676	0.60	0.39 ± 0.04	0.12 ± 0.01	0.80 ± 0.08	0.25 ± 0.03	112.09 ± 14.02	4.60 ± 0.21	131	3.15 ± 0.11
MR1682	3.20	-		0.44 ± 0.07	0.12 ± 0.02	175.00 ± 30.82	4.53 ± 0.21	137	3.80 ± 0.13
MR1683	0.60	0.23 ± 0.03	0.08 ± 0.01	0.76 ± 0.11	0.27 ± 0.04	200.65 ± 30.38	11.94 ± 0.16	221	2.85 ± 0.09
MR1748	3..45	2.34 ± 0.16	0.53 ± 0.04	3.33 ± 0.50	0.76 ± 0.12	109.39 ± 19.51	6.70 ± 0.33	56	4.38 ± 0.14
MR1686	0.60	0.32 ± 0.04	0.10 ± 0.01	0.61 ± 0.07	0.19 ± 0.02	142.23 ± 19.46	5.46 ± 0.20	151	3.21 ± 0.11
MR1750	2.80	-		2.68 ± 0.22	0.58 ± 0.05	68.12 ± 8.43	1.03 ± 0.28	75	4.58 ± 0.14
MR1751	0.55	0.11 ± 0.02	0.04 ± 0.01	0.64 ± 0.17	0.21 ± 0.06	313.62 ± 83.43	73.07 ± 0.20	157	3.08 ± 0.10
MR1753	1.55	0.38 ± 0.07	0.12 ± 0.02	1.47 ± 0.33	0.45 ± 0.10	171.21 ± 42.31	1.89 ± 0.31	62	3.25 ± 0.11
MR1754	0.60	0.16 ± 0.03	0.04 ± 0.01	0.63 ± 0.11	0.17 ± 0.03	196.88 ± 37.94	11.50 ± 0.21	133	3.61 ± 0.12
MR1756	1.60	-		9.83 ± 0.38	1.94 ± 0.11	51.59 ± 3.43	1.14 ± 0.17	202	5.07 ± 0.17
MR1757	0.5	0.09 ± 0.03	0.02 ± 0.01	0.48 ± 0.07	0.09 ± 0.01	136.96 ± 22.12	4.18 ± 0.22	121	5.10 ± 0.17
MR1759	1.60	-		2.03 ± 0.22	0.41 ± 0.05	102.47 ± 13.45	9.77 ± 0.24	101	5.01 ± 0.18
MR1741	0.45	10.25 ± 2.48	3.06 ± 0.76	19.76 ± 2.02	5.91 ± 0.67	77.64 ± 10.98	2.10 ± 0.30	66	3.35 ± 0.15
MR1744	1.64	-		40.80 ± 3.66	13.29 ± 1.31	62.46 ± 8.82	1.09 ± 0.31	61	3.07 ± 0.11

Table 7.10 - Chosen De estimates and age models for each OSL sample with the age model used.

Sample	De (Gy)	Age (ka)	Age Model	Overdispersion [1] (%)	P value [2]	Core	Location in core[3]
MR1676	0.39 ± 0.04	**0.12 ± 0.01**	MAM-3	20	0.68	M5a.1	T
MR 1682	0.44 ± 0.07	**0.12 ± 0.02**	CAM	175.00 ± 30.82	-	M5a.1	B
MR 1683	0.23 ± 0.03	**0.08 ± 0.01**	MAM-3	20	0.73	M5a.2	T
MR 1748	2.34 ± 0.16	**0.53 ± 0.04**	MAM-3	20	0.7	M5a.2	B
MR 1686	0.32 ± 0.04	**0.10 ± 0.01**	MAM-3	20	0.39	M5a.3	T
MR 1750	2.68 ± 0.22	**0.58 ± 0.05**	CAM	68.12 ± 8.43	-	M5a.3	B
MR 1751	0.11 ± 0.02	**0.04 ± 0.01**	MAM-3	20	0.77	M6.1	T
MR 1753	0.38 ± 0.07	**0.12 ± 0.02**	MAM-3	20	0.74	M6.1	B
MR 1754	0.16 ± 0.03	**0.04 ± 0.01**	MAM-3	20	0.72	M6.2	T
MR 1756	9.83 ± 0.38	**1.94 ± 0.11**	CAM	51.59 ± 3.43	-	M6.2	B
MR 1757	0.09 ± 0.03	**0.02 ± 0.01**	MAM-3	20	0.53	M6.3	T
MR 1759	2.03 ± 0.22	**0.41 ± 0.05**	CAM	102.47 ± 13.45	-	M6.3	B
MR 1741	10.25 ± 2.48	**3.06 ± 0.76**	MAM-3	20	0.55	1.1	T
MR 1744	40.80 ± 3.66	**13.29 ± 1.31**	CAM	62.46 ± 8.82	-	1.1	B

[1]Overdispersion is the overdispersion which is inputted in the model calculations. [2]P value is the proportion of grains which max up the De estimate in the minimum age model. [3]T= Top of core, B = bottom of core.

7.5.3.5   *Chrono-stratigraphic presentation and interpretation of the OSL ages*

In section MR1 the channel is divided by a singular large, slightly irregular lenticular island, MR1.1 (Figure 7.13), with bilateral flow. The island is interpreted from the sedimentology and morphology as being a section of excised floodplain. The ages for this island are 3.06 ± 0.76 ka (at 0.45 m) and 13.29 ± 1.31 ka at 1.64 m. This suggests that the island was excised from a floodplain late Holocene in age although it doesn't determine when excision occurred. It would appear that the floodplain or island has at this location continued to accrete very gradually over the past few thousand years.

In section MR2 the ridge MR2.1 (Figure 7.13) has upper and lower ages of 40 ± 10 and 120 ± 20 years, respectively, give a difference of 20 years at 2σ. Ridge MR2.2 (Figure 7.13) has an older basal age of 1.94 ± 0.11 ka, but similarly young upper despositional age of 40 ± 10 years. The lower age is not considered to represent a basal ridge age, but age of the underlying sand sheet, as the sample is 0.85 m below the current island-channel interface. Ridge MR2.3 (Figure 7.13) has a close to modern upper sample of 20 ± 10 years and a lower age of 410 ± 50 years.

In section MR3 all islands and ridges are interpreted as being depositional. Island MR3.1 (Figure 7.13) is interpreted as modern as the lower sample (MR1682) overlaps with its upper counterpart (MR1676) with lower and upper ages of 120 ± 10 years and 120 ± 20 years, respectively. MR3.2 and MR3.3 (Figure 7.13) have similar basal ages of 530 ± 40 years (MR1748) and 580 ± 50 years (MR1750), respectively, overlapping with one another within 1σ, and upper ages of 80 ± 10 years and 100 ± 10 years. In both these cases the basal ages do not overlap with the upper ages. This suggests that the two ridges in section MR2 have accreted over the past ~500 years and may be still vertically accreting, and that the island (MR2.1) is no more than a one or two hundred years old.

All depositional islands and ridges have close to modern upper ages of 20 to 130 years, indicating that island building processes are ongoing. The basal ages vary with MR 3.2, MR3.3 and MR2.3 (Figure 7.13) giving ages consistent with one another at 2σ and are interpreted to have undergone a building period of ~500 years. There is a general pattern that the basal samples from islands on the right (when looking downstream, to the east) of the channel are younger than the left (when looking downstream, to the east), indicting more recent deposition and more recent reworking of the internal

channel structure to the right. The distributions are similar to that of the modern sample, likely due to bioturbation of the samples and contribution of older grains eroded from the relict floodplain. The left side (when looking downstream, to the east) and centre of the channel (MR1748, MR1750, and MR1759) are older, indicating a more stable island/ ridge form in this location
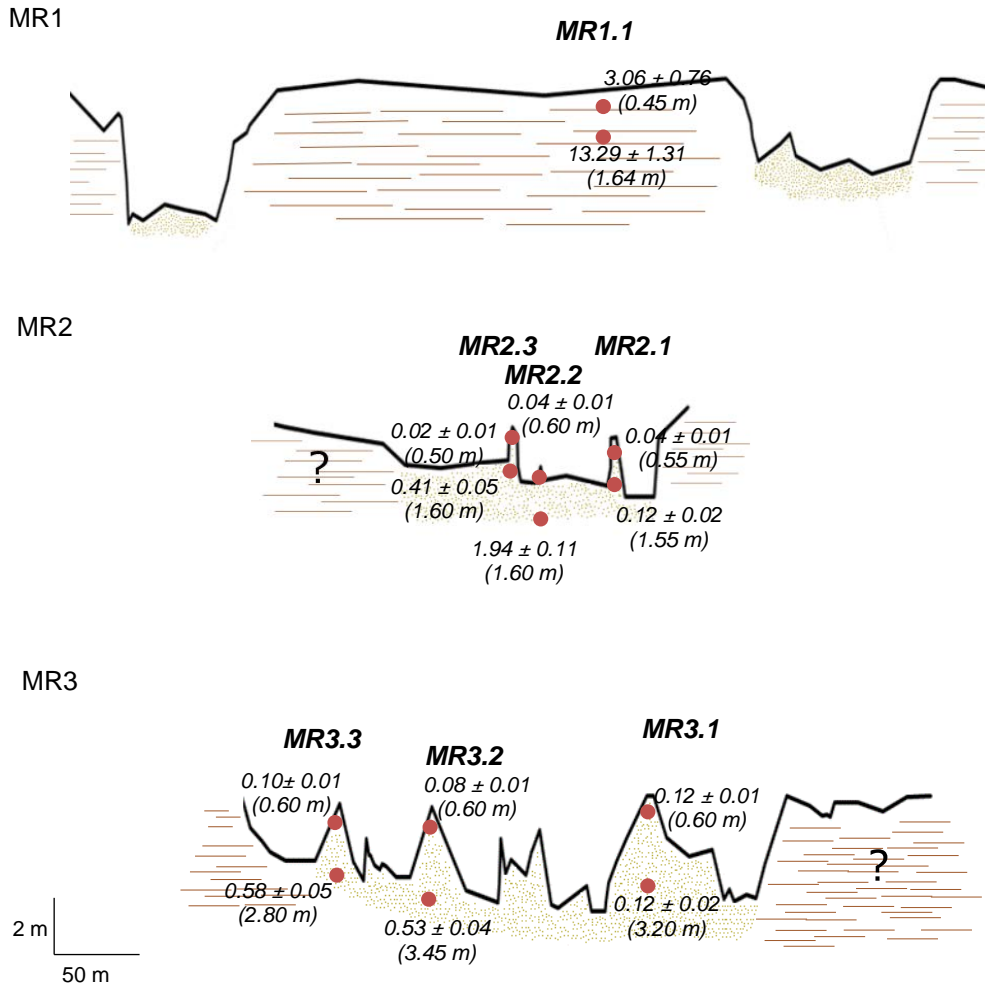
Figure 7.13 - Cross sections from the Marshall River, all sections should be viewed as if facing downstream, with fourteen ages marked by red circles at their respective depths. Cross sections and depths are to scale but downstream distances are not. Stippled areas mark sand beneath the surface. Lines stipulate floodplain type deposits.

7.5.3.6   Deposition rates

Deposition rates for MR3.1 and MR2.1 are not likely to be accurate representations of the rates of deposition throughout the system due to the short time period they cover (Table 7.9). MR1.1 as a large island has much lower rates of deposition than any of the other ridges and small islands. Given that this island is interpreted as being excisional, it is likely to represent the deposition rate of the floodplain. MR3.2, MR3.3 and MR2.3 have similar deposition rates and show ridges as accreting at a rate of between 2.8 and 6.3 m.ka^{-1} (Table 7.9). MR2.2 has a lower accretion rate, and is a smaller ridge. The lower age is interpreted as representing the original channel bed deposit rather than the base of the ridge, so the deposition rate here is a combination of initial in channel accretion followed by ridge building. M3 compared to the other two sections indicated that the within-channel ridges and small islands are accreting (and probably being repeated being destroyed) very much more quickly than the overall floodplain and its associated excised islands along the Marshall River.

Table 7.11 - Accretion rates for islands and ridges. Uncertainties on accretion rates are calculated as using the age +1σ for the upper bound and -1σ for the lower bound.

Island/Ridge	Top age (ka)	Bottom age (ka)	Depth difference (m)	Accretion rate m.ka^{-1}
MR1.1	3.06 ± 0.76	13.29 ± 1.31	1.19	$0.116^{+0.03}_{-0.02}$
MR2.1	0.04 ± 0.01	0.12 ± 0.02	1.00	$12.500^{+7.50}_{-3.41}$
MR2.2	0.04 ± 0.01	1.94 ± 0.11	1.00	$0.526^{+0.04}_{-0.03}$
MR2.3	0.02 ± 0.01	0.41 ± 0.05	1.10	$2.821^{+0.51}_{-0.38}$
MR3.1	0.12 ± 0.01	0.12 ± 0.02	2.60	-
MR3.2	0.08 ± 0.01	0.53 ± 0.04	2.85	$6.333^{+0.79}_{-0.63}$
MR3.3	0.10 ± 0.01	0.58 ± 0.05	2.20	$4.583^{+0.65}_{-0.51}$

The deposition rates calculated are not likely to be indicative of long-term rates, as it does not appear that island/ridge building goes beyond the heights of the islands/ridges currently present in the system. When islands/ridges are small, surface vertical accretion will occur during most flood events but as they grow this rate will decrease because not all flows will be sufficient to reach their upper surfaces.

7.6   Discussion – Anabranching islands in time and space

7.6.1   Development of the Marshall River islands and ridges

The underlying principles of anabranching in the Northern Plains have been extensively investigated (Habeck-Fardy 2013; Tooth and Nanson 1999; Tooth and Nanson 2000a, b; Tooth 2000; Tooth and Nanson 2004; Nanson and Huang 2017) and the conclusion that has been drawn that these systems anabranch to achieve equilibrium is not challenged here.

The cause of anabranching on the Marshall River as a means to maintain dynamic equilibrium has been attributed to the inability of the Marshall River to increase slope, and therefore stream power, by other means (Tooth and Nanson 2004; Nanson and Huang 2017). The anabranches allow the system to achieve maximum flow efficiency (Tooth and Nanson 2000a;b; 2004) (Chapter 2 - 2.2.1), this is displayed by the *H* number for individual anabranches of close to 0.3 (Habeck-Fardy 2013), which is considered to be stable equilibrium, and represents a river at its most efficient (Huang and Chang 2006).

Tooth and Nanson (1999) attributed the actual location of heavily anabranching reaches on the Marshall River to the presence of tributaries, independent of significant changes in the slope or degree of confinement of the trunk stream. Tributaries are likely to trigger anabranching by two dominant mechanisms:

(1) sediment and water to a dry trunk stream prior to or without flow from upstream, encourages growth of vegetation due to increased moisture input so allows for depositional islands to be initiated. Their persistence relies on sediment supply from flood events.

(2) input of water and sediment to a wet trunk channel during flood flow overbank flow leads to linear dissection, where high flow cause local ponding of tributary floodwaters (hydrologic damming) causing high energy periods of flow on floodplains. By the same mechanism, tributary inflows can be dammed by high trunk flow and the mouth is deflect downstream. Where this mechanism occurs many anabranches take the form of differed junction channels, separated from the trunk by large excised floodplain islands or islands developed from channel deposition. (Tooth and Nanson 1999).

When any quantity of flow is present, either via tributaries or throughout the trunk channel, sediment is deposited, although the surface of islands is likely only reached during flood events. The banks appear stable and well vegetated, but the ridges within the channel are dynamic. In cross sections MR2 and MR3 the left side of the channel (facing downstream) is elevated when compared to the right side and from field observations and aerial photographs it appears that there is some infilling and possible inherent stabilisation and atrophying of channels on the left side of the system. The majority of modern island building and likely erosional activity is occurring in the right side of the channel. The island structures themselves, while vegetated, appear to be vulnerable to influx of water as, where vegetation is sparser, sections have been destroyed and removed. It is hypothesised therefore that the islands do not persist in each form for extended periods but are destroyed and rebuilt on a cyclical basis over periods of a few hundred years, as supported by the chronology.

The ages from the islands and ridges of the Marshall River show an onset of the current phase of island building at ~0.5 ka. It can be concluded that, from field observations in agreement with the hydraulic calculations of Habeck-Fardy (2013) and Nanson and Huang (2017) that these systems anabranch to achieve equilibrium. The question arises however, as to why have these islands and ridges existed for no more than 600 years. Is this an indication of the cyclical nature of the system, where there is ongoing formation and removal, or is this the age of a switch to anabranching planform?

The preferred interpretation is that the basal age of these islands, at ~0.5 ka, indicates the maximum lifetime of these islands and that after five hundred years the internal dynamism of the system acts on a cyclic scale. There is field evidence that these islands are being destroyed and rebuilt, yet chronologically this is difficult to define as once an island has been destroyed and a new one built in its place there is no evidence of its previous existence. The apparent atrophying of the left side of the channel suggests significant variation in the depositional behaviour within the channel, but there is little to indicate how the system operates on longer timescales. This cyclic island building supports the evidence from Tooth and Nanson (2000; 2004), Habeck-Fardy (2013) and Nanson and Huang (2017) that the Marshall River is a system in stable equilibrium. The cyclicity of the islands can be interpreted as the process by

which the internal configuration of the ridges and islands in the channel adjust to maintain optimal **H** numbers.

An alternative scenario would be similar to that seen in Chapter 5 of this thesis which constrains the onset of anabranching in Channel Country of the eastern LEB though observation of a reduction in laterally active channels from MIS 5 to MIS 3 and an increase in anabranching from the LGM. However, the systems of the north-western LEB Rivers are very different and the ages show anabranching as starting much more recently, assuming the basal island age indicates the onset of anabranching. Were a planform switch to have occurred at ~0.5 ka that caused anabranching to be initiated, indicating that anabranching has only persisted in this system for the last five hundred years, there would likely be visual evidence of this. One must consider what could have caused a switch to an anabranching planform and what would the river have been like before. There is no surface evidence, either in the field or in aerial photographs, that the river has not always been straight, such as meander scars, scroll bars or oxbow lakes. This implies that the Marshall River has persisted in its current overall form. There is also no indication in either sedimentological or climatic records that any climatic shift occurred at ~0.5 ka that would trigger an adjustment in planform through, for example, a reduction in average or total flow. However, the longterm presence of anabranching beyond this ~0.5 ka cycle is likely to be due to reduced flow due to climatic changes, although its onset cannot be identified.

7.6.2   Comparison to other type 2 and type 4 anabranching

The morphology of the Marshall River is not unique, but 'type 2' (sand dominated island forming) and 'type 4' (sand dominated ridge forming) (Nanson and Knighton 1996) anabranching do not appear to be commonly occurring and/or have not been widely studied and are poorly understood with regards to their temporal variation. From the literature they appear to be unique to Australia where four other 'type 2' and 'type 4' anabranching rivers have been identified.

The other rivers on the Northern Plains which subscribe to a 'type 2' and 'type 4' morphology, are the Sandover-Bundey River and the Woodforde River. There is also the Durack River in the Kimberley region (Wende and Nanson 1998) and Magela Creek in northern Australia in Kakadu National Park (Nanson et al. 1993; Jansen and

Nanson 2004; Tooth et al. 2008). Of these other 'type 2' and 'type 4' rivers only Magela Creek has been systematically dated.

The similarity between these systems is that they are all low slope; the average down-valley slope of Magela Creek and the Durack River are 0.005 m.m^{-1} (Tooth et al. 2008) and 0.008 m.m^{-1} (Wende and Nanson 1998) respectively. Slope of the anabranching reaches on the Northern Plains is ~0.001 m.m^{-1}. The rivers are morphologically similar with steep banks, low width to depth ratios and steep banks.

Magela Creek and the Durack River differ from the Marshall River in that they are located in the tropical monsoon region. The Durack River is of 'type 4' anabranching and is located on the Kimberley Plateau in northwestern Australia, with rainfall of ~700 mm.a^{-1} (Wende and Nanson 1998). It receives over twice as much rainfall than is recorded on the Northern Plains while evapotranspiration is comparable between the two regions. Magela Creek in the southeast of Kakadu National Park ~1200 km NNW of the Marshall River, lies in the humid region. The river differs as it is base level controlled and features 'type 2' anabranching for much of its length but, while being monsoon fed like the Durack River, rainfall is approximately twice as much again at ~1530 mm.a^{-1} and evapotranspiration is slightly lower than the Durack River at ~2580 mm.a^{-1}.

If a widespread planform change were to have occurred it is likely that it would be evidence in the sedimentary record of these similar rivers. No useful chronologies exist for the Durack River, Sandover-Bundey or Woodforde Rivers, however Magela Creek has been systematically dated and shows that islands become younger in a downstream direction and long-term stability of 1.5 – 3.5 ka in upstream islands. The downstream islands in Magela Creek (dated using OSL) are of a similar age to the Marshall River islands from 0.2 – 0.7 ka, and the delta front is modern in age (Tooth et al. 2008). This longitudinal, temporal evolution of anabranch formation is not seen in the Marshall River chronology. Therefore, it is likely that 'type 2' and 'type 4' anabranching are a response to localised variations in hydrological and morphological conditions as opposed to a widespread planform switch due to, for example, climatic changes as seen in Chapter 5.

7.7   Limitations and further research

The limitations of the Marshall River study are the lack of similar rivers for justifiable comparison. We also cannot identify if a previous planform was present, as there is no palaeo-evidence on the floodplain and the current system sits directly on bedrock so we do not know the duration of anabranching as individual ridges and island only represent the most recent event turn over. It is possible that further investigation of the age of the floodplain would give more insight into the preceding system and the onset of anabranching. Therefore, future work should including dating of sediments in a transect away from the channel, along with dating of other similar rivers.

7.8   Chapter summary

Islands and ridges in the Marshall River of the Northern Plains are either depositional or erosional. Depositional islands and ridges are commonly elongate or tear-dropped in shape and streamlined to the direction of flow. Erosional islands tend to be larger and more irregular shaped, although somewhat elongate. Depositional islands tend to form on the lee side of in-channel obstacles, primarily trees, in current shadows, whereas erosional islands form by avulsion or through erosion by flood channels. There is little difference sedimentologically between depositional islands and ridges, and their differentiation appears to be arbitrary, based on the ratio of length to width. There is a slight sedimentological difference to erosional islands, which tend to be finer grained in keeping with the conclusion that they are formed of relict floodplain.

There is little variation in channel width or gradient and there does not appear to be a distinct spatial pattern in island and ridge formation. The channel train appears to be stable, without evidence of lateral movement, but the interior is constant reworked with a lot of variation. The floodplain which makes up the erosional islands is continuing to be eroded and will be contributing older grains to islands downstream and to the modern sample. The system is constantly reworking and actively aggrading. Ridge forms are quite vulnerable until they become stabilised by vegetation, and even then the large flows of water can easily destroy parts of an island.

Through establishing ages for the base of the anabranching ridges and islands in the Marshall River, using OSL, it has been ascertained that island building in the Marshall River is a short-lived process and depositional islands and ridges have a lifetime of

~500 years. The ages indicate that the islands are destroyed and rebuilt on a cyclical basis. The islands and associated channels are formed and reworked over this period in order to adjust channel w/d ratios and to maintain flow pathways and associated flow efficiencies in desert rivers that are invaded by riparian trees seeking moisture

Chapter 8

8 Synthesis and discussion

8.1 Introduction

This thesis has addressed the evolution of anabranching rivers, and their long-term sediment storage characteristics in the arid LEB in central Australia with a particular focus on Cooper Creek in the Channel Country and the Marshall River. Investigation time-scales range from 10^6 to 10^2 years and the rivers in question range from ~1500 km to ~400 km in length. The thesis has addressed facets which are under-represented in past research by specifically relating to anabranching rivers in arid, low slope environments. It has contributed to our understanding of the timescales over which anabranching rivers act, the reasons Australian rivers anabranch and the sediment dynamics of rivers in low slope arid environments. This chapter brings together the findings of each of the three results chapters, establishes how these findings relate to one another and the LEB as a whole, discusses the limitations of the data, and highlights areas for further research.

8.2 Long-term sediment dynamics in arid zone rivers: are all sediment conveyors the same?

Anabranching rivers in the LEB occur in low-gradient settings and all store sediment over timescales from centuries to those spanning multiple glacial cycles, with old sediment being buried at shallow depths in much of the basin (Figure 6.4). In the low-slope arid environments of Australia the sediment conveyors are, in general terms, transport limited. Supply, however, is not high either, with long term erosion rates being some of the lowest in the world. As transport potential is low, storage potential is high. In general, because sediment is moved episodically through the fluvial system (Ferguson 1981), the dynamics of the sediment conveyor allows for sediment to be removed, added, or stored at different points through the system. These processes do not act the same way in all river systems, so what does the presence of these old sediments so close to the surface tell us about the dynamics of the system? In the LEB two sediment storage relationships can be identified.
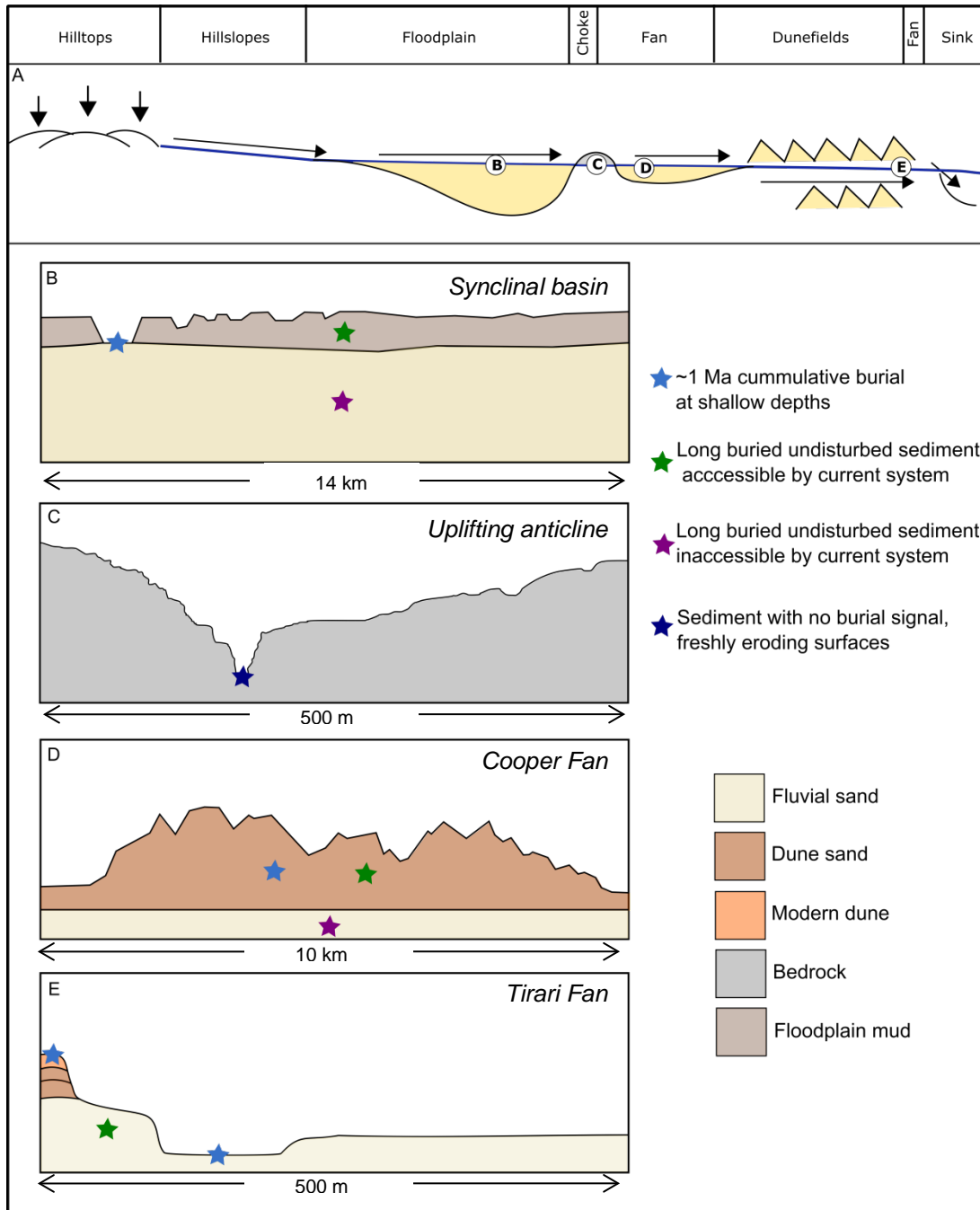
Figure 8.1 - A. Schematic long profile of the Cooper Creek sediment conveyor. B-E. Cross-sections schematically present sediment storage scenarios within the conveyor and show different burial situations and the accessibility of sediment by the modern system. B. Synclinal basin - Cooper floodplain, C. Uplifting anticline - Bedrock channel at the choke, D. Cooper Fan - Gidgealpa dune, E. Tirari fan - Kutjitara West Bluff

The sediment conveyor of Cooper Creek stores sediment in a series of deep sinks and also at the surface. Apparent burial ages, calculated using cosmogenic nuclide burial dating, ranging from ~0.05 Ma to ~1.2 Ma are reported from 'modern' in-channel sediment in Cooper Creek, with apparent burial ages of ~1.06 to ~1.29 Ma in the source-bordering dunes adjacent to the channel. Storage appears to be dominated by storage in both floodplains and dunes with a close relationship between accommodation space and the apparent duration of burial. Examples are discussed below.

Sediment in the channel can be stored at depth such as is seen where floodplains overlie synclinal structures (Figure 8.1), in this scenario deep sediment is not readily accessed by the current channel and can record a single period of complete storage of more than 250 ka (Nanson et al. 2008). In the Cooper-Wilson syncline, where deep storage is possible some alluvial sediment is stored for extended periods (10^5 years). In these settings basin subsidence or ongoing aggradation upstream of the Innamincka Dome essentially removes sediment from the sediment conveyor. In the same location sediment stored close to the surface (i.e. upper 2 m) can also have long burial durations (10^4 - 10^5 yr) in a single period of complete storage, and differs from deep buried sediment in that it is more accessible by the modern system. The old sediment which is accessed episodically during high magnitude events is incorporated into the modern mobile fraction with a long cumulative burial signal of 10^5 – 10^6 yr reflecting multiple instances of long shallow burial and remobilisation, up to 1.2 Ma. This availability of long buried sediment at shallow depths appears to be defining characteristic of the Cooper Creek sediment conveyor, with several locations where this is the case, with storage further amplified where source bordering dunes are present (Figure 8.2 – D; E). Dunes allow for transfer of sediment between storage points, and also for long term burial during periods where dunes are immobile. For example, at Gidgealpa (Figure 8.1 – D), a similar scenario as in the synclinal storage is seen in the dunes, where sediment is stored at < 8m depth for ~192 - 288 ka (Cohen et al. 2010), and has cumulative burial duration of 1.3 – 1.9 Ma (T. Fujioka 2018, pers comm. 11 March). At the most downstream site, at Kutjitara West Bluff (Figure 8.1 – E), a further sediment store is introduced, as the channel at this location is laterally active and is eroding into older, elevated fluvial deposits up to 350 ka (Magee 1997), thus introducing sediment with an extensive

storage signal into the channel and providing material that can be supplied to source bordering dunes, hence the similarity in burial durations in both the dunes and channel at Kutjitara West Bluff . In contrast to this, at the Innamincka Choke (Figure 8.1 – C) the channel is flowing over bedrock and there is no extensively buried sediment, either from a single event or cumulative events. The location of elevated burial signals in the Cooper Creek sediment conveyor, therefore, is a function of accommodation space including synclinal structures, dunes and palaeo-fluvial deposits.

In contrast to the eastern LEB, the western LEB presents a more simple sediment transfer system. In the three catchments analysed by Struck et al. (2018a) there is a direct relationship between distance downstream and burial duration, with sediment being stored, predominantly in the channel or floodplain, for progressively longer periods in a downstream direction (Struck et al. 2018a). The apparent cumulative minimum burial durations of ~0.4 – 0.8 Ma only deviate from this correlation where tributary inputs dilute the burial signal (Struck et al. 2018a). When assessing the causes of the variation in burial duration for the two systems, sediment cover (e.g. the nature of the upstream source areas) should also be considered (Figure 8.2). Given the greater area of the Cooper Creek catchment when compared to the western LEB (246×10^3 km^2 and 105×10^3 km^2 (Struck et al. 2018a) respectively) there is more sediment available, in terms of sand plains, alluvium, lacustrine deposits and dunes, to contribute to the channel and to therefore alter the burial signal within the fluvial realm (Figure 8.2). Despite being approximately twice the area of the western LEB, the Cooper Creek catchment has approximately three times the surface area covered by sediments as the western catchments, even though the percentage sediment cover for the two regions are similar. In addition, the Neales and Macumba catchments feature large areas of silcrete and gibber surface (~10 – 40% of the upstream area) (Struck et al. 2018a). Silcrete is highly resistant to weathering so is likely to contribute relatively little material and gibbers store sediment at shallow depths for extended periods (10^5-10^6 yrs) (Fujioka et al. 2005; Fisher et al. 2014; Struck et al 2018b), but are highly erosion resistant. So despite the sediment contributed from gibber surfaces having a decreased ratio of ^{26}Al/^{10}Be, indicating burial, the amount is small, so unlikely to have a great effect on the in channel ratio.
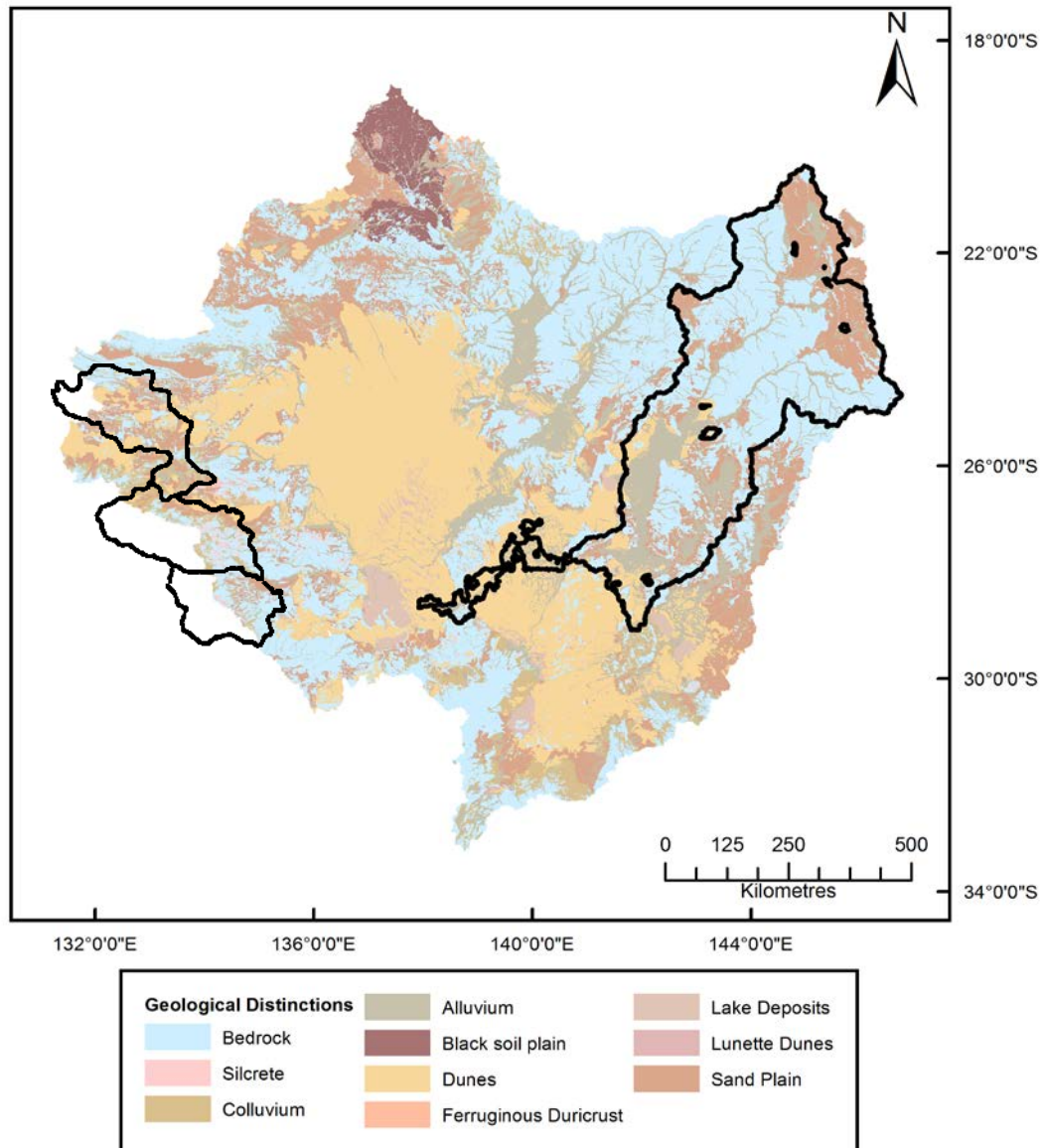
Figure 8.2 – Surface geology of the LEB with subdivisions for bedrock and differing sedimentary cover, adapted from 1:1 M surface geology of Australia (Raymond 2012).

When compared to other sediment conveyors the dynamics of the low slope arid systems of the LEB tend towards to extended periods of sediment storage. In high discharge humid-environment rivers, such as the Amazon and the Po, the dynamics of the sediment conveyor differ greatly to rivers in the arid zone. In the Amazon River, due to short transport and residence times (<0.5 Ma, in-channel sediment is derived from upland areas and does not show significant burial. Where burial does

occur sediment is not buried for extended durations close to the surface but at depth (10 – 20 m). Sediment with a burial signal >0.5 Ma is only accessed during channel avulsions and is then reworked into the floodplain rather than being transmitted downstream. Here, apparent burial durations of >3 Ma have been detected (Wittman et al. 2015). Similarly, in the Po River, $^{26}Al/^{10}Be$ ratios are close to the surface production ratio of 6.7 implying little or no addition of long-buried sediment into the channel (Wittman et al. 2016).

8.3 Spatial and temporal occurrence of anabranching in the LEB

8.3.1 Controls on the spatial occurrence of anabranching in the Australian arid zone

Of the 19 major rivers in the LEB (Habeck-Fardy and Nanson 2014), 14 have an anabranching planform for much of their length and, of these, nine anabranch for more than 50% of their length accumulating a total anabranching length of ~4000 km. Given the prevalence of this channel pattern, what is it that causes its occurrence, or not, in any given location? Chapters 5 and 7 addressed the evolution of anabranching in two different rivers in very different sedimentary and geomorphic settings in the LEB, spanning from the late Pelistocene to the present day.

'Type 1' (muddy, cohesive, anastomosing) anabranching (classification system of Nanson and Knighton 1996) occurs in the Channel Country, but only in the upper to middle reaches of Cooper Creek and the Diamantina River (Figure 8.3) whilst the lower reaches (proximal to Kati Thanda-Lake Eyre) are predominantly single thread. In the two largest tributaries in the LEB (Cooper Creek and the Diamantina River) the change from anabranching to single thread planforms is consistent with an increase in slope downstream of the Gason-Cooryana Dome (Figure 8.3). Type 1 anabranching can persist over very low gradients with slopes as low 0.0001 m.m^{-1} being able to maintain discharges of close to 10 000 m^3.s^{-1} (Smith 1983; Smith et al. 1989) whereas meandering requires a moderate gradient to persist. This 'type 1' anabranching is considered to be stable over extended period (Rust and Nanson 1986) that occurs when the valley slope is less than the minimum slope required for the given sediment load, and in order to achieve equilibrium the slope would have to adjust. However, the Channel Country reaches of Cooper Creek and the Diamantina

River cannot increase slope due to localised tectonics. The uplifting Innamincka and Gason-Cooryana Domes result in reduced slope upstream (Jansen et al. 2013).

In the Marshall River 'type 2' and 'type 4' anabranching exist, these are defined, , by Nanson and Knighton (1996) as island ('type 2') and ridge ('type 4') form anabranching. The cause of anabranching on the Marshall River is also likely to be slope related. As described by Tooth and Nanson (2004), unlike conditions in the adjacent single-thread Plenty River that is transporting a load of medium sand at the same gradient as the Marshall, the coarse sand and granule grainsize in the latter exceeds that that can be carried by the available stream power in a single wide channel. The channel deposits sediment as islands and ridges to reduce w/d ratios and thereby increase individual channel (anabranch) efficiency.

A further spatial control on anabranching in the LEB is presented by Morón and Amos (2018), this being grain size and by inference geology. Whereby, anabranching occurs where sediment is coarser grained. The Neales River has similar longitudinal changes between anabranching and single thread planforms to Cooper Creek and a number of other anabranching LEB rivers (Morón and Amos 2018). Low stream power and an inability to therefore move coarser sediment was found to initiate anabranching in the Neales River (Morón and Amos 2018). This is also seen in the Northern Plains, on the Sandover-Bundy River, where tributary input of coarser sediment initiates the formation of in channel islands (Tooth and Nanson 2000a). Further evidence of grainsize as a control on anabranching is also the Marshall and the Plenty rivers which despite flowing parallel under the same hydrological and slope conditions, the Marshall River anabranches and the Plenty River does not, with the Marshall River being the more coarse grained of the two.

Therefore, it appears that the different forms anabranching in the LEB are located in settings where adjustment through an increase in slope cannot readily provide the required stream power for the imposed sediment load and this would warrant further investigation with grainsize analysis of the sediment from Cooper Creek. The question of when the LEB adopted such anabranching planforms, and why, forms the focus of the discussion below.
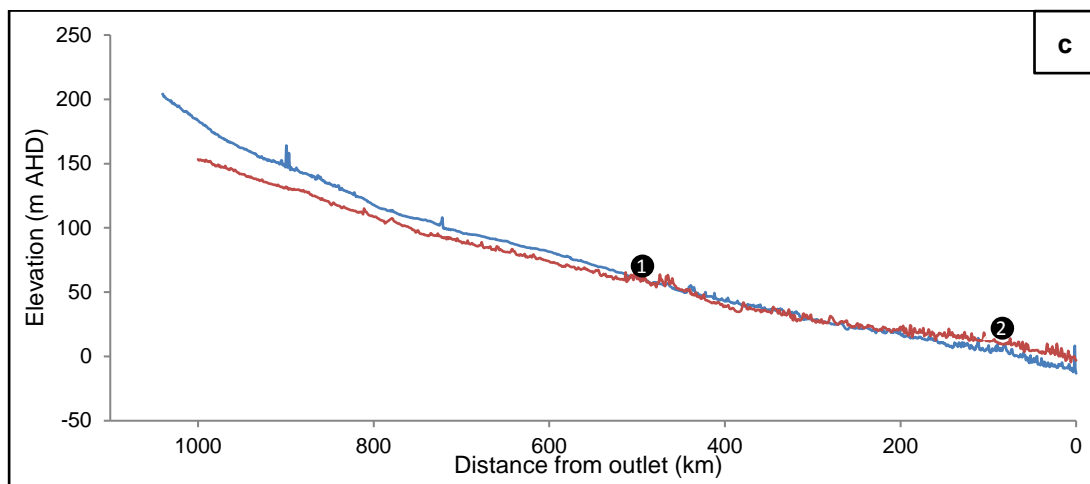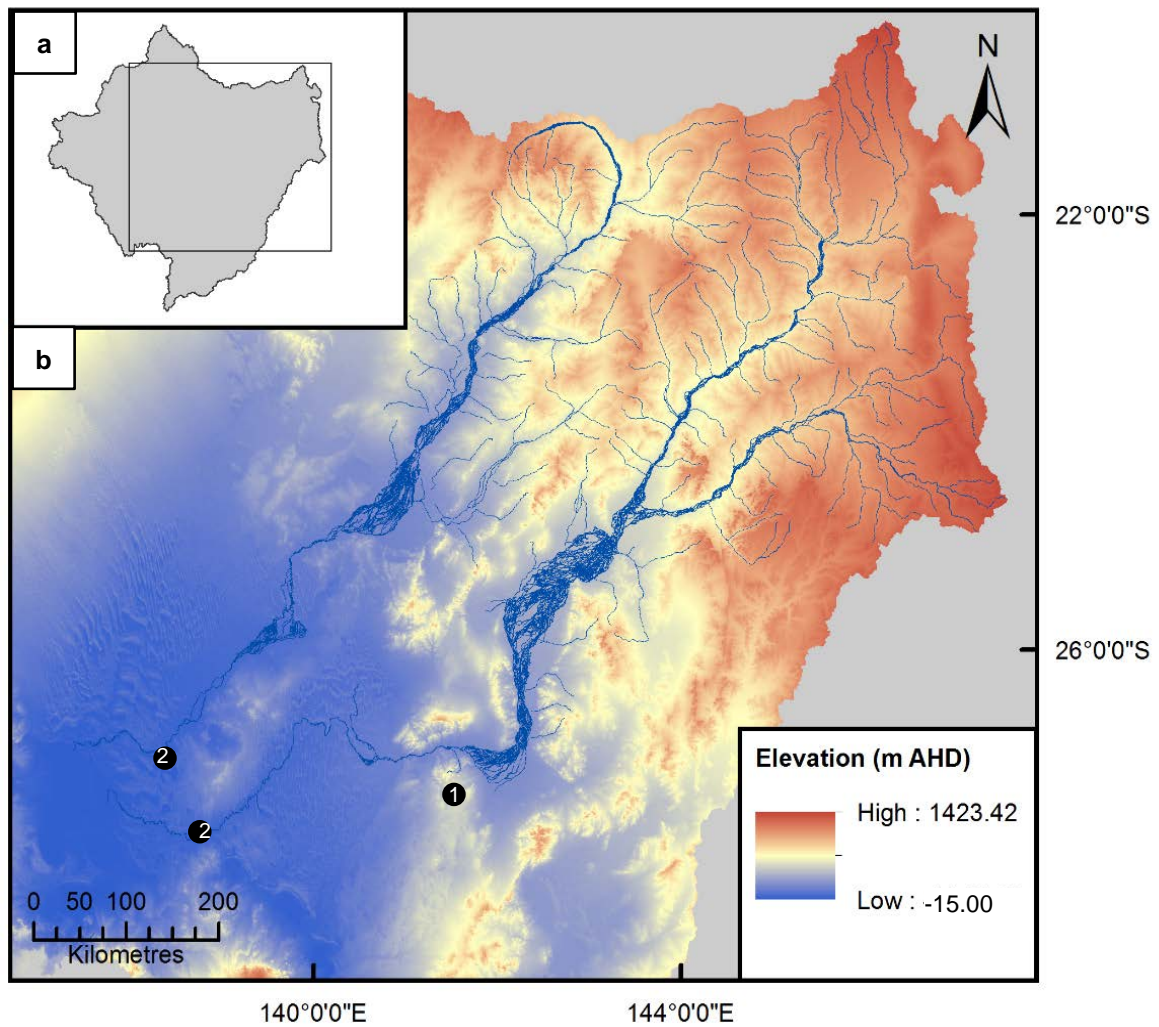
Figure 8.3 – (a) Location of area in the LEB. (b)Digital elevation model from the 1-arc second SRTM, with the Diamantina River and Cooper Creek marked, black stars show where the channels intersect with the Innamincka (1) and Gason-Cooryana (2) Domes. (c) Long profiles of Cooper Creek (blue) and the Diamantina River (red) from the start of the main channel (start of floodplain) to the outlet at Kati Thanda-Lake Eyre. Black stars mark the location on the long profile of the Innamincka (1) and Gason-Cooryana (2) Domes. Long profiles are derived from the 1-arc second SRTM.

8.3.2 Temporal occurrence of anabranching in the LEB

Chapters 5 and 7 addressed the evolution of anabranching in two different rivers in different areas of the LEB. The prior chronology of anabranching deposits combined with that measured in this study spans the Late Pleistocene to the present day.

From the chronologies two different instigators for anabranching have been identified. In the eastern LEB, the control on anabranching appears to be climate related as close correlations can be made with global climate variations and with previous work on late Wuaternary climate fluctuations in the LEB. Based on the data presented in Chapter 5, meandering rivers dominated prior to 28 ka with a peak in sandy deposition seen in the data compilation during MIS 5c. From ~95 ka to ~28 ka there is a continuous decline in the frequency of sand deposits, with an increase in the frequency of mud deposits. This transition from meandering to anabranching would have been gradual with the older mud deposits likely to represent overbank and floodplain deposits. Since MIS 5 the bedload was muddier, with flow cutting into the existing floodplain and mud infilling the existing channels. By ~28 ka a switch in dominance had occurred with a minimum in meandering deposits and a continued increase in anabranching deposits. After 28 ka the switch to a mud dominated anabranching planform appears to have been essentially completed.

In the LEB MIS 5 was wetter than present (Hesse et al. 2004) and fluvial conditions dominated (Nanson et al. 1992) with a number of highstands at Kati Thanda-Lake Eyre from 75 – 100 ka (Magee et al. 2004; Cohen et al. 2015). It was after the MIS 5 pluvial (90-120 ka) that Nanson et al. (1992) suggested a switch from meandering to anabranching occurred, although the data presented here suggests that that the switch was more gradual. The wetter conditions of MIS 5 were able to maintain large laterally active meandering rivers, as reflected in the prevalence of meandering deposits in the dataset, and this is interpreted to be a function of enhanced discharge due to elevated precipitation in the headwater regions. This enhanced discharge was likely seen throughout the LEB with the lake high stand also seen at Lake Frome during MIS 5 where in MIS 5c water was of sufficient depth for Lake Frome and Kati Thanda-Lake Eyre to be connected (Cohen et al. 2011). Further evidence that this wetter period is widespread, beyond the LEB, is seen at Lake Gregory in northern Australia, where a megalake phase was identified around 100-90 ka with

volumes four times that at present (Bowler et al. 2001). This also coincides with enhanced fluvial activity in the Gulf of Carpentaria based on evidence of increased sedimentation rates on the Gilbert Fan delta (Nanson et al. 1991; 2005; Reeves et al. 2008).

An increase in precipitation during MIS 5 is also evidenced with high speleothem deposition/growth rates in the southern arid-zone (Ayliffe et al. 1998). From MIS 5 aridity and/or hydrological variability gradually increased in central Australia presumably transforming it to a landscape of low runoff coefficients (Costelloe et al. 2005) and high transmission losses (Knighton and Nanson 1994a; Costelloe 2013). This is reflected in the frequency of meandering deposits starting to decrease from MIS 5. During MIS 4 and early MIS 3 there was also slightly enhanced fluvial activity, although not as great as in MIS 5 (Nanson et al. 2008).

MIS 3 in the Channel Country fluvial record shows that sandy meandering channels appear to have returned during a period of enhanced wetness and associated fluvial activity. There appears to have been a return to a general drying trend in the LEB with fluvial activity being markedly suppressed after early MIS 3 (Nanson et al 2008). The reduction in meandering deposits leading up to the transition is reflected elsewhere in the climate record, with Lakes Eyre and Frome in drying phases from ~48 ka culminating in the current playa condition (Cohen et al. 2015). Sea levels were also lower during MIS 3 than at any other time during the last glacial cycle aside from the LGM (Lambeck and Chapell 2001) and sea surface temperatures in the Southern Ocean were also lowered (Barrows et al. 2007) indicating a cool dry climate. This corresponds to reducing fluvial activity which we interpret from the sedimentary record and is supported by the absence of water in Kati Thanda-Lake Eyre, implying a reduced input from tropically-sourced runoff (Magee et al. 2004). Increasing aridity in the LEB is supported by evidence of dune building from 40 ka (Hesse et al. 2004).

In the LGM, the Channel Country dataset shows the final reduction in the deposition of meandering deposits and marks the start of an increase in anabranching deposits. The climatic conditions in the LGM are debated. Aeolian process appear to have dominated with a peak in aridity (Fitzsimmons et al. 2014) allowing for deflation of the Kati Thanda-Lake Eyre surface into surrounding dunes (Hesse et al. 2004). This

dune building period has been identified elsewhere in Australia, corresponding with low sea-level and a supply of material from the continental shelf (Lees 1992).

After this time sedimentological evidence elsewhere in the LEB shows that the climate was becoming more variable than previous interglacials. During the early Holocene there was an increase in effective precipitation in arid Australia (Singh and Luly 1991; McCarthy and Head 2001; Magee et al. 2004), resulting in a low-level lake phase at Kati Thanda-Lake Eyre (Magee et al. 2004), although there was no return to fluvial conditions of the magnitude seen during MIS 5 and MIS 3 (Nanson et al. 1992). After ~5 ka, the climate became ENSO dominated and there is evidence of variability in fluvial activity with a series of pluvial events on the Mt Chambers fan and intermittent increased lake-levels at Lake Callabonna (Gliganic et al. 2014). This climatic variability has not produced conditions conducive to a return to a meandering planform.

The metamorphosis from high discharge meandering to anabranching, which in this case is described as 'type 1c' anabranching (cohesive sediment, semi-arid, mud-dominated), corresponds with a climatic change from a warm, wet climate to a cooler, drier, more variable climate. The temperature increase and moisture increase in the mid-Holocene, which saw an increase in precipitation to ~5 ka (Cohen et al. 2012), appears not to have been sufficient to trigger a further transition back to the laterally active sandy system that characterised parts of MIS 5, 4 and 3 as well.

A question arises, given the strong probable climatic cause identified for anabranching in the eastern LEB. Has all anabranching in the LEB been initiated on the same timescale and due to the same influencing factors? Chapter 7 investigated the age of anabranching islands on the Marshall River in the northwestern LEB. These anabranching deposits are sedimentologically very different to those of Cooper Creek and the Diamantina River and represent an equilibrium state, island and ridge form anabranching, rather than the muddy anastomosing planform. The cycle on which the island and ridge building phase lasts is ~500 years. Anabranching in the Marshall River is likely a function of the current climatic regime as in Cooper Creek, due to the arid climate resulting in insufficient flow to provide the required stream power for the given bedload and the tectonically quiescent environment. However, when those climatic conditions triggered a shift to an anabranching

planform on the Marshall River remains unknown as the initial onset of anabranching cannot however be dated due to the cyclic nature of the system, which removes the traces of the previous island building phase.

8.4 Late Quaternary arid zone channel metamorphosis: a global phenomenon?

Given the broad correlation of changes in planform to glacial/interglacial changes the question arises as to whether other rivers, globally, have experienced similar planform changes in the Late Quaternary? Information on arid zone river responses to climate change for much of the Late Quaternary is scant and studies which directly approach whether planform metamorphosis has occurred appear to be even more limited. The discussion below engages with the available literature on river response to Quaternary climate change and investigates whether rivers outside of the LEB have responded in the same manner to climatic changes, first in Australia, then other arid and semi-arid areas, and finally globally.

The fluvial planform adjustments in the Channel Country broadly correspond to glacial-interglacial cycles, as presented in Chapter 5. Given that glacial-interglacial scale climate change is determined to be approximately globally synchronous, at least at the resolution proffered by fluvial deposits, one might expect corresponding fluctuations in discharge and planform changes elsewhere in the arid zone, possibly globally.

8.4.1 An Australian perspective

In Australia, comparisons can be drawn between the rivers investigated in this thesis and other rivers with chronologies covering the Late Quaternary. The Neales River, in the western LEB shows similarly enhanced fluvial activity during MIS 5, with active channels that are synchronous with a lake high-stand in Kati Thanda-Lake Eyre (Croke et al. 1996). Further enhanced fluvial activity is seen during MIS 3 in the Neales River, where channel incision was occurring (Croke et al. 1996), implying enhanced stream power, which is also seen in the Cooper Creek stratigraphy as an increase in meandering type deposition (Nanson et al. 1992). A general drying trend is identified from 30 ka during the LGM the Neales River becoming ephemeral and

aeolian deposition occurring (Croke et al. 1996) inferring that during this time is when those parts of the Neales River which are anabranching became established.

While periods of enhanced and supressed fluvial activity appear to be synchronous throughout the LEB, there is also evidence of enhanced and fairly synchronous fluvial activity in the Murray-Murrumbidgee basin in southeastern Australia during MIS 5 and MIS 3 (Page et al. 1991; Page et al. 1996). Here, however, there no evidence of any major corresponding planform change until the development of highly sinuous meanders after the Yanco phase that ended about 12ka The Murrumbidgee River also shows enhanced fluvial activity during the LGM (Mueller et al. in press).

8.4.2   A global perspective

Looking at arid and semi-arid regions beyond Australia, rivers for comparison are few and far between. The first issue arises in that analogues for direct comparison are rare, due the uniqueness of the LEB, with its arid environment, low slope, tectonic quiescence and endorheic drainage. Secondly, arid zone rivers are not widely investigated, and even less so for those representing the entire time period from MIS 5 to the present.

The Inland Niger Delta in Mali provides the only other comprehensively described example of Knighton and Nanson's (1996) 'type 1c' anabranching (Makaske 2001). While the Inland Niger Delta is, as a result of more rapid subsidence, is accreting more quickly, anabranching is shown to be a long-lived stable planform as in Cooper Creek. The stratigraphy is shown to be similar, with sandy deposits underlying ~4-5 m of mud. The similarity to Cooper Creek is marked, with a semi-static avulsion regime and slow accretion. The similarity between the systems continues with the presence of dunes, which form adjacent to, and can partially infringe on, the channels. Given the geomorphic, sedimentological and climatological similarities between the systems it is likely formation occurred due to similar reasons, however no chronology exists.

With the sparse chronological evidence available, a general trend for fluvial fluctuations to correlate to climate fluctuations is seen. Examples from the Arabian Peninsula (Parker 2010) and India (Jain and Tandon 2003) show enhanced fluvial

activity commonly during MIS 5, with fan formation and channel incision, respectively. The Arabian Peninsula shows enhanced fluvial activity with three distinct pulses of fan aggradation from ~160 ka to the early Holocene (Farraj and Harvey 2004) and an increase in fluvial sand deposition throughout the region (Parker 2010). These phases of enhanced fluvial activity are dated at MIS 5, and tentatively at MIS 3 (Parker 2010). Enhanced dune building is also seen during MIS 5, attributed to a greater supply of sediment. The deposits of the Arabian Peninsula are poorly and sporadically dated but the presence of alluvial fan and sand deposits, implies a different planform in the past compared to the highly ephemeral and in places entirely absent river systems seen today.

In India, the rivers of the Thar Desert show a succession of planform changes from MIS 5 to present, in particular for the Luni basin (Jain and Tandon 2003). During MIS 5 these rivers were braided with gravel beds, a planform which continued during MIS 4. During MIS 3 landscape stability and pedogensis was occurring with meandering channels from 54 - 30 ka (Srivastava et al. 2001). A transition to ephemeral sand bed streams occurred at MIS 2 with enhanced aeolian activity (Jain and Tandon 2003). The transition appears to have been reversed at the start of the Holocene with channel incision followed by a transition through gravel braided, and meandering channels ~14 ka to ~3 ka, by which point the system was aeolian dominated. At two of the four sites incision and floodplain development has occurred since ~1 ka (Jain and Tandon 2003). Overall, it is concluded that gravel bed, braided planforms dominated during wetter phases, MIS 5 and early MIS 1, and ephemeral rivers and sheet floods dominated during drier phases.

More recent changes seen in arid zone rivers are also seen in the Nile River where at ~20 ka BP it switched from a seasonally regulated braided river to a sinuous suspended load system coinciding with a shift to warmer wetter headwater conditions (Adamson et al. 1980).

When approaching rivers on a global scale, a large amount of the research relating to changes during the Holocene exists (e.g. Macklin and Lewin 2003; Macklin et al. 2005; Macklin et al. 2006). While a few longer archives do exist, they are largely from Europe (e.g. Fuller et al. 1998; Howard et al. 2007), where many rivers have, historically, been glacially influenced. A general trend is present that river planforms

and behaviour have been identified to correlate to the same cyclicity as seen in the global glacial–interglacial/stadial-interstadial cycles (Vandenberghe 2002), with rivers responding to climatically forced changes in discharge through incision, when discharge is enhanced, and deposition, when discharge is reduced. Incisional events can also be represented as an erosional gap in the depositional series, an example of which is seen in the Thames River, UK where the erosional gaps, indicating enhanced fluvial activity, correspond to interglacials (Büdel 1977).

A somewhat global trend is seen in temperate zone high relief European and American rivers, where the aggradation episodes coincide with stadials/glacials and incision phases coincide with interstadials/interglacials (e.g. Fuller et al. 1998; Blum et al. 2000). Given the lack of relief in central Australia, it is unlikely that the rivers would respond to global climate changes in the same manner. This is also reflected in aeolian activity where dune building phases, indicating greater sediment availability, during MIS 2 occur in a number of rivers worldwide including the rivers in this thesis, the rivers of the Luni Basin, India (Jain and Tandon 2003) and a number of rivers in north west Europe (e.g. Maas River and Schelde River, Netherlands (Kasse 2002).

A key difference between the rivers of the LEB, and other arid rivers, and the majority of global rivers, is the fluctuations in planforms seen after the LGM to ~14 ka. This is due to the input of sediment through glacial melt which frequently initiated a switch to a braided planform with incision occurring after 14 ka, when sediment load reduced (e.g. Mississippi River; Teller 1987; Wright 1987). Post-glacial, there was also an increase in vegetation cover in temperate zones, reducing sediment supply and aiding the return to meandering rivers (Kozarski 1991; Starkel 1991; Jain and Tandon 2003). This did not occur in the LEB, as vegetation cover has always remained sparse.

8.4.3 Summary

In conclusion, late Quaternary channel metamorphosis is not well documented nor well constrained, but a switch from meandering to anabranching appears to be unusual. While all global rivers appear to respond similarly to global climate change with changes in discharge, the way that this change manifests varies due to basin characteristics, with the rivers of the LEB responding with a switch to anabranching

due to the low slope environment, and low stream power. In the LEB, and other arid basins, the changes correlating with climatic changes are superimposed on an overall trend of increasing aridity.

8.5 Conclusions

This thesis had three key conclusions derived from each of the results chapters.

Chapter 5 raised the question of how we analyse geochronological data from different sources and how we can justify the conclusions we draw. What was created is a method by which we can objectively distinguish signal from noise. The conclusion of Chapter 5 was that kernel density estimates (KDEs) are the most reliable way of presenting geochronological datasets and can be easily utilised in creating a synthetic dataset, with a given set of statistical characteristics, to simulate what could be considered a level of noise for a set of observed data. It was established, therefore, that the variations seen in the fluvial geochronology data had significance given that they were distinguishable from the random noise. As the data was concluded to be useful, and fit for purpose, the interpretation was made that in the Channel Country, 'type 1' anabranching (Nanson and Knighton 1996), was initiated due to increasing aridity, most likely driven by global climate fluctuations. The transition to anabranching is interpreted as having begun at the end of MIS 5 when sand transport started to decrease substantially. The increase in mud deposition and contemporaneous sand deposition, is indicative of floodplain deposition and muddy infill. There was an increase in sand deposition during MIS 3, but not to MIS 5 levels likely indicating a return in dominance to meandering systems. However, by the LGM a switch to anabranching had been completed in the lowest slope regions of the eastern LEB, with channels cutting into the previous floodplain deposits and channels being infilled. The more downstream reaches of the eastern LEB rivers are of slightly greater slope and do not anabranch, suggesting that they are above the threshold slope for the initiation of anabranching. Overall, it was established that, when compared to other rivers in the arid zone and globally the initiation of anabranching in the LEB appears to be somewhat unique.

The quantification of sediment storage/burial in the Cooper Creek system in Chapter 6, using terrestrial cosmogenic nuclides, shows burial of up to 1.2 Ma, driven by low

slope and highly variable flow in Cooper Creek. Apparent burial is related to accommodation space in the system, with prolonged apparent burial in areas of large accommodation space, and minimal apparent burial where accommodation space is limited. Therefore, apparent burial duration in Cooper Creek is closely related to the morphology of the channel and valley setting. This is in contrast to the Western LEB where there is an overall increase in burial with distance downstream. This further differs from more humid fluvial systems, where long buried sediment is only accessed when floodplains are reworked through channel avulsion.

Chapter 7 shows that anabranching ridges and islands in the Marshall River are formed by a balance between alluvial erosion and deposition in this dynamic system. An example of one of the large islands showed it to be relatively long-lived; 3 ka at 0.45 m and 13 ka at 1.64 m depth. It is made up of finer sediment that has accreted more slowly than the sandy ridges that characterise other reaches of the Marshall River. The narrow depositional ridges that create relatively narrow and well-defined multiple anabranching channels are formed largely of medium sand and show no distinct stratigraphy. From those dated they appear to have a maximum lifetime of ~500 years, as if being created, destroyed and rebuilt on a cyclical scale of about this periodicity in order to maintain an equilibrium sand-transporting system. Anabranching in the northwestern LEB is somewhat unique and is also initiated by slope, as the channel is close to bedrock so is unable to increase slope by down cutting.

Overall it can be concluded that arid rivers vary greatly, even within the LEB. The sediment conveyors are not the same and the potential for sediment storage and a burial signal in the system depends on quantity of available sediment cover and accommodation space within the system. The location of anabranching in the LEB can be linked, in general, to the arid climate and the low slopes. Anabranching is initiated where energy gradients and discharges are less than that required to transfer the sediment loads that are supplied. In the case of the Channel Country, the metamorphosis of planform from meandering to anabranching is due to Late Quaternary climate change greatly reducing flow discharges under conditions where localised tectonics and sedimentation have reduced gradients. On the Northern Plains, the presence of anabranching is specific to the endogenic characteristics of a

river in regards to specific combinations of grainsize and slope that cause one river to anabranch in order to maintain equilibrium, when an adjacent river does not.

Reference List

Adamson, D.A., Gasse, F., Street, F.A. and Williams, M.A.J., 1980. Late Quaternary history of the Nile. *Nature*, *288*(5786), pp.50.

Aitken, M.J., 1976. Thermoluminescent age evaluation and assessment of error limits: revised system. *Archaeometry, 18*(2), pp.233-238.

Aitken, M.J., 1998. *An Introduction to Optical Dating.* Oxford University Press, Oxford.

Aitken, M.J. and Mejdahl, V., 1985. *Thermoluminescence dating (Vol. 359).* Academic Press, London.

Aitken, M.J., Tite, M.S. and Reid, J., 1964. Thermoluminescent dating of ancient ceramics. *Nature*, *202*(4936), pp.1032.

Aitken, M.J., Zimmerman, D.W. and Fleming, S.J., 1968. Thermoluminescent dating of ancient pottery. *Nature*, *219*(5153), pp.442.

Al Farraj, A. and Harvey, A.M., 2004. Late Quaternary interactions between aeolian and fluvial processes: a case study in the northern UAE. *Journal of Arid Environments*, *56*(2), pp.235-248.

Al-Masrahy, M.A. and Mountney, N.P., 2015. A classification scheme for fluvial–aeolian system interaction in desert-margin settings. *Aeolian Research, 17*, pp.67-88.

Alexandrov, Y., Laronne, J.B. and Reid, I., 2003. Suspended sediment transport in flash floods of the semiarid northern Negev, Israel. *International Association of Hydrological Sciences Publication, 278,* pp.346-352.

Allen, J.R.L., 1982. Longitudinal bedforms and secondary flows. *Sedimentary Structures: Their Character and Physical Basis (Developments in Sedimentology 30A and 30B)* Elsevier, New York, pp.1-52.

Allen, P.A., 2008. From landscape into geological history. *Nature, 451*(7176), pp.274-276.

Alley, N.F., 1998. Cainozoic stratigraphy, palaeoenvironments and geological evolution of the Lake Eyre Basin. *Palaeogeography, Palaeoclimatology, Palaeoecology, 144*(3-4), pp.239-263.

Arnold, L.J. and Roberts, R.G., 2009. Stochastic modelling of multi-grain equivalent dose (De) distributions: Implications for OSL dating of sediment mixtures. *Quaternary Geochronology*, *4*(3), pp.204-230.

Arnold, L.J., Roberts, R.G., Galbraith, R.F. and DeLong, S.B., 2009. A revised burial dose estimation procedure for optical dating of young and modern-age sediments. *Quaternary Geochronology*, *4*(4), pp.306-325.

Ayliffe, L.K., Marianelli, P.C., Moriarty, K.C., Wells, R.T., McCulloch, M.T., Mortimer, G.E. and Hellstrom, J.C., 1998. 500 ka precipitation record from south-eastern Australia: evidence for interglacial relative aridity. *Geology*, *26*(2), pp.147-150.

Bailey, R.M. and Arnold, L.J., 2006. Statistical modelling of single grain quartz De distributions and an assessment of procedures for estimating burial dose. *Quaternary Science Reviews, 25*(19-20), pp.2475-2502.

Bailey, R.M., Smith, B.W. and Rhodes, E.J., 1997. Partial bleaching and the decay form characteristics of quartz OSL. *Radiation Measurements*, *27*(2), pp.123-136.

Balco, G. and Rovey, C.W., 2008. An isochron method for cosmogenic-nuclide dating of buried soils and sediments. *American Journal of Science, 308*(10), pp.1083-1114.

Balco, G., Stone, J.O., Lifton, N.A. and Dunai, T.J., 2008. A complete and easily accessible means of calculating surface exposure ages or erosion rates from [10]Be and [26]Al measurements. *Quaternary geochronology, 3*(3), pp.174-195.

Barrows, T.T., Juggins, S., De Deckker, P., Calvo, E. and Pelejero, C., 2007. Long-term sea surface temperature and climate change in the Australian–New Zealand region. *Paleoceanography*, *22*(2).

Bastin G and the ACRIS Management Committee, 2008. *Rangelands 2008 — Taking the Pulse,* National Land and Water Resources Audit, Canberra.

Bateman, M.D., Frederick, C.D., Jaiswal, M.K., and Singhvi, A.K., 2003. Investigations into the potential effects of pedoturbation on luminescence dating. *Quaternary Science Reviews, 22*(10), 1169-1176.

Bateman, M.D., Boulter, C.H., Carr, A.S., Frederick, C.D., Peter, D. and Wilder, M., 2007. Preserving the palaeoenvironmental record in drylands: bioturbation and its significance for luminescence-derived chronologies. *Sedimentary Geology*, *195*(1), pp.5-19.

Berger, G.W., 1990. Effectiveness of natural zeroing of the thermoluminescence in sediments. *Journal of Geophysical Research: Solid Earth, 95*(B8), pp.12375-12397.

Berger, G.W. and Luternauer, J.J., 1987. Preliminary fieldwork for thermoluminescence dating studies at the Fraser River delta, British Columbia. *Geological Survey of Canada Paper, 87*, pp.901-904.

Bierman, P.R. and Caffee, M., 2001. Slow rates of rock surface erosion and sediment production across the Namib Desert and escarpment, southern Africa. *American Journal of Science, 301*(4-5), pp.326-358.

Bierman, P.R. and Caffee, M., 2002. Cosmogenic exposure and erosion history of Australian bedrock landforms. *Geological Society of America Bulletin 114*(7), pp. 787-803.

Bierman, P. and Steig, E.J., 1996. Estimating rates of denudation using cosmogenic isotope abundances in sediment. *Earth Surface Processes and Landforms, 21*(2), pp.125-139.

Bierman, P.R., Albrecht, A., Bothner, M.H., Brown, E.T., Bullen, T.D., Gray, L.B. and Turpin, L., 1998. Erosion, weathering, and sedimentation. In: C. Kendall and J.J. McDonnell (eds.). *Isotope tracers in catchment hydrology*, Elsevier, pp. 647-678.

Bierman, P.R., Reuter, J.M., Pavich, M., Gellis, A.C., Caffee, M.W. and Larsen, J., 2005. Using cosmogenic nuclides to contrast rates of erosion and sediment yield in a semi-arid, arroyo-dominated landscape, Rio Puerco Basin, New Mexico. *Earth Surface Processes and Landforms, 30*(8), pp.935-953.

Bishop, P., 2007. Long-term landscape evolution: linking tectonics and surface processes. *Earth Surface Processes and Landforms, 32*(3), pp.329-365.

Blum, M.D., Guccione, M.J., Wysocki, D.A., Robnett, P.C. and Rutledge, E.M., 2000. Late Pleistocene evolution of the lower Mississippi River valley, southern Missouri to Arkansas. *GSA Bulletin*, *112*(2), pp.221-235.

Bowler, J.M., Wyrwoll, K.H. and Lu, Y., 2001. Variations of the northwest Australian summer monsoon over the last 300,000 years: the paleohydrological record of the Gregory (Mulan) Lakes System. *Quaternary International*, *83*, pp.63-80.

Bowler, J.M., Johnston, H., Olley, J.M., Prescott, J.R., Roberts, R.G., Shawcross, W. and Spooner, N.A., 2003. New ages for human occupation and climatic change at Lake Mungo, Australia. *Nature, 421*(6925), pp.837.

Bowman, H.H., 2003. *The flow hydraulics of Cooper Creek through the Innamincka Dome*. Unpublished BSc (Hons) thesis, School of Geosciences, University of Wollongong.

Bridge, J. and Demicco, R., 2008. *Earth surface processes, landforms and sediment deposits.* Cambridge University Press.

Bridgland, D. and Westaway, R., 2008. Climatically controlled river terrace staircases: a worldwide Quaternary phenomenon. *Geomorphology*, *98*(3-4), pp.285-315.

Brown, E.T., Brook, E.J., Raisbeck, G.M., Yiou, F. and Kurz, M.D., 1992. Effective attenuation lengths of cosmic rays producing ^{10}Be and ^{26}Al in quartz: Implications for exposure age dating. *Geophysical Research Letters, 19*(4), pp.369-372.

Brown, E.T., Stallard, R.F., Larsen, M.C., Raisbeck, G.M. and Yiou, F., 1995. Denudation rates determined from the accumulation of in situ-produced ^{10}Be in the Luquillo Experimental Forest, Puerto Rico. *Earth and Planetary Science Letters, 129*(1-4), pp.193-202.

Bull, L.J., 2002. *Dryland rivers: hydrology and geomorphology of semi-arid channels.* John Wiley & Sons.

Bullard, J.E. and Livingstone, I., 2002. Interactions between aeolian and fluvial systems in dryland environments. *Area, 34*(1), pp.8-16.

Bullard, J.E. and McTainsh, G.H., 2003. Aeolian-fluvial interactions in dryland environments: examples, concepts and Australia case study. *Progress in Physical Geography, 27*(4), pp.471-501.

Buylaert, J.P., Jain, M., Murray, A.S., Thomsen, K.J., Thiel, C. and Sohbati, R., 2012. A robust feldspar luminescence dating method for Middle and Late Pleistocene sediments. *Boreas, 41*(3), pp.435-451.

Bunn, S. E., Thoms, M. C., Hamilton, S. K., and Capon, S. J. 2006, Flow variability in dryland rivers: boom, bust and the bits in between. *River Research and Applications, 22*(2), pp. 179-186.

Bureau of Meteorology, 2015. *Hydrologic Reference Stations*. Accessed:15/02/2016, http://www.bom.gov.au/water/hrs/index.shtml

Bureau of Meteoroloy, 2016. *Intensity-Frequency-Duration*. Accessed:04/09/2016 http://www.bom.gov.au/water/designRainfalls/ifd/

Bureau of Meteorology, 2018. *Climate data online*. Accessed:10/08/2018, http://www.bom.gov.au/climate/data/index.shtml

Büdel, J., 1977. *Klima-Geomorphologie*. Gebrüder Borntraeger Verlagsbuchhandlung, Berlin.

Callen, R.A. and Bradford, J., 1992. Cooper Creek fan and Strzelecki Creek–hypsometric data, Holocene sedimentation, and implications for human activity. *Mines and Energy Review*, *158*, pp.52-57.

Callen, R.A. and Nanson, G.C., 1992. Formation and age of dunes in the Lake Eyre Depocentres. *Geologische Rundschau, 81*(2), pp.589-593.

Cantalice, J.R.B., Cunha Filho, M., Stosic, B.D., Piscoya, V.C., Guerra, S.M. and Singh, V.P., 2013. Relationship between bedload and suspended sediment in the sand-bed Exu River, in the semi-arid region of Brazil. *Hydrological sciences journal, 58*(8), pp.1789-1802.

Chang, H.H., 1980, Geometry of gravel streams. *Journal of the Hydraulics Division, 106*(9), pp. 1443-1456.

Chapot, M.S., Roberts, H.M., Duller, G.A.T. and Lai, Z.P., 2012. A comparison of natural-and laboratory-generated dose response curves for quartz optically stimulated luminescence signals from Chinese Loess. *Radiation Measurements, 47*(11-12), pp.1045-1052.

Child, D., Elliott, G., Mifsud, C., Smith, A.M. and Fink, D., 2000. Sample processing for earth science studies at ANTARES. *Nuclear Instruments and Methods in Physics Research Section B: Beam Interactions with Materials and Atoms*, *172*(1-4), pp.856-860.

Chmeleff, J., von Blanckenburg, F., Kossert, K. and Jakob, D., 2010. Determination of the ^{10}Be half-life by multicollector ICP-MS and liquid scintillation counting. *Nuclear Instruments and Methods in Physics Research Section B: Beam Interactions with Materials and Atoms*, *268*(2), pp.192-199.

Ciampalini, A., Persano, C., Fabel, D. and Firpo, M., 2015. Dating Pleistocene deltaic deposits using in-situ 26Al and 10Be cosmogenic nuclides. *Quaternary Geochronology*, *28*, pp.71-79.

Clapp, E.M., Bierman, P.R., Schick, A.P., Lekach, J., Enzel, Y. and Caffee, M., 2000. Sediment yield exceeds sediment production in arid region drainage basins. *Geology, 28*(11), pp.995-998.

Codilean, A.T., 2006. Calculation of the cosmogenic nuclide production topographic shielding scaling factor for large areas using DEMs. *Earth Surface Processes and Landforms, 31*(6), pp.785-794.

Cohen, T.J., Nanson, G.C., Larsen, J.R., Jones, B.G., Price, D.M., Coleman, M. and Pietsch, T.J., 2010. Late Quaternary aeolian and fluvial interactions on the Cooper Creek Fan and the association between linear and source-bordering dunes, Strzelecki Desert, Australia. *Quaternary Science Reviews, 29*(3-4), pp.455-471.

Cohen, T.J., Nanson, G.C., Jansen, J.D., Jones, B.G., Jacobs, Z., Treble, P., Price, D.M., May, J.H., Smith, A.M., Ayliffe, L.K. and Hellstrom, J.C., 2011. Continental aridification and the vanishing of Australia's megalakes. *Geology, 39*(2), pp.167-170.

Cohen, T.J., Jansen, J.D., Gliganic, L.A., Larsen, J.R., Nanson, G.C., May, J.H., Jones, B.G. and Price, D.M., 2015. Hydrological transformation coincided with megafaunal extinction in central Australia. *Geology, 43*(3), pp.195-198.

Coleman, M., 2002. *Alluvial, aeolian and lacustrine evidence of climatic flow regime changes over the past 250 ka, Cooper Creek near Innamincka, South Australia.* Unpublished PhD thesis, School of Geosciences, University of Wollongong.

Cooke, R.U., Warren, A. and Goudie, A.S., 1993. *Desert Geomorphology.* CRC Press.

Costelloe, J.F., Grayson, R.B. and McMahon, T.A., 2005. Modelling stream flow for use in ecological studies in a large, arid zone river, central Australia. *Hydrological Processes: An International Journal, 19*(6), pp.1165-1183.

Costelloe, J.F., 2013. Hydrological assessment and analysis of the Cooper Creek catchment, South Australia. *A report to the South Australian Arid Lands Natural Resources Management Board, Port Augusta.*

Craig, H. and Poreda, R.J., 1986. Cosmogenic 3He in terrestrial rocks: The summit lavas of Maui. *Proceedings of the National Academy of Sciences, 83*(7), pp.1970-1974.

Croke, J., Magee, J. and Price, D., 1996. Major episodes of Quaternary activity in the lower Neales River, northwest of Lake Eyre, central Australia. *Palaeogeography, Palaeoclimatology, Palaeoecology, 124*(1-2), pp.1-15.

Croke, J.C., Magee, J.W. and Wallensky, E.P., 1999. The role of the Australian Monsoon in the western catchment of Lake Eyre, central Australia, during the Last Interglacial. *Quaternary International, 57*, pp.71-80.

Crossman, S. and Li, O., 2015. *Surface Hydrology lines (regional)*[downloaded dataset] Accessed:04/04/2016. https://ecat.ga.gov.au/geonetwork/srv/eng/catalog.search?node=srv#/metada ta/1186e898-14b5-812e-e053-10a3070a76f0

Cunningham, A.C., and Wallinga, J., 2012. Realizing the potential of fluvial archives using robust OSL chronologies. *Quaternary Geochronology, 12*, pp.98-106.

Daniels, F., Boyd, C.A. and Saunders, D.F., 1953. Thermoluminescence as a research tool. *Science, 117*(3040), pp.343-349.

Dannhaus, N., Wittmann, H., Krám, P., Christl, M. and Von Blanckenburg, F., 2018. Catchment-wide weathering and erosion rates of mafic, ultramafic, and granitic rock from cosmogenic meteoric 10Be/9Be ratios. *Geochimica et Cosmochimica Acta, 222,* pp.618-641.

Darvill, C.M., 2013. Cosmogenic nuclide analysis. *British society for geomorphology, geomorphological techniques,* pp.25.

Davis, M., Matmon, A., Fink, D., Ron, H. and Niedermann, S., 2011. Dating Pliocene lacustrine sediments in the central Jordan Valley, Israel—Implications for

cosmogenic burial dating. *Earth and Planetary Science Letters, 305*(3-4), pp.317-327.

Davis, M., Matmon, A., Rood, D.H. and Avnaim-Katav, S., 2012. Constant cosmogenic nuclide concentrations in sand supplied from the Nile River over the past 2.5 my. *Geology, 40*(4), pp.359-362.

Dawson, N.M., Ahern, C.R., 1974. Soils. In: N.M. Dawson, C.R. Ahern, and D.E. Boyland (eds.). Western arid region, land use study, Part 1. Queensland Dept. Primary Industries Tech. Bull. 12,Brisbane, pp. 18–46.

Dehnert, A. and Schlüchter, C., 2008. Sediment burial dating using terrestrial cosmogenic nuclides. *Eiszeitalter und Gegenwart (Quaternary Science Journal,) 57*, pp.210-225.

Desilets, D. and Zreda, M., 2003. Spatial and temporal distribution of secondary cosmic-ray nucleon intensities and applications to in situ cosmogenic dating. *Earth and Planetary Science Letters, 206*(1-2), pp.21-42.

Desilets, D., Zreda, M. and Prabu, T., 2006. Extended scaling factors for in situ cosmogenic nuclides: new measurements at low latitude. *Earth and Planetary Science Letters, 246*(3-4), pp.265-276.

Diaz, H.F., and Bradley, R.S. 2004. *The Hadley Circulation: Present, Past and Future.* Springer Netherlands.

Dibble, H.L., Aldeias, V., Jacobs, Z., Olszewski, D.I., Rezek, Z., Lin, S.C., Alvarez-Fernández, E., Barshay-Szmidt, C.C., Hallett-Desguez, E., Reed, D. and Reed, K., 2013. On the industrial attributions of the Aterian and Mousterian of the Maghreb. *Journal of Human Evolution, 64*(3), pp.194-210.

Dorsaz, J.M., Gironás, J., Escauriaza, C. and Rinaldo, A., 2013. The geomorphometry of endorheic drainage basins: implications for interpreting and modelling their evolution. *Earth Surface Processes and Landforms, 38*(15), pp.1881-1896.

Duller, G.A.T., 1996. Recent developments in luminescence dating of Quaternary sediments. *Progress in Physical Geography, 20*(2), pp.127-145.

Duller, G.A. and Murray, A.S., 2000. Luminescence dating of sediments using individual mineral grains. *Geologos*, *5*(8).

Duller, G.A.T., Bøtter-Jensen, L. and Murray, A.S., 2000. Optical dating of single sand-sized grains of quartz: sources of variability. *Radiation Measurements*, *32*(5), pp.453-457.

Duller, G.A.T., 2012. Improving the accuracy and precision of equivalent doses determined using the optically stimulated luminescence signal from single grains of quartz. *Radiation Measurements*, *47*(9), pp.770-777.

Dunai, T.J., 2000. Scaling factors for production rates of in situ produced cosmogenic nuclides: a critical reevaluation. *Earth and Planetary Science Letters, 176*(1), pp.157-169.

Dunai, T.J., 2010. *Cosmogenic nuclides: principles, concepts and applications in the earth surface sciences*. Cambridge University Press.

Dunkerley, D.L. 1992. Channel geometry, bed material, and inferred flow conditions in ephemeral stream systems, Barrier Range, Western NSW, Australia. *Hydrological Processes, 6*(4), 417-433.

Dunkerley, D.L., 2011. Desert soils. *Arid zone geomorphology: process, form and change in drylands*, pp.101-129.

Dunne, J., Elmore, D. and Muzikar, P., 1999. Scaling factors for the rates of production of cosmogenic nuclides for geometric shielding and attenuation at depth on sloped surfaces. *Geomorphology, 27*(1-2), pp.3-11.

Durcan, J.A. and Duller, G.A., 2011. The fast ratio: a rapid measure for testing the dominance of the fast component in the initial OSL signal from quartz. *Radiation Measurements*, *46*(10), pp.1065-1072.

Fagan, S.D., 2001. *Channel and floodplain characteristics of Cooper Creek, central Australia*. Unpublished PhD thesis, School of Geosciences, University of Wollongong.

Fagan, S.D. and Nanson, G.C., 2004. The morphology and formation of floodplain-surface channels, Cooper Creek, Australia. *Geomorphology, 60(1-2),* pp.107-126.

Fink, D. and Smith, A., 2007. An inter-comparison of ^{10}Be and ^{26}Al AMS reference standards and the ^{10}Be half-life. *Nuclear Instruments and Methods in Physics Research Section B: Beam Interactions with Materials and Atoms*, *259*(1), pp.600-609.

Finlayson, B., 2010. Rivers in Australia. *Frontiers of Earth Science in China, 4*(4), pp.375-385.

Finlayson, B.L., and McMahon, T.A. 1988, Australia vs the world: a comparative analysis of streamflow characteristics. *Fluvial geomorphology of Australia*, pp.17-40.

Finlayson, B.L. and Brizga, S.O., 1993. Anastomosing channels and arroyo development on the Nogoa River, Central Queensland, Australia. *Sedimentary Geology, 85(1-4),* pp.179-190.

Fisher, A., Fink, D., Chappell, J. and Melville, M., 2014. ^{26}Al/^{10}Be dating of an aeolian dust mantle soil in western New South Wales, Australia. *Geomorphology*, *219*, pp.201-212.

Fitzsimmons, K.E., Cohen, T.J., Hesse, P.P., Jansen, J., Nanson, G.C., May, J.H., Barrows, T.T., Haberlah, D., Hilgers, A., Kelly, T. and Larsen, J., 2013. Late Quaternary palaeoenvironmental change in the Australian drylands. *Quaternary Science Reviews, 74*, pp.78-96.

Freeman, M.J., 1986, *Huckitta SF53–11: 1:250,000 geological map series, Explanatory notes*. Darwin, Department of Mines and Energy and Northern Territory Geological Survey, pp.58.

Frostick, L.E., Reid, I. and Layman, J.T., 1983. Changing Size Distribution of Suspended Sediment in Arid-Zone Flash Floods. In: J. D. Collinson and J. Lewin (eds.). *Modern and Ancient Fluvial Systems,* International Association of Sedimentologists, Special publication 6, Blackwell Scientific Publications, Oxford, pp.97-106.

Fryirs, K., 2013. (Dis) Connectivity in catchment sediment cascades: a fresh look at the sediment delivery problem. *Earth Surface Processes and Landforms, 38*(1), pp.30-46.

Fryirs, K.A., Brierley, G.J., Preston, N.J. and Kasai, M., 2007. Buffers, barriers and blankets: the (dis) connectivity of catchment-scale sediment cascades. *Catena*, *70*(1), pp.49-67.

Fuchs, M. and Lang, A., 2001. OSL dating of coarse-grain fluvial quartz using single-aliquot protocols on sediments from NE Peloponnese, Greece. *Quaternary Science Reviews, 20*(5-9), pp.783-787.

Fujioka, T., Chappell, J., Honda, M., Yatsevich, I., Fifield, K. and Fabel, D., 2005. Global cooling initiated stony deserts in central Australia 2–4 Ma, dated by cosmogenic ^{21}Ne-^{10}Be. *Geology, 33*(12), pp.993-996.

Fujioka, T. and Chappell, J., 2010. History of Australian aridity: chronology in the evolution of arid landscapes. *Geological Society, London, Special Publications, 346*(1), pp.121-139.

Fujioka, T. and Chappell, J., 2011. Desert landscape processes on a timescale of millions of years, probed by cosmogenic nuclides. *Aeolian Research, 3*(2), pp.157-164.

Fuller, I.C., Macklin, M.G., Lewin, J., Passmore, D.G. and Wintle, A.G., 1998. River response to high-frequency climate oscillations in southern Europe over the past 200 ky. *Geology*, *26*(3), pp.275-278.

Gaisser, T.K., Engel, R. and Resconi, E., 2016. *Cosmic rays and particle physics.* Cambridge University Press.

Galbraith, R.F., 2005. *Statistics for fission track analysis*. Chapman and Hall/CRC.

Galbraith, R.F. and Roberts, R.G., 2012. Statistical aspects of equivalent dose and error calculation and display in OSL dating: an overview and some recommendations. *Quaternary Geochronology, 11*, pp.1-27.

Galbraith, R.F., Roberts, R.G., Laslett, G.M., Yoshida, H. and Olley, J.M., 1999. Optical dating of single and multiple grains of quartz from Jinmium rock shelter, northern Australia: Part I, experimental design and statistical models. *Archaeometry, 41*(2), pp.339-364.

Gibling, M.R., Nanson, G.C. and Maroulis, J.C., 1998. Anastomosing river sedimentation in the Channel Country of central Australia. *Sedimentology, 45*(3), pp.595-619.

Gliganic, L.A., Jacobs, Z. and Roberts, R.G., 2012. Luminescence characteristics and dose distributions for quartz and feldspar grains from Mumba rockshelter, Tanzania. *Archaeological and Anthropological Sciences*, *4*(2), pp.115-135.

Gliganic, L.A., Cohen, T.J., May, J.H., Jansen, J.D., Nanson, G.C., Dosseto, A., Larsen, J.R. and Aubert, M., 2014. Late-Holocene climatic variability indicated by three natural archives in arid southern Australia. *The Holocene*, *24*(1), pp.104-117.

Gliganic, L.A., May, J.H. and Cohen, T.J., 2015. All mixed up: using single-grain equivalent dose distributions to identify phases of pedogenic mixing on a dryland alluvial fan. *Quaternary international, 362*, pp.23-33.

Gliganic, L.A., Cohen, T.J., Meyer, M. and Molenaar, A., 2017. Variations in luminescence properties of quartz and feldspar from modern fluvial sediments in three rivers. *Quaternary Geochronology, 41*, pp.70-82.

Gosse, J.C. and Phillips, F.M., 2001. Terrestrial in situ cosmogenic nuclides: theory and application. *Quaternary Science Reviews*, *20*(14), pp.1475-1560.

Graf, W.L., 1988. *Fluvial processes in dryland rivers*. Springer-Verlag, New York.

Graf, W.H., 1984. *Hydraulics of sediment transport.* Water Resources Publication.

Granger, D.E. and Muzikar, P.F., 2001. Dating sediment burial with in situ-produced cosmogenic nuclides: theory, techniques, and limitations. *Earth and Planetary Science Letters, 188*(1-2), pp.269-281.

Granger, D.E. and Smith, A.L., 2000. Dating buried sediments using radioactive decay and muogenic production of ^{26}Al and ^{10}Be. *Nuclear Instruments and Methods in Physics Research Section B: Beam Interactions with Materials and Atoms, 172*(1-4), pp.822-826.

Granger, D.E., Kirchner, J.W. and Finkel, R., 1996. Spatially averaged long-term erosion rates measured from in situ-produced cosmogenic nuclides in alluvial sediment. *The Journal of Geology, 104*(3), pp.249-257.

Guérin, G., Mercier, N. and Adamiec, G., 2011. Dose-rate conversion factors: update. *Ancient TL*, *29*(1), pp.5-8.

Guralnik, B., Matmon, A., Avni, Y., Porat, N. and Fink, D., 2011. Constraining the evolution of river terraces with integrated OSL and cosmogenic nuclide data. *Quaternary Geochronology, 6(1),* pp.22-32.

Guralnik, B., Li, B., Jain, M., Chen, R., Paris, R.B., Murray, A.S., Li, S.H., Pagonis, V., Valla, P.G. and Herman, F., 2015. Radiation-induced growth and isothermal decay of infrared-stimulated luminescence from feldspar. *Radiation Measurements*, *81*, pp.224-231.

Gurnis, M., Müller, R.D. and Moresi, L., 1998. Cretaceous vertical motion of Australia and the AustralianAntarctic discordance. *Science, 279*(5356), pp.1499-1504.

Gutierrez, M. and Benito, G., 2005. *Climatic geomorphology*. Amsterdam: Elsevier.

Habeck-Fardy, A., 2013. *River Channel Self-Adjustment Towards Equilibrium: Endogenic And Exogenic Influences On Distinctly Different River Types In The Lake Eyre Basin Of Arid Central Australia*, Unpublished PhD Thesis,

School of Earth and Environmental Sciences, University of Wollongong, Australia.

Habeck-Fardy, A. and Nanson, G.C. 2014, Environmental character and history of the Lake Eyre Basin, one seventh of the Australian continent. *Earth-Science Reviews*, 132, pp.39-66.

Hammer, U.T. 1986. Saline lakes: distribution and uses. In: D. T. Waite (ed.). *Evaluating saline waters in a plains environment.* Universidad de Regina pp. 1-22.

Heerdegen, R., 2001. *The geomorphological role of rivers*. Oxford University Press

Heimsath, A.M., Chappell, J. and Fifield, K., 2010. Eroding Australia: rates and processes from Bega Valley to Arnhem Land. *Geological Society, London, Special Publications, 346*(1), pp.225-241.

Heisinger, B., 1998. *Muon Induced Production of Radionuclides.* Unpublished PhD Thesis, Technical University of Munich, Germany

Heisinger, B., Lal, D., Jull, T.A.J., Kubik, P.W., Ivy---Ochs, S., Neumaier, S., Knie, K., Lazarev, V., and Nolte, E., 2002a, Production of selected cosmogenic radionuclides by muons 1. Fast muons: *Earth and Planetary Science Letters, 200*, pp.345–355.

Heisinger, B., Lal, D., Jull, T.A.J., Kubik, P.W., Ivy---Ochs, S., Knie, K., and Nolte, E., 2002b, Production of selected cosmogenic radionuclides by muons: 2.Capture of negative muons: *Earth and Planetary Science Letters, 200*, pp. 357–369.

Hesse, P.P., 2010. The Australian desert dunefields: formation and evolution in an old, flat, dry continent. *Geological Society, London, Special Publications*, *346*(1), pp.141-164.

Hesse, P., 2011. Sticky dunes in a wet desert: formation, stabilisation and modification of the Australian desert dunefields. *Geomorphology*, *134*(3-4), pp.309-325.

Hesse, P.P., 2016. How do longitudinal dunes respond to climate forcing? Insights from 25 years of luminescence dating of the Australian desert dunefields. *Quaternary International, 410*, pp.11-29.

Hesse, P.P., Magee, J.W. and van der Kaars, S., 2004. Late Quaternary climates of the Australian arid zone: a review. *Quaternary International, 118*, pp.87-102.

Hidy, A.J., Gosse, J.C., Pederson, J.L., Mattern, J.P. and Finkel, R.C., 2010. A geologically constrained Monte Carlo approach to modeling exposure ages from profiles of cosmogenic nuclides: An example from Lees Ferry, Arizona. *Geochemistry, Geophysics, Geosystems*, *11*(9).

Howard, A.D. 1982, Equilibrium and time scales in geomorphology: Application to sand-bed alluvial streams. *Earth Surface Processes and Landforms*, 7(4), pp.303-325.

Howard, A.J., Bridgland, D., Knight, D., McNabb, J., Rose, J., Schreve, D., Westaway, R., White, M.J. and White, T.S., 2007. The British Pleistocene fluvial archive: East Midlands drainage evolution and human occupation in the context of the British and NW European record. *Quaternary Science Reviews*, *26*(22-24), pp.2724-2737.

Hostetler, S.W., 1995. Hydrological and thermal response of lakes to climate: description and modeling. In *Physics and chemistry of Lakes*. Springer, Berlin, Heidelberg. pp.63-82

Houston, J. and Hartley, A.J., 2003. The central Andean west-slope rainshadow and its potential contribution to the origin of hyper-aridity in the Atacama Desert. *International Journal of Climatology, 23(12),* pp.1453-1464.

Huang, H.Q. and Chang, H.H., 2006. Scale independent linear behavior of alluvial channel flow. *Journal of Hydraulic Engineering*, *132*(7), pp.722-730.

Huang, H.Q., and Nanson, G.C. 2007, Why some alluvial rivers develop an anabranching pattern. *Water Resources Research*, *43*(7).

Huang, H.Q., Nanson, G.C., and Fagan, S.D. 2002, Hydraulic geometry of straight alluvial channels and the principle of least action. *Journal of Hydraulic Research*, 40(2), 153-160.

Huang, H.Q., Chang, H.H. and Nanson, G.C., 2004. Minimum energy as the general form of critical flow and maximum flow efficiency and for explaining variations in river channel pattern. *Water Resources Research*, *40*(4).

Huntley, D.J., Godfrey-Smith, D.I. and Thewalt, M.L., 1985. Optical dating of sediments. Nature, 313(5998), pp.105.

Hwang, J.N., Lay, S.R. and Lippman, A., 1994. Nonparametric multivariate density estimation: a comparative study. *IEEE Transactions on Signal Processing, 42*(10), pp.2795-2810.

Jacobs, Z., Wintle, A.G., Roberts, R.G. and Duller, G.A., 2008. Equivalent dose distributions from single grains of quartz at Sibudu, South Africa: context, causes and consequences for optical dating of archaeological deposits. *Journal of Archaeological Science, 35*(7), pp.1808-1820.

Jacobs, Z., Hayes, E.H., Roberts, R.G., Galbraith, R.F. and Henshilwood, C.S., 2013. An improved OSL chronology for the Still Bay layers at Blombos Cave, South Africa: further tests of single-grain dating procedures and a re-evaluation of the timing of the Still Bay industry across southern Africa. *Journal of Archaeological Science*, *40*(1), pp.579-594.

Jaeger, K.L., Sutfin, N.A., Tooth, S., Michaelides, K. and Singer, M., 2017. Geomorphology and sediment regimes of intermittent rivers and ephemeral streams. In*: Intermittent Rivers and Ephemeral Streams (pp. 21-49).* Academic Press.

Jain, M. and Tandon, S.K., 2003. Fluvial response to Late Quaternary climate changes, western India. *Quaternary Science Reviews*, *22*(20), pp.2223-2235.

Jain, M., Murray, A.S. and Bøtter-Jensen, L., 2003. Characterisation of blue-light stimulated luminescence components in different quartz samples: implications for dose measurement. *Radiation Measurements*, *37*(4), pp.441-449.

Jain, M., Murray, A.S., and Botter-Jensen, L. (2004). Optically stimulated luminescence dating: how significant is incomplete light exposure in fluvial environments? [Datation par luminescence stimulée optiquement: quelle signification en cas de blanchiment incomplet des sédiments fluviatiles?]. *Quaternaire, 15*(1), pp.143-157.

Jankowski, N.R., 2014. *Chronologies in context: reconciling the optical dating of quartz with its sedimentary environment.* Unpublished PhD Thesis, School of Earth and Environmental Sciences, University of Wollongong, Australia.

Jankowski, N.R. and Jacobs, Z., 2018. Beta dose variability and its spatial contextualisation in samples used for optical dating: An empirical approach to examining beta microdosimetry. *Quaternary Geochronology, 44*, pp.23-37.

Jankowski, N.R., Jacobs, Z. and Goldberg, P., 2015. Optical dating and soil micromorphology at MacCauley's Beach, new South Wales, Australia. *Earth Surface Processes and Landforms*, *40*(2), pp.229-242.

Jansen, J. D., and Nanson, G. C. 2004, Anabranching and maximum flow efficiency in Magela Creek, northern Australia. *Water Resources Research,40(4):* W04503.

Jansen, J.D., Nanson, G.C., Cohen, T.J., Fujioka, T., Fabel, D., Larsen, J.R., Codilean, A.T., Price, D.M., Bowman, H.H., May, J.H. and Gliganic, L.A., 2013. Lowland river responses to intraplate tectonism and climate forcing quantified with luminescence and cosmogenic [10]Be. *Earth and Planetary Science Letters,* 366, pp.49-58.

Judd, D. A., Rutherfurd, I. D., Tilleard, J. W., and Keller, R. J. (2007). A case study of the processes displacing flow from the anabranching Ovens River,

Victoria, Australia. *Earth Surface Processes and Landforms, 32*(14), 2120-2132.

Kasse, C., 2002. Sandy aeolian deposits and environments and their relation to climate during the Last Glacial Maximum and Lateglacial in northwest and central Europe. *Progress in physical Geography*, *26*(4), pp.507-532.

Kernich A. L., Pain, C. F., Clarke, J. D. A. and Fitzpatrick, A. D., 2009, Geomorphology of a dryland fluvial system: the Lower Balonne River, southern Queensland, *Australian Journal of Earth Sciences*, 56:S1, S139-S153,

Kingsford, R. T. and Thompson, J. R., 2006, Desert or Dryland rivers of the World: an Introduction. In: R.T. Kingsford (ed.). *Ecology of Desert Rivers*, Cambridge University Press: Cambridge, pp.3–10.

Klein, J., Giegengack, R., Middleton, R., Sharma, P., Underwood, J.R. and Weeks, R.A., 1986. Revealing histories of exposure using in situ produced ^{26}Al and ^{10}Be in Libyan desert glass. *Radiocarbon, 28*(2A), pp.547-555.

Knighton, A.D. and Nanson, G.C., 1994a. Flow transmission along an arid zone anastomosing river, Cooper Creek, Australia. *Hydrological Processes, 8*(2), pp.137-154.

Knighton, A.D., and Nanson, G.C., 1994b. Waterholes and their significance in the anastomosing channel system of Cooper Creek, Australia. *Geomorphology 9*(4), 311-324.

Knighton, A.D. and Nanson, G.C., 1997. Distinctiveness, diversity and uniqueness in arid zone river systems. In D.S.G. Thomas (ed.). *Arid Zone Geomorphology: Process, Form and Change in Drylands, 2nd Edition*, John Wiley and Sons, pp.185-203.

Knighton, A.D. and Nanson, G.C., 2001. An event-based approach to the hydrology of arid zone rivers in the Channel Country of Australia. *Journal of Hydrology, 254(1-4),* pp.102-123.

Kober, F., Ivy-Ochs, S., Zeilinger, G., Schlunegger, F., Kubik, P.W., Baur, H. and Wieler, R., 2009. Complex multiple cosmogenic nuclide concentration and histories in the arid Rio Lluta catchment, northern Chile. *Earth Surface Processes and Landforms*, *34*(3), pp.398-412.

Kohl, C.P. and Nishiizumi, K., 1992. Chemical isolation of quartz for measurement of in-situ-produced cosmogenic nuclides. *Geochimica et Cosmochimica Acta*, *56*(9), pp.3583-3587.

Korschinek, G., Bergmaier, A., Faestermann, T., Gerstmann, U.C., Knie, K., Rugel, G., Wallner, A., Dillmann, I., Dollinger, G., Von Gostomski, C.L. and Kossert, K., 2010. A new value for the half-life of ^{10}Be by heavy-ion elastic recoil detection and liquid scintillation counting. *Nuclear Instruments and Methods in Physics Research Section B: Beam Interactions with Materials and Atoms*, *268*(2), pp.187-191.

Kotwicki, V., 1986. *Floods of Lake Eyre*. Engineering and Water Supply Department, Adelaide.

Kozarski, S., 1991. Warta—a case study of a lowland river. *Temperate Palaeohydrology*, pp.189-215.

Kubik, P.W., Christl, M., and Alfimov, V., 2009. New Primary ^{10}Be standard and T1/2 for AMS at ETH. *Ion Beam Physics, ETH Zurich Annual repor*t, pp. 12.

Kurz, M.D., 1986a. Cosmogenic helium in a terrestrial igneous rock. *Nature, 320*(6061), pp.435-439.

Kurz, M.D., 1986b. In situ production of terrestrial cosmogenic helium and some applications to geochronology. *Geochimica et Cosmochimica Acta, 50*(12), pp.2855-2862.

Laity, J. 2008. *Deserts and deserts environments.* Hoboken, NJ. Wiley.

Lake Eyre Basin Scientific Advisory Panel., 2008. *State of the basin 2008: Rivers assessment.* Commonwealth of Australia, Canberra,

Lal, D., 1991. Cosmic ray labelling of erosion surfaces: in situ nuclide production rates and erosion models. *Earth and Planetary Science Letters, 104*(2-4), pp.424-439.

Lambeck, K. and Chappell, J., 2001. Sea level change through the last glacial cycle. *Science*, *292*(5517), pp.679-686.

Lang, A., 1994. Infra-red stimulated luminescence dating of Holocene reworked silty sediments. *Quaternary Science Reviews, 13(5-7),* pp.525-528.

Langford, R.P., 1989. Fluvial-aeolian interactions: Part I, modern systems. *Sedimentology, 36*(6), pp.1023-1035.

Laronne, J.B., and Reid, I. 1993. Very high rates of bedload sediment transport by ephemeral desert rivers. *Nature, 366*(6451), pp.148.

Larsen, J.R., 2011. Aspects of the contempory amd Quaternary hydrology of the Lake Eyre Basin. Unpublished PhD Thesis, School of Earth and Environmental Sciences, University of Wollongong Australia

Latrubesse, E.M. 2008, Patterns of anabranching channels: The ultimate end-member adjustment of mega rivers. *Geomorphology, 101(1),* pp.130-145.

Lees, B.G., 1992. Geomorphological evidence for late Holocene climatic change in northern Australia. *The Australian Geographer*, *23*(1), pp.1-10.

Leon, J.X. and Cohen, T.J., 2012. An improved bathymetric model for the modern and palaeo Lake Eyre. *Geomorphology, 173*, pp.69-79.

Leopold, L.B. and Bull, W.B., 1979. Base level, aggradation, and grade. Proceedings of the *American Philosophical Society, 123*(3), pp.168-202.

Leopold, L.B., and Wolman, M.G. 1957, River channel patterns: Braided, meandering and straight. *U.S. Geol. Surv. Prof. Pap., 282-B.*

Leopold, L.B., and Wolman, M.G. 1960, River meanders. *Geological Society of America Bulletin, 71*(6), pp.769-793.

Leopold, L.B., Wolman, M.G., and Miller, J.P., 1964. *Fluvial Processes in Geomorphology*, W. H. Freeman, New York.

Lepper, K., Larsen, N.A. and McKeever, S.W., 2000. Equivalent dose distribution analysis of Holocene eolian and fluvial quartz sands from Central Oklahoma. *Radiation Measurements, 32*(5-6), pp.603-608.

Lewin, J. and Macklin, M.G., 2003. Preservation potential for Late Quaternary river alluvium. *Journal of Quaternary Science, 18*(2), pp.107-120.

Li, B. and Li, S.H., 2012. Luminescence dating of Chinese loess beyond 130 ka using the non-fading signal from K-feldspar. *Quaternary Geochronology, 10*, pp.24-31.

Li, B., Li, S.H. and Wintle, A., 2008. Overcoming environmental dose rate changes in luminescence dating of waterlain deposits. *Geochronometria, 30(1),* pp.33-40.

Lifton, N.A., Bieber, J.W., Clem, J.M., Duldig, M.L., Evenson, P., Humble, J.E. and Pyle, R., 2005. Addressing solar modulation and long-term uncertainties in scaling secondary cosmic rays for in situ cosmogenic nuclide applications. *Earth and Planetary Science Letters, 239*(1-2), pp.140-161.

Lüthgens, C., Neuhuber, S., Grupe, S., Payer, T., Peresson, M. and Fiebig, M., 2017. Geochronological investigations using a combination of luminescence and cosmogenic nuclide burial dating of drill cores from the Vienna Basin. *Zeitschrift der Deutschen Gesellschaft für Geowissenschaften, 168(1),* pp.115-140.

Mabbutt, J.A., 1965, The weathered land surface in central Australia: *Zeitschrift für Geomorphologie, 9,* pp.82–114.

Mabbutt, J.A., 1967. Denudation chronology in central Australia: Structure, climate and landform inheritance in the Alice Springs area. In: J.N. Jennings and J.A. Mabbutt (eds.). *Landform studies from Australia and New Guinea.* Australian National University Press Canberra. pp.144-181

Mabbutt, J.A., 1977. *Desert landforms: an introduction to systematic geomorphology*. MIT Press, Cambridge, Massachusetts.

Mackin, J., 1948. Concept of the graded river. *Geological Society of America Bulletin, 59*(5), pp.463-512.

Macklin, M.G. and Lewin, J., 2003. River sediments, great floods and centennial-scale Holocene climate change. *Journal of Quaternary Science: Published for the Quaternary Research Association*, *18*(2), pp.101-105.

Macklin, M.G., Johnstone, E. and Lewin, J., 2005. Pervasive and long-term forcing of Holocene river instability and flooding in Great Britain by centennial-scale climate change. *The Holocene*, *15*(7), pp.937-943.

Macklin, M.G., Benito, G., Gregory, K.J., Johnstone, E., Lewin, J., Michczyńska, D.J., Soja, R., Starkel, L. and Thorndycraft, V.R., 2006. Past hydrological events reflected in the Holocene fluvial record of Europe. *Catena*, *66*(1-2), pp.145-154.

Magee, J.W., 1997. *Late Quaternary environments and palaeohydrology of Lake Eyre, arid central Australia*. Unpublished PhD Thesis. Australian National University, Australia.

Magee, J.W., Bowler, J.M., Miller, G.H. and Williams, D.L.G., 1995. Stratigraphy, sedimentology, chronology and palaeohydrology of Quaternary lacustrine deposits at Madigan Gulf, Lake Eyre, South Australia. *Palaeogeography, Palaeoclimatology, Palaeoecology*, *113*(1), pp.3-42.

Magee, J.W., Miller, G.H., Spooner, N.A. and Questiaux, D., 2004. Continuous 150 ky monsoon record from Lake Eyre, Australia: insolation-forcing implications and unexpected Holocene failure. *Geology, 32*(10), pp.885-888.

Makaske, B. 2001, Anastomosing rivers: a review of their classification, origin and sedimentary products. *Earth-Science Reviews*, *53*(3), 149-196.

Maroulis, J.C., 2000. *Stratigraphy and mid-to-late quaternary chronology of the Cooper Creek floodplain, southwest Queensland, Australia.* Unpublished PhD Thesis, School of Geosciences, University of Wollongong, Australia.

Maroulis, J.C. and Nanson, G.C., 1996. Bedload transport of aggregated muddy alluvium from Cooper Creek, central Australia: a flume study. *Sedimentology, 43*(5), pp.771-790.

Maroulis, J.C., Nanson, G.C., Price, D.M. and Pietsch, T., 2007. Aeolian–fluvial interaction and climate change: source-bordering dune development over the past~ 100 ka on Cooper Creek, central Australia. *Quaternary Science Reviews, 26*(3-4), pp.386-404.

Marsaglia, G., 1995. DIEHARD, a battery of tests for random number generators. Department of Statistics and Supercomputer Computations Research Institute, Florida State University.

Marti, K. and Craig, H., 1987. Cosmic-ray-produced neon and helium in the summit lavas of Maui. *Nature, 325*(6102), pp.335.

Masarik, J. and Beer, J., 1999. Simulation of particle fluxes and cosmogenic nuclide production in the Earth's atmosphere. *Journal of Geophysical Research: Atmospheres, 104*(D10), pp.12099-12111.

Mather, A.E., Stokes, M. and Whitfield, E., 2017. River terraces and alluvial fans: the case for an integrated Quaternary fluvial archive. *Quaternary Science Reviews, 166*, pp.74-90.

Matsumoto, M. and Nishimura, T., 1998. Mersenne twister: a 623-dimensionally equidistributed uniform pseudo-random number generator. *ACM Transactions on Modeling and Computer Simulation (TOMACS), 8*(1), pp.3-30.

May, J.H., Barrett, A., Cohen, T.J., Jones, B.G., Price, D. and Gliganic, L.A., 2015. Late Quaternary evolution of a playa margin at Lake Frome, South Australia. *Journal of Arid Environments, 122*, pp.93-108.

Mayya, Y.S., Morthekai, P., Murari, M.K. and Singhvi, A.K., 2006. Towards quantifying beta microdosimetric effects in single-grain quartz dose distribution. *Radiation Measurements*, *41*(7), pp.1032-1039.

McCarthy, L. and Head, L., 2001. Holocene variability in semi-arid vegetation: new evidence from Leporillus middens from the Flinders Ranges, South Australia. *The Holocene*, *11*(6), pp.681-689.

McMahon, T.A. 1979, Hydrological characteristics of arid zones. The Hydrology of Areas of Low Precipitation. *Proceedings of the Canberra Symposium. International Association of Hydrological Sciences Publication No. 128*. IAHS Press, Wallingford, pp.105–123.

McMahon, T. A., Finlayson, B. L., Haines, A. T., and Srikanthan, R. 1992. *Global runoff: continental comparisons of annual flows and peak discharges.* Catena Verlag.

McMahon, T.A., Murphy, R., Little, P., Costelloe, J.F., Peel, M.C., Chiew, F.H.S., Hayes, S., Nathan, R., Kandel, D.D., 2005. *Hydrology of Lake Eyre Basin.* Report to Department of Environment and Heritage, Canberra

McMahon, T.A., Murphy, R.E., Peel, M.C., Costelloe, J.F. and Chiew, F.H., 2008. Understanding the surface hydrology of the Lake Eyre Basin: part 2—streamflow. *Journal of Arid Environments, 72*(10), pp.1869-1886.

McMahon, T.A., Murphy, R.E., Peel, M.C., Costelloe, J.F. and Chiew, F.H., 2008b. Understanding the surface hydrology of the Lake Eyre Basin: part 1—rainfall. *Journal of Arid Environments, 72*(10), pp.1853-1868.

McTainsh, G., and Strong. C., 2007. The role of aeolian dust in ecosystems. *Geomorphology 89*(1), pp.39-54.

Mejdahl, V., 1979. Thermoluminescence dating: beta-dose attenuation in quartz grains. *Archaeometry, 21*(1), pp.61-72.

Mejdahl, V., 1986. Thermoluminescence dating of sediments. *Radiation Protection Dosimetry, 17*(1-4), pp.219-227.

Meybeck, M., Green, P. and Vörösmarty, C., 2001. A new typology for mountains and other relief classes: an application to global continental water resources and population distribution. *Mountain Research and Development, 21*(1), pp.34-45.

Miall, A.D., 1977. A review of the braided-river depositional environment. *Earth-Science Reviews, 13*(1), pp.1-62.

Middleton, N., and Thomas, D. 1997, *World atlas of desertification* (2nd edition). Arnold, Hodder Headline, PLC.

Mifsud, C., Fujioka, T. and Fink, D. (2013), `Extraction and purication of quartz in rock using hot phosphoric acid for in situ cosmogenic exposure dating', *Nuclear Instruments and Methods in Physics Research Section B: Beam Interactions with Materials and Atoms 294*, 203-207.

Milliman, J. D. and Meade, R. H. 1983, Worldwide delivery of river sediment to the oceans. *Journal of Geology*, *91*, pp.1–21.

Moore, P.D., 1998. Desert ecology: Life in the upper crust. *Nature*, *393*(6684), 419-420.

Morón, S., Edmonds, D.A. and Amos, K., 2017. The role of floodplain width and alluvial bar growth as a precursor for the formation of anabranching rivers. *Geomorphology, 278,* pp.78-90.

Morón, S. and Amos, K.J., 2018. Downstream grain-size changes associated with a transition from single channel to anabranching. *Sedimentology, 65(5),* pp.1590-1610.

Mueller, D., Jacobs, Z., Cohen T.J., Price, D.M., Reinfelds, I.V. and Shulmeister, J., In press. Revisiting an arid LGM using fluvial archives: A luminescence chronology for palaeochannels of the Murrumbidgee River, southeastern Australia. *Journal of Quaternary Science*

Murray, A.S., and Roberts, R.G. (1997). Determining the burial time of single grains of quartz using optically stimulated luminescence. *Earth and Planetary Science Letters, 152*(1), 163-180.

Murray, A.S. and Roberts, R.G., 1997. Determining the burial time of single grains of quartz using optically stimulated luminescence. *Earth and Planetary Science Letters, 152*(1-4), pp.163-180.

Murray, A.S., and Wintle, A.G. (2000). Luminescence dating of quartz using an improved single-aliquot regenerative-dose protocol. *Radiation measurements, 32*(1), 57-73.

Murray, A. S., Olley, J. M., and Caitcheon, G. G. (1995). Measurement of equivalent doses in quartz from contemporary water-lain sediments using optically stimulated luminescence. *Quaternary Science Reviews, 14*(4), 365-371.

Nanson G.C., 2013. Anabranching and Anastomosing Rivers. In: J. F. Shroder (ed.). *Treatise on Geomorphology, Volume 9*, San Diego: Academic Press. pp. 330-345.

Nanson, G.C. and Croke, J.C., 1992. A genetic classification of floodplains. *Geomorphology, 4*(6), pp.459-486.

Nanson, G.C., and Huang, H.Q. 1999, Anabranching rivers: divided efficiency leading to fluvial diversity. Varieties of Fluvial Form, 7, pp.477-494.

Nanson, G.C., and Huang, H.Q., 2008. Least action principle, equilibrium states, iterative adjustment and the stability of alluvial channels. *Earth Surface Processes and Landforms, 33*(6), pp.923-942.

Nanson, G.C. and Huang, H.Q., 2017. Self-adjustment in rivers: Evidence for least action as the primary control of alluvial-channel form and process. *Earth Surface Processes and Landforms, 42*(4), pp.575-594.

Nanson, G.C. and Knighton, A.D., 1996., Anabranching rivers: their cause, character and classification. *Earth surface processes and landforms, 21(3)*, pp.217-239.

Nanson, G.C., Rust, B.R., and Taylor, G., 1986. Coexistent mud braids and anastomosing channels in an arid-zone river: Cooper Creek, central Australia. *Geology, 14*(2), 175-178.

Nanson, G.C., Young, R.W., Price, D.M., and Rust, B.R., 1988. Stratigraphy, sedimentology and late Quaternary chronology of the Channel Country of western Queensland. *Fluvial geomorphology of Australia*, pp. 151-175.

Nanson, G.C., Price, D.M., Short, S.A., Page, K.J., Nott, J.F., 1991. Major episodes of climatic change in Australia over the last 300,000 years. In: R. Gillespie (ed.) *Quaternary Dating Workshop Department of Biogeography, Geomorphology, Research School of Earth Sciences,* Australian National University, Canberra, pp. 45–50.

Nanson, G.C., Price, D.M. and Short, S.A., 1992. Wetting and drying of Australia over the past 300 ka. *Geology, 20*(9), pp.791-794.

Nanson, G.C., East, T.J. and Roberts, R.G., 1993. Quaternary stratigraphy, geochronology and evolution of the Magela Creek catchment in the monsoon tropics of northern Australia. *Sedimentary Geology*, *83*(3-4), pp.277-302.

Nanson, G.C., Chen, X.Y. and Price, D.M., 1995. Aeolian and fluvial evidence of changing climate and wind patterns during the past 100 ka in the western Simpson Desert, Australia. *Palaeogeography, Palaeoclimatology, Palaeoecology, 113*(1), pp.87-102.

Nanson, G.C., Tooth, S. and Knighton, A.D., 2002. A global perspective on dryland rivers: perceptions, misconceptions and distinctions. In: L. J. Bull and M. J. Kirkby (eds.). *Dryland rivers: hydrology and geomorphology of semi-arid channels*, John Wiley and Sons, pp.17-54.

Nanson, G.C., Jones, B.G., Price, D.M. and Pietsch, T.J., 2005. Rivers turned to rock: Late Quaternary alluvial induration influencing the behaviour and morphology of an anabranching river in the Australian monsoon tropics. *Geomorphology*, *70*(3-4), pp.398-420.

Nanson, G.C., Price, D.M., Jones, B.G., Maroulis, J.C., Coleman, M., Bowman, H., Cohen, T.J., Pietsch, T.J. and Larsen, J.R., 2008. Alluvial evidence for major climate and flow regime changes during the middle and late Quaternary in eastern central Australia. *Geomorphology, 101*(1-2), pp.109-129.

Nathan, R.P., Thomas, P.J., Jain, M., Murray, A.S. and Rhodes, E.J., 2003. Environmental dose rate heterogeneity of beta radiation and its implications for luminescence dating: Monte Carlo modelling and experimental validation. Radiation Measurements, 37(4-5), pp.305-313.

Neff, E.L., 1967. Discharge frequency compared to long-term sediment yields. *Publication of International Association of Hydrological Sciences, 75*, pp. 236-242.

Nezu, I., Nakagawa, H. and Tominaga, A., 1985. Secondary currents in a straight channel flow and the relation to its aspect ratio. In *Turbulent shear flows 4*, Springer, Berlin, Heidelberg, pp. 246-260.

Nichols, G., 2007. Fluvial systems in desiccating endorheic basins. *Sedimentary Processes, Environments and Basins: A Tribute to Peter Friend*, pp.569-589.

Nishiizumi, K., 2004. Preparation of 26Al AMS standards. *Nuclear Instruments and Methods in Physics Research Section B: Beam Interactions with Materials and Atoms*, *223*, pp.388-392.

Nishiizumi, K., Lal, D., Klein, J., Middleton, R. and Arnold, J.R., 1986. Production of ^{10}Be and ^{26}Al by cosmic rays in terrestrial quartz in situ and implications for erosion rates. *Nature, 319*(6049), pp.134.

Nishiizumi, K., Klein, J., Middleton, R. and Arnold, J.R., 1987. Long-lived cosmogenic nuclides in the Derrick Peak and Lazarev iron meteorites. In *Lunar and Planetary Science Conference (Vol. 18)*.

Nishiizumi, K., Kohl, C.P., Arnold, J.R., Dorn, R., Klein, I., Fink, D., Middleton, R. and Lal, D., 1993. Role of in situ cosmogenic nuclides 10Be and 26Al in the

study of diverse geomorphic processes. *Earth surface processes and landforms, 18(5),* pp.407-425.

Nishiizumi, K., Imamura, M., Caffee, M.W., Southon, J.R., Finkel, R.C. and McAninch, J., 2007. Absolute calibration of ^{10}Be AMS standards. *Nuclear Instruments and Methods in Physics Research Section B: Beam Interactions with Materials and Atoms, 258*(2), pp.403-413.

Norris, T.L., Gancarz, A.J., Rokop, D.J. and Thomas, K.W., 1983. Half-life of 26Al. *Journal of Geophysical Research: Solid Earth*, *88*(S01).

Olley, J., Caitcheon, G. and Murray, A., 1998. The distribution of apparent dose as determined by optically stimulated luminescence in small aliquots of fluvial quartz: implications for dating young sediments. *Quaternary Science Reviews, 17*(11), pp.1033-1040.

Olley, J.M., Caitcheon, G.G. and Roberts, R.G., 1999. The origin of dose distributions in fluvial sediments, and the prospect of dating single grains from fluvial deposits using optically stimulated luminescence. *Radiation Measurements, 30*(2), pp.207-217.

Osterkamp, W.R., 1998. Processes of fluvial island formation, with examples from Plum Creek, Colorado and Snake River, Idaho. *Wetlands*, *18*(4), pp.530-545.

Otto, J.C., Schrott, L., Jaboyedoff, M. and Dikau, R., 2009. Quantifying sediment storage in a high alpine valley (Turtmanntal, Switzerland). *Earth Surface Processes and Landforms, 34*(13), pp.1726-1742.

Page, K.J., Nanson, G.C. and Price, D.M., 1991. Thermoluminescence chronology of late quaternary deposition on the riverine plain of South-Eastern Australia. *The Australian Geographer*, *22*(1), pp.14-23.

Page, K., Nanson, G. and Price, D., 1996. Chronology of Murrumbidgee river palaeochannels on the Riverine Plain, southeastern Australia. *Journal of Quaternary Science*, *11*(4), pp.311-326.

Parker, A.G., 2010. Pleistocene climate change in Arabia: developing a framework for hominin dispersal over the last 350 ka. In *The evolution of human populations in Arabia*. Springer, Dordrecht, pp. 39-49

Peel, M.C., McMahon, T.A., Finlayson, B.L. and Watson, F.G., 2001. Identification and explanation of continental differences in the variability of annual runoff. *Journal of Hydrology, 250*(1-4), pp.224-240.

Peel, M. C., Finlayson, B. L., and McMahon, T. A. 2007, Updated world map of the Köppen-Geiger climate classification. *Hydrology and earth system sciences discussions, 4*(2)*, pp.439-473.

Peng J, Dong ZB, Han FQ, Long H, Liu XJ, 2013. R package numOSL: numeric routines for optically stimulated luminescence dating. *Ancient TL*, *31*(2), pp 41-48

Phillips, J.D. and Slattery, M.C., 2006. Sediment storage, sea level, and sediment delivery to the ocean by coastal plain rivers. *Progress in Physical Geography, 30*(4), pp.513-530.

Phillips, F.M., Leavy, B.D., Jannik, N.O., Elmore, D. and Kubik, P.W., 1986. The accumulation of cosmogenic chlorine-36 in rocks: A method for surface exposure dating. *Science, 231*(4733), pp.41-43.

Portenga, E.W. and Bierman, P.R., 2011. Understanding Earth's eroding surface with 10 Be. *GsA Today, 21*(8), pp.4-10.

Powell, D.M., 2009. Dryland rivers: processes and forms. In: *Geomorphology of desert environments (pp. 333-373)*. Springer, Dordrecht.

Powell, D.M., Reid, I., Laronne, J.B. and Frostick, L., 1996. Bed load as a component of sediment yield from a semiarid watershed of the northern Negev. *IAHS Publications-Series of Proceedings and Reports-Intern Assoc Hydrological Sciences, 236*, pp.389-398.

Prescott, J.R. and Hutton, J.T., 1994. Cosmic ray contributions to dose rates for luminescence and ESR dating: large depths and long-term time variations. *Radiation measurements*, *23*(2-3), pp.497-500.

Puckridge, J.T., Sheldon, F., Walker, K.F. and Boulton, A.J., 1998. Flow variability and the ecology of large rivers.: *Marine and Freshwater Research, 49*, pp.55-72.

Quigley, M.C., Clark, D. and Sandiford, M., 2010. Tectonic geomorphology of Australia. *Geological Society, London, Special Publications, 346*(1), pp.243-265.

Raymond, O., Liu, S., Gallagher, R., Zhang, W., and Highet, L., 2012. *Surface Geology of Australia 1:1 million scale (2012 edition)*, Commonwealth of Australia (Geoscience Australia).

Reeves, J.M., Chivas, A.R., García, A., Holt, S., Couapel, M.J., Jones, B.G., Cendón, D.I. and Fink, D., 2008. The sedimentary record of palaeoenvironments and sea-level change in the Gulf of Carpentaria, Australia, through the last glacial cycle. *Quaternary International*, *183*(1), pp.3-22.

Reid, I. and Laronne, J.B., 1995. Bed load sediment transport in an ephemeral stream and a comparison with seasonal and perennial counterparts. *Water Resources Research, 31*(3), pp.773-781.

Reid, I., and Frostick, L.E. 1987, Flow dynamics and suspended sediment properties in arid zone flash floods. Hydrological Processes 1, pp.239–253.

Reid, I., and Frostick, L.E. 1989. Channel form, flows and sediments in deserts. In: D.S.G. Thomas (ed.). *Arid Zone Geomorphology,* London and New York, Belhaven Press and Halsted Press, pp.117-135.

Reynolds, J.F., Smith, D.M.S., Lambin, E.F., Turner, B.L., Mortimore, M., Batterbury, S.P., Downing, T.E., Dowlatabadi, H., Fernández, R.J., Herrick, J.E. and Huber-Sannwald, E., 2007. Global desertification: building a science for dryland development. *Science, 316*(5826), pp.847-851.

Rhodes, E.J., Singarayer, J.S., Raynal, J.P., Westaway, K.E. and Sbihi-Alaoui, F.Z., 2006. New age estimates for the Palaeolithic assemblages and Pleistocene succession of Casablanca, Morocco. *Quaternary Science Reviews*, *25*(19), pp.2569-2585.

Rittenour, T. M., 2008. Luminescence dating of fluvial deposits: applications to geomorphic, palaeoseismic and archaeological research. *Boreas, 37*(4), 613-635.

Rittenour, T.M., Goble, R.J. and Blum, M.D., 2005. Development of an OSL chronology for Late Pleistocene channel belts in the lower Mississippi valley, USA. *Quaternary Science Reviews, 24(23-24)*, pp.2539-2554.

Rixhon, G., Briant, R.M., Cordier, S., Duval, M., Jones, A. and Scholz, D., 2017. Revealing the pace of river landscape evolution during the Quaternary: recent developments in numerical dating methods. *Quaternary Science Reviews, 166*, pp.91-113.

Romans, B.W., Castelltort, S., Covault, J.A., Fildani, A. and Walsh, J.P., 2016. Environmental signal propagation in sedimentary systems across timescales. *Earth-Science Reviews, 153*, pp.7-29.

Rust, B.R., 1981. Sedimentation in an arid-zone anastomosing fluvial system; Cooper's Creek, central Australia. *Journal of Sedimentary Research*, *51*(3), pp.745-755

Rust, B.R., and Nanson, G.C., 1986. Contemporary and palaeo-channel patterns and the late Quaternary stratigraphy of Cooper Creek, southwest Queensland, Australia. *Earth Surface Processes and Landforms, 11*(6), 581-590.

Sadler, P.M., 1981. Sediment accumulation rates and the completeness of stratigraphic sections. *The Journal of Geology, 89*(5), pp.569-584.

Sandiford, M., Wallace, M. and Coblentz, D., 2004. Origin of the in situ stress field in south-eastern Australia. *Basin Research, 16*(3), pp.325-338.

Schaller, M., Von Blanckenburg, F., Hovius, N. and Kubik, P.W., 2001. Large-scale erosion rates from in situ-produced cosmogenic nuclides in European river sediments. *Earth and Planetary Science Letters*, *188*(3-4), pp.441-458.

Schaller, M., Von Blanckenburg, F., Veldkamp, A., Tebbens, L.A., Hovius, N. and Kubik, P.W., 2002. A 30 000 yr record of erosion rates from cosmogenic ^{10}Be in Middle European river terraces. *Earth and Planetary Science Letters*, *204*(1-2), pp.307-320.

Schumer, R. and Jerolmack, D.J., 2009. Real and apparent changes in sediment deposition rates through time. *Journal of Geophysical Research (Earth Surface), 114*.

Schumm, S.A. 1968, Speculations concerning paleohydrologic controls of terrestrial sedimentation. *Geological Society of America Bulletin, 79*(11), pp.1573-1588.

Schumm, S.A., 1977. *The fluvial system (Vol. 338)*. New York: Wiley.

Schumm, S.A., 1981. Evolution and response of the fluvial system, sedimentologic implications. In: F. G. Ethridge and R. M. Flores (eds.). *Recent and ancient nonmarine depositional environments*, S*ociety of Economic Palaeontologists and Mineralogists Special Publication, 31,* pp.19–29.

Schumm, S.A. 1985, Patterns of alluvial rivers. *Annual Review of Earth and Planetary Sciences*, *13*(1), pp.5-27.

Schumm, S.A., and Lichty, R.W., 1965. Time, space, and causality in geomorphology. *American Journal of Science, 263*(2), pp.110-119.

Sharma, K.D. and Murthy, J.S.R., 1994. Modelling sediment transport in stream channels in the arid zone of India. *Hydrological processes, 8*(6), pp.567-572.

Silberberg, R. and Tsao, C.H., 1990. Spallation processes and nuclear interaction products of cosmic rays. *Physics Reports, 191(6),* pp.351-408.

Silverman, B.W., 1986. *Density Estimation for Statistics and Data Analysis.* Chapman and Hall, New York.

Sim, A.K., Thomsen, K.J., Murray, A.S., Jacobsen, G., Drysdale, R. and Erskine, W., 2014. Dating recent floodplain sediments in the Hawkesbury-Nepean River system, eastern Australia using single-grain quartz OSL. *Boreas, 43(1),* pp.1-21.

Simpson, J.A. and Fagot, W.C., 1953. Properties of the low energy nucleonic component at large atmospheric depths. *Physical Review, 90*(6), pp.1068.

Singh, G. and Luly, J., 1991. Changes in vegetation and seasonal climate since the last full glacial at Lake Frome, South Australia. *Palaeogeography, Palaeoclimatology, Palaeoecology*, *84*(1-4), pp.75-86.

Smith, D. G. 1983. Anastomosed fluvial deposits: modem examples from western Canada. In: J. D. Collinson and J. Lewin (eds.). *Modern and Ancient Fluvial Systems, Special Publication of the International Association of Sedimentologists, 6,* pp. 155-168.

Smith, B.W. and Rhodes, E.J., 1994. Charge movements in quartz and their relevance to optical dating. *Radiation Measurements, 23*(2-3), pp.329-333.

Smith, N.D., Cross, T.A., Dufficy, J.P. and Clough, S.R. 1989, Anatomy of an avulsion. *Sedimentology, 36*(1), pp.1-23.

Spooner, N.A., 1992. Optical dating: preliminary results on the anomalous fading of luminescence from feldspars. *Quaternary Science Reviews, 11*(1-2), pp.139-145.

Spooner, N.A., 1994. The anomalous fading of infrared-stimulated luminescence from feldspars. *Radiation Measurements, 23*(2-3), pp.625-632.

Starkel, L., 1991. The Vistula River Valley: a case study for central Europe. In: L. Starkel, K.J. Gregory, J.B. Thornes (eds.). *Temperate Palaeohydrology: Fluvial Processes in the Temperate Zone during the Last 15000 Years.* Wiley, New York, pp. 171–188.

Stewart, G.A., Perry, R.A., 1962. Part I. Introduction and summary description of the Alice Springs area. In: R.A. Perry (ed.). *General Report on Lands of the Alice Springs Area, Northern Territory, 1956–1957. CSIRO Land Research Series No. 6* pp. 9–19.

Štor, T., Schaller, M., Merchel, S., Martínek, K., Rittenour, T., Rugel, G. and Scharf, A., 2019. Quaternary evolution of the Ploučnice River system (Bohemian Massif) based on fluvial deposits dated with optically stimulated luminescence and in situ produced cosmogenic nuclides. *Geomorphology, 329*, pp.152-169.

Struck, M., Jansen, J.D., Fujioka, T., Codilean, A.T., Fink, D., Fülöp, R.H., Wilcken, K.M., Price, D.M., Kotevski, S., Fifield, L.K. and Chappell, J., 2018a. Tracking the ^{10}Be - ^{26}Al source-area signal in sediment-routing systems of arid central Australia. *Earth Surface Dynamics, 6*(2), pp.329-349.

Struck, M., Jansen, J.D., Fujioka, T., Codilean, A.T., Fink, D., Egholm, D.L., Fülöp, R.H., Wilcken, K.M. and Kotevski, S., 2018b. Soil production and transport on postorogenic desert hillslopes quantified with 10 Be and 26 Al. *Bulletin of the Geological Society of America*, *130*(5-6), pp.1017-1040.

Stoddart, D.R. 1978. Geomorphology in China. *Progress in Physical Geography, 2*, pp.187–236.

Stone, J.O., 2000. Air pressure and cosmogenic isotope production. *Journal of Geophysical Research: Solid Earth, 105*(B10), pp.23753-23759.

Surovell, T.A. and Brantingham, P.J., 2007. A note on the use of temporal frequency distributions in studies of prehistoric demography. *Journal of Archaeological Science, 34*(11), pp.1868-1877.

Surovell, T.A., Finley, J.B., Smith, G.M., Brantingham, P.J. and Kelly, R., 2009. Correcting temporal frequency distributions for taphonomic bias. *Journal of Archaeological Science, 36*(8), pp.1715-1724.

Syvitski, J.P. and Milliman, J.D., 2007. Geology, geography, and humans battle for dominance over the delivery of fluvial sediment to the coastal ocean. *The Journal of Geology, 115*(1), pp.1-19.

Teller, J.T., 1987. Proglacial lakes and the southern margin of the Laurentide Ice Sheet. In: W.F. Ruddiman, H.E. Wright Jr. (eds.). *North America and Adjacent Oceans During the Last Deglaciation. The Geology of North America,* Geological Society of America, Boulder, Colorado, pp. 39–69.

Tetzlaff, G. and Bye, J.A.T., 1978. Water balance of Lake Eyre for the flooded period January 1974-June 1976. *Transactions of the Royal Society of Australia, 102*, pp.91-6.

Thomas, D.S. and Bailey, R.M., 2017. Is there evidence for global-scale forcing of Southern Hemisphere Quaternary desert dune accumulation? A quantitative method for testing hypotheses of dune system development. Earth Surface Processes and Landforms, 42(14), pp.2280-2294.

Thomas, D.S. and Burrough, S.L., 2012. Interpreting geoproxies of late Quaternary climate change in African drylands: implications for understanding environmental change and early human behaviour. *Quaternary International, 253,* pp.5-17.

Thompson, C.J., Fryirs, K. and Croke, J., 2016. The disconnected sediment conveyor belt: patterns of longitudinal and lateral erosion and deposition during a catastrophic flood in the Lockyer Valley, South East Queensland, Australia. *River Research and Applications, 32*(4), pp.540-551.

Thoms, M., Beyer. P.J., and Rogers, K.H., 2006. Variability, complexity and diversity: The geomorphology of river ecosystems in dryland regions. In: R. Kingsford (ed.). *Ecology of Desert Rivers*, Cambridge University Press, pp.47-75.

Tockner, K. and Stanford, J.A., 2002. Riverine flood plains: present state and future trends. *Environmental conservation, 29(3),* pp.308-330.

Tooth, S., 1997. *The morphology, dynamics and Late Quaternary sedimentary history of ephemeral drainage systems on the Northern Plains of central Australia.* Unpublished PhD Thesis, School of Geosciences, University of Wollongong, Australia.

Tooth, S., 2000a. Process, form and change in dryland rivers: a review of recent research. *Earth-Science Reviews*, *51*(1), pp.67-107.

Tooth, S., 2000b. Downstream changes in dryland river channels: the Northern Plains of arid central Australia. *Geomorphology, 34(1-2),* pp.33-54.

Tooth, S., 2013. Dryland fluvial environments: assessing distinctiveness and diversity from a global perspective. *Treatise on Geomorphology*, *9*, pp.612-644.

Tooth, S. and Nanson, G. C., 1999, Anabranching rivers on the Northern Plains of arid central Australia. *Geomorphology, 29*(3), pp.211-233.

Tooth, S. and Nanson, G. C., 2000a, The role of vegetation in the formation of anabranching channels in an ephemeral river, Northern plains, arid central Australia. *Hydrological Processes*, *14*(16-17), pp.3099-3117.

Tooth, S. and Nanson, G. C., 2000b, Equilibrium and nonequilibrium conditions in dryland rivers, *Physical Geography*, *21*(3), pp.183-211.

Tooth, S. and Nanson, G.C., 2004. Forms and processes of two highly contrasting rivers in arid central Australia, and the implications for channel-pattern discrimination and prediction. *Geological Society of America Bulletin, 116*(7-8), pp.802-816.

Tooth, S., Jansen, J.D., Nanson, G.C., Coulthard, T.J. and Pietsch, T., 2008. Riparian vegetation and the late Holocene development of an anabranching river: Magela Creek, northern Australia. *Geological Society of America Bulletin, 120*(7-8), pp.1021-1035.

Turner, M., Bari, M., Amirthanathan, G. and Ahmad, Z., 2012. Australian network of hydrologic reference stations-advances in design, development and

implementation. In: *Hydrology and Water Resources Symposium 2012,* Engineers Australia, pp. 1555.

United Nations Environment Program (UNEP). 2006. *Global deserts outlook.* Accessed:14/02/2016.

https://www.unenvironment.org/resources/report/global-deserts-outlook

Vandenberghe, J., 2002. The relation between climate and river processes, landforms and deposits during the Quaternary. *Quaternary International*, *91*(1), pp.17-23.

Vermeesch, P., 2007. CosmoCalc: An Excel add-in for cosmogenic nuclide calculations. *Geochemistry, Geophysics, Geosystems*, *8*(8).

Vermeesch, P., 2012. On the visualisation of detrital age distributions. *Chemical Geology, 312,* pp.190-194.

Vermeesch, P., Fenton, C.R., Kober, F., Wiggs, G.F.S., Bristow, C.S. and Xu, S., 2010. Sand residence times of one million years in the Namib Sand Sea from cosmogenic nuclides. *Nature Geoscience, 3*(12), pp.862.

Waddams, J.A., 1958. Lattice defects and the physicochemical properties of quartz. In: *Die Staublungenerkrankungen*, Steinkopff, Heidelberg, pp.40-53.

Walker, M.J.C., 2005. *Quaternary dating methods.* John Wiley and Sons.

Walling, D.E., 1983. The sediment delivery problem. *Journal of hydrology, 65(1-3)*, pp.209-237.

Walling, D.E. and Kleo, A.H.A., 1979. Sediment yield of rivers in areas oflow precipitation: a global view. In: *The Hydrology of Areas of Low Precipitation. IAHS Publication No. 128.* Institute of Hydrology, Wallingford, pp.479-493.

Wallinga, J. (2002). Optically stimulated luminescence dating of fluvial deposits: a review. *Boreas, 31*(4), pp.303-322.

Ward, R., 1978. *Floods: a geographical perspective*. Wiley, New York.

Warner, R.F., 1988. *Fluvial geomorphology of Australia*. Academic Press.

Warren, S.E., 1978. Thermoluminescence dating of pottery: an assessment of the dose-rate from rubidium. *Archaeometry, 20*(1), pp.71-72.

Wasson, R.J., 1983a. The Cainozoic history of the Strzelecki and Simpson dunefields (Australia), and the origin of the desert dunes. *Zeitschrift für Geomorphologie, 45*, pp.85-115.

Wasson, R.J., 1983b. Dune sediment types, sand colour, sediment provenance and hydrology in the Strzelecki-Simpson dunefield, Australia. In *Developments in Sedimentology (Vol. 38),* Elsevier, pp.165-195.

Wende, R., and Nanson, G.C. 1998. Anabranching rivers: ridge-form alluvial channels in tropical northern Australia. *Geomorphology, 22*(3), 205-224.

Whipple, K.X. and Tucker, G.E., 2002. Implications of sediment-flux-dependent river incision models for landscape evolution. *Journal of Geophysical Research: Solid Earth, 107*(B2), pp.ETG-3.

Williams, M., 2015. Interactions between fluvial and eolian geomorphic systems and processes: examples from the Sahara and Australia. *Catena, 134,* pp.4-13.

Willenbring, J.K., Codilean, A.T. and McElroy, B., 2013. Earth is (mostly) flat: Apportionment of the flux of continental sediment over millennial time scales. *Geology*, *41*(3), pp.343-346.

Wintle, A.G., 1973. Anomalous fading of thermo-luminescence in mineral samples. *Nature, 245*(5421), pp.143.

Wintle, A.G., 1997. Luminescence dating: laboratory procedures and protocols. *Radiation Measurements*, *27*(5), pp.769-817.

Wintle, A.G. and Huntley, D.J., 1980. Thermoluminescence dating of ocean sediments. *Canadian Journal of Earth Sciences, 17*(3), pp.348-360.

Wittmann, H. and Von Blanckenburg, F., 2009. Cosmogenic nuclide budgeting of floodplain sediment transfer. *Geomorphology, 109*(3-4), pp.246-256.

Wittmann, H. and von Blanckenburg, F., 2016. The geological significance of cosmogenic nuclides in large lowland river basins. *Earth Science Reviews, 159*, pp.118-141.

Wittmann, H., Von Blanckenburg, F., Maurice, L., Guyot, J.L. and Kubik, P.W., 2011. Recycling of Amazon floodplain sediment quantified by cosmogenic ^{26}Al and ^{10}Be. *Geology*, *39*(5), pp.467-470.

Wittmann, H., Von Blanckenburg, F., Dannhaus, N., Bouchez, J., Gaillardet, J., Guyot, J.L., Maurice, L., Roig, H., Filizola, N. and Christl, M., 2015. A test of the cosmogenic ^{10}Be(meteoric)/^{9}Be proxy for simultaneously determining basin-wide erosion rates, denudation rates, and the degree of weathering in the Amazon basin. *Journal of Geophysical Research: Earth Surface*, *120*(12), pp.2498-2528.

Wittmann, H., Malusà, M.G., Resentini, A., Garzanti, E. and Niedermann, S., 2016. The cosmogenic record of mountain erosion transmitted across a foreland basin: Source-to-sink analysis of in situ ^{10}Be, ^{26}Al and ^{21}Ne in sediment of the Po river catchment. *Earth and Planetary Science Letters*, *452*, pp.258-271.

Wolkowinsky, A.J. and Granger, D.E., 2004. Early Pleistocene incision of the San Juan River, Utah, dated with ^{26}Al and ^{10}Be. *Geology, 32*(9), pp.749-752.

Wolman, M.G. and Leopold, L.B., 1957. River flood plains: some observations on their formation, *No. 282-C,* US Government Printing Office, pp. 87-109.

Wright Jr., H.E., 1987. Synthesis; the land south of the ice sheets. In: W.F. Ruddiman and H.E. Wright Jr. (eds.). *North America and Adjacent Oceans During the Last Deglaciation: the Geology of North America.* Geological Society of America, Boulder, Colorado, pp.479–488.

Wright, V.P. and Marriott, S.B., 1993. The sequence stratigraphy of fluvial depositional systems: the role of floodplain sediment storage. *Sedimentary geology, 86(3-4),* pp.203-210.

Wyrick, J.R. and Klingeman, P.C., 2011. Proposed fluvial island classification scheme and its use for river restoration. *River Research and Applications*, *27*(7), pp.814-825.

Xu, J. 1999. Grain-size characteristics of suspended sediment in the Yellow River, China. *Catena, 38*, 243–263.

Yanes, Y., Wolf, D. and Faust, D., 2019. Paleoenvironmental reconstruction and sedimentary processes in Drylands. *Quaternary Research, 91(1)*, pp.1-3.

Yang, C. T., and Song, C. 1979, Theory of minimum rate of energy dissipation. *Journal of the Hydraulics Division, 105*(7), pp.769-784.

Yang, C. T., Song, C., and Woldenberg, M. J. (1981). Hydraulic geometry and minimum rate of energy dissipation. *Water Resources Research, 17*(4), pp.1014-1018.

Appendix A

A Fluvial data compilation

A.1 Meandering channel and anabranching deposits

The deposits used in chapter 5 of this thesis have been dated using OSL and TL. The age estimates of these deposits were refined to 94 values (Figure 4.5). These age estimates are taken from Rust and Nanson (1986), Nanson et al. (1988), Maroulis (2000), Fagan (2001), Coleman (2002), and Nanson (2013, pers comm. 3 August).

Of these 94 values 50% are sandy deposits which are interpreted as being from sand load, laterally active meandering rivers (Table A.1), and 50% are from muddy deposits (Table A.2) which are interpreted as being from 'type 1' anabranching deposits described as muddy anastomosing (Nanson and Knighton 1996).

Table A.1 - Table of age estimate from sand deposits from Channel Country used for data analysis in Chapter 5

River	Site i	Site ii	Dating method [a]	Lab code [b]	Age ka	±1σ error ka	Sample depth m	Deposition Rate[c] m.ka⁻¹	Reference [d]
Cooper Ck.	Chookoo	CH-2 trench	TL	W2054/W2055	98.4	10.5	4.44	45.41	2.95	Maroulis (2000)
Cooper Ck.	Chookoo	CH-3 trench	TL	W2057	81.6	7.4	3.9	47.79	3.97	Maroulis (2000)
Cooper Ck.	Chookoo	CH-3 trench	TL	W2058	103.0	10	6.1	59.22	5.24	Maroulis (2000)
Cooper Ck.	Chookoo	CH-D	TL	W1710	92.4	9	6.85	74.13	6.58	Maroulis (2000)
Cooper Ck.	Chookoo	CH-G	TL	W1717	99.2	10.7	9.3	93.75	9.13	Maroulis (2000)
Cooper Ck.	Chookoo	CH-M	TL	W2059	48.6	3.8	5.3	109.05	7.91	Maroulis (2000)
Cooper Ck.	Chookoo	CH-S	TL	W3567	63.5	3.9	4.3	67.72	3.92	Maroulis et al. 2007
Cooper Ck.	Cullyamurra, Transect 1	AH1-1	TL	W2669	9.7	1.3	2.8	288.66	34.11	Coleman (2002)
Cooper Ck.	Cullyamurra, Transect 1	AH2-1	TL	W2580	18.3	2.1	8.5	464.48	47.81	Coleman (2002)
Cooper Ck.	Cullyamurra, Transect 1	AH2-1	TL	W2670	20.1	2.9	2.8	139.30	17.56	Coleman (2002)
Cooper Ck.	Cullyamurra, Transect 1	AH2-1	TL	W2671	62.5	7.7	14.7	235.20	25.80	Coleman (2002)
Cooper Ck.	Cullyamurra, Transect 1	AH3-1	TL	W2581	6.0	0.5	2.7	450.00	34.62	Coleman (2002)
Cooper Ck.	Cullyamurra, Transect 1	AH4-1	TL	W2582	27.8	2.5	5.6	201.44	16.62	Coleman (2002)
Cooper Ck.	Durham Downs Rd	F/P6	TL	W1707	75.6	6.9	8	105.82	8.85	Maroulis (2000)

River	Site i	Site ii	Dating method[a]	Lab code[b]	Age ka	±1σ error ka	Sample depth m	Deposition Rate[c] m.ka^{-1}	Reference[d]
Cooper Ck.	Durham dune	DD1	TL	W1713	118	13	10	84.75	8.41	Maroulis (2000)
Cooper Ck.	Durham dune	DD3	TL	W1714	95.5	8.5	6	62.83	5.13	Maroulis (2000)
Cooper Ck.	Goonbabinna Waterhole	T1	TL	W2053	5.3	0.4	4.8	905.66	63.56	Maroulis (2000)
Cooper Ck.	Maapoo Waterhole	M/H2	TL	W4266	89.5	7.7	4.5	50.28	3.98	Nanson (unpub.)[e]
Cooper Ck.	Maapoo Waterhole	M/H3	TL	W4268	61.2	3.3	2.3	37.58	1.92	Nanson (unpub.)[e]
Cooper Ck.	Maapoo Waterhole	MW/H1	TL	W4263	62.3	3.9	1.8	28.89	1.70	Nanson (unpub.)[e]
Cooper Ck.	Maapoo Waterhole	MW/H1	TL	W4259	70.8	4.2	4.2	59.32	3.32	Nanson (unpub.)[e]
Cooper Ck.	Maapoo Waterhole	MW/H1	TL	W4260	122	19	8	65.57	8.84	Nanson (unpub.)[e]
Cooper Ck.	Mt Howitt	Trench 1/1	TL	W2290/W2291	61.1	5.2	5.1	82.62	6.47	Maroulis (2000)
Cooper Ck.	Mt Howitt	Trench 1/3	TL	W2295	95.8	8.3	4.7	49.06	3.91	Maroulis (2000)
Cooper Ck.	Naccowlah Waterhole	Exc. 1	TL	W551/W552	210.0	58.4	3.4	16.19	3.52	Rust & Nanson (1986)
Cooper Ck.	Naccowlah Waterhole	Exc. 2 (TL8)	TL	W567	251.5	73.5	4.2	16.70	3.78	Rust & Nanson (1986)
Cooper Ck.	Narberry Waterhole	NH1	TL	W2029	146	11	7	47.95	3.36	Maroulis (2000)
Cooper Ck.	Narberry Waterhole	NH2	TL	W2297	92.1	10.6	4	43.43	4.48	Maroulis (2000)

River	Site i	Site ii	Dating method [a]	Lab code [b]	Age (ka)	$\pm 1\sigma$ error (ka)	Sample depth (m)	Deposition Rate [c] ($m.ka^{-1}$)	Reference [d]
Cooper Ck.	Shire Rd	SR1	TL	W2030	10.5	0.9	3	285.71	22.56	Maroulis (2000)
Cooper Ck.	Shire Rd	SR1	TL	W2031	38.1	3.5	6	157.48	13.25	Maroulis (2000)
Cooper Ck.	Shire Rd	SR2	TL	W2032	34.5	3.6	1.5	43.48	4.11	Maroulis (2000)
Cooper Ck.	Shire Rd	SR2	TL	W2033	58.3	6.3	9	154.37	15.06	Maroulis (2000)
Cooper Ck.	Shire Rd	SR2	TL	W2033	58.3	6.3	9	154.37	15.06	Maroulis (2000)
Cooper Ck.	Shire Rd	SR3	TL	W2037	29.9	2.6	1.5	51.90	4.28	Maroulis (2000)
Cooper Ck.	Shire Rd	SR3	TL	W2038	77.5	6.6	9	116.13	9.11	Maroulis (2000)
Cooper Ck.	Shire Rd	SR3	TL	W2039	133	15	12	90.23	9.14	Maroulis (2000)
Cooper Ck.	Shire Rd	SR3-T	TL	W2296	41.9	5.1	5.1	121.72	13.21	Maroulis (2000)
Cooper Ck.	Shire Rd	SR5	TL	W2045	137	14	9	65.69	6.09	Maroulis (2000)
Cooper Ck.	Shire Rd	SR5	TL	W2046	454	174	15	33.04	9.15	Maroulis (2000)
Cooper Ck.	Shire Rd	SR6	TL	W2048	169	83	6	35.50	11.69	Maroulis (2000)
Cooper Ck.	Shire Rd	SR7	TL	W2050	147	18	7.6	51.70	5.64	Maroulis (2000)
Cooper Ck.	Shire Rd	SR8	TL	W2052	164	25	6	36.59	4.84	Maroulis (2000)

River	Site i	Site ii	Dating method [a]	Lab code [b]	Age ka	±1σ error ka	Sample depth m	Deposition Rate [c] m.ka⁻¹		Reference [d]
Diamantina R.	Brighton Downs		TL	W582	97	10	10	103.09	9.63	Nanson et al. (1988)
Diamantina R.	Bulia Rd Crossing	Exc-4	TL	W843	140	21	2.1	15.00	1.96	Nanson et al. (1988)
Thomson R.	Longreach	H3	TL	W638	109	11	2.9	26.61	2.44	Nanson et al. (1988)
Thomson R.	Longreach	H3	TL	W605	128.3	14.2	4.8	37.41	3.73	Nanson et al. (1988)
Western R.		H3	TL	W598	35.8	2.7	6.6	184.36	12.93	Nanson et al. (1988)
Western R.		H4	TL	W599	41.5	3.5	4.6	110.84	8.62	Nanson et al. (1988)

[a] *TL—thermoluminescence, OSL-MGA—optically stimulated luminescence, multiple-grain aliquot;* [b] *Laboratory code, where two labcodes are presentd a weighted mean has been taken of the two samples as they are from the same unit.* [c] *Calculated using depth and age;* [d] *Work in which the age originally appeared;* [e] *Nanson (2013, pers comm. 3 August)*

Table A.2 – Table of age estimate from mud deposits from the Channel Country used for data analysis in Chapter 5

River	Site i	Site ii	Dating method [a]	Lab code [b]	Age ka	±1σ error ka	Sample depth m	Deposition Rate [b] m.ka⁻¹	Reference [d]
Cooper Ck.	Chookoo	CH-3 trench	TL	W2056	33.3	2.6	3.7	111.11	8.05	Maroulis (2000)
Cooper Ck.	Chookoo	CH-G	TL	W1715	54.2	5.2	3	55.35	4.85	Maroulis (2000)
Cooper Ck.	Chookoo	CH-G	TL	W1716	67.1	5.8	6	89.42	7.11	Maroulis (2000)
Cooper Ck.	Durham Downs Rd	F/P1	TL	W1700	38.9	3.1	1.5	38.56	2.85	Maroulis (2000)
Cooper Ck.	Durham Downs Rd	F/P1	TL	W1701	100	18	3	30.00	4.58	Maroulis (2000)
Cooper Ck.	Durham Downs Rd	F/P3	TL	W1703	7.8	0.8	1.5	192.31	17.89	Maroulis (2000)
Cooper Ck.	Durham Downs Rd	F/P3	TL	W1704	32.7	2.4	4.5	137.61	9.41	Maroulis (2000)
Cooper Ck.	Durham Downs Rd	F/P3	TL	W1705	37.4	3	6	160.43	11.91	Maroulis (2000)
Cooper Ck.	Durham Downs Rd	F/P6	TL	W1706	2.5	0.3	2	800.00	85.71	Maroulis (2000)
Cooper Ck.	Karmona pipeline	SF12-1	TL	re-W2850	5.1	0.4	1.5	294.12	21.39	Fagan (2001)
Cooper Ck.	Karmona pipeline	SF12-1	OSL-MGA	W2854	7.2	0.5	1.53	212.50	13.80	Fagan (2001)
Cooper Ck.	Karmona pipeline	SF13-3	TL	W2852	8.4	0.7	1.2	142.86	10.99	Fagan (2001)
Cooper Ck.	Karmona pipeline	SF14-4	TL	W2853	2.4	0.2	1.5	625.00	48.08	Fagan (2001)
Cooper Ck.	Karmona pipeline	SF15-5	TL	W2843	2.6	0.2	0.7	269.23	19.23	Fagan (2001)

Continued over page....

River	Site i	Site ii	Dating method [a]	Lab code [b]	Age ±1σ error		Sample depth	Deposition Rate [b]		Reference [d]
					ka	ka	m	m.ka⁻¹		
Cooper Ck.	Karmona pipeline	SF16-2	TL	W2851	74.6	7.6	1.5	20.11	1.86	Fagan (2001)
Cooper Ck.	Levee A, crest	SF5	OSL-MGA	re-2844	4.2	0.3	1.14	271.43	18.10	Fagan (2001)
Cooper Ck.	Levee A, crest	SF7	OSL-MGA	re-2845	6.1	0.6	1.53	250.82	22.46	Fagan (2001)
Cooper Ck.	Levee A, crest	SF8	OSL-MGA	re-2846	7.5	0.6	2.02	269.33	19.95	Fagan (2001)
Cooper Ck.	Levee A, distal	SF1	OSL-MGA	re-2839	21.1	1.4	1.55	73.46	4.57	Fagan (2001)
Cooper Ck.	Levee A, distal	SF2	TL	W2840	20.5	1.5	2.09	101.95	6.95	Fagan (2001)
Cooper Ck.	Levee A, distal	SF3	TL	W2841	18.4	1.8	0.72	39.13	3.49	Fagan (2001)
Cooper Ck.	Levee A, distal	SF4	TL	W2842	22.6	2.1	1.13	50.00	4.25	Fagan (2001)
Cooper Ck.	Maapoo waterhole	MW/H1	TL	W4264	97.9	10.1	19	194.08	18.15	Nanson (unpub.)[e]
Cooper Ck.	Maapoo waterhole	MW/H1	TL	W4261	131	8	15.7	119.85	6.90	Nanson (unpub.) [e]
Cooper Ck.	Maapoo waterhole	MW/H1	TL	W4265	160	15	11	68.75	5.89	Nanson (unpub.) [e]
Cooper Ck.	Mt Howitt	Trench 1/2	TL	W2292	0.33	0.04	0.8	2424.24	2417.70	Maroulis (2000)
Cooper Ck.	Mt Howitt	Trench 1/2	TL	W2293	2.6	0.2	2.85	1096.15	113.40	Maroulis (2000)
Cooper Ck.	Mt Howitt	Trench 1/2	TL	W2294	16.7	1.5	4.8	287.43	25.13	Maroulis (2000)

River	Site i	Site ii	Dating method[a]	Lab code[b]	Age ka	±1σ error ka	Sample depth m	Deposition Rate[b] m.ka^{-1}		Reference[d]
Cooper Ck.	Naccowlah waterhole	Exc. 1	TL	W553	51	4.5	2.2	43.14	3.50	Rust & Nanson (1986)
Cooper Ck.	South Narberry waterhole	NH3	TL	W1041	14.5	1.6	1	68.97	6.85	Maroulis (2000)
Cooper Ck.	Shire Rd	SR4	TL	W2040	11.3	1	1.5	132.74	10.79	Maroulis (2000)
Cooper Ck.	Shire Rd	SR6	TL	W2047	14.4	1.4	3	208.33	18.46	Maroulis (2000)
Cooper Ck	Shire Rd	SR7	TL	W2049	63.1	12.2	3	47.54	7.70	Maroulis (2000)
Cooper Ck	Shire Rd	SR8	TL	W2051	53.9	4	3	55.66	3.85	Maroulis (2000)
Cooper Ck	Wilsons Swamp	SF10	TL	W2848	1.2	0.1	1.35	1125.0	86.54	Fagan (2001)
Cooper Ck.	Wilsons Swamp	SF11	OSL-MGA	re-W2849	7.3	0.5	1.87	256.16	16.42	Fagan (2001)
Cooper Ck.	Wilsons Swamp	SF9	TL	W2847	0.3	0.05	0.9	3000.0	428.5	Fagan (2001)
Diamantina R.	Brighton Downs		TL	W581	2	0.5	0.6	300.00	60.00	Nanson et al. (1988)
Diamantina R.	Davenport Downs		TL	W623	17	1.6	5.5	323.53	27.83	Nanson et al. (1988)
Diamantina R.	Davenport Downs		TL	W624	85	9.2	9.2	108.24	10.57	Nanson et al. (1988)
Thomson R.	Longreach	H2	TL	W602	4.9	0.5	3.4	693.87	64.25	Nanson et al. (1988)
Thomson R.	Longreach	H2	TL	W603	10.3	0.8	5.5	533.98	38.49	Nanson et al. (1988)

Continued over page….

River	Site i	Site ii	Dating method [a]	Lab code [b]	Age ±1σ error		Sample depth	Deposition Rate [b]		Reference [d]
					ka	ka	m	m.ka⁻¹		
								1587.3	512.0	
Western R.	H1		TL	W595	0.63	0.3	1	0	3	Nanson et al. (1988)
Western R.	H1		TL	W596	17.4	1	3	172.41	9.37	Nanson et al. (1988)
Western R.	H2		TL	W597	85	10	5.5	64.71	6.81	Nanson et al. (1988)
Western R.	H3		TL	W637	19.8	1.6	1.6	80.81	6.04	Nanson et al. (1988)
Western R.	H5		TL	W601	11.2	2	2.8	250.00	37.88	Nanson et al. (1988)

[a]*TL—thermoluminescence, OSL-MGA—optically stimulated luminescence, multiple-grain aliquot;* [b]*Laboratory code, where two labcodes are presentd a weighted mean has been taken of the two samples as they are from the same unit.* [c] *Calculated using depth and age;* [d]*Work in which the age originally appeared;* [e]*Nanson (2013, pers comm. 3 August)*

Table A.3 - *Statistics of meandering and anabranching datasets and their associated errors.*

Statistical parameter	Meandering	Meandering error	Meandering % error	Anabranching	Anabranching error	Anabranching % error
n	47	47	47	47	47	47
Mean	92.18	15.37	12.09	30.92	3.13	10.79
Median	81.60	7.40	9.74	16.70	1.50	9.29
Min	5.30	0.40	5.39	0.30	0.04	5.75
Max	454.00	174.00	49.11	160.00	18.00	47.62
Range	448.70	173.60	43.72	159.70	17.96	41.87
Lower quartile	41.70	3.55	8.51	5.60	0.50	7.83
Upper quartile	120.00	12.00	11.84	44.95	3.55	10.57
Interquartile range	78.30	8.45	3.33	39.35	3.05	2.74
Standard deviation	75.36	28.75	8.09	36.79	4.15	6.57
Variance	5802.25	844.61	66.79	1383.05	17.58	44.06
Skew	2.56	4.19	3.15	1.72	1.97	4.15
Kurtosis	10.34	20.04	10.73	2.70	3.50	20.97

B Kernel density band width estimation

B.1 Bandwidth selection

Bandwidth for kernel density estimates can be selected visually by comparing different bandwidths, and selecting that which doesn't over or under smooth. Figure B.1 shows bandwidth comparisons for bandwidths of 5, 10, 15, 20, and calculated using Silverman's rule (Silverman 1986).
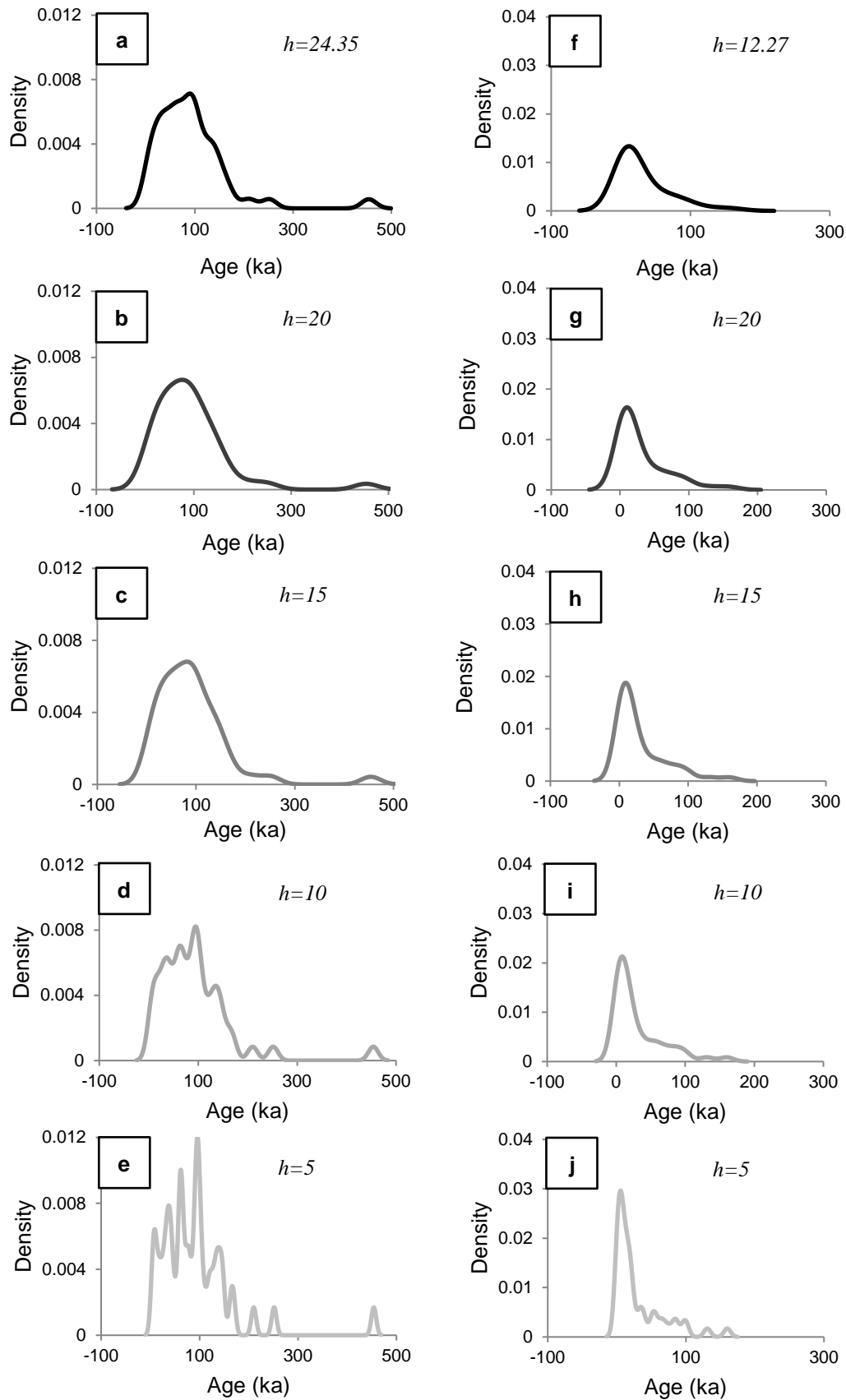
Figure B.1 - Bandwidth comparison for observed sand (a-e) and observed mud deposits (f-j). Bandwidths for a and f are calculated using Silvermans' rule of thumb' (Silverman, 1986).

Appendix C

C Cosmogenic nuclide extraction, measurements and calculations

This appendix outlines the methods used in calculating burial ages and erosion rates using cosmogenic ^{10}Be and ^{26}Al. The samples were prepared at the University of Wollongong (UOW) and the Australian Nuclear Science and Technology Organisation (ANSTO). The quartz separation and purification procedure, detailed below (C.1.1), is based on the protocols of Kohl and Nishiizumi (1992) and Mifsud et al. (2013). Be and Al were then extracted as oxides (C.1.2) using the ion chromatography method of Child et al. (2000).

C.1 Sample preparation

C.1.1 Quartz purification

Samples were collected as bulk sediment samples from channel beds and dune surfaces, and sieved, retaining the 250 – 500 μm grainsize fraction, ~300g of which was then purified to quartz through the following steps:

1. Samples rinsed to remove fine grained solids, repeat rinse until no suspended solids remain.

2. Samples underwent HCl/HNO^3 leach on hotplate for 24 hrs at 100 degrees. Repeated 3-5 times. Removes carbonates, sulphides, hydroxides, and metals and allows for HF to attack solid inclusions in grains.

3. Samples cleaned with H$_2$0 and fines discarded.

4. Samples placed in high-density polyethylene (HDPE) bottles with a mix of 2-4% HF and 2% HNO$_3$. Acid mix is used for optimal quartz purity. Leeched 2-4 times for 46 hours at 80°C whilst being constantly rotated (using 'hot dog' rollers).

5. Samples washed with MilliQ water and dried.

6. Quartz purity assessed. Quartz aliquots (0.2 – 0.3 g) extracted into Savillex vials. 2 mL 48% HF & 1 mL 32% HNO_3, closed vials heated at 120°C until dissolved.

7. Dissolved samples dried down at 120°C and the residue redissolved in 5 mL 1M HNO_3. Transferred to 10Ml tubes and made up to 10 ml with 1M HNO3. These were sent for ICPMS measurement.

8. The target is <200 ppm aluminium. Samples were 93.17 – 264.57 ppm.

9. To visually assess the purity of the quartz 1 g of each sample was placed in 50 ml Teflon beakers and 15 mL of 48% HF and 2.5 mL of $HClO_4$ was added. These were covered with Teflon watch glasses and placed on a hotplate at ~80 °C for 12 hours. Once dissolved they were fumed to dry. A spot <2 mm in diameter and white to pale yellow was expected. If this was not the result, further purification was needed and then the sample was reassessed.

C.1.2   Beryllium and aluminium extraction

Beryllium and aluminium extract was completed in two batches of eight (batch 1) and four (batch 2) samples each sample consisting of 30- 44 g pf purified quartz (Table C.1)

1. Each sample of purified quartz was added to a 1 L Nalgene Teflon bottle with ~0.3 – 0.45 g of a ^{9}Be carrier solution (the spike) (Table C.1). Spike for first batch was 1090 µg.g^{-1} and 1280 µg.g^{-1} for batch 2. The spike is necessary as there is no naturally occurring ^{9}Be in the samples, and only small quantities of ^{10}Be, making acquisition of sufficient quantities of BeO for measurement difficult. The amount of ^{10}Be is obtained from the ratio of ^{10}Be/^{9}Be so the quantity of ^{9}Be must be known. Al did not require a spike as there were sufficient quantities to obtain enough AL_2O_3.

2. A blank was also prepared with the carrier and HF but no sample.

3. Sample was dissolved in 48% hydrofluoric acid (HF) relative to the weight of the sample using Equation C.1 and 10 ml of nitric acid (HNO_3) to maintain the reactivity of HF.

$$V^{HF} = 1.1 \frac{335 \, M}{80}$$

Equation C.1 - Equation for calculating required amount of HF where V^{HF} is volume of HF and M is mass of sample

4. Sample bottles were placed on orbital shaker at 200 rpm for ~72 hours to dissolve quartz completely. After first 24 hours the orbital shaker was heated to 50°C to aid dissolution.

5. Two 1-4 ML aliquots were taken for ICP-OES.

6. Samples were transferred to 250 mL Teflon beakers and 5 mL of $HClO_4$ added to each sample. Beakers were placed on a hotplate.

7. After ~72 hrs samples are dried to a droplet and 2 mL 37% HCl and 10mL HNO_3 were added to redissolve the sample.

8. The sampleswere dried again and taken up in 5mL 1 M HNO_3. Solution was now yellow due to Fe present. The repetition of the evaporation and dissolution step ensures removal of HF and boron (as BF_3). Fe, Ti, Al, Be, alkali elements and alkali earth elements are retained as chlorine salts.

9. The samples were then transferred to 50 mL centrifuge tubes and 30 mL of MilliQ water was added.

10. A pH meter was calibrated between pH 4 and 7.

11. The pH of the samples in the 50 ml centrifuge tubes was adjusted to 7.8 with ammonia (NH_3) and 1 M HNO_3. This causes the Be and Al to precipitate with Fe and Ti while Na, K, Mg and Ca stay in solution. After 4 hours the pH was checked and adjusted back to 7.8 if necessary.

12. Samples were centrifuged for 10 mins at 3600 rpm which causes the precipitate to collect as a gel at the bottom of the tubes and the supernatant can be decanted to waste.

13. The samples were washed twice in 5mL MilliQ water and centrifuged for 10 min at 3600 rpm.

14. The cleaned precipitate was dissolved in 5 mL 37% HCl for >12 hrs. The resulting solution is yellow due to Fe.

15. Fe and some Ti was removed using anion exchange columns.

a. 8g of Dowex 1X-8 200 mesh anion exchange resin in exchange columns was conditioned using 20mL 1 *M* HCl, 20mL 2 *M* HCl, 20mL 4 *M* HCl, 20mL 8 *M* HCl, 50mL 9 *M* HCl and the conditioning solution was discarded.

b. A 50ml Teflon beaker was placed under each column

c. The samples were centrifuged for 2 mins at 3600 rpm then added to the columns.

d. Centrifuge tubes were washed four times with 5 ml of 9M HCl and the rinse added to the columns.

e. Fe(III) remains in columns as Cl- complexes and is seen as brown stains in the top of the column. Ti (IV) stays in columns as $TiCL_6$, whereas cationic Ti and Ti (III) wash through resin. The eluent contains Be, Al and Ti.

f. Used anion columns were kept until Be and Al processing completed.

16. The solutions, in Teflon beakers, have 2.5 mL of $HClO_4$ added and were placed on hot plates at 160 °C.

17. Once the sample had dried to a droplet 5 mL of HNO_3 was added and the contents of the beaker were transferred to a 50 mL centrifuge tube and 25 mL of MilliQ is added.

18. Al was separated from Be and Ti by adjusting the pH to 11.5 with 1 *M* HNO_3 and 50% and dilute $NaOH_2$. Be and Ti form insoluble hydroxides and Al stays in solution.

19. The sample was centrifuged for 10 mins a 3600 rpm. The supernatant was transferred to new tubes and the residue retained.

20. The Al was recovered from the supernatant by adjusting the pH to ~7.8 with 50% and 1 M HNO_3 and dilute $NaOH_2$ and the sample was left for 12 hours. The Al precipitates and was washed twice, with the supernatant then being discarded.

21. The Be was separated using cation exchange chromatography

a. 8g of Dowex 50W-X8 200 mesh cation exchange resin in exchange columns was conditioned using 20mL 4 *M* HNO_3, 20mL 2 *M* HNO_3, 20mL 0.5 *M* HNO_3, 250 mL of Milli-Q water and the conditioning solution was discarded.

b. Immediately prior to sample addition, columns were conditioned with 50 mL of 0.25 M H_2SO_4 + 0.015% H_2O_2 and drained to the top of the resin this complexes the Ti into a negative ion which drains and the Be was retained.

c. Sample was centrifuged for 10 minutes then added to column, sample should drip through at ~1 drip per second and will be yellow if titanium is present. The sample was collected in 250 mL Teflon beakers.

d. Tubes from which sample was poured had 20 mL of 0.25 M H_2SO_4 + 0.015% H_2O_2 added and were centrifuged for 3 – 5 mins. These were then added to columns.

e. 200 mL more 0.25 M H_2SO_4 + 0.015% H_2O_2 was added. Where elutant was still yellow 40 mL more acid mix was added. Once elutant was clear, beakers weremoved to the fume cupboard and retained until Be extraction was complete.

f. 20 mL of 1.2 M HNO_3 was added to each sample column and the elutant collected in centrifuge tubes marked: Be/1.2 M wash

g. 40 mL of 1.2 M HNO_3 was added to each sample column and the elutant collected in centrifuge tubes marked: Be/F1

h. 40 mL of 1.2 M HNO_3 was added to each sample column and the elutant collected in centrifuge tubes marked: Be/F2

i. Used columns were kept in case of need for reprocessing

22. The pH of the 1.2 M wash, F1 and F2 were adjusted to 7.8 using with dilute and 1 M HNO_3 and concentrated NH_3.

23. The hydroxide precipitate coagulated, after which the tubes were centrifuged at 3000 rpm for 10 mins and the supernatants were discarded.

24. Residue was washed twice with Milli-Q water and spun at 3000 rpm for 10 mins and supernatant discarded.

25. Last drops of wash were removed with pipette.

C.1.3   Oxide production

1. One crucible used for each Be and Al sample.

2. Masses of crucibles and lids were recorded to 0.0001 mg.

3. A separate pipette and centrifuge tube were cleaned with 1 *M* HNO$_3$ for each sample.

4. Samples are added to crucibles with pipette and 2 – 3 drops of HNO$_3$ were used to rinse the remainder. If more than one tube for a sample contained Be, these were combined into one crucible.

5. Crucibles were placed in the oven at 90 °C over night.

6. Samples were placed in muffle furnace at 200 °C for at least 1 hr.

7. Muffle furnace was gradually increased to 800 °C. 120 °C for 10 min, 160 °C for 15 min, 200 °C for 15 min, 800 °C. Samples were left for 6 hours. This converts hydroxides to oxides.

8. Muffle furnace temperature was reduced to 100 °C and samples were removed.

9. Crucibles were weighed once cooled and masses record.

C.1.4 Cathode loading

1. Pin was inserted into cathode with small stempel.

2. Cathode number engraved on cathode and recorded in loading book

3. In fume hood, sample was weighed and balance tared.

4. 4 mg niobium (Nb) was added into cathode.

5. BeO is transferred from crucible to mortar and mass difference in crucible recorded.

6. Four times the amount of BeO was added in Nb in the mortar.

7. Nb and BeO were mixed well with spatula and added to cathode with funnel.

8. Pin pressed into cathode with pill press to specified pressure.

9. Sample surface in cathode inspected under microscope and cleaned with alcohol wipe.

10. Repeated with AlO.

C.1.5 AMS measurement and concentration calculation

Measurements of ^{10}Be/^{9}Be and ^{26}Al/^{27}Al for all samples were completed on a 10MV ANTARES at ANSTO (Fink and Smith, 2007). Standard KN-5-2 was used for ^{10}Be/^{9}Be ratios (Nishiizumi et al. 2007). All ^{26}Al/^{27}Al ratios were corrected according to the full chemistry procedural blank's ^{26}Al count rate. Uncertainties on 10Be were calculated in quadrature from the measurement uncertainties (counting statistics, standard normalisation, blank correction), 2% standard reproducibility and 1%

uncertainty in the Be spike concentration. Final ^{26}Al uncertainties were calculated in quadrature using AMS uncertainties, 3% standard reproducibility and 4% ICP-OES uncertainty.

$$N_{^{10}Be} = \frac{^{10}Be}{^{9}Be} \frac{\dfrac{m_{^9Be}}{L} m_a(^9Be)}{m_{qtz}}$$

Equation C.2 – Calculation of concentrations for 10Be: where $\frac{^{10}Be}{^9Be}$ is the blank corrected measurement from AMS $m_a(^9Be)$is the atomic mass of ^9Be; $m_{qtz}$is the mass of dissolved clean quartz; $m_{^9Be}$ is the 9BE added in the carrier; L is Avogadro's number.

$$N_{^{26}Al} = \frac{^{26}Al}{^{27}Al} \frac{\dfrac{m_{^{27}Al}}{L} m_a(^{27}Al)}{m_{qtz}}$$

Equation C.3 – Calculations of concentrations for ^{26}Al: where $\frac{^{26}Al}{^{27}Al}$ is the blank corrected measurement from AMS; $m_a(^{27}Al)$ is the atomic mass of ^{27}Al; $m_{qtz}$is the mass of dissolved clean quartz; $m_{^{27}Al}$ is the 27Al measured by ICP-OES; L is Avogadro's number.

Table C.1- Cosmogenic nuclide measurement data

Sample	AMS ID	Production scaling factor[a]	Sample Mass (g)	10Be/9Be ratio (10^-15)[b,c,d]	9Be carrier mass[e]	10Be 10^6 at.g-1	26Al/27Al ratio (10^-15)[d,f,i]	27Al icp conc µg.g-1	26Al 10^6 at.g-1	Ratio
BR2	A2592/B5745	0.80	40.243	837.56 ± 16.71	0.316[1]	0.48 ± 0.010	861.29 ± 141.86	124.72	2.25 ± 0.40	4.68 ± 0.84
BW1	A2710/B6017	0.86	39.57	924.00 ± 16.07	0.297[2]	0.52 ± 0.017	348.01 ± 19.24	264.57	2.06 ± 0.15	3.93 ± 0.31
WDFS1	A2597/B5757	0.79	40.163	767.54 ± 11.01	0.311[1]	0.43 ± 0.006	905.88 ± 211.15	126.81	2.39 ± 0.61	5.52 ± 1.42
CO1	A2591/B5744	0.79	40.436	873.33 ± 13.03	0.315[1]	0.50 ± 0.007	638.12 ± 57.48	145.27	1.86 ± 0.23	3.76 ± 0.48
CB1	A2709/B6016	0.78	42.91	939.35 ± 23.63	0.298[2]	0.49 ± 0.018	407.01 ± 29.35	194.69	1.77 ± 0.16	3.60 ± 0.34
WN1	A2598/B5751	0.82	30.262	1878.50 ± 31.83	0.315[1]	1.42 ± 0.024	1819.84 ± 159.76	129.98	5.09 ± 0.52	3.57 ± 0.38
CHFS1	A2593/B5746	0.80	40.373	887.90 ± 15.14	0.318[1]	0.51 ± 0.006	1509.24 ± 75.62	100.69	3.25 ± 0.23	6.39 ± 0.49
NETFS1	A2595/B5748	0.84	40.014	927.17 ± 14.06	0.316[1]	0.53 ± 0.008	910.73 ± 130.32	162.16	3.04 ± 0.50	5.70 ± 0.94
PP-DS1	A2596/B5749	0.79	40.778	1013.60 ± 17.07	0.313[1]	0.57 ± 0.010	745.37 ± 68.81	130.52	1.90 ± 0.23	3.36 ± 0.41
KWBFS1	A2594/B5747	0.79	41.296	760.37 ± 12.59	0.314[1]	0.42 ± 0.006	741.70 ± 83.58	111.14	1.62 ± 0.22	3.84 ± 0.52
KWBDS1	A2711/B6018	0.79	40.71	723.20 ± 14.66	0.388[2]	0.52 ± 0.018	502.11 ± 22.29	157.86	1.77 ± 0.12	3.41 ± 0.25
KWBDS2	A2712/B6019	0.79	43.09	670.14 ± 18.70	0.465[2]	0.55 ± 0.022	513.99 ± 24.43	171.45	1.97 ± 0.14	3.61 ± 0.28

[a] *combined atmospheric pressure/latitude scaling factor using the time-independent scaling of Dunai (2000);* [b] *normalised to standard KN-5-2 (Nishiizumi et al., 2007);* [c] *corrected for blank of 9.58 ± 2.06 x10^-15;* [d] *uncertainties at 1-σ;* [e] 9Be *carrier solution concentrations of 1) 1090 ± 15 mg·g^-1 2) 1128 ± 22 mg·g^-1;* [f] 26Al/27Al *normalised to SRM KN-4-2 at aratio of 30 960 a 10^-15 (Nishiizumi 2004);* [i] *corrected for blank*

C.2   Denudation rates and burial ages

C.2.1   Scaling and production rates

In order to calculate catchment denudation rates and burial duration production rates of Schaller et al. (2001) were used with ^{10}Be sea level high latitude (SLHL) production rates as follows: 4.5 ± 0.5 atoms.g^{-1}.y^{-1} for high energy neutrons from Balco et al. (2008) ^{10}Be calibration site dataset, utilising the time-independent altitude-latitude scaling scheme of Dunai (2000) with a half-life for ^{10}Be of 1.387 ± 0.012 Ma (Chmeleff et al. 2010; Korschinek et al. 2010); and 0.097 ± 0.007 atoms.g^{-1}.y^{-1} for slow muons and 0.085 ± 0.012 atoms.g^{-1}.y^{-1} for fast muons from Kubik et al. (2009) and based on Heisinger et al. (2002a,b).

For ^{26}Al, high energy neutron production was scaled to ^{10}Be production at a ratio of 6.1 to give 30.38 atoms.g^{-1}.y^{-1}; 0.805 ± 0.073 g^{-1}.y^{-1} was used for slow muon production and 0.715 ± 0.086 g^{-1}.y^{-1} for fast muon production from Heisinger et al. (2002a;b). This gives a total ^{26}Al production rate of 31.90 g^{-1}.y^{-1} and a ^{10}Be production rate of 4.68 g^{-1}.y^{-1}.

All of the production rates were corrected, using the time-independent scaling scheme of Dunai (2000), for altitude and latitude and following Codilean (2006), for topographic shielding. These values were then used in CosmoCalc 3.0 (Vermeesch et al. 2007).

C.2.2 Denudation rates

Denudation rate calculations use a single nuclide, in this case ^{10}Be. The calculations assume steady state erosion and negligible burial. i.e burial age T = 0. Equation C.4, is used by Cosmocalc 3.0 (Vermeesch 2007) when given the calculated scaling, measured ^{10}Be concentration and ^{10}Be error to calculate denudation rate.

$$N_{10_{Be}(\epsilon)} = P_{10_{Be}} \sum_{i=0}^{3} \frac{S_{P(i)}F_i}{\lambda_{10_{Be}} + \frac{\epsilon\rho}{\Lambda_i}}$$

Equation C.4 – The denudation rate as calculated by Cosmocalc 3.0 where: $N_{10_{Be}}$ is the measured ^{10}Be concentration; $P_{10_{Be}}$ is the total SLHL surface production rate of ^{10}Be; F_i is the relative ^{10}Be production rates; $\lambda_{10_{Be}}$ is the radioactive decay constant of ^{10}Be ($5 \times 10^{-7}.yr^{-1}$); ρ is the density of overburden at 2.65 g.cm^{-3}; $S_{P(i)}$ is the production scaling factors, calculated after Dunai (2000); and Λ_i is the attenuation lengths. (Vermeesch 2007).

C.2.3 Burial age calculation

Burial age calculations were performed using Cosmocalc 3.0 (Vermeesch 2007) with the two nuclide 'Burial-Erosion' model with ^{26}Al and ^{10}Be using the Newton method. Cosmocalc 3.0 performs Equation C.5 which in its simplest form assumes exposure followed by a single phase of burial followed by minor exposure. Erosion is assumed to be steady state, therefore T = ∞ (Vermeesch 2007). The resultant value is a minimum burial age and a burial corrected denudation rate.

$$\left[\begin{array}{l} f_{10_{Be}}(\epsilon, T): N_{10_{Be}} = P_{10_{Be}}\, e^{-\lambda^{10_{Be}}\tau} \sum_{i=0}^{3} \frac{S_{P(i),^{10}Be}F_{i,^{10}Be}}{\lambda_{10_{Be}} + \frac{\epsilon\rho}{\Lambda_i},^{10}Be} \quad (a) \\[3em] f_{26_{Al}}(\epsilon, T): N_{26_{Al}} = P_{26_{Al}}\, e^{-\lambda^{26_{Al}}\tau} \sum_{i=0}^{3} \frac{S_{P(i),^{26}Al}F_{i,^{26}Al}}{\lambda_{26_{Al}} + \frac{\epsilon\rho}{\Lambda_i},^{26}Al} \quad (b) \end{array} \right.$$

Equation C.5 – Equations for (a) ^{10}Be and (b) ^{26}Al to calculate burial (Vermeesch 2007). $N_{10_{Be}}$ and $N_{26_{Al}}$ are the measured ^{10}Be and ^{26}Al concentrations; $P_{10_{Be}}$ and $P_{26_{Al}}$ are the total SLHL surface production rates of ^{10}Be and ^{26}Al ; $F_{i,^{10}Be}$ and $F_{i,^{26}Al}$ are the relative ^{10}Be and ^{26}Al production rates; $\lambda_{10_{Be}}$ is the radioactive decay constant of ^{10}Be ($5 \times 10^{-7}.yr^{-1}$) and $\lambda_{26_{Al}}$ is the radioactive decay constant of ^{26}Al ($9.83 \times 10^{-7}.yr^{-1}$); ρ is the density of overburden at 2.65 g.cm^{-3}; $S_{P(i)}$ is the production scaling factor, calculated after Dunai (2000); and Λ_i is the attenuation lengths.

Due to the shorter half-life of ^{26}Al, the equations can be rearranged to be a function of the denudation rate (Equation C.6a):

$$\text{T} = \frac{^{26}Al}{\lambda_{^{26}Al}} \, ln\left(\frac{P_{^{26}Al}}{N_{^{26}Al}} \sum_{i=0}^{3} \frac{S_{P(i),^{26}Al}F_{i,^{26}Al}}{\lambda_{^{26}Al} + \frac{\epsilon\rho}{\Lambda_i},\,^{26}Al}\right) \qquad (a)$$

Where ϵ is given as (Equation C.6b) (Vermeesch 2007):

$$\lambda_{^{26}Al} \, ln\left(\frac{P_{^{10}Be}}{N_{Be}} \sum_{i=0}^{3} \frac{S_{P(i),^{26}Al}F_{i,^{26}Al}}{\lambda_{^{10}Be} + \epsilon\rho/\Lambda_{i,}\,^{10}Be}\right)$$
$$- \lambda_{^{26}Al} \, ln\left(\frac{P_{^{26}Al}}{N_{^{26}Al}} \sum_{i=0}^{3} \frac{S_{P(i),^{26}Al}F_{i,^{26}Al}}{\lambda_{^{26}Al} + \epsilon\rho/\Lambda_i,\,^{26}Al}\right) = 0 \qquad (b)$$

Equation C.6 – Equation for burial, by solving (b) for ϵ, ϵ can then be substituted into (a) to give burial duration. $N_{^{10}Be}$ and $N_{^{26}Al}$ are the measured ^{10}Be and ^{26}Al concentrations; $P_{^{10}Be}$ and $P_{^{26}Al}$ are the total SLHL surface production rates of ^{10}Be and ^{26}Al ; $F_{i,^{10}Be}$ and $F_{i,^{26}Al}$ are the relative ^{10}Be and ^{26}Al production rates; $\lambda_{^{10}Be}$ is the radioactive decay constant of ^{10}Be (5 x 10^{-7}.yr^{-1}) and $\lambda_{^{26}Al}$ is the radioactive decay constant of ^{26}Al (9.83 x 10^{-7}.yr^{-1}); ρ is the density of overburden at 2.65 g.cm^{-3}; $S_{P(i)}$ is the production scaling factor, calculated after Dunai (2000); and Λ_i is the attenuation length.

Appendix D

D OSL dating of the Marshall River

D.1 Introduction

This appendix outlines the intrinsic luminescence characteristics of the 15 samples from the Marshall River discussed in Chapter 7, as well as the measurement and distribution of D_e values from these samples and how they were combined for final D_e, and subsequently, age estimation. This appendix also details the dosimetry for each of these samples.

No two grains are behaviourally the same. Rather, each grain displays variabilities within their luminescence properties, not only within the depositional setting of the samples, but within each individual sample. These inter-grain variations can be been seen in: 1) the brightness of the OSL signal (Duller and Murray 2000); 2) the contribution of the fast, medium, and slow components to the signal as seen in the decay curve shape (Jain et al. 2003); and 3) the shape of the dose response curves (Gliganic et al. 2012; Rhodes et al. 2006). A total of 13 200 individual grains of 180–212 μm, HF-etched quartz from the Marshall River samples were measured using a Risø TL/OSL reader fitted with a U-340 filter at the University of Wollongong for D_e determination. Of these 13 200 grains not all give an accurate estimate of the D_e. The OSL signal is taken by integrating the signal from the sum of the first 0.22 s of stimulation and the background is taken as the average of the last 0.3 s of stimulation. Following D_e measurement, each grain was systematically interrogated against a series of rejection criteria to ensure that an accurate and meaningful D_e value was determined. The final D_e determination for each sample was then made using only those grains that pass these criteria.

OSL samples were prepared for single grain analysis of 180–212 μm quartz using the standard quartz extraction and purification method of Wintle (1997) outlined below.

D.2 Sample preparation

1. Samples were sieved at 90, 125, 180, 212, 250 μm.

2. The 180-212 μm fraction was then immersed in 10% HCl to remove carbonate

   $$2 HCl + CO_3(-2) \rightarrow H_2CO_3 \longleftrightarrow CO_2(g) + H_2O(l) + 2Cl-$$

3. The samples were then cleaned with distilled water.

4. Immersed in 10% H_2O_2 for 24 hours to remove organics and cleaned with distilled water.

   $$2(H_2O_2) +c \rightarrow 2H_2O + CO_2$$

5. The samples were then re-sieved at 180 and 212 μm to remove any smaller grains that had been disaggregated during the sample preparation.

6. The samples then underwent density separation with sodium polytungstate (SPT) to isolate the Quartz grains; first at 2.7 g cm^{-3}, to remove heavy minerals which constituted approximately 5 – 10% of the sample then at 2.62 g cm^{-3} to remove feldspars. Feldspar content was minimal.

7. The samples were then etched with 40% HF for 40 minutes to remove the outer, alpha irradiated layer, and to remove any feldspars that had not been removed by density separation. And sieved again at 180-212 to removed grains reduced in size by etching. Standard sample prep method (Wintle 1997).

D.3 Luminescence measurements

All measurements for D_e determination and dose recovery tests use the single aliquot regenerative dose (SAR) procedure of Murray and Wintle (2000) on 180–212 µm grains. The sequences all use the measurement durations and fixed temperatures shown in Table D.1. A test dose of 300 s was used (~22 Gy), as initial measurements with a test dose of 100 s (~7.3 Gy) gave poor return of usable grains as only a few grains had a sufficiently bright test dose OSL signal above background.

Table D.1 – The SAR procedure (Murray and Wintle 2000) used on all samples from the Marshall River for dose recovery and D_e determination.

Step Number	Step Procedure
1	Preheat @ PH1 at 5 °C/s and hold for 10 s
2	Stimulate with green laser at 125 °C for 2 s to induce OSL signal from natural or regenerative dose.
3	Irradiate with test dose
4	Preheat @ PH2 at 5 °C/s and hold for 5 s
5	Stimulate using green laser at 125 °C for 2 s to induce OSL signal from natural or regenerative dose.
6	Irradiate at regenerative dose
7	Repeat steps 1-6 for R1 - R_n, 0 and R1.
8	Stimulate with infrared laser at 50 °C
9	Repeat steps 1-5

D.4 Single grain dose recovery tests

The dose recovery tests establish the most appropriate measurement parameters in terms of preheat (PH1) and cutheat (PH2), steps 1 and 4 in the SAR procedure.

The dose recovery tests were conducted on one sample, with four different preheat/cutheat combinations investigated. Prior to D_e measurement, the samples were bleached in natural sunlight for 48 hours and rested for a further 48 hours. A laboratory beta irradiation of ~7.3 Gy was given as a surrogate natural dose before running the SAR procedure as normal (Table D.1). A total of 500 grains were measured for each of four different temperature combinations, each using a 160°C cutheat (PH2) and preheat (PH1) of 180 °C, 200 °C, 220 °C and 240 °C, with the exception of 180 °C/160 °C where only 400 grains were measured). Grains were analysed in R using the NumOSL package (Peng et al. 2013) and screened using the same rejection criteria as used for the measurements for D_e determination. A weighted mean recovered dose for each sample was calculated using the central age model (Galbraith et al. 1999) and this value used to calculate a measured-to-given dose ratio (Table D.2).

Table D.2 – Results of dose recovery tests at four different preheat-cutheat combinations. Measured dose is presented as a weight mean calculated using the central age model (Galbraith et al. 1999).

PH1	PH2	Number grains		Given Dose (Gy)	Measured Dose (Gy) (CAM)	Measured to given ratio	OD%
		Measured	Accepted				
180	160	400	114	7.3	7.26 ± 0.07	0.99 ± 0.02	4.99 ± 0.99
200	160	500	117	7.3	6.47 ± 0.11	0.89 ± 0.02	14.63 ± 1.52
220	160	500	68	7.3	6.49 ± 0.15	0.89 ± 0.03	13.43 ± 2.11
240	160	500	116	7.3	6.35 ± 0.12	0.87 ± 0.02	15.84 ± 1.56

Figure D.1 – Radial plots of four preheat-cutheat combination, shaded region centred upon the weighted mean D_e determined using the central age (Galbraith et al. 1999). If the data conformed to typical statistical assumptions then 95% of the data in each plot ought to fall within the shaded grey band – shown at 2 σ. This is not the case for any sample shown here indicating a degree of overdispersion is present within each sample.
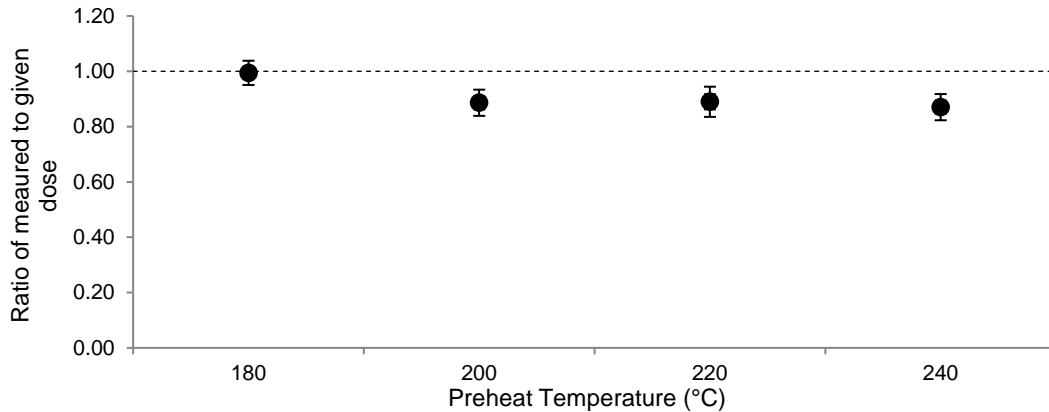
Figure D.2 – Results of dose recovery test. The ratio of measured to given dose is plotted for each preheat-cutheat temperature combination. Errors are displayed at one and two sigma.

Only a PH1/PH2 temperature combination of 180/160 °C gives a ratio within either 1σ (or 2σ) of unity. Higher temperatures (200 °C, 220 °C, 240 °C) systematically underestimate the given dose, with none being consisted with unity at 2σ. The overdispersion values range from 4.99% to 15.84% and are systematically higher for higher temperatures. Given these results, a temperature combination of 180 °C (PH1) and 160 °C (PH2) was chosen.

D.5 Luminescence characteristics

D.5.1 Application of rejection criteria

From the 14 subsurface island and ridge samples and one modern channel sample (MR-SS-1) from the Marshall River, a total of 13 200 grains were measured. The rejection criteria used to screen the Marshall River samples can be divided into three categories: signal related, growth curve related and D_e related (Table D.3) and were applied sequentially using the standard error in their application. When fitting the curve for the regenerative doses each data point was weighted by its inverse variance, the 'GOK' (general order kinetics) model was used with 500 Monte Carlo repeats for the curve fit. The D_e was then calculated using interpolation. Where a GOK curve could not be fitted, the R function iteratively attempted to fit a linear fit, single saturation exponential, single saturation exponential plus linear, and double saturation exponential curve to the data. If no appropriate fit was determined the D_e for the associated grain was rejected.

A significant proportion of grains within each of the Marshall River samples produced negative D_e values. In addition to the rejection criteria applied via NumOSL (Peng et al. 2013), therefore, any D_e value that had a D_e value that did not intersect with 0 Gy was rejected as they cannot represent a true dose (rejection criteria 12 in Table D.3). This criterion was only applied to those grains that had not been removed by any previously applied criterion. A final visual assessment of the dose response curves of all accepted to grains was then made to verify that the fitted curves were satisfactory.

Table D.3 - Rejection criteria used by R function calSARED. These criteria are applied in sequential order.

[1]*Rejection criterion 12 was applied in addition, and is not part of the R function calSARED*

	Number	Reject if:	Definition
Signal related	1	TN <3σ Background	If the test dose of the natural signal is within 3σ of background
	2	RSE >20%	If the relative standard error on the natural test dose is >20%
Growth curve related	3	Recycling ≠ 1	If the ratio between and R5/R1 does not intersect with 1 at 2sigma
	4	Recycling ≠ 1± 10%	If the ratio between R6/R5 is not within 10% of unity, so between 0.9 and 1.1, indicating feldspar contamination.
	5	Recuperation >20%	If recuperation (ratio of 0 dose to natural) exceeds 20% [1]
	6	FOM >10	If the figure of merit exceeds 10%, the curve does not sufficiently satisfy the characteristics of the model curve.
Equivalent dose related	7	No D_e	Unable to calculate D_e by interpolation
	8	Failed curve fit	Unable to fit a growth curve through the measurements from the SAR protocol.
	9	Saturated in LN/TN	The grain has reached its maximum dose absorption
	10	Failed D_e	Failed to calculated D_e
	11	Failed D_e error	Failed to calculated D_e error
	12[1]	Negative D_e	Negative values that do not intersect with 0 at 3σ

Criterion 5 was only applied to samples 1741 and 1744 as the D_e of the grains was higher than the other samples. In grains with a low D_e recuperation is often high as an artefact of the high signal-to-noise ratio of the natural OSL signal, as opposed to signal build-up over the SAR cycles. Criteria 6 was not applied to samples 1741 and

1744, preventing unnecessary rejections as curve fits were adequate without this criteria.

The twelve rejection criteria were applied sequentially to the samples (Table D.3). A total of 13 200 grains were measured with 1821 (13.8%) passing all the rejection criteria and being used in the D_e determination. For each sample between 7.5 and 22.5% of the total measured grains were accepted. The majority of grains were rejected due to signal-related criteria, with between 59.6 and 78.3% 291 and 856 grains for each sample failing on criteria 1 and 2. (Table D.4). A small number of grains, between 1.6 and 6.9%, were rejected based on the recycling ratio between the first and fifth regenerative doses not being within unity at 2σ. Even smaller numbers, less than 2% of grains for all samples except MR1750 where 7.6% grains failed, failed with the recycling ratio between the sixth and fifth regenerative doses not being within 10% of unity, thus indicating the presence of an infrared signal inferring feldspar contamination. Of the remaining grains between 3.8 and 13.8% grains failed as the figure of merit was not sufficient to satisfy the model used to fit the growth curve. The remaining rejection criteria, 7 – 12 (Table D.3), failed only a small number of grains, mostly less than 1.8% grains with the exception of MR 1750 and MR1744 where 2.2 and 4.8% grains failed to calculate an estimate of the dose. The reduction in the number of rejected grains for each criterion applied is likely to be due to removal of unsuitable grains that may fail on more than one criteria being removed by the preceding criteria.

Table D.4 - Number of grains that were rejected for each of the rejection criteria. 1 only applied to 1741 and 1744. 2 applied to all samples except 1741 and 1744

Sample	Total Measured	Total Accepted #	Total Accepted %	1	2	3	4	5	6	7	8	9	10	11	12
MR-SS-1	900	147	16.3	528	102	37	18	-	56	1	0	1	0	1	9
MR1676	1000	131	13.1	558	126	44	19	-	116	4	0	0	1	0	1
MR1682	1000	137	13.7	574	117	44	16	-	97	6	0	6	2	0	0
MR1683	1000	221	22.5	482	116	67	20	-	82	4	0	4	0	0	4
MR1686	1000	151	15.1	548	135	34	16	-	108	3	0	2	1	0	2
MR1748	500	56	11.2	317	63	19	10	-	33	1	0	1	0	0	0
MR1750	1000	75	7.5	495	118	69	76	-	138	22	2	3	1	0	1
MR1751	1300	157	12.1	856	144	47	24	-	68	0	0	1	0	0	3
MR1753	500	62	12.4	329	60	8	10	-	24	6	0	0	0	0	1
MR1754	1000	133	13.3	660	94	53	18	-	38	1	0	1	0	0	2
MR1756	1000	202	20.2	582	102	28	20	-	56	8	0	1	0	0	1
MR1757	1000	121	12.1	648	106	40	15	-	61	2	0	2	0	1	4
MR1759	1000	101	10.1	665	118	41	8	-	62	2	0	1	0	0	2
MR1741	500	66	13.2	340	50	28	6	1	-	2	0	5	1	0	1
MR1744	500	61	12.2	291	65	24	8	2	-	24	0	25	0	0	0

D.5.2 Signal brightness

D.5.2.1 Sensitivity

Not all grains will possess suitable signal or respond in the same way during the OSL measurement protocol. Duller et al. (2000) and Duller and Murray (2000), amongst others, have shown that less than 30% of the grains contribute to 90- 95% of the signal from a sample where aliquots are measured. The intrinsic brightness of the grains within each sample and between samples varies greatly. The sensitivity of each grain was measured by dividing the signal (counts) of the background corrected test dose of the natural (T_N) by the given test dose in Gy to give a value in counts/Gy. This corrects for the variable dose rates and differing test doses used on different machines. The background-corrected T_N signal for each grain was counted as the OSL counts in the first 0.2 s of optical stimulation with the average background count of the last 0.3 s of stimulation subtracted. The brightness distribution was assessed using cumulative light sum plots (Duller and Murray 2000), which plot the cumulative light sum as a function of the cumulative contribution of each grain to the total amount grains measured. The cumulative light sum plots are accompanied by a table of the percentage of grains that have poor (<10 counts.Gy^{-1}), moderate (10-100 counts. Gy^{-1}) and high (>100 counts. Gy^{-1}), while arbitrary these divisions have precedent from Jankowski (2014) and Jacobs et al. (2013).

The divisions are applied to: 1) all the grains measured (Table D.5), and 2) only those grains which pass the rejection criteria (Table D.6). There is some variability in the luminescence sensitivity of the grains measured for each sample, the lowest sensitivities are between ~-3 and -1 cts.Gy^{-1}, the highest values for any sample vary substantially from ~1300 cts.Gy^{-1} to ~15 000 cts.Gy^{-1}, a greater than one order of magnitude difference ,when looking at all grains. When looking at only the accepted grains, this variation is significantly reduced with a difference of ~ 6000 cts.Gy^{-1} from ~500 to ~6500. Variation in the lowest sensitivities is similarly low as with all grains, with a variation of ~4–8 cts.Gy^{-1}. For all grains of all samples, the majority of grains have sensitivity from 0–10 cts.Gy^{-1} (45–69%) for all grains and when also incorporating those < 0, (63–84%) Only 11–23% of grains have sensitivities of 10–100 cts.Gy^{-1} and only 5–15% with >100 cts.Gy^{-1}.

Table D.5 - Number of grains for each sample (all grains) which fall into sensitivity categories of cts.Gy^{-1} <0, 0-10, 10-100 and >100

Sample	# grains	<0		<10		10-100		>100		Min	Mean	Max
		#	%	#	%	#	%	#	%			
MR-SS1	900	182	20	502	56	153	17	63	7	-3.12	55.99	14734.48
MR1676	1000	210	21	557	56	155	16	78	8	-1.49	58.42	14459.22
MR1682	1000	223	22	543	54	161	16	73	7	-1.24	45.95	6072.74
MR1683	1000	142	14	486	49	227	23	145	15	-2.92	93.83	10456.76
MR1686	1000	208	21	544	54	173	17	75	8	-1.50	61.13	12488.06
MR1748	500	105	21	313	63	58	12	24	5	-1.23	24.59	1940.62
MR1750	1000	154	15	527	53	205	21	114	11	-2.90	137.19	14195.96
MR1751	1300	296	23	775	60	167	13	62	5	-1.90	28.82	6337.51
MR1753	500	91	18	327	65	55	11	27	5	-1.80	69.62	13117.88
MR1754	1000	224	22	581	58	123	12	72	7	-1.45	44.73	5797.71
MR1756	1000	204	20	539	54	186	19	71	7	-1.96	51.12	4416.42
MR1757	1000	217	22	594	59	127	13	62	6	-1.39	38.23	4028.64
MR1759	1000	221	22	619	62	111	11	49	5	-1.57	25.07	2491.66
MR1741	500	116	23	296	59	59	12	29	6	-1.32	27.82	1372.21
MR1744	500	100	20	289	58	77	15	34	7	-1.34	39.17	2965.15

When only the accepted grains are considered, the grain proportions for each category differ with the sensitivities of all grains being >0 cts.Gy^{-1}. This result is considered to be due to these 'negative' signal grains all failing the rejection criteria of having a T_N greater than background plus 3 sigma or a relative standard error of >20%. The proportion of grains with <10 cts.Gy^{-1} is substantially smaller with only 1–28% of grains meeting this criteria of low sensitivity, again likely due to them not passing the rejection criteria relating to the T_N . 56–73% of the accepted grains are within the 10–100 cts.Gy^{-1} division, which is a substantially larger proportion of the grains than when all grains considered. The brightest grains account for proportionally more grains in the accepted grains with 15–37% with >100 cts.Gy^{-1}.

The differences in luminescence sensitivity do not appear to be systematic according to sediment deposition mode, depth in core, machine used, or distance downstream.
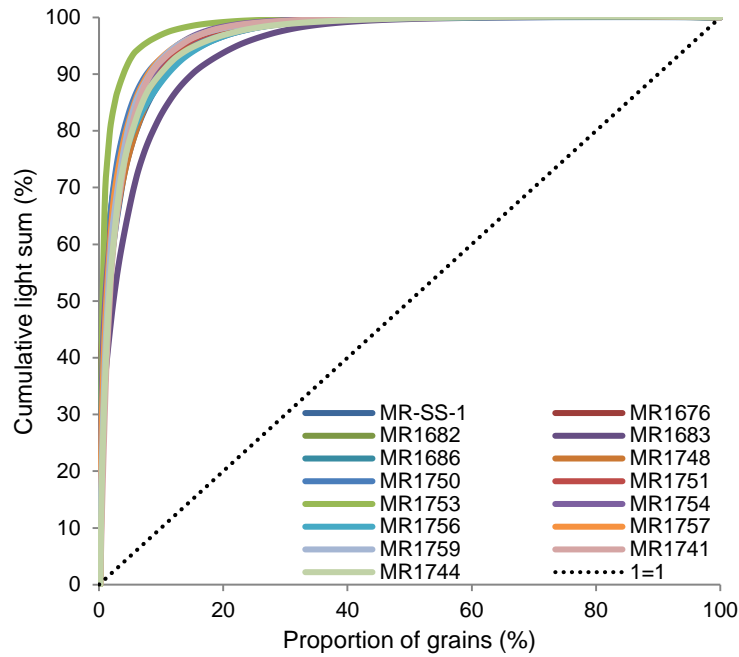
Figure D.3- Cumulative light sum plot of all samples. These curves show the background corrected TN signals. The 1=1 line represents a scenario where all grains contribute the same proportion of luminescence to the total.
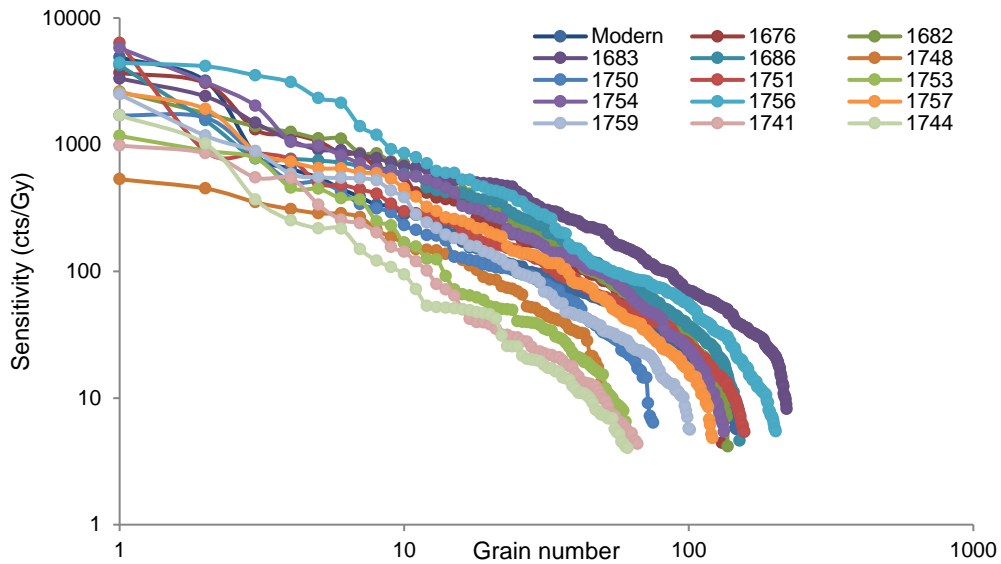
Figure D.4- Sensitivity plot showing the TN sensitivities(counts/Gy)of the accepted grains of each sample in descending rank order.

Table D.6 - Number of grains for each sample (only grains which pass rejection criteria) which fall into sensitivity categories of cts.Gy^{-1}<0, 0-10, 10-100 and >100

Sample	# grains	<10		10-100		>100		Min	Mean	Max
		#	%	#	%	#	%			
MR-SS1	147	13	9	108	73	26	18	5.66	127.68	4894.50
MR1676	131	7	5	80	61	44	34	4.41	185.35	3681.11
MR1682	137	4	3	88	64	45	33	4.14	181.05	2620.79
MR1683	221	3	1	136	62	82	37	8.18	172.55	3324.97
MR1686	151	7	5	95	63	49	32	4.59	168.40	4232.28
MR1748	56	6	11	32	57	18	32	8.37	99.93	532.82
MR1750	75	4	5	47	62	24	32	6.36	144.30	1702.05
MR1751	157	14	9	110	70	33	21	5.39	125.18	6337.51
MR1753	62	9	15	40	65	13	21	4.90	113.26	1170.83
MR1754	133	10	8	75	56	48	36	5.40	207.76	5797.71
MR1756	202	15	7	133	66	54	27	5.44	212.42	4416.42
MR1757	121	7	6	77	64	37	31	4.82	143.08	2573.38
MR1759	101	5	5	72	71	24	24	5.60	128.31	2491.66
MR1741	66	17	26	37	56	12	18	4.34	85.05	981.42
MR1744	61	17	28	35	57	9	15	4.02	87.25	1700.05

D.5.3 OSL decay curves

When applying the rejection criteria no lower limit was placed on the fast ratio on the T_N. The fast component is taken from the signal of the first 0.02 s, the medium and slow components from 0.18 - 0.2 s, and the background from 1 - 1.8 s. Durcan and Duller (2011) suggest that a fast ratio of 20 indicates an OSL signal that is ~90% fast component, determined using blue LEDs on aliquots. Duller (2012) applied a fast ratio of 20, and a range of increasing values to single grains. Here a fast ratio of 20 is taken to indicate a fast component dominated grain. There is a large amount of variation in the fast ratios of the Marshall River samples only MR1686 and MR1682 have more than 25% of grains with a fast ratio >20. The majority of samples have more than 50%

of grains with a fast ratio <10. A greater fast ratio indicates a faster decaying OSL signal. The Marshall River samples show a range of decay times (Figure D.5) in addition to the range of signal brightnesses, as discussed in D.3.2.

Table D.7 - Number of accepted grains for sample which have a fast ratio of <5, 5-10, 10-15, 15-20, >20. Lower bound of each category is inclusive.

Sample	Total # grains	Fast ratio range – number and percentage of grains									
		<5		5-10		10-15		15-20		>20	
		#	%	#	%	#	%	#	%	#	%
MR-SS1	147	86	59	33	22	12	8	8	5	8	5
MR1676	131	15	11	35	27	27	21	19	15	35	27
MR1682	137	19	14	42	31	24	18	13	9	39	28
MR1683	221	131	59	47	21	19	9	12	5	12	5
MR1686	151	18	12	44	29	26	17	15	10	48	32
MR1748	56	22	39	22	39	4	7	4	7	4	7
MR1750	75	17	23	25	33	7	9	15	20	11	15
MR1751	158	78	50	39	25	20	13	8	5	12	8
MR1753	62	37	60	11	18	4	6	6	10	4	6
MR1754	133	71	54	38	29	10	8	5	4	8	6
MR1756	202	106	52	43	21	22	11	10	5	21	10
MR1757	121	59	49	31	26	10	8	5	4	16	13
MR1759	101	59	58	27	27	4	4	2	2	9	9
MR1741	66	32	48	16	24	6	9	5	8	7	11
MR1744	61	37	65	11	19	5	9	0	0	4	7

D.5.4 Dose response curves

In all cases the response of the OSL signal with each additional laboratory dose was best explained by a general order kinetics (GOK) function (Guralnik et al. 2015). Figure D.5 also shows that the majority of grains have a D_e that plots in the lower part of the curve where growth is approximately linear, as is common in low samples D_e.

$$y = a * [1 - (1 + b * c * x)^{(-1/c)}] + d$$

Equation D.1 - The general order kinetics (GOK) curve equation.
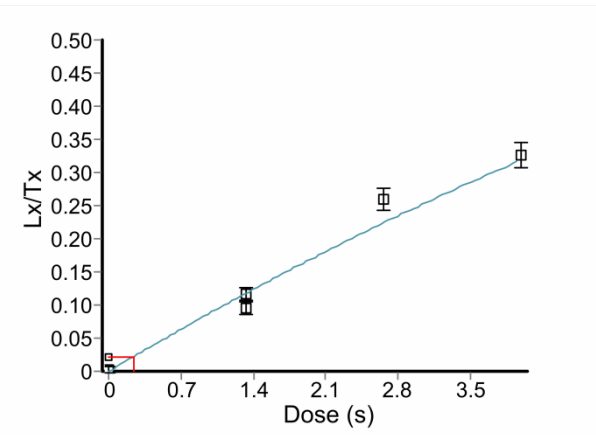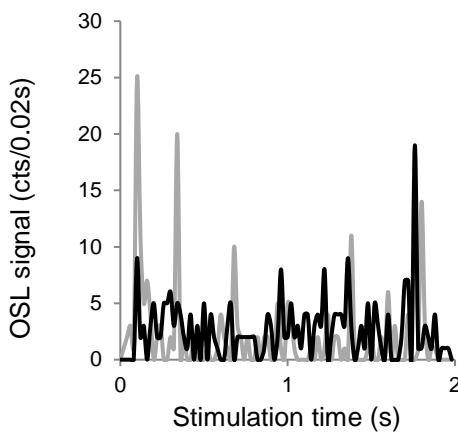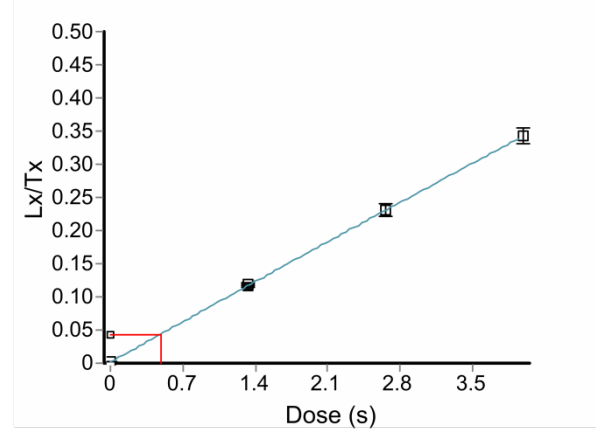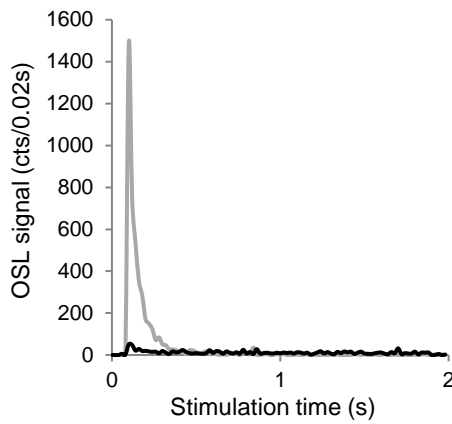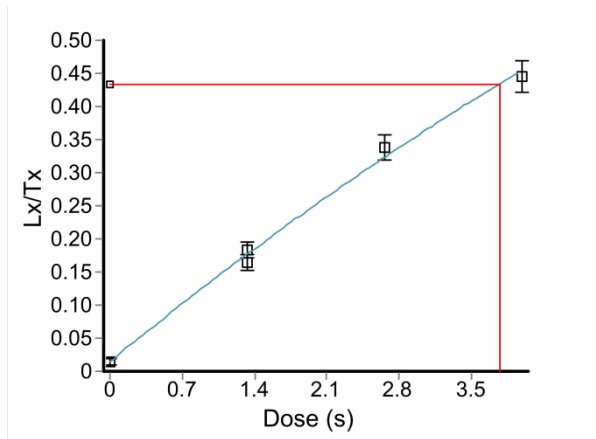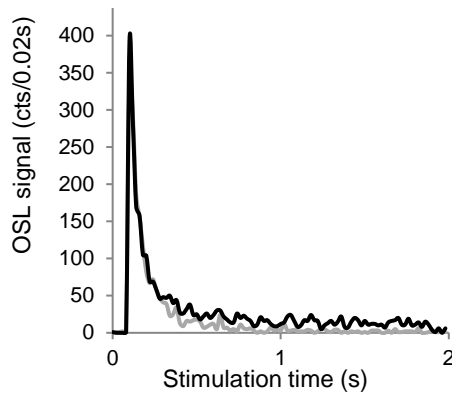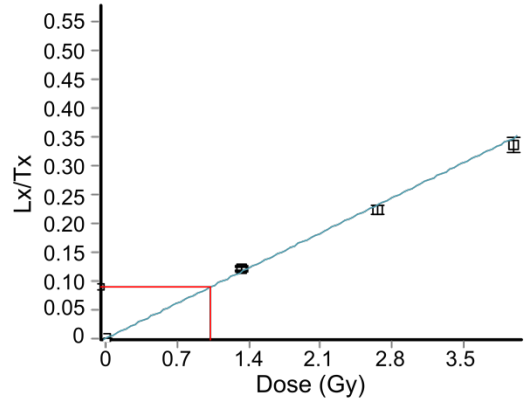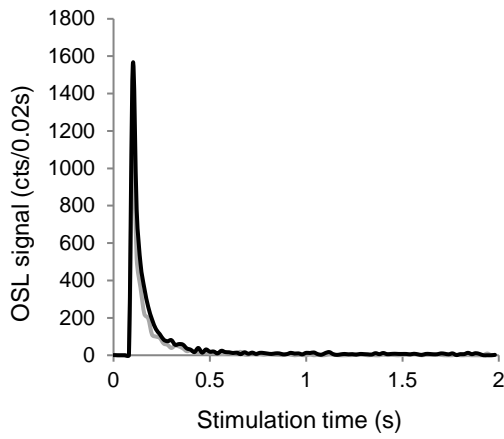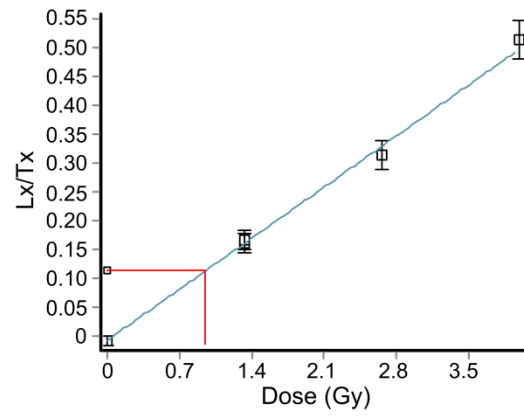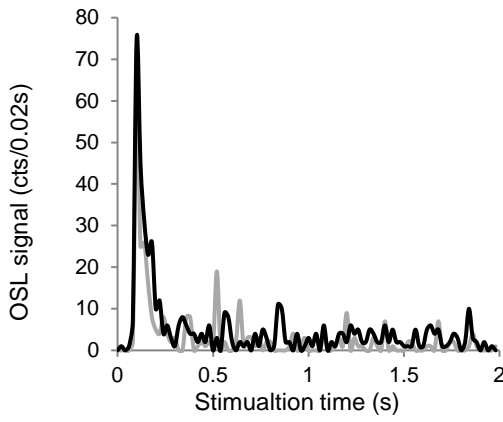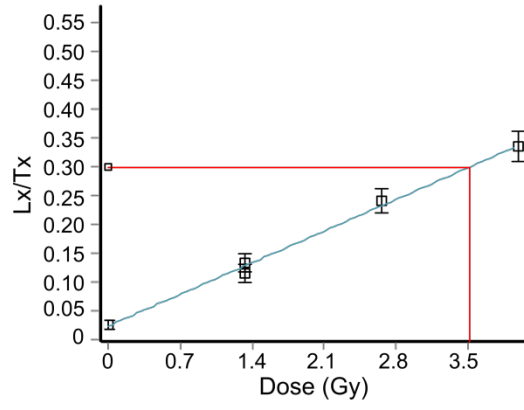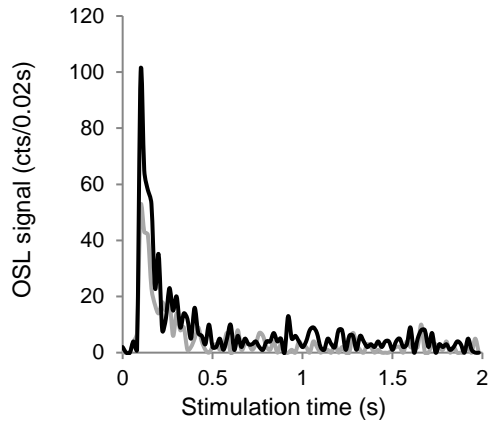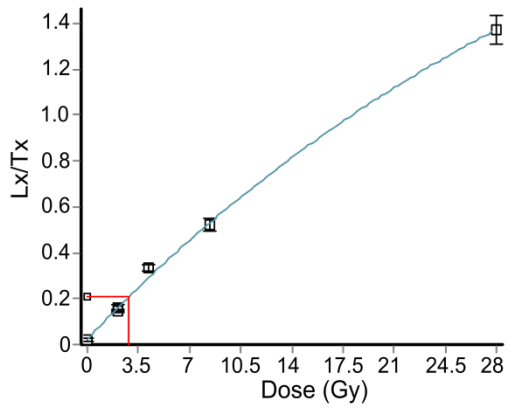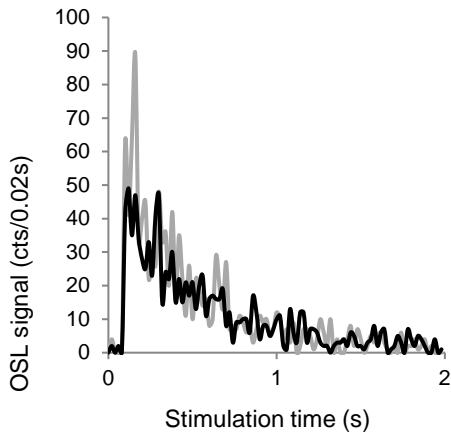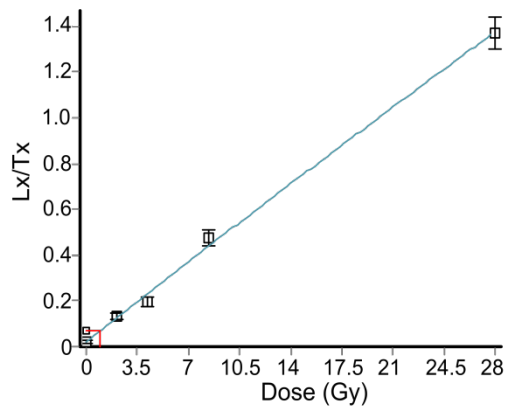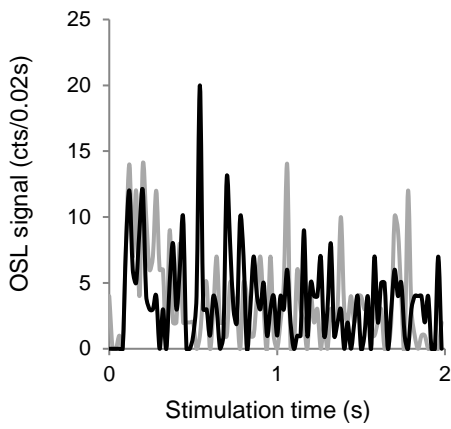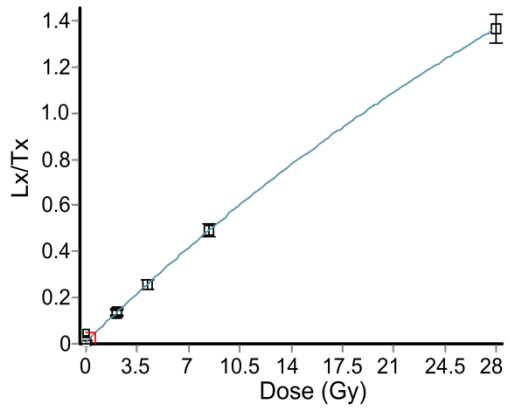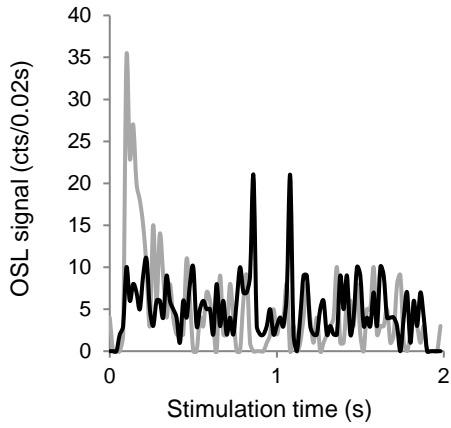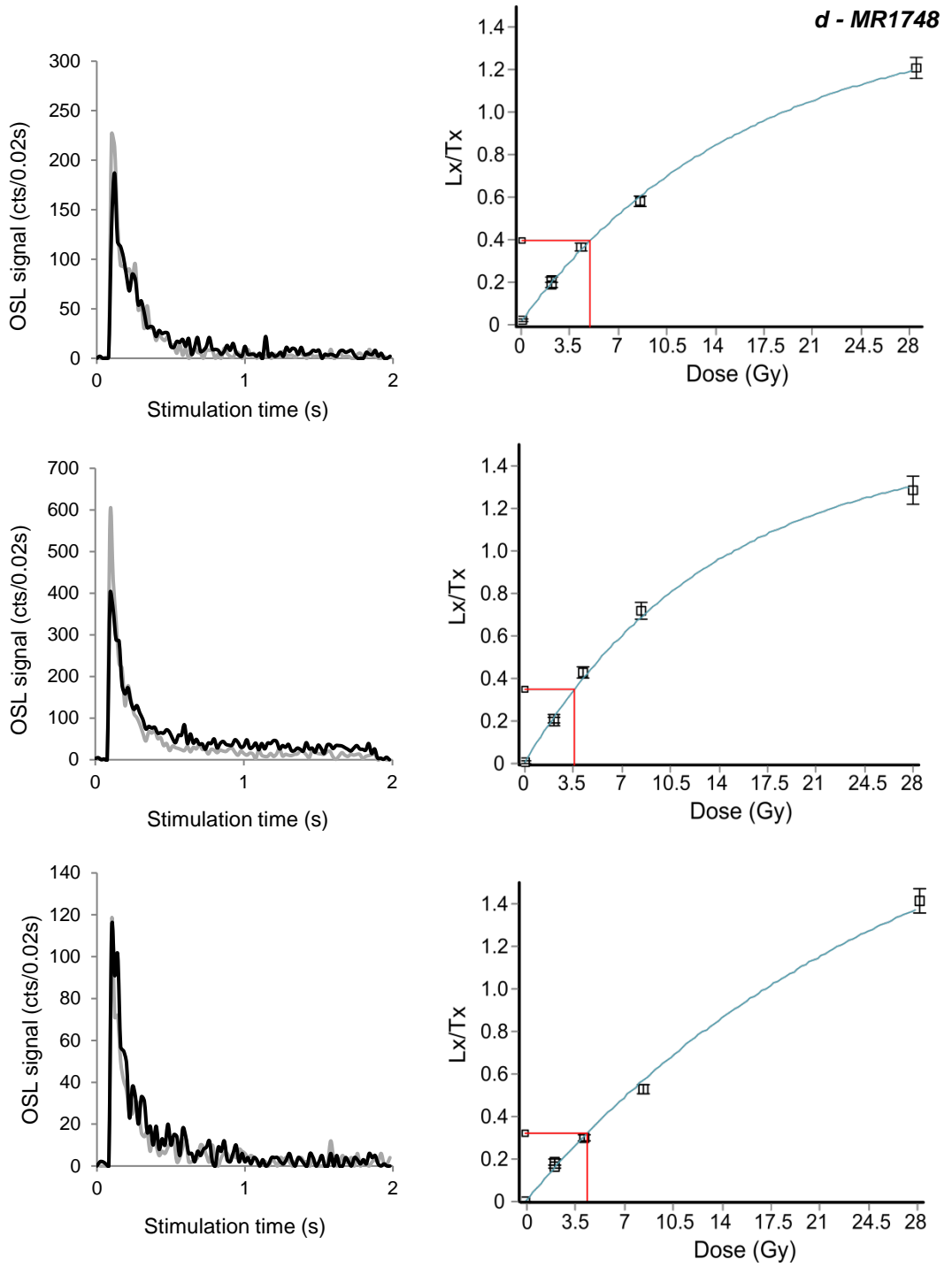
b - MR1682
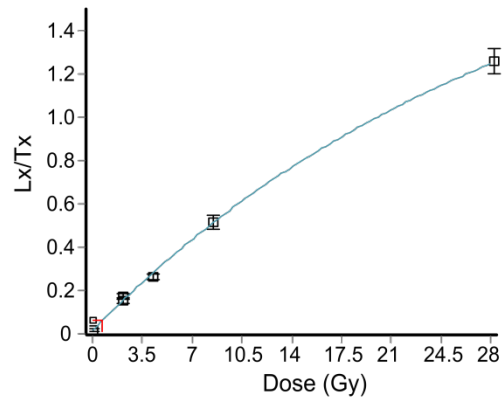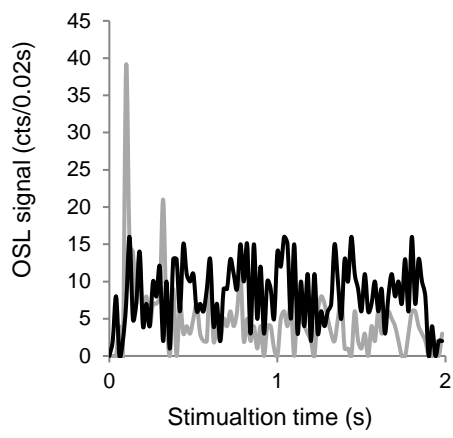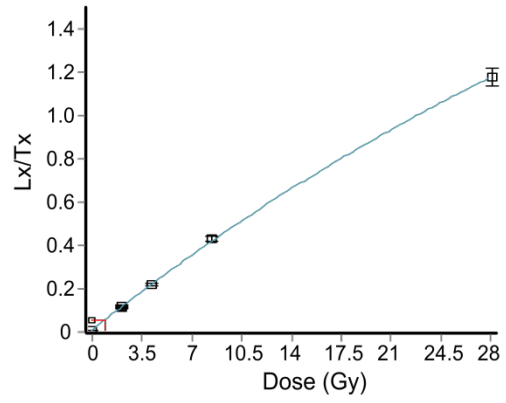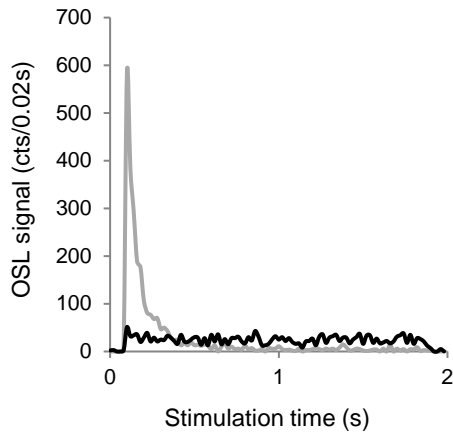
b - MR1682

c - MR1683

d - MR1748

e – MR1686
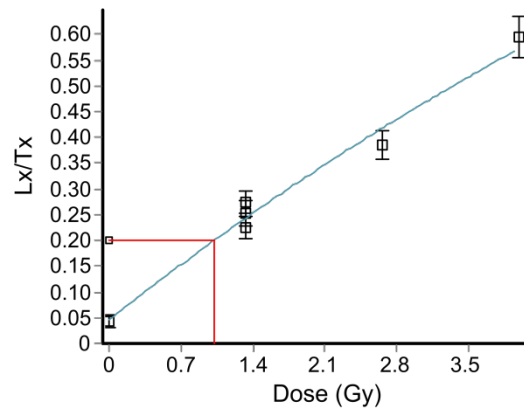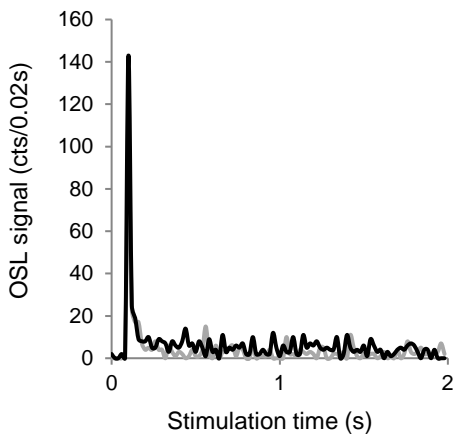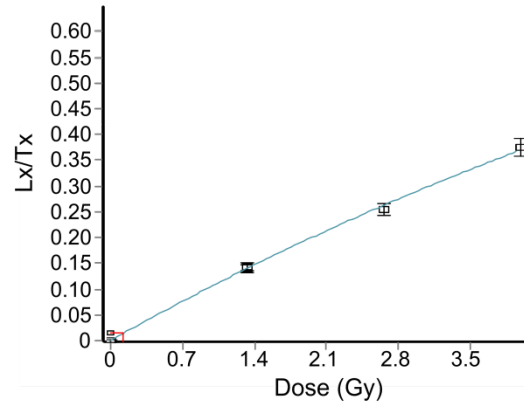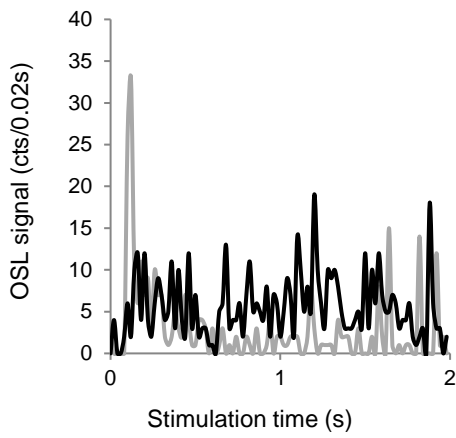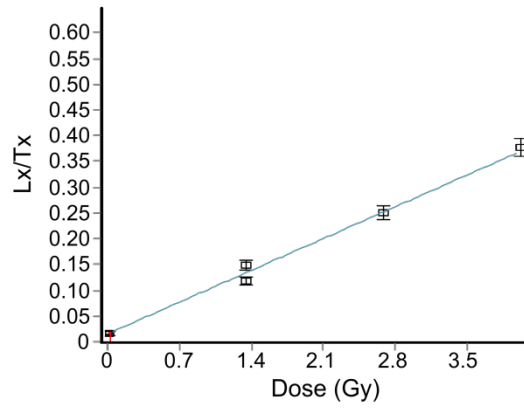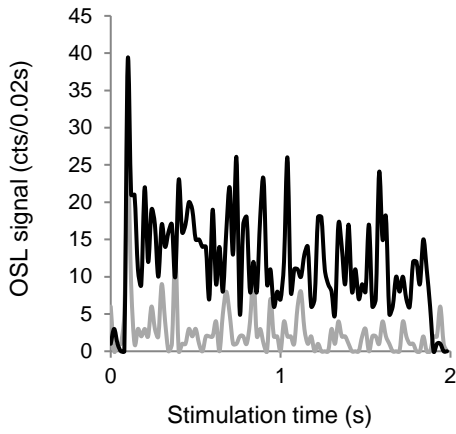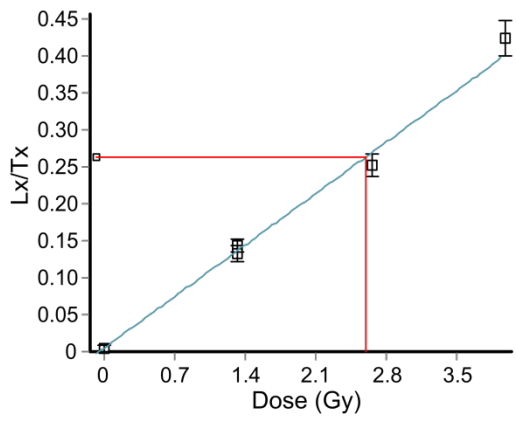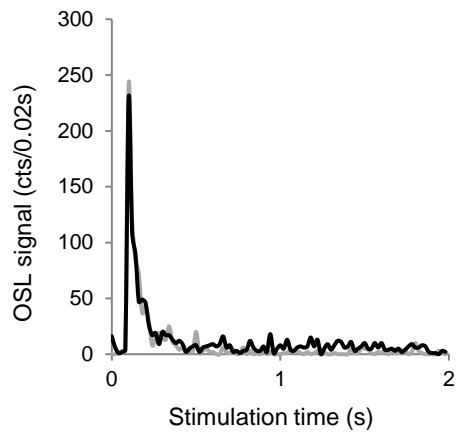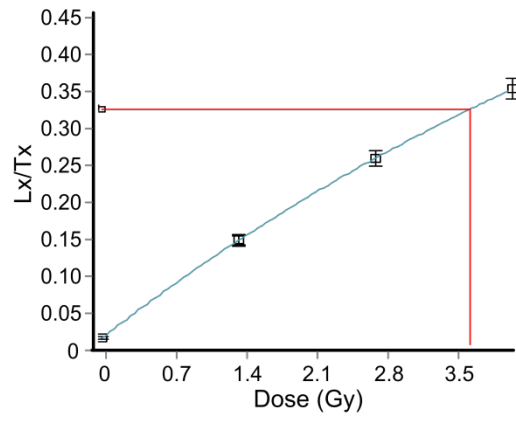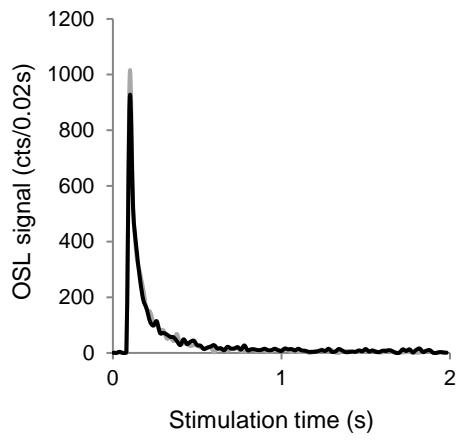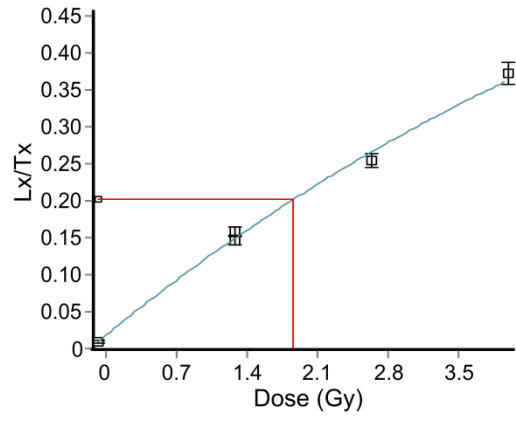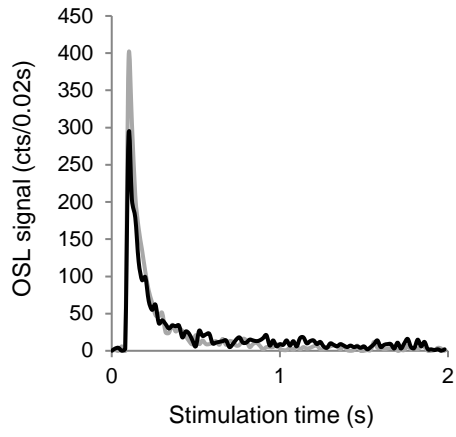
g – MR1751
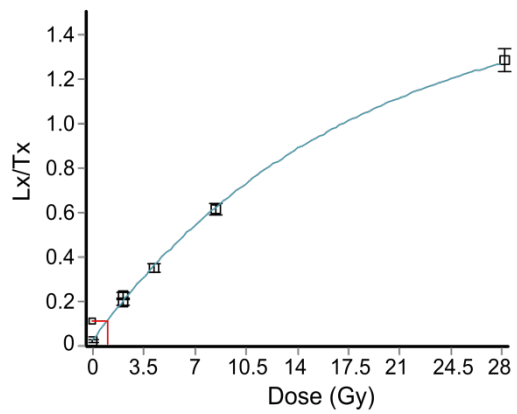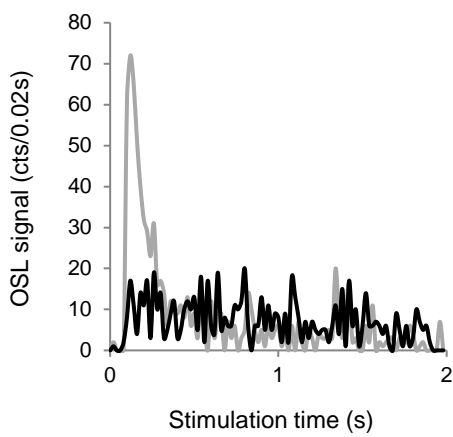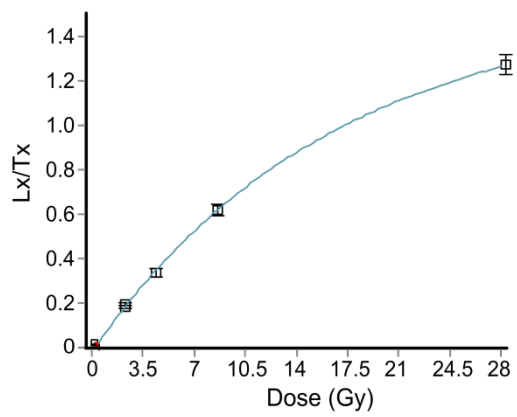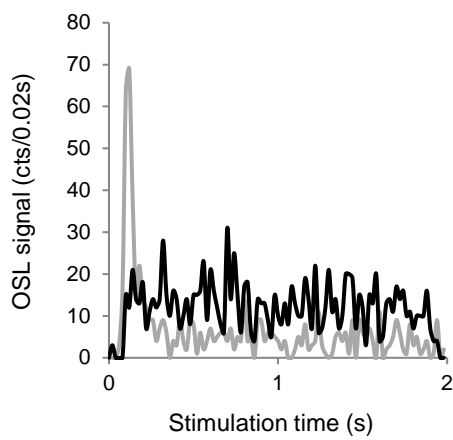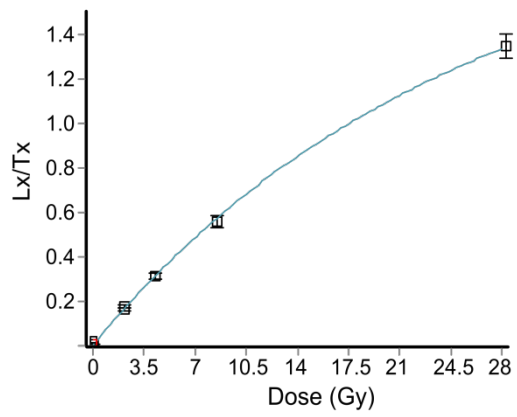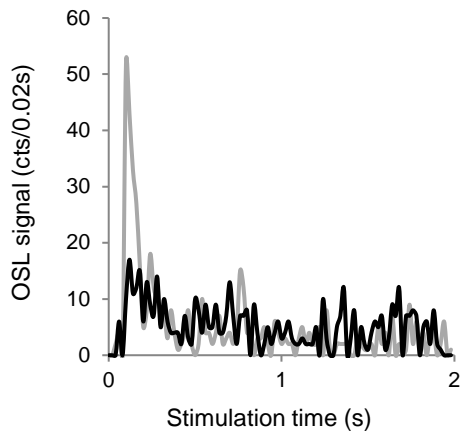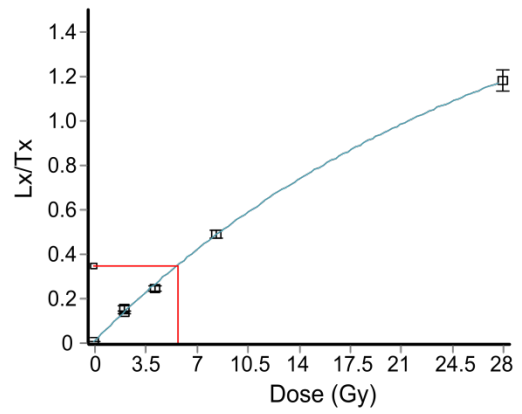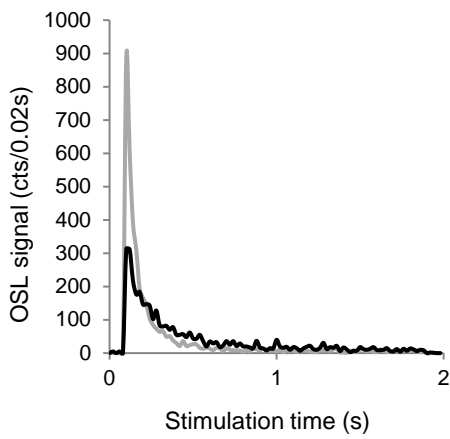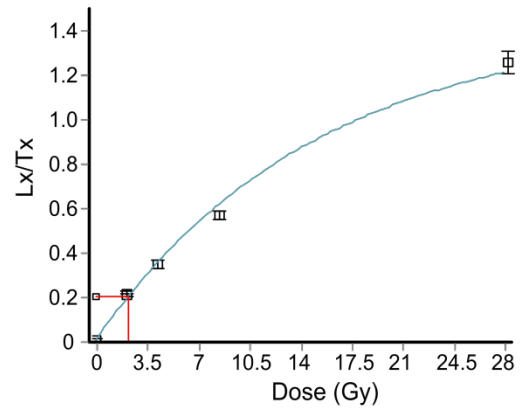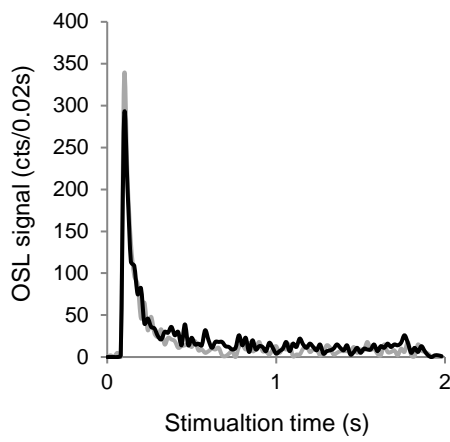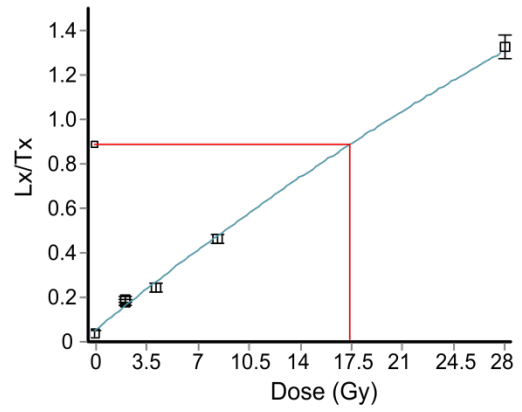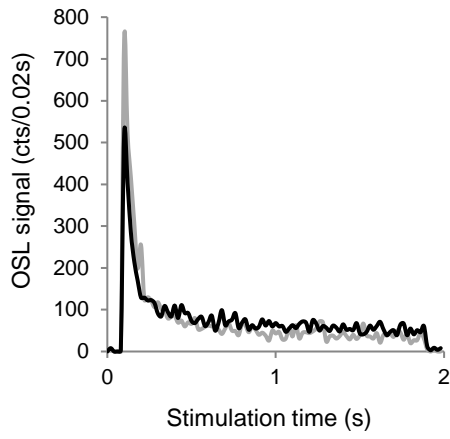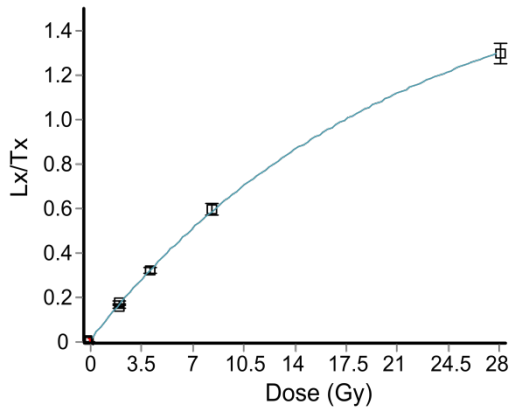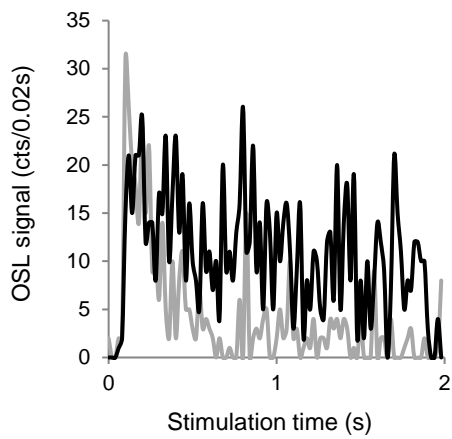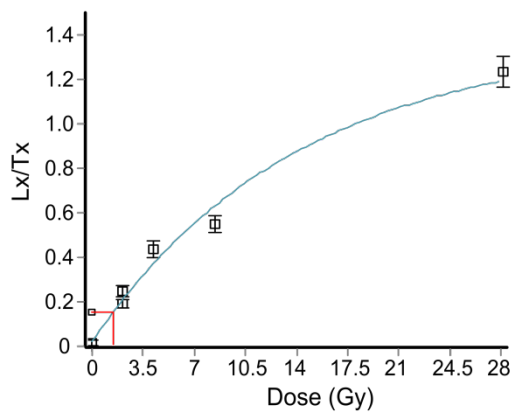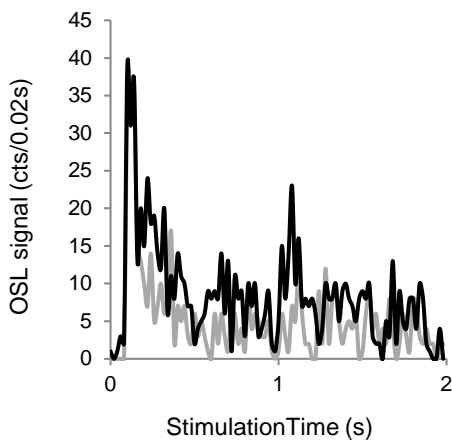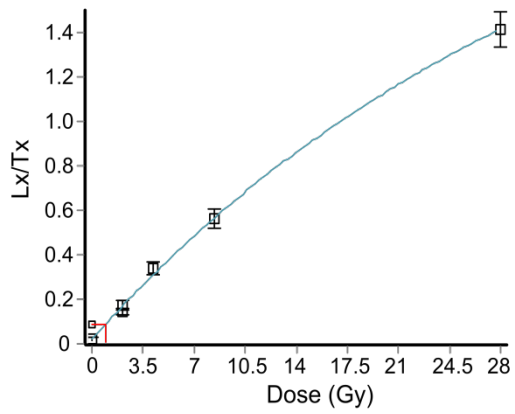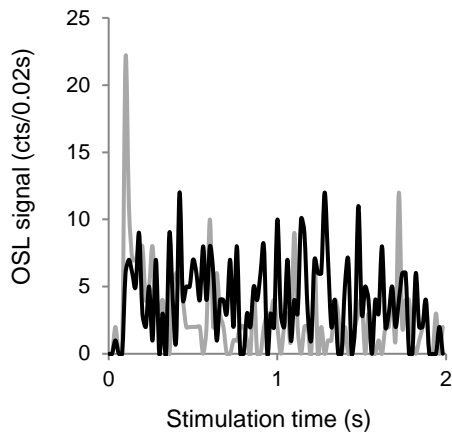
i – MR1754

j – MR1756
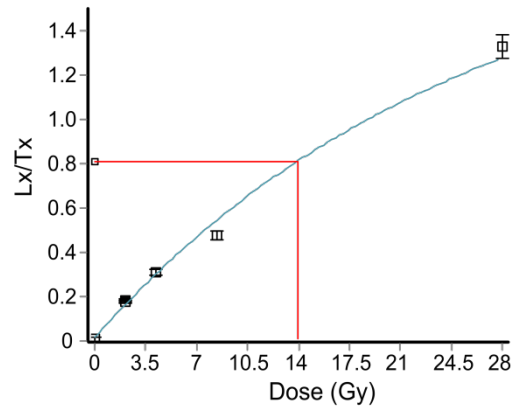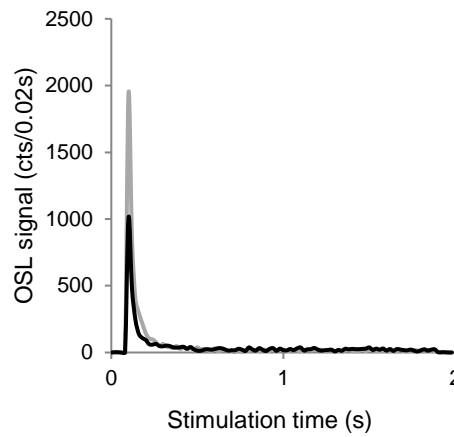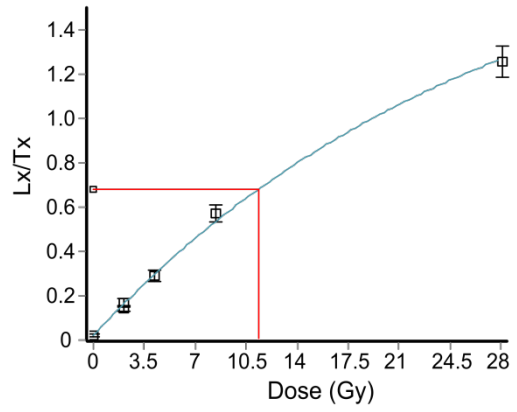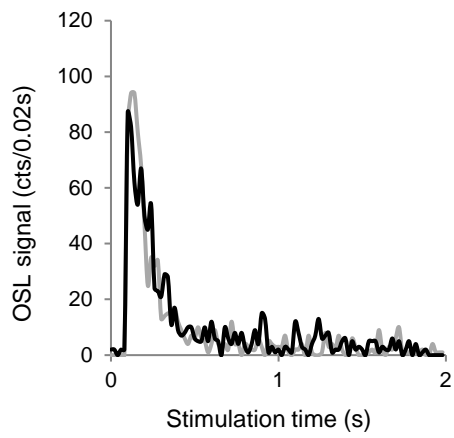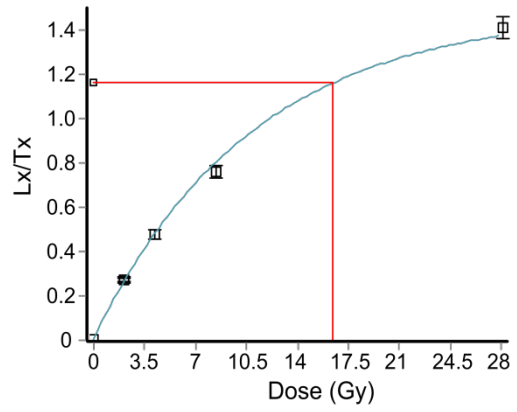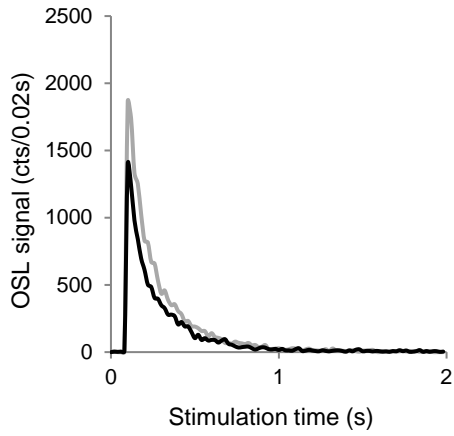
k – MR1757
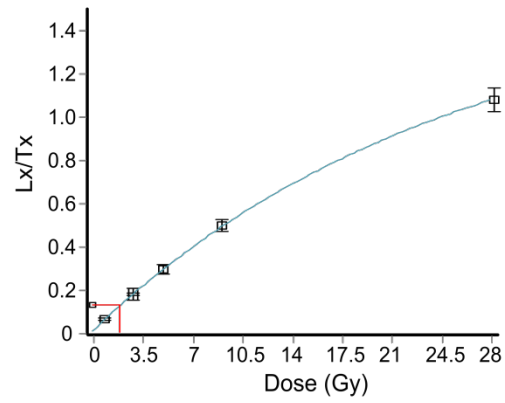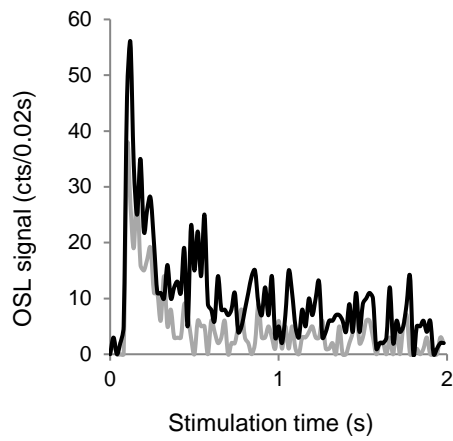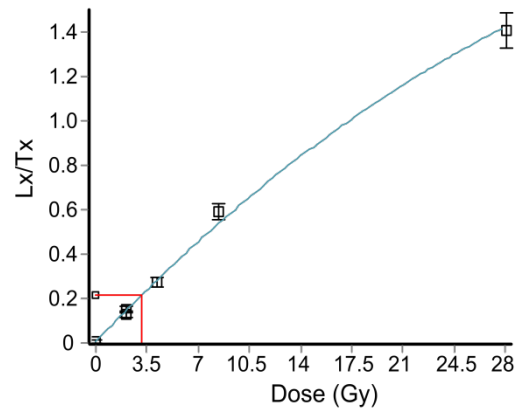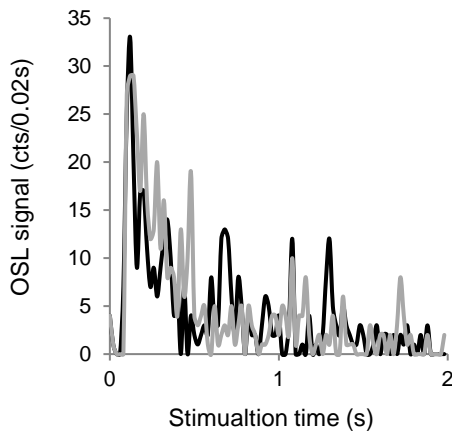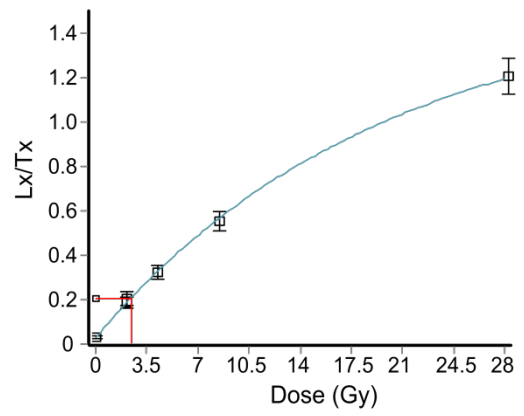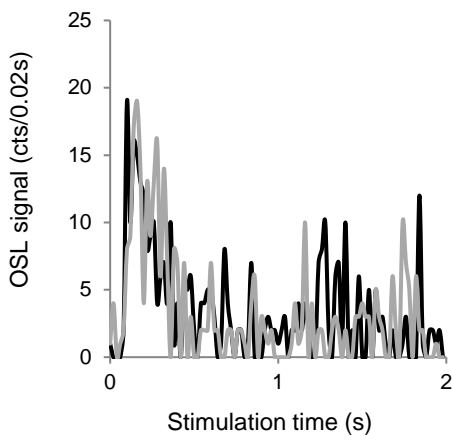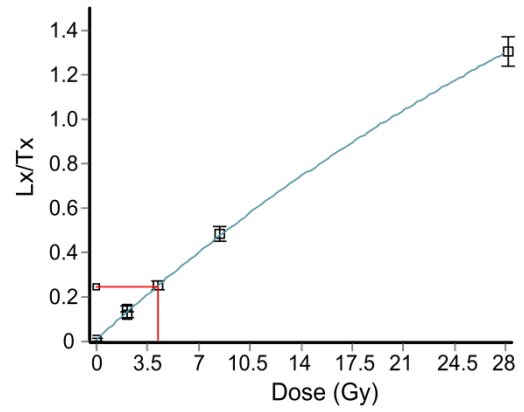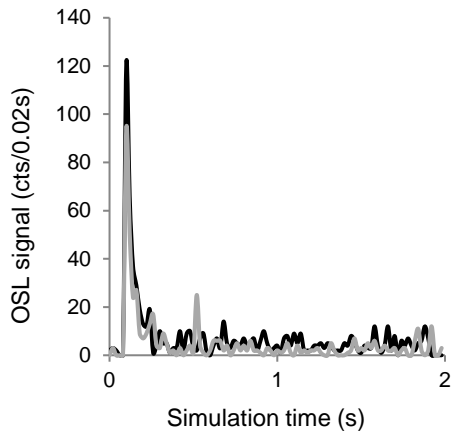
M – MR1741
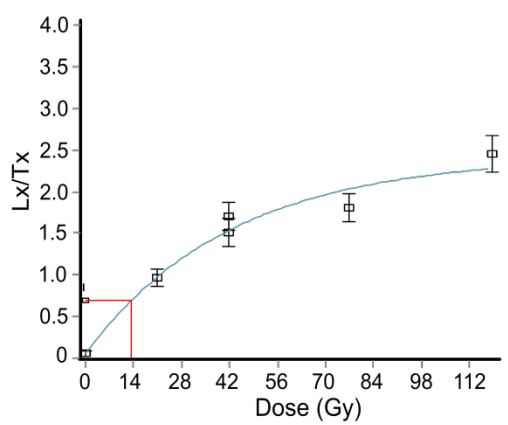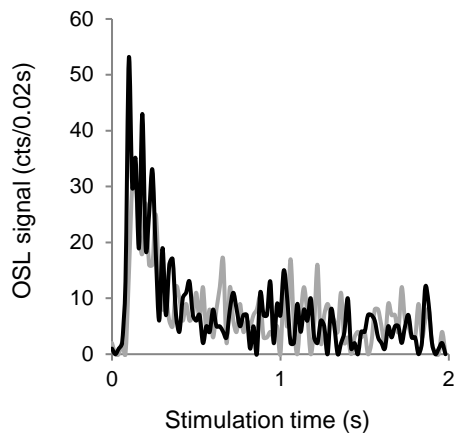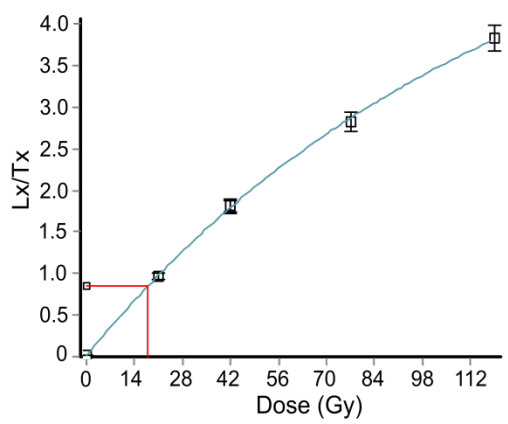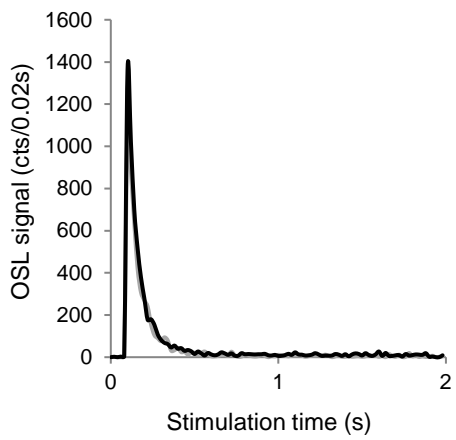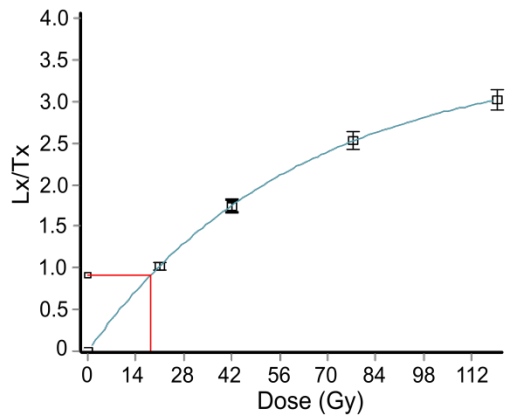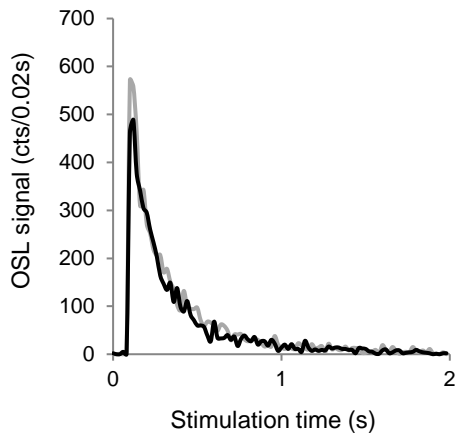
n – MR1744
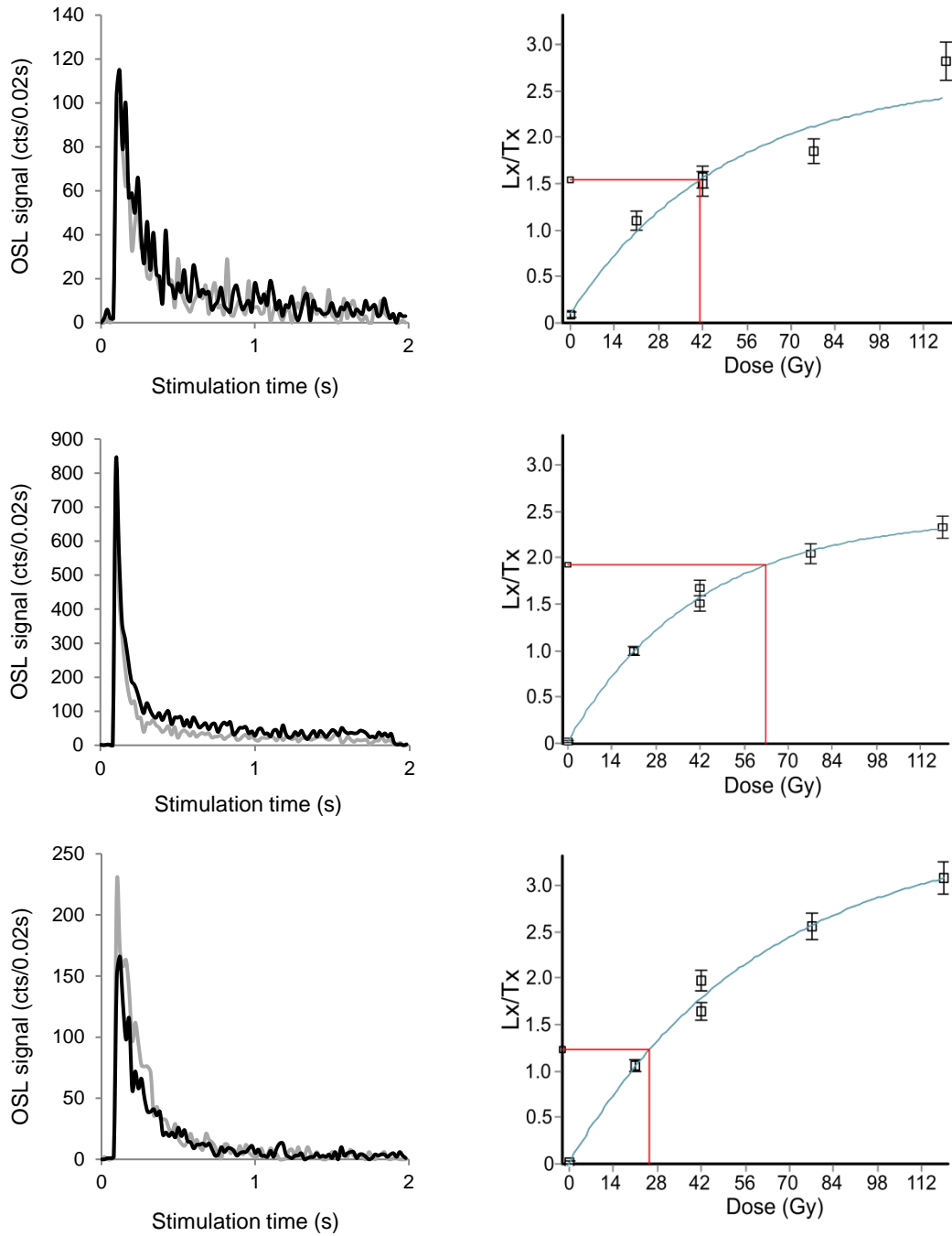
Figure D.5 – OSL decay curves and dose response curves from three grains chosen from accepted grains of all samples. Decay curve plots show decay of natural signal (grey) and decay of the test dose on the natural signal (black).

D.6 Distribution of grains

All the samples have more spread than would be expected, assuming a normal distribution (Table D.8), i.e. they are overdispersed. The overdispersion values, obtained from the central age model (Galbraith et al. 1999), for the Marshall River samples vary from 51.59 ± 3.43 to $313.62 \pm 83.43\%$. These high overdispersion values are considered an indicator of a sample which has been heterogeneously bleached or dosed, or contains multiple dose populations (either discrete or continuous). While it is likely that there are a number of origins of the D_e values within the samples, the most likely causes of a highly overdispersed distribution in these samples are:

1) variation in the degree of bleaching of grains due transport in a highly turbid water column followed by rapid deposition and burial, resulting in a heterogeneously bleached sample (Berger 1990)

2) variable environmental dose due to beta dose heterogeneity from the presence of heavy minerals (Jankowski et al. 2015; Mayya et al. 2006)

3) downward movement of younger surface grains through bioturbation from plant roots (Bateman et al. 2007)

4) incorporation of older grains from eroded floodplain deposits.

Given the probable sources of variation within the D_e distributions, the higher D_e grains are not likely to be representative of the most recent deposition event, therefore a weighted mean, as obtained by the central age model would overestimate the burial age. It would be assumed given the likelihood of incomplete bleaching and the incorporation of older, unbleached grains, that the lowest D_e population would be consistent with the most recent solar resetting and thus, calculation of the burial age should use the minimum age model (Galbraith et al. 1999). However, each sample will be assessed as to whether the minimum age model is appropriate.

Table D.8 - Summary of accepted grains with min and maximum ED, the central age model estimate (Galbraith, 1999) of each sample and the overdispersion

Sample	grains	grains = 0 at 2σ		Min	Max	CAM	OD	Skew
	#	#	%	Gy	Gy	Gy	%	
MR-SS1	147	116	79	-3.93 ± 2.22	12.67 ± 0.27	0.41 ± 0.13	382.10 ± 126.30	66.92 ± 0.20
MR1676	131	49	37	-2.31 ± 0.84	5.54 ± 0.94	0.80 ± 0.08	112.09 ± 14.02	4.60 ± 0.21
MR1682	137	68	50	-3.53 ± 1.46	6.58 ± 0.93	0.44 ± 0.07	175.00 ± 30.82	4.53 ± 0.21
MR1683	221	114	52	-7.76±3.43	25.28±7.14	0.76 ± 0.11	200.65 ± 30.38	11.94 ± 0.16
MR1686	151	73	48	-3.09 ± 2.34	4.59 ± 0.15	0.61 ± 0.07	142.23 ± 19.46	5.46 ± 0.20
MR1748	56	9	16	-3.60 ± 2.75	28.55 ± 2.02	3.33 ± 0.50	109.39 ± 19.51	6.70 ± 0.33
MR1750	75	18	24	-1.67 ± 0.88	6.95 ± 0.37	2.68 ± 0.22	68.12 ± 8.43	1.03 ± 0.28
MR1751	157	106	68	-4.09 ± 1.69	23.66 ± 0.87	0.64 ± 0.17	313.62 ± 83.43	73.07 ± 0.20
MR1753	62	31	50	-2.77 ± 1.99	15.56 ± 0.93	1.47 ± 0.33	171.21 ± 42.31	1.89 ± 0.31
MR1754	133	73	55	-2.84 ± 1.26	16.07 ± 1.61	0.63 ± 0.11	196.88 ± 37.94	11.50 ± 0.21
MR1756	202	19	9	-3.34 ± 2.46	29.71 ± 26.31	9.83 ± 0.38	51.59 ± 3.43	1.14 ± 0.17
MR1757	121	67	55	-4.38 ± 2.47	4.67 ± 0.43	0.48 ± 0.07	136.96 ± 22.12	4.18 ± 0.22
MR1759	101	9	9	-4.55 ± 1.63	14.97 ± 1.47	2.03 ± 0.22	102.47 ± 13.45	9.77 ± 0.24
MR1741	66	10	15	0.13 ± 0.27	118.24 ± 38.66	19.76 ± 2.02	77.64 ± 10.98	2.10 ±0.30
MR1744	61	13	21	-1.09 ± 2.29	118.06 ± 12.92	40.80 ± 3.66	62.46 ± 8.82	1.09 ± 0.31

D.7 D_e determination

Of the grains that were measured, between 7.5 and 22.5% (Table D.4) passed all rejection criteria and were used for each age calculation. The sample D_e for each sample was determined using either the unlogged 3-parameter minimum age model (Arnold et al. 2009) and the unlogged central age model (Galbraith et al. 1999). For all samples unlogged age models were used as all samples had at least one grain whose D_e, while greater than zero, still intersected with zero at 3-sigma, making log values unavailable.

Age models for final D_e calculation were chosen by assessing the distribution through radial plots and histograms. The radial plots use an linear D_e scale (rather than the more usual logarithmic scale) due to the prevalence of low D_e grains and use absolute standard errors on the x-axis (rather than the more usual relative standard errors on the x-axis) as the relative standard errors are often large due to being "relative to something small" (Galbraith and Roberts 2012).

When using the unlogged minimum age model the value of overdispersion input into the model was calculated as 10, 15 and 20% of the D_e estimate obtained using the unlogged central age model (Lee Arnold 2017, pers. comm., 29 August 2017). The unlogged minimum age model was applied as a number of the samples showed a large population of low D_e grains within the distributions. This can be seen in Figure D.7 as a dominant lower edge on the distribution.

The model was tested with user defined overdispersion values of 10, 15 and 20% and it was found that 20% gave the most samples where it was possible to calculate the D_e and also gave the highest *p* values. The *p* value is the proportion of grains which are included in the MAM-3 D_e, the maximum possible being 1.00. *P*-values range from 0.39 to 0.77 indicating low dose populations which incorporate between 39 and 77% of the grains.

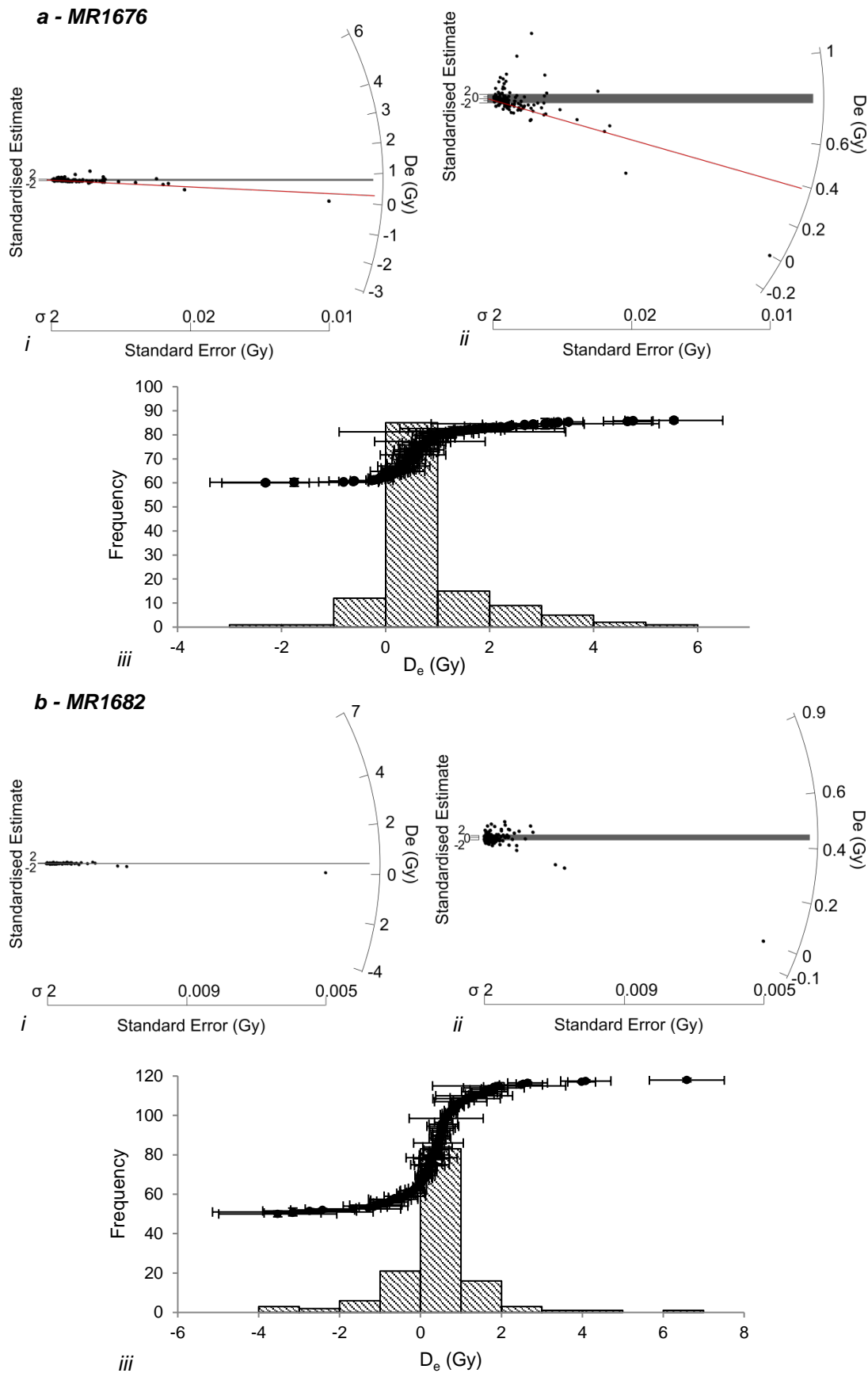While all samples showed some younger grains, and a high overdispersion also indicative of heterogeneous bleaching, the minimum age model was not appropriate for all samples. In the case of MR1682, MR1750, MR1756, MR1759, and MR1744 the minimum model could not calculate a D_e estimate indicating that insufficient low dose grains were present to be interpreted as the dominant population. MR1682,

MR1750, MR1759, and MR1744 contain only a small number of low dose grains compared to the rest of the population (Figure D.6-b, f, l, n). MR1756 appears, from its radial plots to contain a large number of low dose grains (Figure D.6 – j), however the model calculated a minimum age with a p-value of 0.1 indicating the minimum age only incorporated 10% of the grains, which was not deemed sufficient for an accurate minimum age.

Those samples with ages calculated using MAM-3 (unlogged) are, with the exception of MR1748 and MR1753, from the upper part of the cores so are those mostly likely to have been affected by bioturbation and the infiltration of younger grains. None of the samples with ages calculated using CAM (unlogged) are from the upper part of the core.

Table D.9 - Estimates of D_e and burial age for all samples using the 3 parameter minimum age model where possible and the central age model (Galbraith et al.1999) With overdispersion from the CAM (Galbraith et al. 1999) and skew from (Bailey and Arnold 2006).

OSL code	MAM - 3	CAM	OD	Skew	*p*	n
	Gy	Gy	%			
MR-SS-1	-	0.41 ± 0.13	382.10 ± 126.30	66.92 ± 0.20	0.68	147
MR1676	0.39 ± 0.04	0.80 ± 0.08	112.09 ± 14.02	4.60 ± 0.21		131
MR1682	-	0.44 ± 0.07	175.00 ± 30.82	4.53 ± 0.21	0.73	137
MR1683	0.23 ± 0.03	0.76 ± 0.11	200.65 ± 30.38	11.94 ± 0.16	0.7	221
MR1748	2.34 ± 0.16	3.33 ± 0.50	109.39 ± 19.51	6.70 ± 0.33	0.39	56
MR1686	0.32 ± 0.04	0.61 ± 0.07	142.23 ± 19.46	5.46 ± 0.20		151
MR1750	-	2.68 ± 0.22	68.12 ± 8.43	1.03 ± 0.28	0.77	75
MR1751	0.11 ± 0.02	0.64 ± 0.17	313.62 ± 83.43	73.07 ± 0.20	0.74	157
MR1753	0.38 ± 0.07	1.47 ± 0.33	171.21 ± 42.31	1.89 ± 0.31	0.72	62
MR1754	0.16 ± 0.03	0.63 ± 0.11	196.88 ± 37.94	11.50 ± 0.21		133
MR1756	-	9.83 ± 0.38	51.59 ± 3.43	1.14 ± 0.17	0.53	202
MR1757	0.09 ± 0.03	0.48 ± 0.07	136.96 ± 22.12	4.18 ± 0.22		121
MR1759	-	2.03 ± 0.22	102.47 ± 13.45	9.77 ± 0.24	0.55	101
MR1741	10.25 ± 2.48	19.76 ± 2.02	77.64 ± 10.98	2.10 ±0.30		66
MR1744	-	40.80 ± 3.66	62.46 ± 8.82	1.09 ± 0.31	0.68	61

a - MR1676

b - MR1682

c – MR1693

d – MR1748

e - MR1686

i

ii

iii

f - MR1750

i

ii

iii

g - MR1751

i

ii

iii

h - MR1753

i

ii

iii

i - MR1754

j - MR1756

k - MR1757

l - MR1759
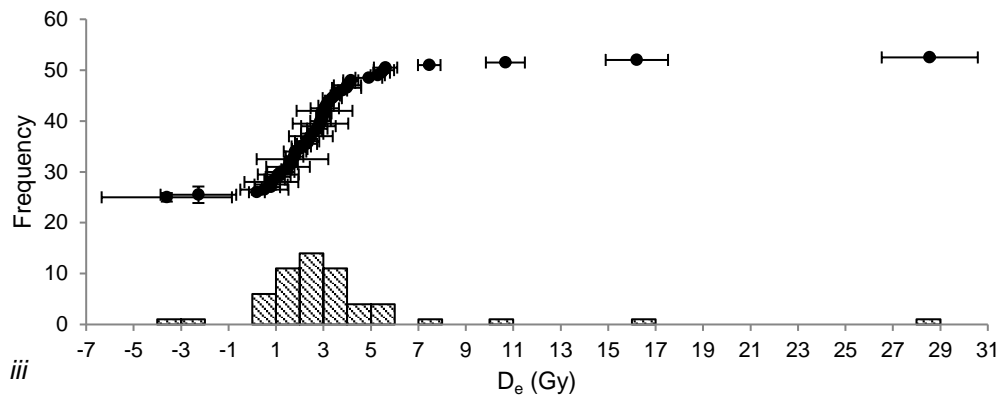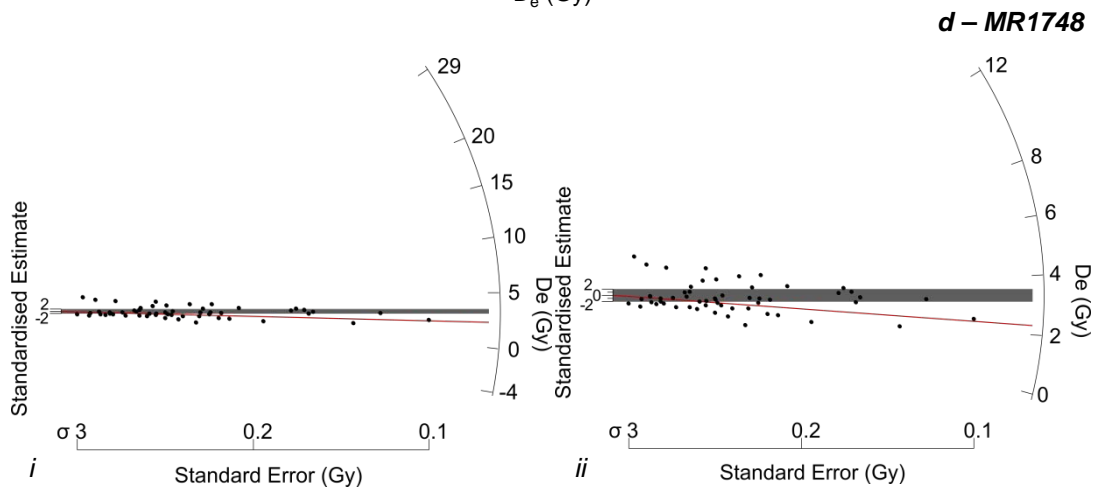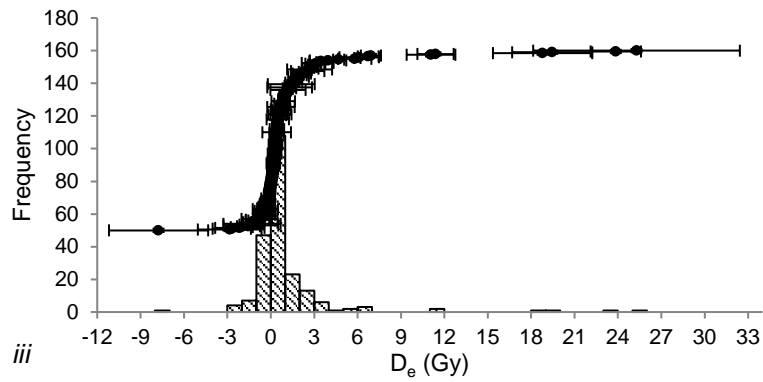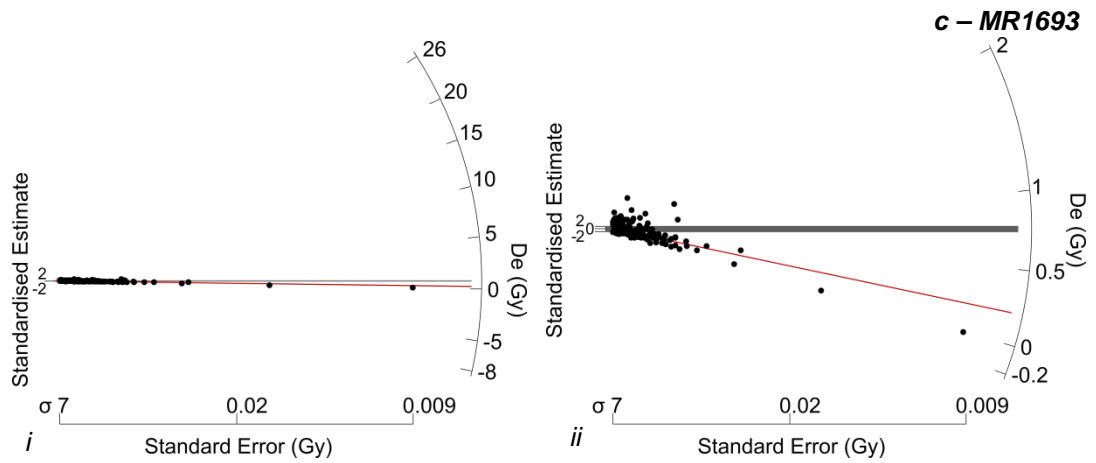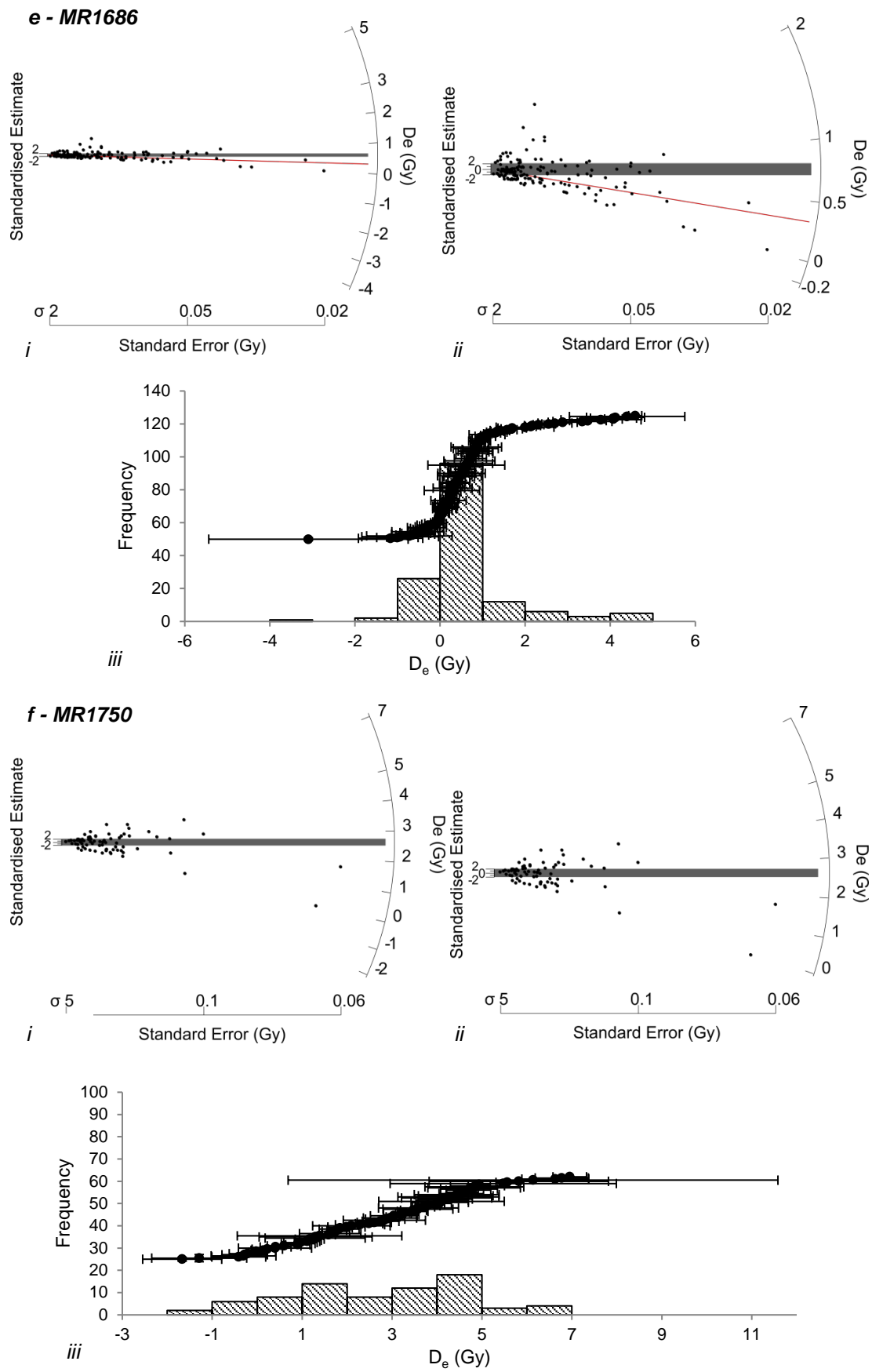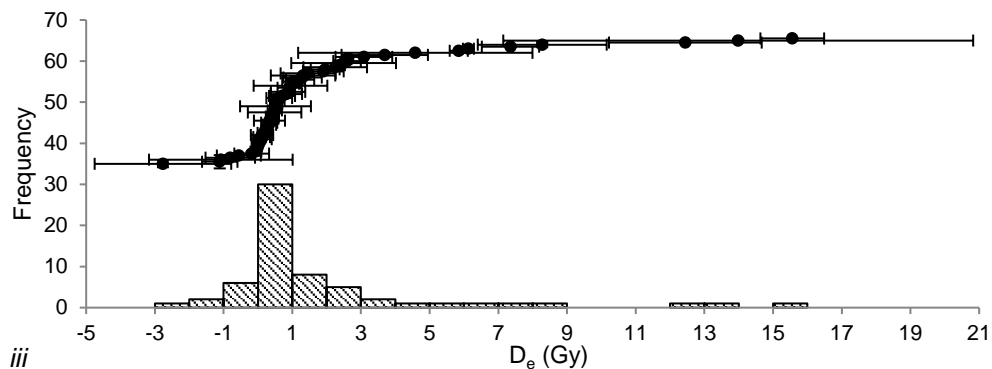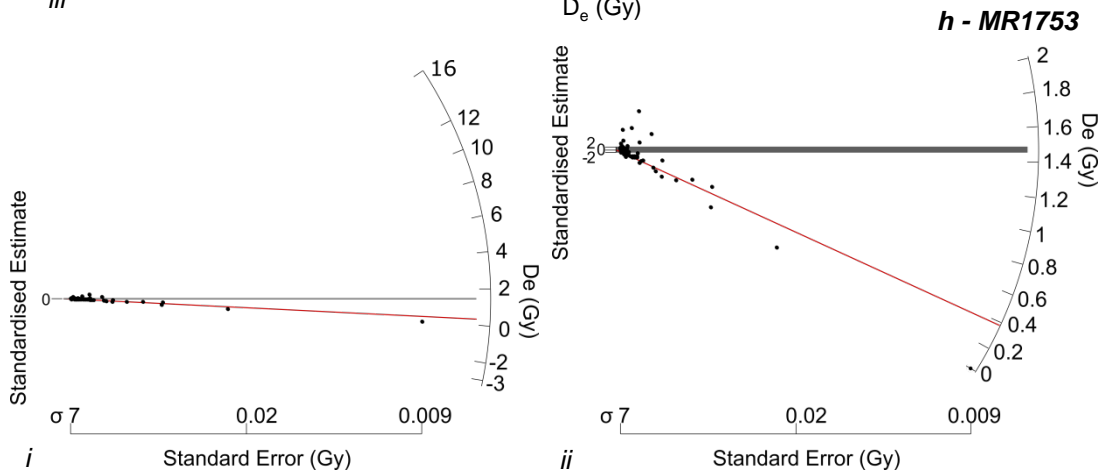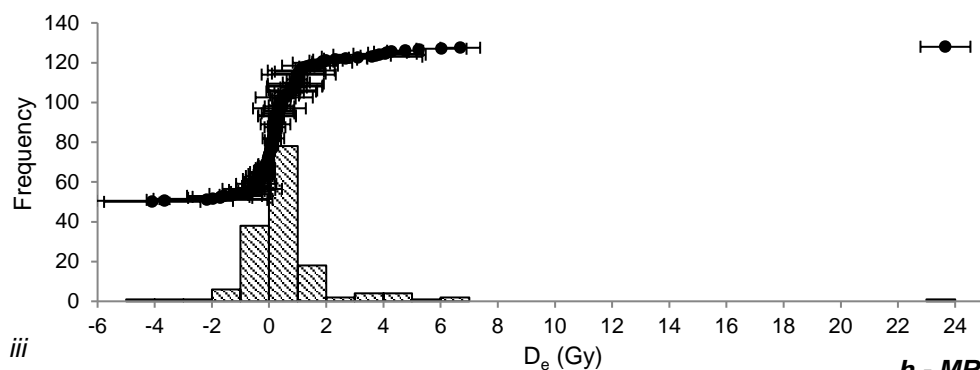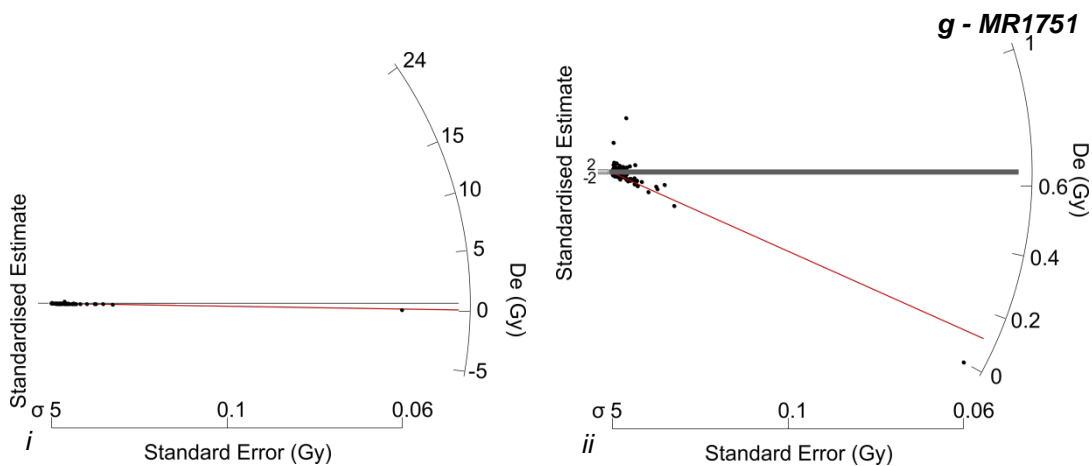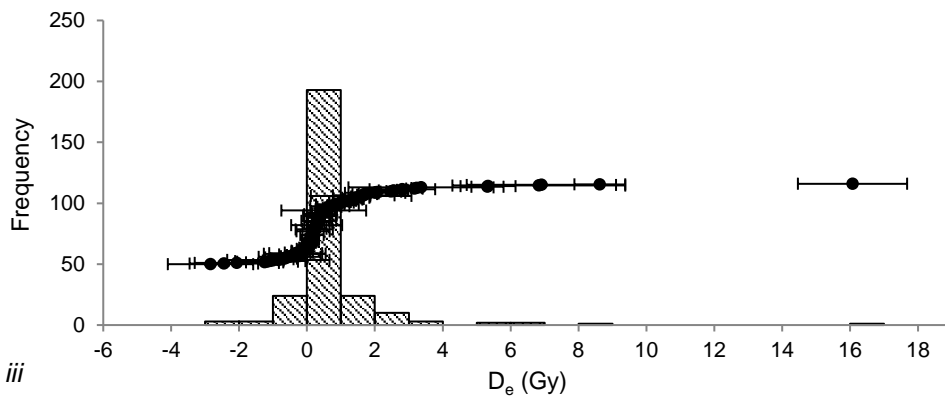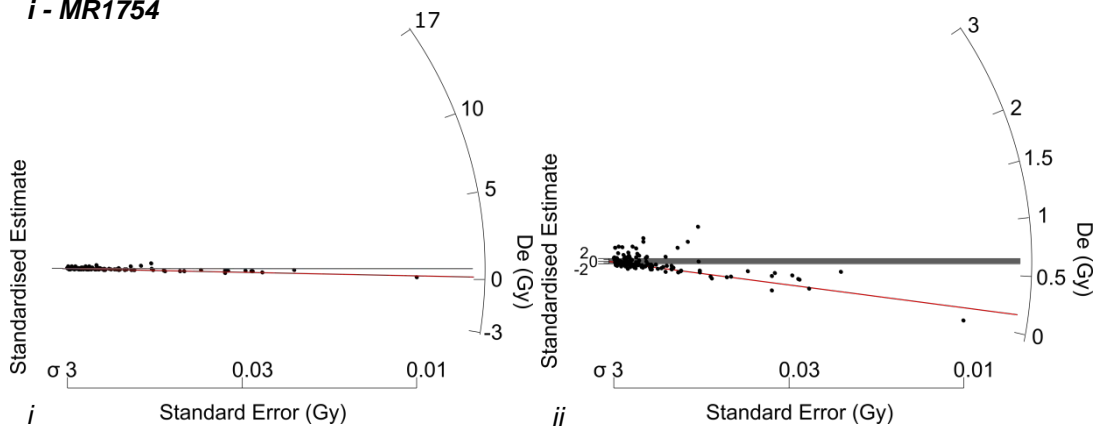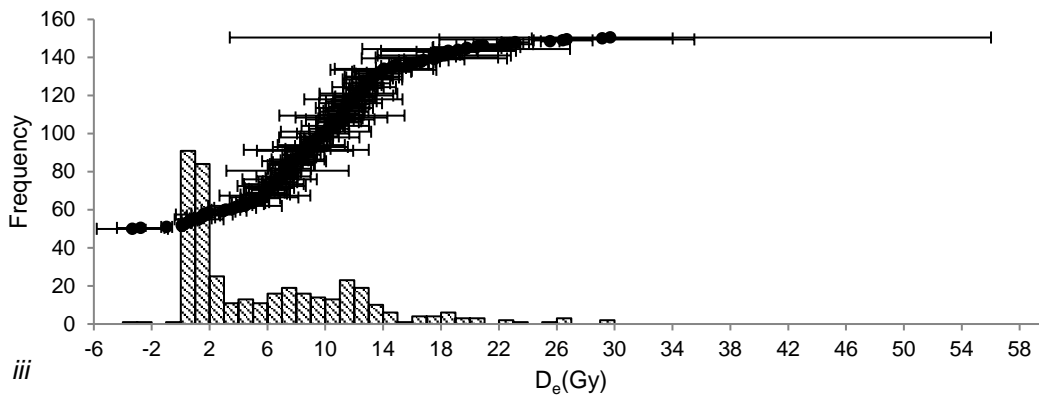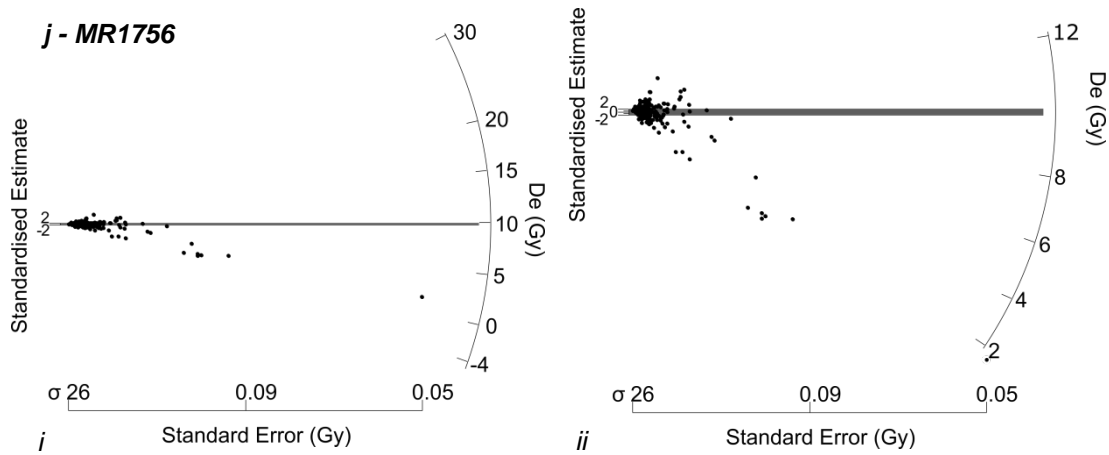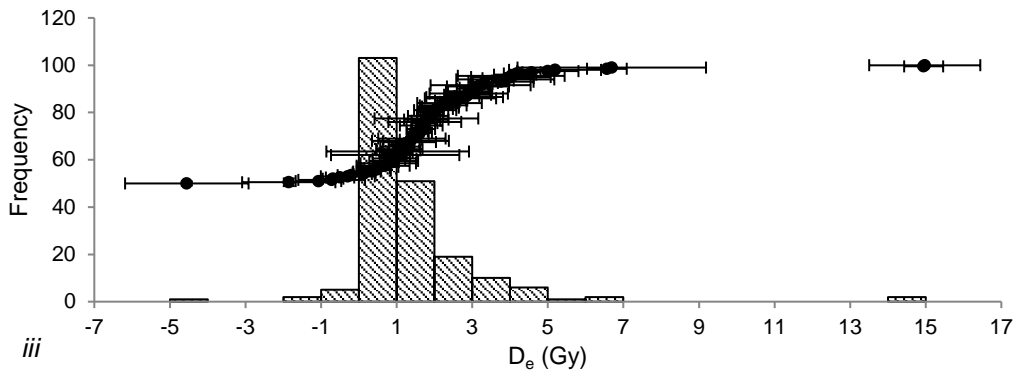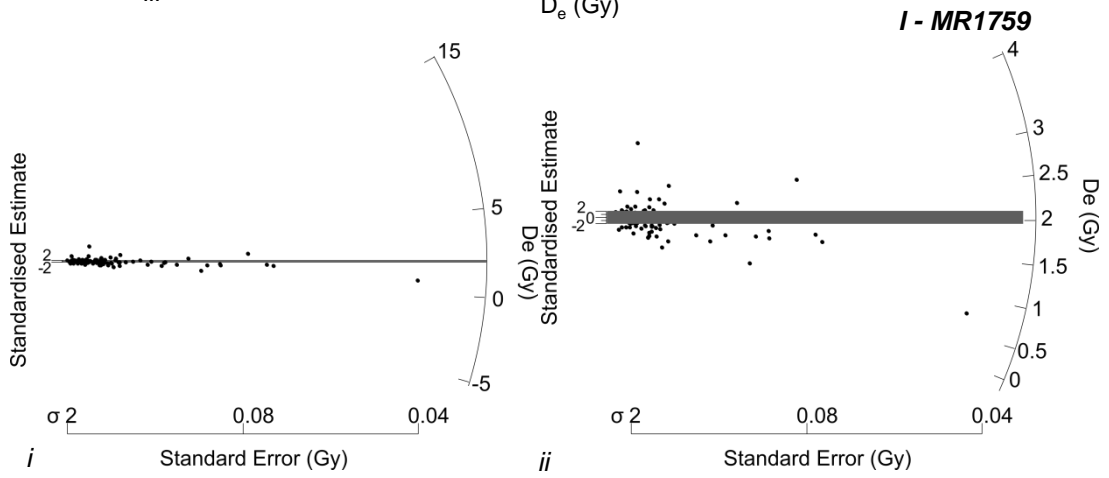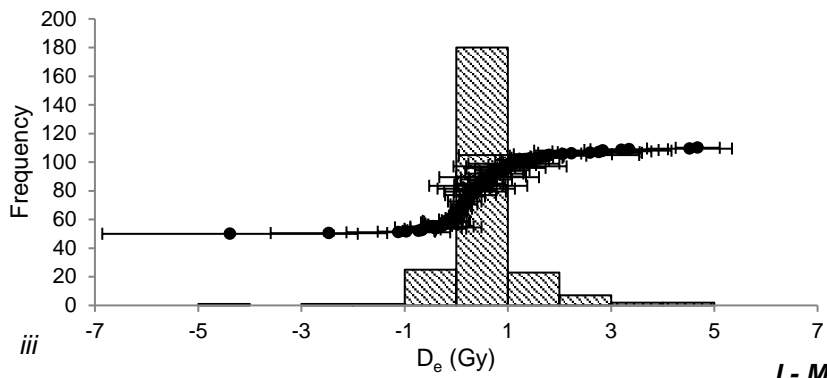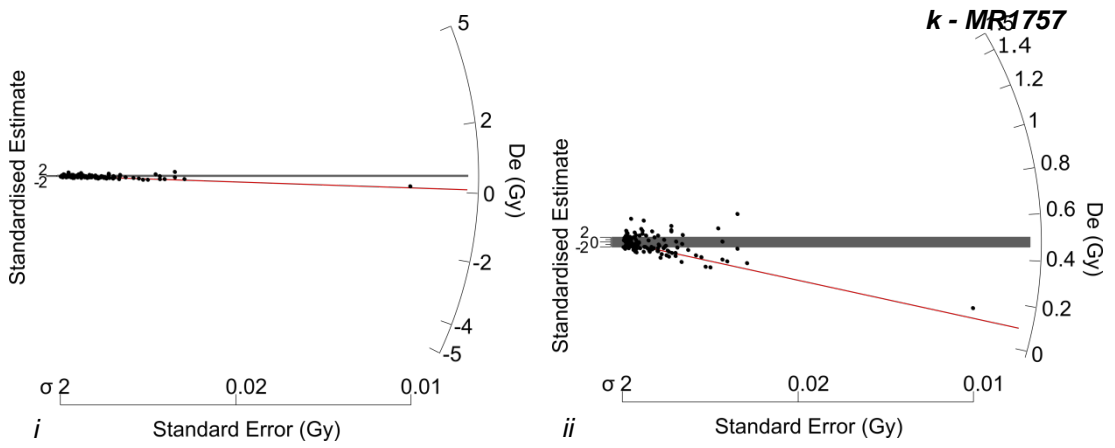
m - MR1741
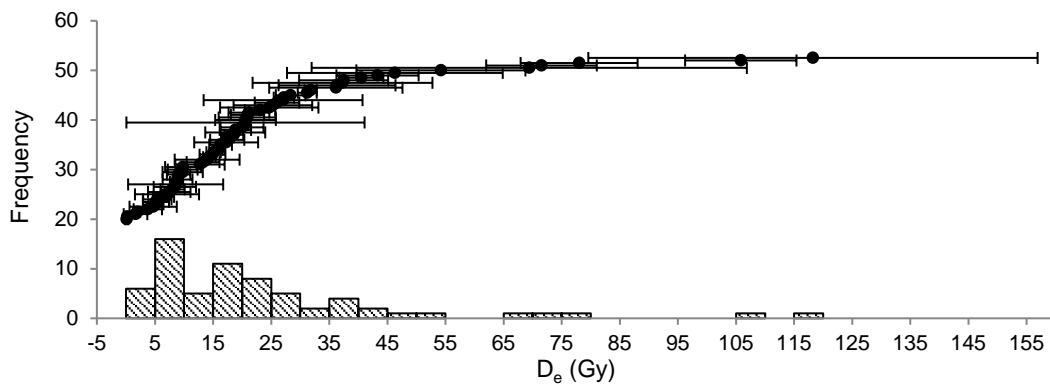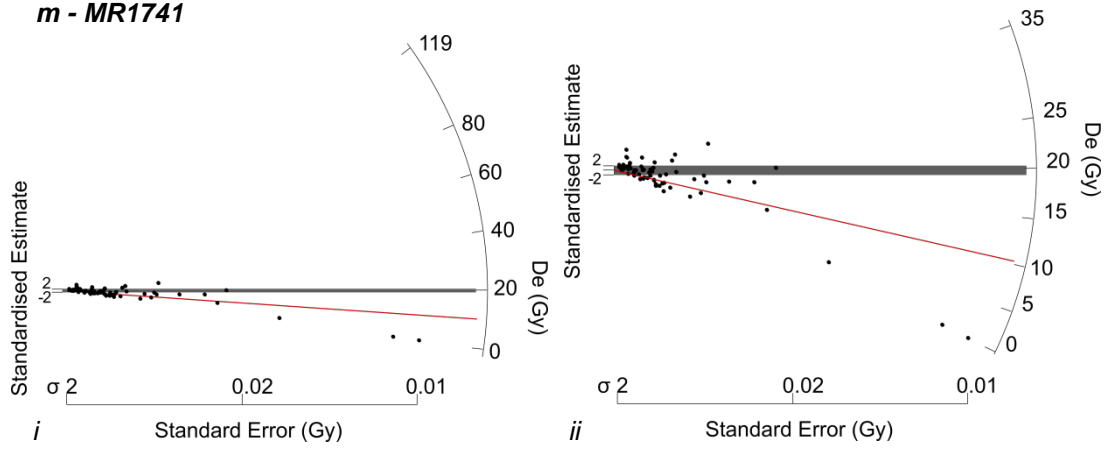
n - MR1744
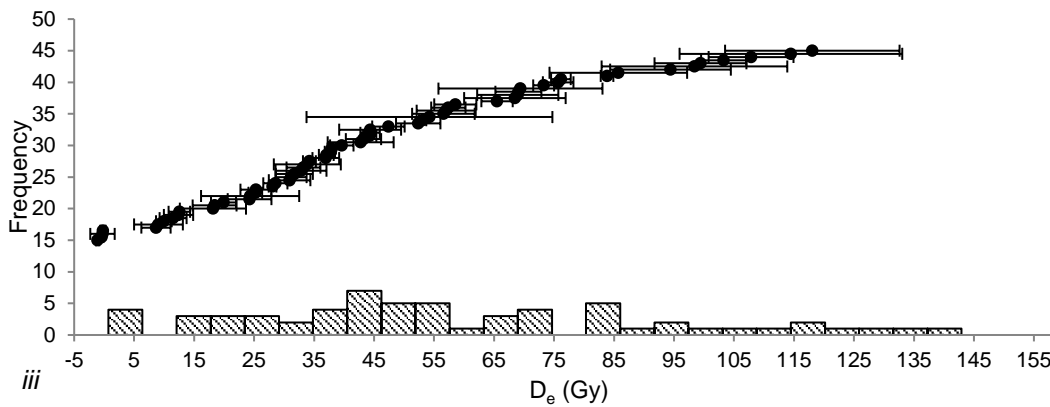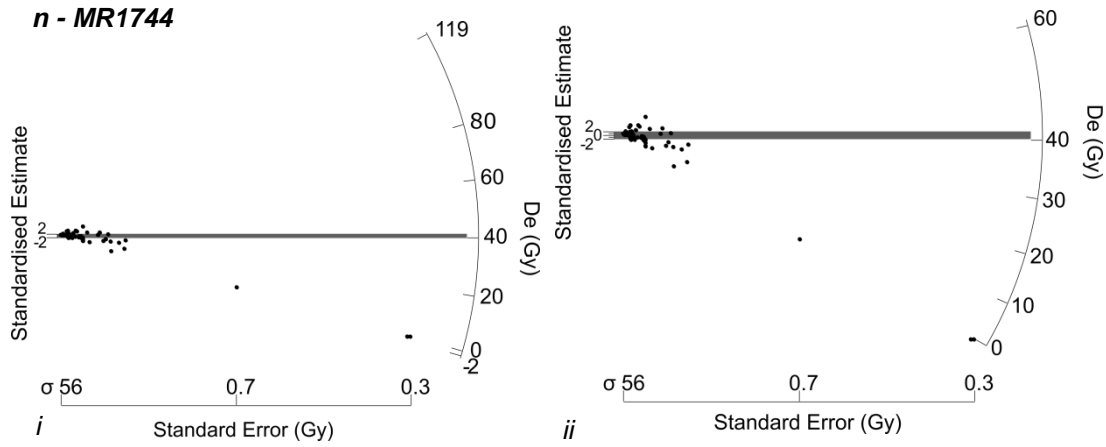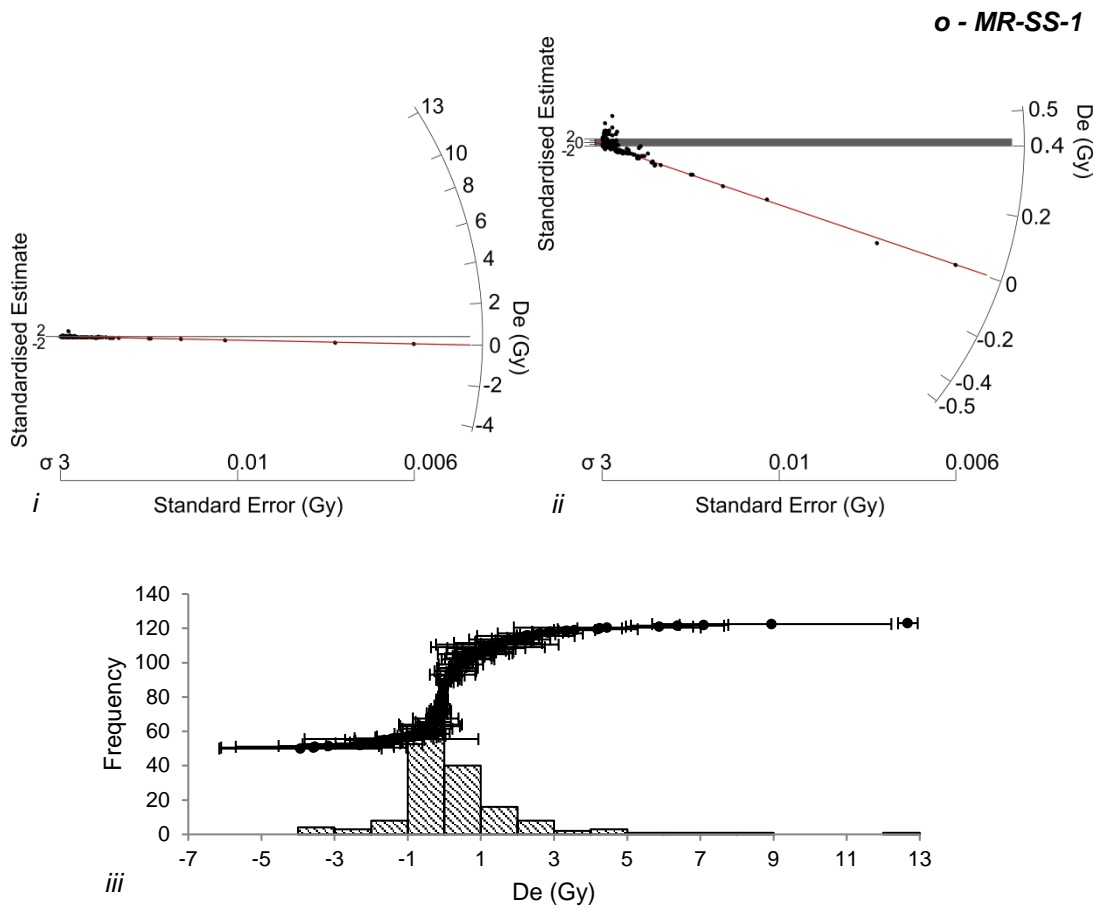
Figure D.6 - D_e distributions for each sample from the Marshall River displayed as i)radial plots with linear y-axes, and standard error on x-axes; ii)radial plots zoomed in to show z-axes; iii) Histograms with 1 Gy bin widths and ranked plot of ages. Grey shaded areas on radial plots show the central age model (Galbraith et al. 1999) estimates of burial dose with 2-sigma errors. Red line on radial plot shows unlogged 3-parameter minimum age model (Arnold et al. 2009) estimate of burial dose, where applied.

D.8   Environmental dose rate determination:

All samples were measured by Inductively coupled plasma mass spectrometry/optical emission spectrometry (ICPMS/OES), thick source alpha counting (TSAC), Geiger Müller beta counting (GMBC) and x-ray fluorescence (XRF). Five samples were also measured by high resolution gamma spectrometry (HRGS), using a well detector.

D.8.1   Beta dose rates

Table D.10 – Beta dose rates measured using: [1] ICPMS/OES for potassium, uranium and thorium; [2]TSAC for uranium and thorium, ICP-OES for potassium; [3]XRF for potassium, uranium and thorium;[4] TSAC for uranium and thorium, XRF for potassium;, [5]GMBC for uranium ,thorium and potassium.[6]HRGS for uranium thorium and potassium.

Sample	ICP-MS/-OES[1]	ICP-OES+ TSAC[2]	XRF[3]	XRF+ TSAC[4]	GMBC[5]	HRGS[6]
MR1676	1.79 ± 0.05	2.04 ± 0.07	2.06 ± 0.05	2.04±0.07	2.06 ± 0.05	
MR1682	2.23 ± 0.06	2.45 ± 0.08	2.14 ± 0.06	2.51 ± 0.08	2.42 ± 0.10	
MR1683	1.72 ± 0.05	1.94 ± 0.06	1.70 ± 0.05	1.96 ± 0.06	1.90 ± 0.07	
MR1748	2.73 ± 0.07	2.84 ± 0.09	2.78 ± 0.07	2.85 ± 0.09	3.03 ± 0.11	2.87 ± 0.08
MR1686	1.97 ± 0.05	2.11 ± 0.07	2.18 ± 0.06	2.16 ± 0.07	2.10 ± 0.11	
MR1750	2.99 ± 0.08	3.04 ± 0.09			3.32 ± 0.11	2.64 ± 0.08
MR1751	1.90 ± 0.05	2.08 ± 0.07	1.86 ± 0.05	2.11 ± 0.07	1.99 ± 0.08	
MR1753	1.80 ±0.05	1.94 ± 0.06	2.14 ± 0.07	2.00 ± 0.05	2.10 ± 0.08	
MR1754	2.22 ± 0.06	2.42 ± 0.08	2.16 ± 0.06	2.36 ± 0.08	2.41 ± 0.09	
MR1756	3.47 ± 0.09	3.13 ± 0.11	2.70 ± 0.07	3.07 ± 0.11	3.39 ± 0.14	2.97 ± 0.08
MR1757	3.40 ± 0.09	2.64 ± 0.10	3.01 ± 0.08	2.70 ± 0.10	3.35 ± 0.13	3.12 ± 0.09
MR1759	3.05 ± 0.08	3.04 ± 0.11	2.74 ± 0.07	3.16 ± 0.11	3.24 ± 0.14	3.04 ± 0.11
MR1741	2.02 ± 0.05	2.03 ± 0.09	2.06 ± 0.05	2.11 ± 0.09	2.18 ± 0.12	
MR1744	2.02 ± 0.05	2.03 ± 0.07	1.91 ± 0.05	2.05 ± 0.07	2.04 ± 0.08	
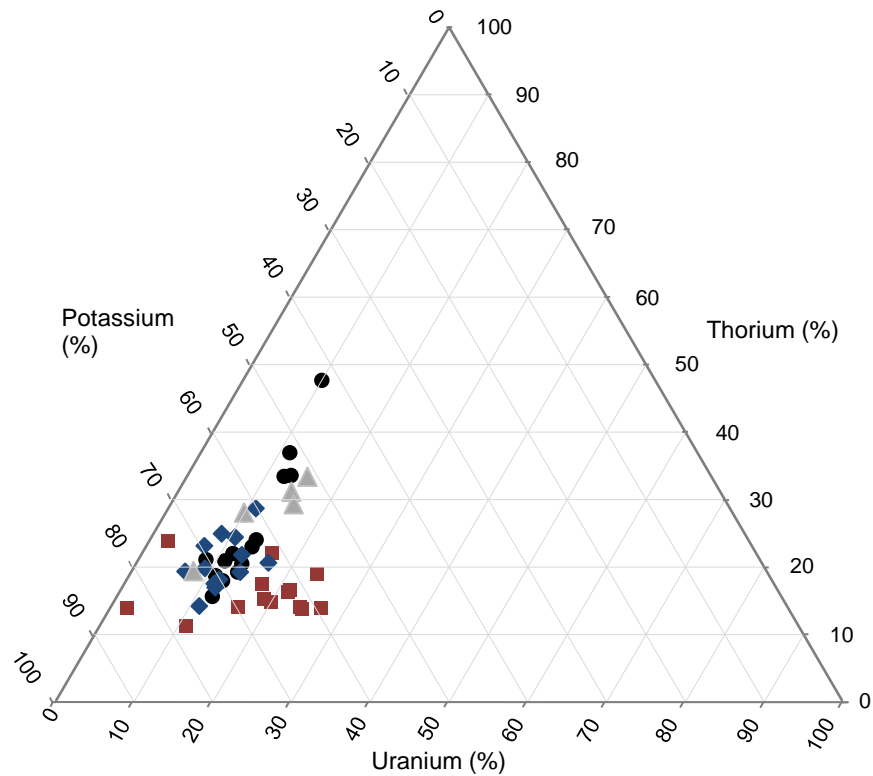
Figure D.7 - Ternary plot of percentage contributions to beta dose rate of uranium, thorium and potassium using TSAC/GMBC (red squares,) ICPMS (grey triangles), XRF (blue diamonds) and HRGS (black circles).

Beta dose rates vary between the determination methods used. Table D.10 and Figure D.8 show the results of the different methods and the variation between them. In general ICPMS/OES and XRF give a lower beta dose rate than GMBC and HRGS. When measuring dose rate using GMBC, the proportion of beta dose from uranium is higher than other methods (Figure D.7).

D.8.2 Gamma Dose rates
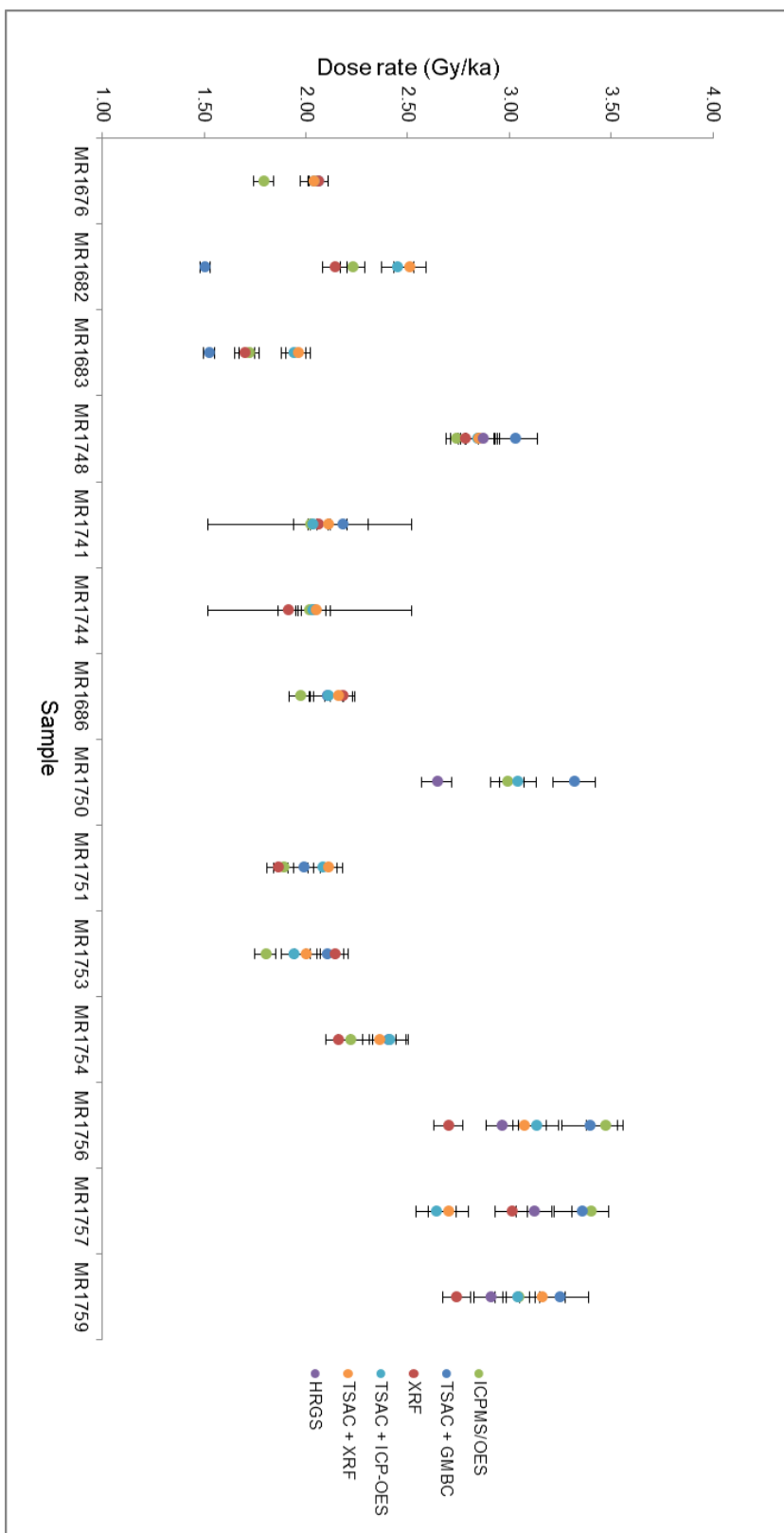
Figure D.8 - Comparison plot of all beta dose determination for each sample using ICPMS/OES, TSAC + GMBC, XRF, TSAC + ICPMS, TSAC + XRF, and HRGS. Each measurement has error bars at 1-sigma and 2-sigma.

Table D.11 - Gamma dose rates measured using: [1]ICPMS/OES for potassium, uranium and thorium; [2]TSAC for uranium and thorium, ICP-OES for potassium; [3]XRF for potassium, uranium and thorium;[4] TSAC for uranium and thorium, XRF for potassium;, [5]TSAC for uranium ,thorium and potassium.

Sample	ICPMS	ICPMS+ TSAC/GM BC	XRF	XRF+ TSAC	TSAC	HRGS
MR1676	1.11 ± 0.04	1.27 ± 0.07	1.12 ± 0.04	1.27 ± 0.07	1.28 ± 0.07	
MR1682	1.47 ± 0.05	1.70±0.09	1.32 ± 0.04	1.72 ± 0.1	1.41±0.10	
MR1683	1.01 ± 0.03	1.11±0.05	0.96 ± 0.03	1.12 ± 0.05	0.98 ± 0.05	
MR1686	1.33 ± 0.04	1.31±0.07	1.48±0.05	1.32 ± 0.07	1.12 ± 0.08	
MR1748	1.78 ± 0.06	1.71 ± 0.09	1.87 ± .06	1.71 ± 0.09	1.29 ± 0.09	2.15 ± 0.04
MR1750	1.70 ± 0.05	1.65 ± 0.09			1.16 ± 0.08	1.69 ± 0.05
MR1751	1.22 ± 0.04	1.29 ± 0.07	1.16±0.04	1.30±0.07	1.11 ± 0.07	
MR1753	1.25± 0.04	1.31 ± 0.07	1.30 ± 0.04	1.37 ± 0.07	1.17 ± 0.07	
MR1754	1.36 ± 0.04	1.46 ± 0.08	1.35 ± 0.04	1.48 ± 0.08	1.19 ± 0.08	
MR1756	2.94 ± 0.09	2.09 ± 0.12	1.90 ± 0.06	2.07 ± 0.12	1.57 ± 0.12	2.41 ± 0.04
MR1757	3.02 ± 0.09	2.00 ± 0.12	2.32 ± 0.07	2.02 ± 0.12	1.63 ± 0.13	2.68 ± 0.05
MR1759	2.57 ± 0.08	2.17 ± 0.13	1.93 ± 0.06	2.21 ± 0.13	1.68 ± 0.14	2.32 ± 0.04
MR1741	1.44 ± 0.05	1.35 ± 0.12	1.40 ± 0.04	1.37 ± 0.13	1.19 ± 0.13	
MR1744	1.34 ± 0.04	1.25 ± 0.08	1.17 ± 0.04	1.26 ± 0.08	1.09 ± 0.08	
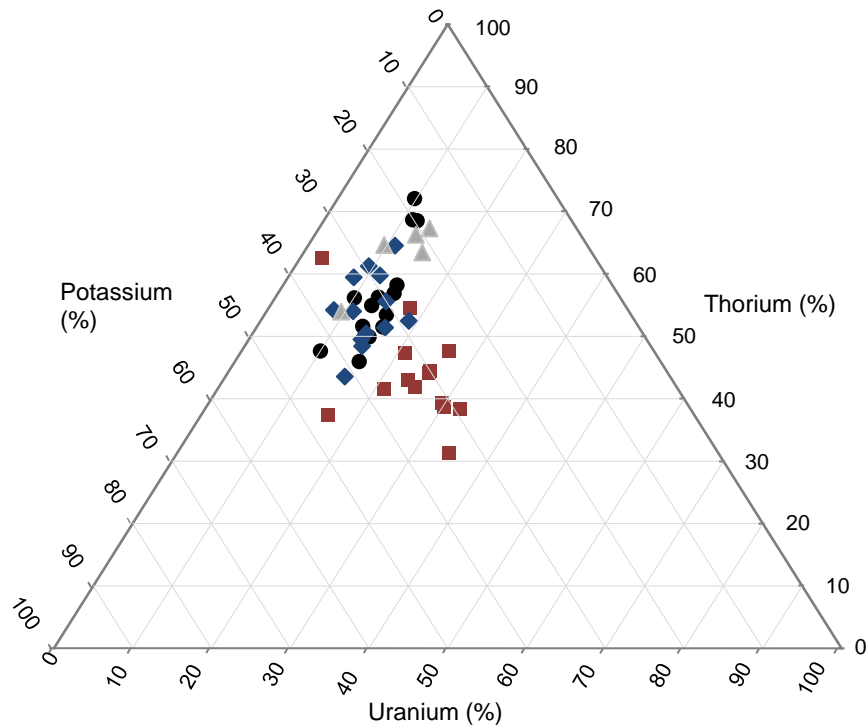
Figure D.9 – Ternary plot of percentage contributions to gamma dose rate of uranium, thorium and potassium using TSAC/GMBC (red squares,) ICPMS (grey triangles), XRF (blue diamonds) and HRGS (black circles).

Similarly to beta dose rates, the gamma dose rates also vary between the determination methods used. Table D.11 and Figure D.10; show the results of the different methods and the variation between them. In general ICPMS/OES gives a higher gamma dose rate than GMBC and HRGS (Table D.11). When measuring dose rate using GMBC/TSAC, the proportion of gamma dose from uranium is generally higher than other methods (Figure D.9), whilst the ICPMS, HRGS and XRF methods show similar proportions of all contributing elements.
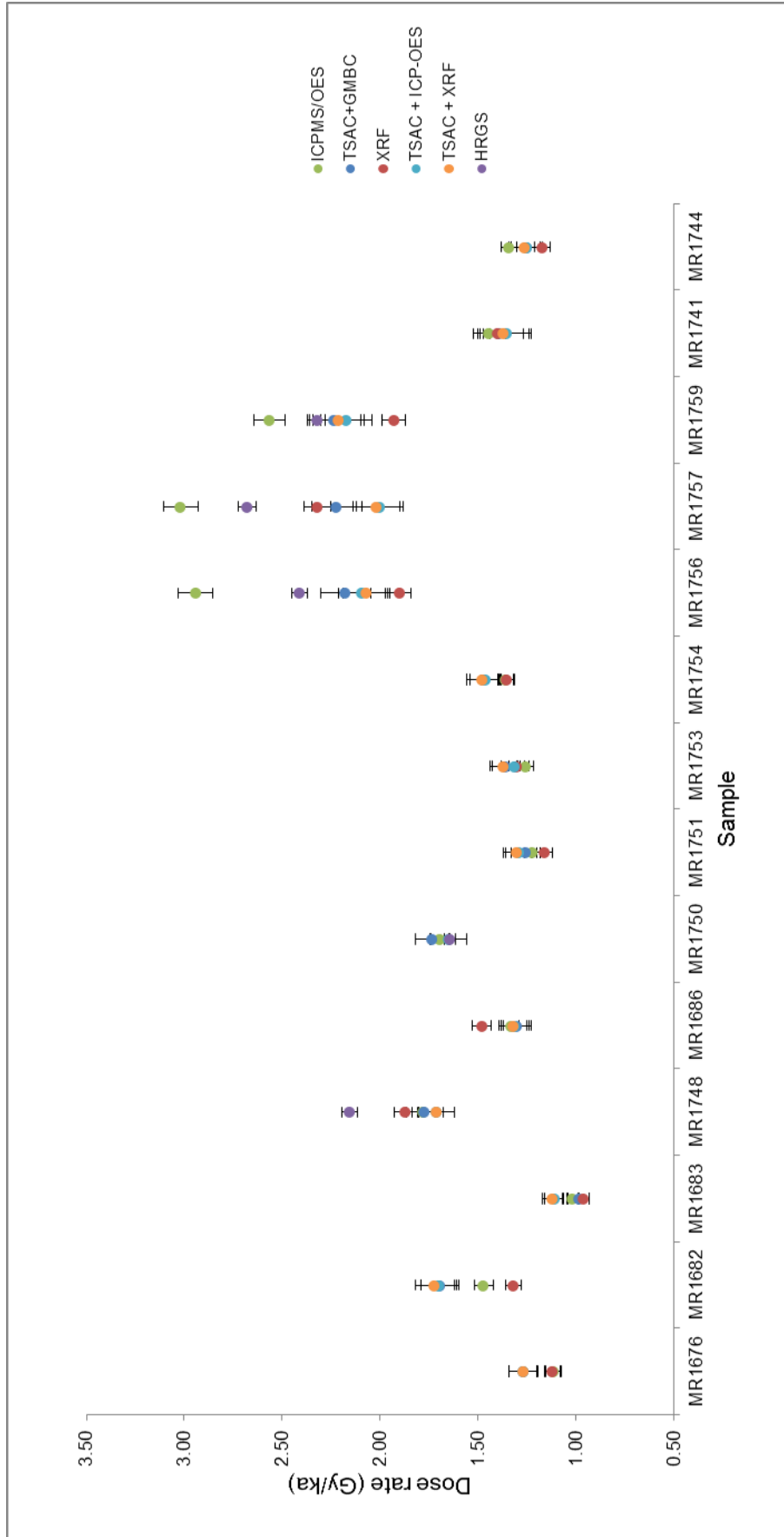
Figure D.10- Comparison plot of all gamma dose determination for each sample using ICPMS/OES, TSAC + GMBC, XRF, TSAC + ICPMS, TSAC + XRF, and HRGS. Each measurement has error bars at 1-sigma and 2-sigma.

D.8.3 Alpha dose rates

An internal alpha dose rate of 0.03 ± 0.01 is assumed for all samples, coming from the radioactive decay of uranium and thorium within the crystal lattice of each quartz grain. This value is based upon values calculated by Bowler et al. (2003) for quartz in Australia.

D.8.4 Cosmic dose rates

Cosmic dose rates (Table D.12) were calculated using the adjustments of Prescott and Hutton (1994) incorporating the elevation above sea-level, geomagnetic latitude, and sample depth with a sediment density of 2.95 $g.cm^3$ used for all overburden. An uncertainty of 15% was added to each estimate of cosmic ray dose. The cosmic dose rate varies from 0.15 ± 0.02 $Gy.ka^{-1}$ to 0.20 ± 0.03 $Gy.ka^{-1}$

D.8.5 Moisture content

Measurements of moisture content at time of sampling were taken for each sample using equation 1. At the time of sampling the water content varied from 0.66 – 6.51% (Table D.12). Given the ephemeral nature of the river and infrequent flows an assumed long term average of $4 \pm 2\%$ was used in dose rate calculations, at 2σ this value encompasses all measured water contents.

$$M_n \ = \ ((W_w - W_d)/W_w) \text{ x } 100$$

Equation D.2 -Equation to calculate water content of a sample where M_n = moisture content (%) of sample, W_W = wet weight of the sample W_d = weight of the sample after drying.

Table D.12 - Cosmic dose rates and water content for all OSL samples. Water content (measured) is the current water content at time of sampling. Water content (assumed)is that which is used in the dose rate calculations.

Sample	Cosmic	Water content (measured)	Water content (assumed)
MR1676	0.20 ± 0.03	1.16	4 ± 2
MR1682	0.15 ± 0.02	1.43	4 ± 2
MR1683	0.20 ± 0.03	1.46	4 ± 2
MR1748	0.15 ± 0.02	0.86	4 ± 2
MR1686	0.20 ± 0.03	1.27	4 ± 2
MR1750	0.16 ± 0.02	0.66	4 ± 2
MR1751	0.20 ± 0.03	2.10	4 ± 2
MR1753	0.18 ± 0.03	2.37	4 ± 2
MR1754	0.18 ± 0.03	1.81	4 ± 2
MR1756	0.16 ± 0.02	2.69	4 ± 2
MR1757	0.18 ± 0.03	2.10	4 ± 2
MR1759	0.16 ± 0.02	5.19	4 ± 2
MR1741	0.16 ± 0.02	3.26	4 ± 2
MR1744	0.16 ± 0.02	6.51	4 ± 2

D.8.6 Total Environmental Dose rate

Total environmental does rates (Table D.12) are the total of each of the dose rate contributors. The errors are obtained through summing, in quadrature, the known random and systematic errors of the internal alpha, beta, gamma, and cosmic dose rates and accounting for the attenuation due to water content. As seen in Table D.10; Table D.11; Figure D.9 and Figure D.11 there is some variability in the dose rate depending on the method used. This variability by method is continued when the total dose rate is calculated (Table D.13). The variability between the methods used for dose rate determination is most likely the result of where in the radioactive decay chain the measurement is taking place. GMBC and TSAC are both emission-counting based methods that measure the present-day radiation flux of the sediments coming from the entire decay chain series of radionuclides. These methods explicitly assume that the

current state of (dis)equilibrium in the sediments prevailed throughout the period of burial. In contrast, XRF and ICP-MS measure the elemental concentration of the element at the head of the decay chain (i.e., U, Th) and explicitly assume that the decay chain is in equilibrium. It is only with HRGS that the state of (dis)equilibrium can be examined. Although the HRGS measurements made on five samples show no evidence of disequilibrium, the GMBC and TSAC measurements were considered to be a more reliable means of dose rate determination and used throughout this study for age estimation.

Table D.13 - Total environmental dose rate calculated using [1] ICPMS/OES for potassium, uranium and thorium; [2] TSAC for uranium and thorium, ICP-OES for potassium; [3] XRF for potassium, uranium and thorium, XRF for potassium; [4] TSAC for uranium and thorium; [5] TSAC for uranium and thorium and GMBC for potassium.; [5] TSAC for uranium and thorium and GMBC for potassium. [6] HRGS for uranium thorium and potassium, for all samples from Marshall River, incorporating: water content and cosmic dose rates.

Sample	ICPMS[1]	ICPOES+ TSAC[2]	XRF[3]	XRF+ TSAC[4]	TSAC/GMBC[5]	HRGS[6]
1676	2.77 ± 0.08	3.13 ± 0.11	2.75 ± 0.08	3.13 ± 0.11	3.15 ± 0.11	
1682	3.43 ± 0.09	3.83 ± 0.13	3.21 ± 0.09	3.90 ± 0.14	3.80 ± 0.13	
1683	2.62 ± 0.08	2.90 ± 0.10	2.55 ± 0.08	2.92 ± 0.10	2.85 ± 0.09	
1686	3.13 ± 0.09	3.22 ± 0.12	3.44 ± 0.10	3.28 ± 0.12	3.21 ± 0.11	
1748	4.14 ± 0.12	4.17 ± 0.14	4.26 ± 0.12	4.17 ± 0.14	4.38 ± 0.14	4.61 ± 0.12
1750	4.27 ± 0.12	4.27 ± 0.14			4.58 ± 0.14	3.94 ± 0.10
1751	2.96 ± 0.09	3.18 ± 0.11	2.88 ± 0.08	3.22 ± 0.11	3.08 ± 0.10	
1753	2.89 ± 0.08	3.06 ± 0.11	3.10 ± 0.09	3.29 ± 0.11	3.25 ± 0.11	
1754	3.29 ± 0.10	3.55 ± 0.13	3.33 ± 0.10	3.62 ± 0.13	3.61 ± 0.12	
1756	5.87 ± 0.17	4.77 ± 0.18	4.24 ± 0.12	4.71 ± 0.18	5.07 ± 0.17	4.94 ± 0.12
1757	5.90 ± 0.17	4.30 ± 0.17	4.91 ± 0.14	4.36 ± 0.17	5.10 ± 0.17	5.35 ± 0.13
1759	5.16 ± 0.15	4.78 ± 0.19	4.30 ± 0.12	4.92 ± 0.19	5.01 ± 0.18	4.81 ± 0.12
1741	3.26 ± 0.09	3.17 ± 0.16	3.23 ± 0.09	3.24 ± 0.16	3.35 ± 0.15	
1744	3.14 ± 0.09	3.06 ± 0.11	2.89 ± 0.08	3.09 ± 0.11	3.07 ± 0.11	

D.9   Age calculation

For all 14 island samples, single-grain OSL burial ages were calculated. In its simplest form the age equation is presented in Equation D.3. This incorporates the total environmental dose and the estimate of dose as decided by the age models (Table D.13; Table D.14). When comparing the different methods used for dose rate determination different burial ages are produced, although these ages overlap within 2-sigma (Figure D.11), attributed to the uncertainty of the D_e being greater than the uncertainty on the dose rate leading to age estimates that are insensitive to the dose rate determination method.For the final ages for interpretation, dose rate determination by TSAC and GMBC was used.

$$Burial\ Age = \frac{Dose\ estimate}{Total\ environmental\ dose}$$

Equation D.3 - The basic OSL equation which divides the measurement of dose estimate by the calculated total environmental dose to give a burial age.

Table D.14- Chosen D$_e$ and age estimates for each OSL sample with the age model used including the overdispersion and the MAM-3 P value.

Sample	D$_e$ (Gy)	Age (ka)	Age Model	Overdispersion [1] (%)	P value [2]	Core	Location in core[3]
MR1676	0.39 ± 0.04	**0.12 ± 0.01**	MAM-3	20	0.68	MR3.1	T
MR 1682	0.44 ± 0.07	**0.12 ± 0.02**	CAM	175.00 ± 30.82	-	MR3.1	B
MR 1683	0.23 ± 0.03	**0.08 ± 0.01**	MAM-3	20	0.73	MR3.2	T
MR 1748	2.34 ± 0.16	**0.53 ± 0.04**	MAM-3	20	0.7	MR3.2	B
MR 1686	0.32 ± 0.04	**0.10 ± 0.01**	MAM-3	20	0.39	MR3.3	T
MR 1750	2.68 ± 0.22	**0.58 ± 0.05**	CAM	68.12 ± 8.43	-	MR3.3	B
MR 1751	0.11 ± 0.02	**0.04 ± 0.01**	MAM-3	20	0.77	MR2.1	T
MR 1753	0.38 ± 0.07	**0.12 ± 0.02**	MAM-3	20	0.74	MR2.1	B
MR 1754	0.16 ± 0.03	**0.04 ± 0.01**	MAM-3	20	0.72	MR2.2	T
MR 1756	9.83 ± 0.38	**1.94 ± 0.11**	CAM	51.59 ± 3.43	-	MR2.2	B
MR 1757	0.09 ± 0.03	**0.02 ± 0.01**	MAM-3	20	0.53	MR2.3	T
MR 1759	2.03 ± 0.22	**0.41 ± 0.05**	CAM	102.47 ± 13.45	-	MR2.3	B
MR 1741	10.25 ± 2.48	**3.06 ± 0.76**	MAM-3	20	0.55	MR1.1	T
MR 1744	40.80 ± 3.66	**13.29 ± 1.31**	CAM	62.46 ± 8.82	-	MR1.1	B

[1]*Overdispersion is the overdispersion which is input in the model calculation for 3-MAM ages or the value from the CAM for CAM ages.* [2]*P value is the proportion of grains which max up the D$_e$ estimate in the minimum age model.* [3]*T= Top of core, B = bottom of core.*
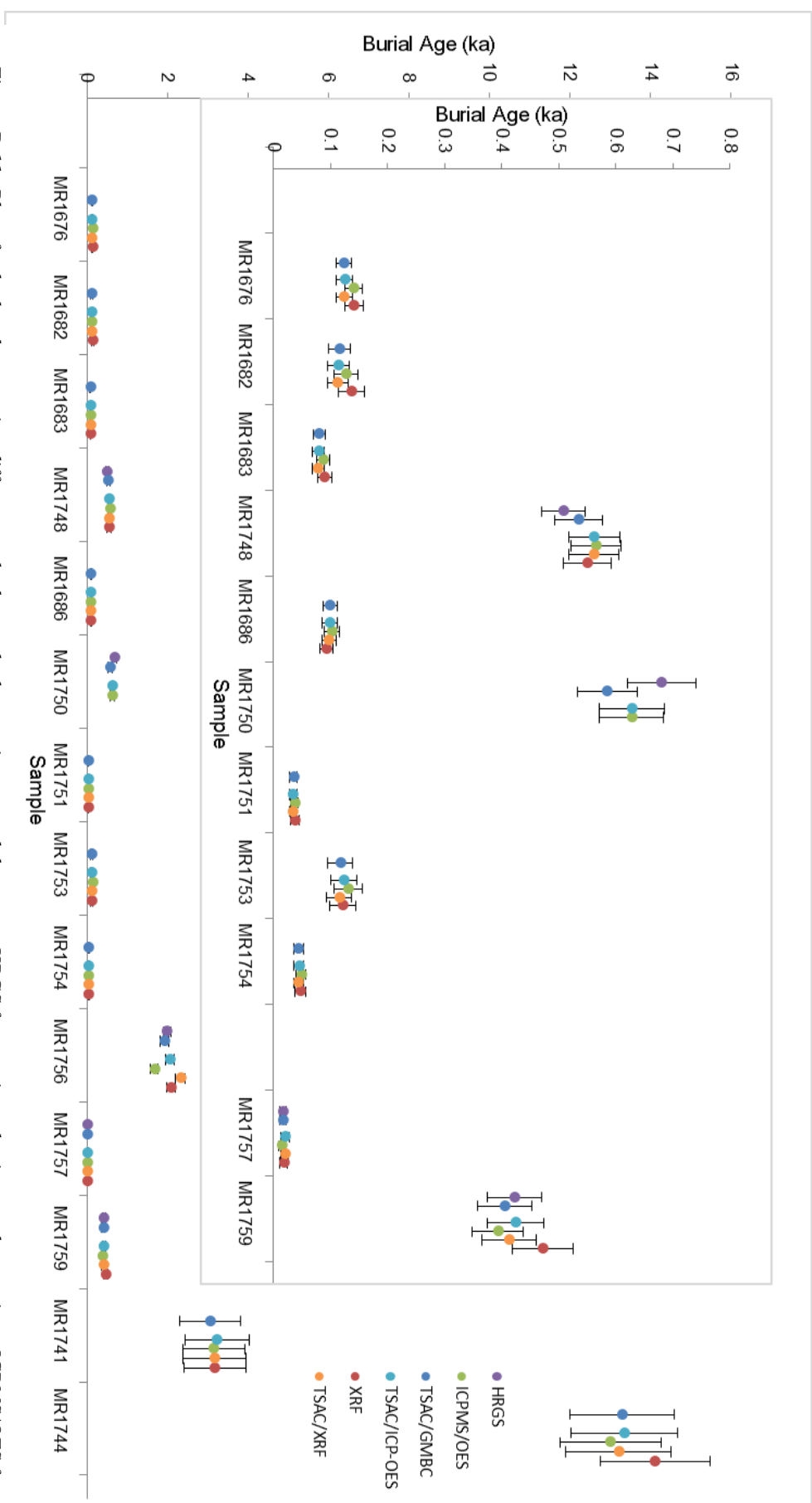
Figure D.11 - Plot of calculated ages using different methods to calculate environmental dose rate: HRGS for uranium, thorium, and potassium; ICPMS/OES for potassium, uranium and thorium; TSAC for uranium and thorium and ICP-OES for potassium; TSAC for uranium and thorium and GMBC for potassium; XRF for potassium, uranium, and thorium; TSAC for uranium and thorium, XRF for potassium. All incorporating water content and cosmic dose rate.

Appendix E

E   Marshall River grainsize analysis

This appendix contains the results of laser diffraction grain size analysis for seven cores from the ridges and islands of the Marshall River (Figure E.1). These same ridges and islands are dated using OSL in chapter 7. These results (Figure E.2) are all based on the less than 1.5 mm (1500 μm) grainsize fraction. In these samples, the contribution of grains larger than 1.5 mm is minimal and where these grains are present it is noted in Table E.1 a-g.
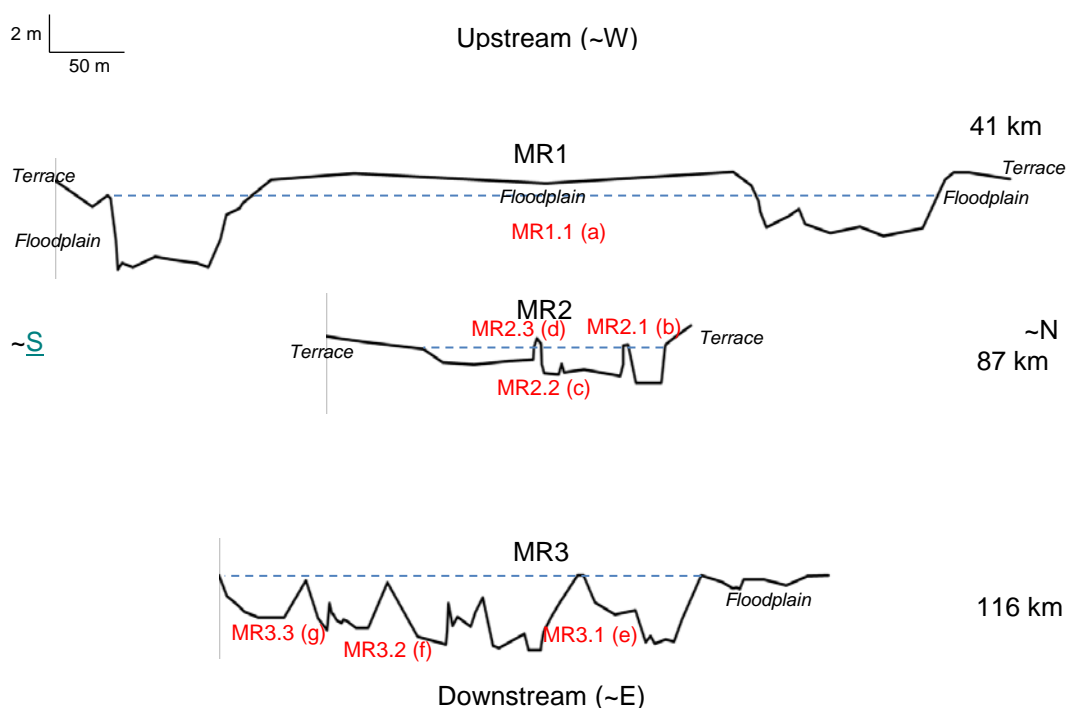
Figure E.1 - Cross-sections and coring sites of the Marshall River surveyed. Scale applies to cross-sections only. Downstream distance is not to scale. (a) – (g) correspond to Figure E.2 and Table E.1.
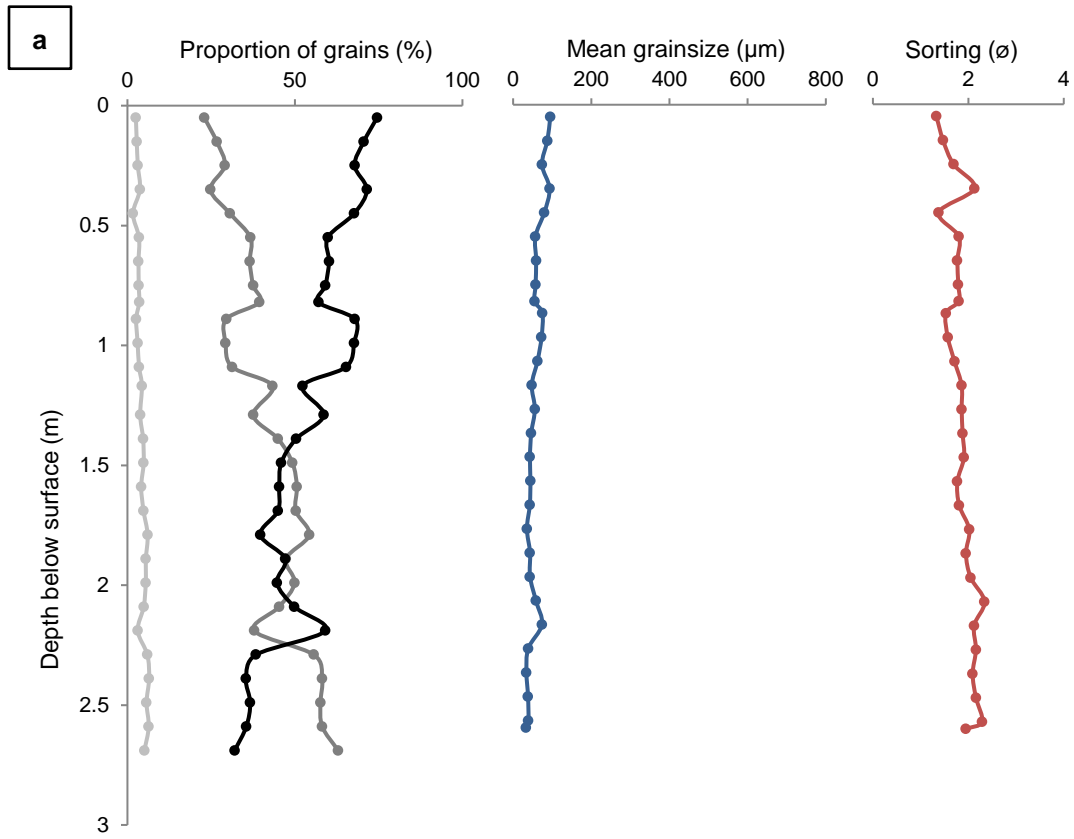
figure continued over page...
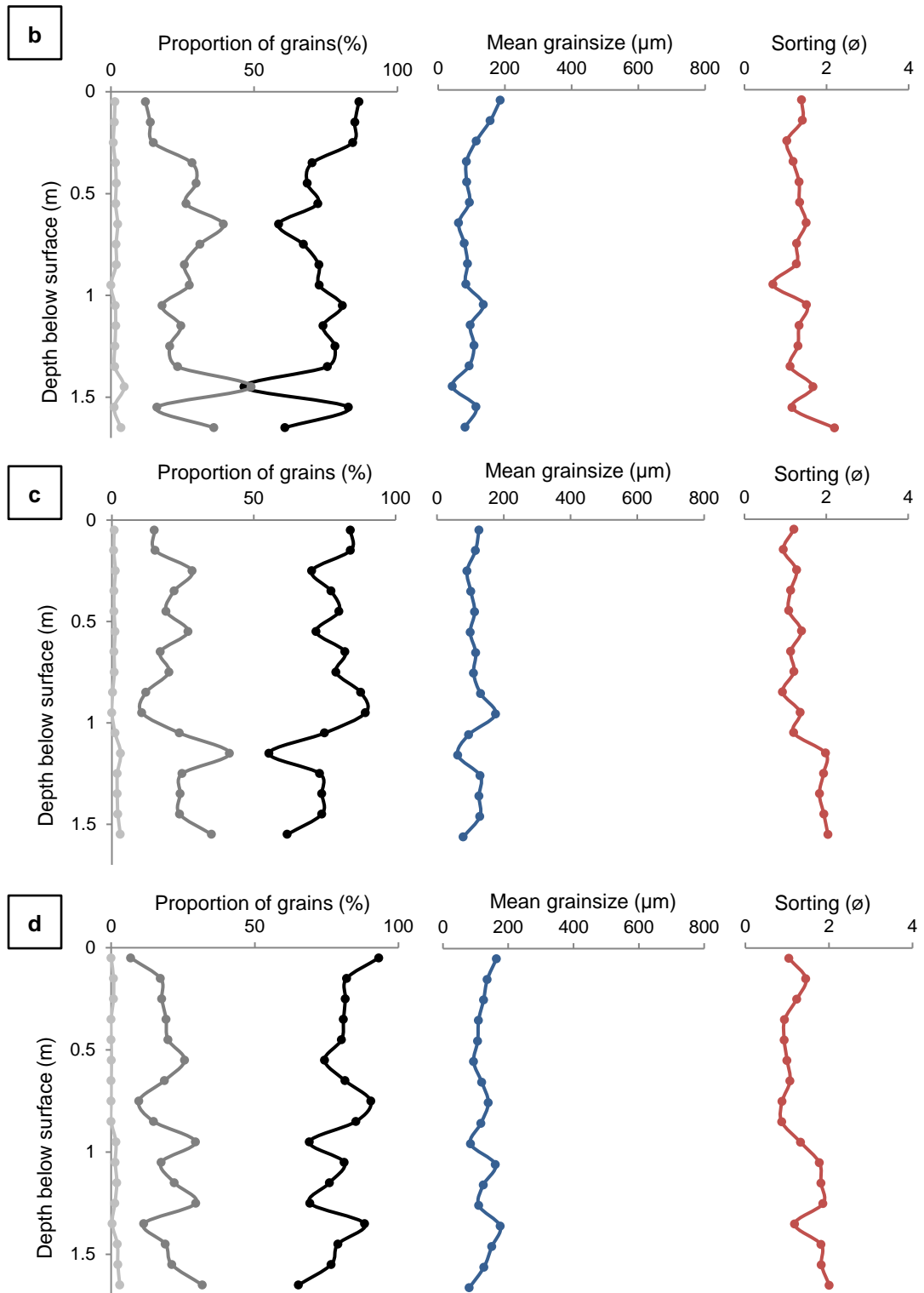
figure continued over page…
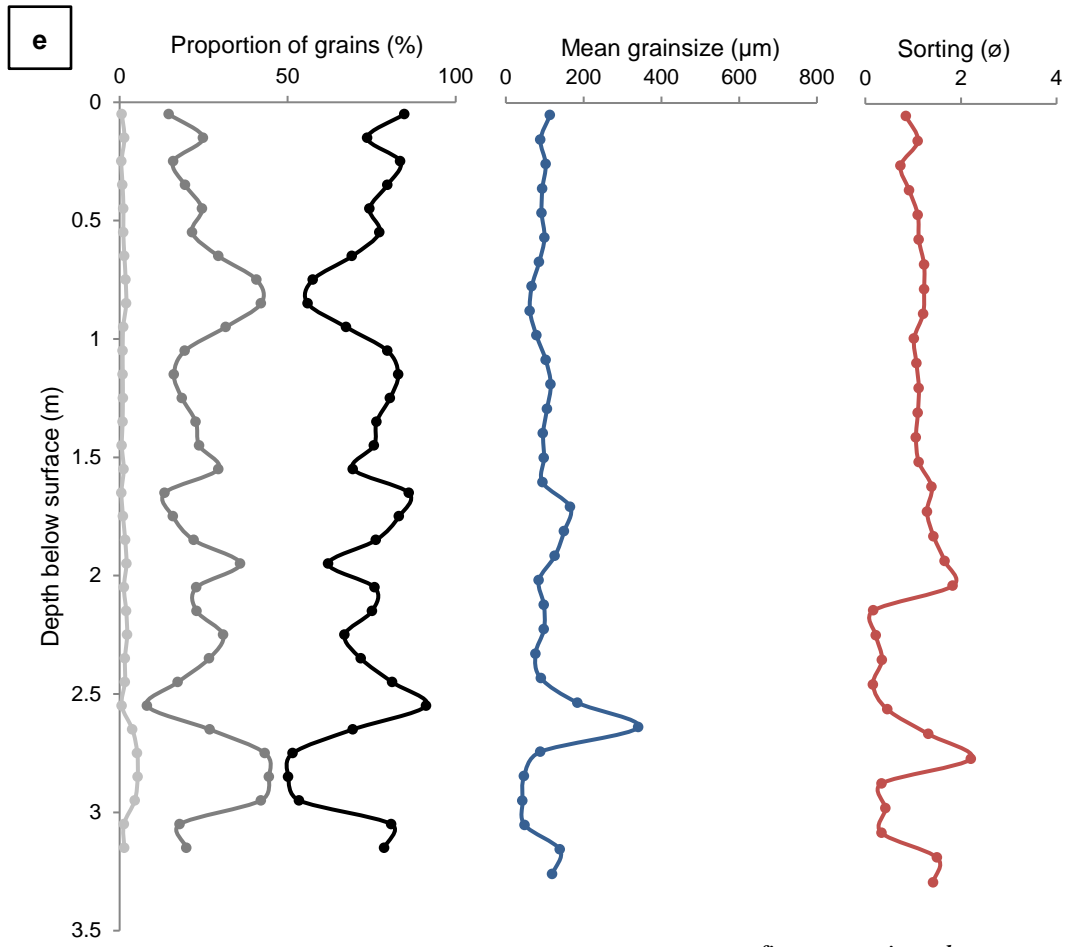
figure continued over page…
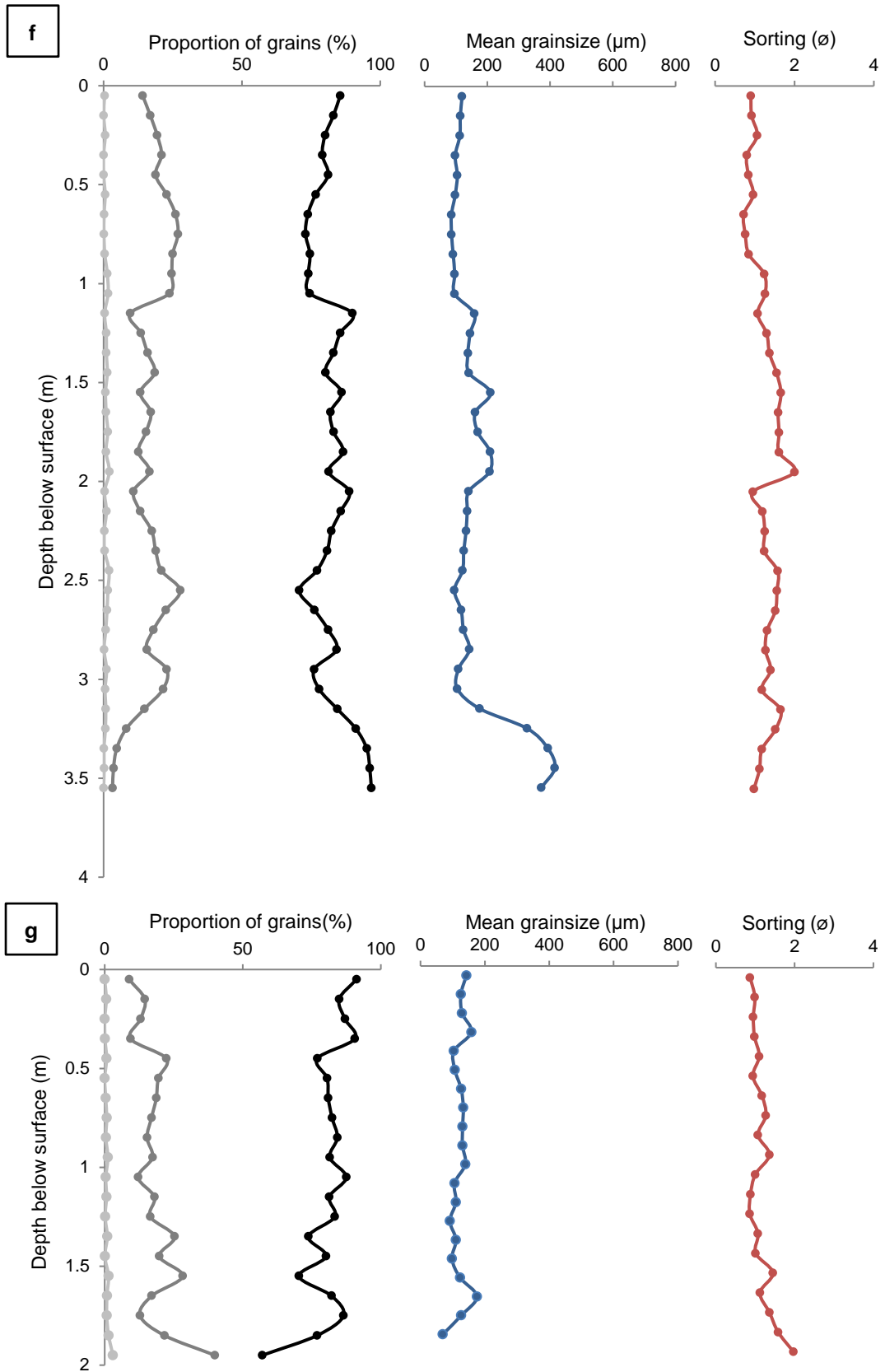
Figure E.2- Depth profiles of grainsize distributions of seven cores from the Marshall River. Percentage proportion of clay (light grey), silt (dark grey), and sand (black); mean grainsize (µm); and standard deviation in phi (ø) units as a proxy of sorting (the greater the ø value, the poorer the sorting of the sediment) are shown at 10 cm intervals for all cores. a) MR1.1; b) MR2.1; c) MR2.2; d)MR2.3; e) MR3.1; f)MR3.2; g)MR3.3

Table E.1 – Tables of grainsize measurements from Malvern Mastersizer 2000. Corresponding to Figure E.1 – a-g. Grainsize distribution is shown as percentages of sand, silt and clay, the mean grainsize and the standard deviation expressed as sorting. The percentage of the initial sample weight that is greater than 1500 µm is also shown, as this is too large to measure using laser diffraction in the Malvern Mastersizer 2000.

a

Core	Depth (m)	Sand (%)	Silt (%)	Clay (%)	Mean (µm)	Sorting (ø)	Grains > 1500 µm (% weight)
MR1.1.1	0.00 – 0.10	74.52	22.96	2.52	95.17	3.39	
MR1.1.1	0.10 – 0.20	70.57	26.65	2.78	87.60	3.51	
MR1.1.1	0.20 – 0.30	67.83	29.06	3.11	73.87	3.76	
MR1.1.1	0.30 – 0.40	71.48	24.79	3.73	93.29	3.42	
MR1.1.1	0.40 – 0.50	67.69	30.64	1.67	79.93	3.65	
MR1.1.1	0.50 – 0.60	59.81	36.72	3.46	56.93	4.13	
MR1.1.1	0.60 – 0.70	60.18	36.52	3.31	58.92	4.09	
MR1.1.1	0.70 – 0.80	59.07	37.55	3.38	57.48	4.12	
MR1.1.2	0.80 – 0.84	57.04	39.44	3.52	55.17	4.18	
MR1.1.2	0.84 – 0.94	67.86	29.52	2.62	74.90	3.74	
MR1.1.2	0.94 – 1.04	67.67	29.29	3.04	72.74	3.78	
MR1.1.2	1.04 – 1.14	65.25	31.27	3.48	62.36	4.00	
MR1.1.2	1.14 – 1.24	52.32	43.35	4.33	47.67	4.39	
MR1.1.2	1.24 – 1.34	58.63	37.56	3.81	55.69	4.17	
MR1.1.2	1.34 – 1.44	50.34	44.98	4.68	46.44	4.43	
MR1.1.2	1.44 – 1.54	45.9	49.26	4.84	43.01	4.54	
MR1.1.2	1.54 – 1.64	45.31	50.58	4.11	44.27	4.50	
MR1.1.2	1.64 – 1.74	44.94	50.26	4.81	42.71	4.55	
MR1.1.3	1.74 – 1.84	39.67	54.29	6.04	35.31	4.82	
MR1.1.3	1.84 – 1.94	47.14	47.34	5.52	43.25	4.53	
MR1.1.3	1.94 – 2.04	44.64	49.9	5.47	43.25	4.53	
MR1.1.3	2.04 – 2.14	49.85	45.28	4.87	58.34	4.10	
MR1.1.3	2.14 – 2.24	59.09	37.83	3.08	73.69	3.76	
MR1.1.3	2.24 – 2.34	38.39	55.66	5.95	38.63	4.69	13.04
MR1.1.3	2.34 – 2.44	35.39	58.14	6.47	34.19	4.87	5.93
MR1.1.3	2.44 – 2.54	36.67	57.62	5.70	38.15	4.71	14.48
MR1.1.3	2.54 – 2.64	35.48	58.15	6.36	39.14	4.68	28.44
MR1.1.3	2.64 – 2.70	32.00	62.93	5.06	33.18	4.91	5.49

b						
Core	Depth (m)	Sand (%)	Silt (%)	Clay (%)	Mean (µm)	Sorting (ø)	Grains > 1500 µm (% weight)
MR2.1.1	0.00 – 0.10	86.54	12.04	1.42	186.29	2.42	
MR2.1.1	0.10 – 0.20	85.1	13.72	1.18	156.2	2.68	
MR2.1.1	0.20 – 0.30	84.38	14.77	0.85	114.01	3.13	
MR2.1.1	0.30 – 0.40	70.23	28.25	1.53	84.84	3.56	
MR2.1.1	0.40 – 0.50	68.48	29.68	1.84	85.42	3.55	
MR2.1.1	0.50 – 0.60	72.16	26.20	1.64	94.22	3.41	
MR2.1.1	0.60 – 0.70	58.48	39.18	2.34	61.63	4.02	
MR2.1.1	0.70 – 0.80	67.18	31.01	1.81	78.54	3.67	
MR2.1.1	0.80 – 0.90	72.55	25.60	1.85	88.30	3.50	
MR2.1.1	0.90 – 1.00	72.66	27.34	0.00	83.49	3.58	
MR2.1.2	1.00 – 1.10	80.71	17.83	1.46	135.74	2.88	
MR2.1.2	1.10 – 1.20	73.98	24.37	1.64	96.60	3.37	
MR2.1.2	1.20 – 1.30	78.14	20.48	1.38	107.82	3.21	
MR2.1.2	1.30 – 1.40	75.51	23.20	1.29	93.16	3.42	
MR2.1.2	1.40 – 1.50	46.46	48.92	4.62	42.22	4.57	
MR2.1.2	1.50 – 1.60	82.86	16.00	1.13	113.81	3.14	
MR2.1.2	1.60 – 1.65	60.66	35.91	3.43	80.61	3.63	

c						
Core	Depth (m)	Sand (%)	Silt (%)	Clay (%)	Mean (µm)	Sorting (ø)	Grains > 1500 µm (% weight)
MR2.2.1	0.00 – 0.10	84.14	15.02	0.84	125.85	2.99	
MR2.2.1	0.10 – 0.20	84.11	15.25	0.65	115.52	3.11	
MR2.2.1	0.20 – 0.30	70.49	28.30	1.21	89.96	3.47	
MR2.2.1	0.30 – 0.40	77.27	21.94	0.78	101.51	3.3	
MR2.2.1	0.40 – 0.50	80.09	19.15	0.76	113.02	3.15	
MR2.2.1	0.50 – 0.60	71.96	26.88	1.15	99.51	3.33	
MR2.2.1	0.60 – 0.70	82.15	17.05	0.80	116.41	3.10	
MR2.2.1	0.70 – 0.80	78.98	20.13	0.89	109.68	3.19	
MR2.2.1	0.80 – 0.90	87.73	12.01	0.27	130.98	2.93	
MR2.2.1	0.90 – 1.00	89.42	10.58	0.00	175.54	2.51	
MR2.2.2	1.00 – 1.10	75.01	23.85	1.13	95.04	3.40	
MR2.2.2	1.10 – 1.20	55.37	41.51	3.12	62.48	4.00	
MR2.2.2	1.20 – 1.30	73.28	24.79	1.93	129.45	2.95	
MR2.2.2	1.30 – 1.40	74.01	24.10	1.88	125.64	2.99	
MR2.2.2	1.40 – 1.50	73.98	23.91	2.11	42.22	4.57	
MR2.2.2	1.50 – 1.60	61.82	35.18	3.00	113.81	3.14	

d

Core	Depth (m)	Sand (%)	Silt (%)	Clay (%)	Mean (µm)	Sorting (ø)	Grains > 1500 µm (% weight)
MR2.3.1	0.00 – 0.10	93.15	6.85	0.00	163.7	2.61	
MR2.3.1	0.10 – 0.20	81.98	17.18	0.84	135.83	2.88	
MR2.3.1	0.20 – 0.30	81.53	17.66	0.81	124.25	3.01	
MR2.3.1	0.30 – 0.40	80.88	19.12	0.00	108.98	3.20	
MR2.3.1	0.40 – 0.50	80.19	19.81	0.00	106.48	3.23	
MR2.3.1	0.50 – 0.60	74.27	25.61	0.12	93.87	3.41	
MR2.3.1	0.60 – 0.70	81.40	18.57	0.02	118.96	3.07	
MR2.3.1	0.70 – 0.80	90.37	9.63	0.00	138.90	2.85	
MR2.3.1	0.80 – 0.90	85.19	14.81	0.00	116.11	3.11	
MR2.3.1	0.90 – 1.00	69.00	29.34	1.67	84.30	3.57	
MR2.3.2	1.00 – 1.10	81.15	17.40	1.45	160.59	2.64	
MR2.3.2	1.10 – 1.20	76.02	22.01	1.97	123.42	3.02	
MR2.3.2	1.20 – 1.30	69.19	29.49	1.32	109.90	3.19	57.61
MR2.3.2	1.30 – 1.40	88.27	11.40	0.33	175.38	2.51	23.83
MR2.3.2	1.40 – 1.50	78.93	18.89	2.18	149.48	2.74	59.19
MR2.3.2	1.50 – 1.60	76.54	21.13	2.33	125.46	2.99	
MR2.3.2	1.60 – 1.65	65.19	31.78	3.03	80.55	3.63	

e						
Core	Depth (m)	Sand (%)	Silt (%)	Clay (%)	Mean (μm)	Sorting (ø)	Grains > 1500 μm (% weight)
MR3.1.1	0.00 – 0.10	84.70	14.66	0.65	113.62	3.14	
MR3.1.1	0.10 – 0.20	73.70	24.86	1.44	89.20	3.49	
MR3.1.1	0.20 – 0.30	83.54	15.92	0.55	102.68	3.28	
MR3.1.1	0.30 – 0.40	79.66	19.47	0.87	93.97	3.41	
MR3.1.1	0.40 – 0.50	74.36	24.50	1.14	92.01	3.44	
MR3.1.1	0.50 – 0.60	77.34	21.57	1.09	99.51	3.33	
MR3.1.1	0.60 – 0.70	69.16	29.42	1.42	85.75	3.54	
MR3.1.1	0.70 – 0.80	57.46	40.75	1.79	66.70	3.91	
MR3.1.1	0.80 – 0.90	55.95	42.10	1.95	62.03	4.01	
MR3.1.1	0.90 – 1.00	67.39	31.54	1.07	78.88	3.66	
MR3.1.2	1.00 – 1.10	79.67	19.44	0.90	102.59	3.29	
MR3.1.2	1.10 – 1.20	82.89	16.17	0.94	115.60	3.11	
MR3.1.2	1.20 – 1.30	80.47	18.56	0.97	105.89	3.24	
MR3.1.2	1.30 – 1.40	76.44	22.68	0.88	95.87	3.38	
MR3.1.2	1.40 – 1.50	75.68	23.66	0.66	98.20	3.35	
MR3.1.2	1.50 – 1.60	69.43	29.38	1.20	94.37	3.41	
MR3.1.2	1.60 – 1.70	86.02	13.43	0.55	165.65	2.59	
MR3.1.2	1.70 – 1.80	83.15	15.85	1.00	149.83	2.74	
MR3.1.2	1.80 – 1.90	76.27	22.06	1.66	126.39	2.98	
MR3.1.2	1.90 – 2.00	62.11	35.87	2.02	84.92	3.56	
MR3.1.3	2.00 – 2.10	75.88	22.83	1.28	97.93	3.35	
MR3.1.3	2.10 – 2.20	75.09	22.95	1.96	98.12	3.35	
MR3.1.3	2.20 – 2.30	66.97	30.81	2.23	76.24	3.71	
MR3.1.3	2.30 – 2.40	71.74	26.67	1.59	90.26	3.47	
MR3.1.3	2.40 – 2.50	81.09	17.33	1.58	184.80	2.44	
MR3.1.3	2.50 – 2.60	91.2	8.16	0.63	340.50	1.55	12.63
MR3.1.3	2.60 – 2.70	69.37	26.81	3.82	88.79	3.49	8.23
MR3.1.3	2.70 – 2.80	51.54	43.23	5.24	46.73	4.42	
MR3.1.3	2.80 – 2.90	50.19	44.46	5.36	43.24	4.53	
MR3.1.3	2.90 – 3.00	53.44	42.04	4.52	48.89	4.35	
MR3.1.4	3.00 – 3.10	80.84	17.90	1.26	139.13	2.85	
MR3.1.4	3.10 – 3.20	78.75	19.89	1.36	119.68	3.06	
MR3.1.4	3.20 – 3.30	75.59	22.81	1.60	116.58	3.10	
MR3.1.4	3.30 – 3.40	77.39	21.39	1.22	111.20	3.17	
MR3.1.4	3.40 – 3.50	57.88	38.62	3.51	65.22	3.94	

f						
Core	Depth (m)	Sand (%)	Silt (%)	Clay (%)	Mean (µm)	Sorting (ø)	Grains > 1500 µm (% weight)
MR3.2.1	0.00 – 0.10	85.52	14.12	0.36	119.56	3.06	
MR3.2.1	0.10 – 0.20	83.09	16.88	0.04	113.89	3.13	
MR3.2.1	0.20 – 0.30	80.07	19.36	0.57	112.31	3.15	
MR3.2.1	0.30 – 0.40	79.06	20.94	0.00	97.58	3.36	
MR3.2.1	0.40 – 0.50	81.18	18.80	0.02	104.27	3.26	
MR3.2.1	0.50 – 0.60	76.66	22.79	0.55	97.44	3.36	
MR3.2.1	0.60 – 0.70	73.82	26.00	0.18	85.52	3.55	
MR3.2.1	0.70 – 0.80	72.99	26.90	0.11	85.98	3.54	
MR3.2.1	0.80 – 0.90	74.59	24.98	0.43	91.13	3.46	
MR3.2.1	0.90 – 1.00	74.06	24.60	1.34	96.01	3.38	
MR3.2.2	1.00 – 1.10	74.52	23.83	1.65	95.83	3.38	
MR3.2.2	1.10 – 1.20	89.94	9.67	0.39	158.9	2.65	
MR3.2.2	1.20 – 1.30	85.54	13.49	0.97	145.18	2.78	
MR3.2.2	1.30 – 1.40	83.11	15.89	1.01	138.2	2.86	
MR3.2.2	1.40 – 1.50	80.18	18.49	1.33	141.54	2.82	
MR3.2.2	1.50 – 1.60	86.03	13.26	0.71	210.36	2.25	
MR3.2.2	1.60 – 1.70	82.01	17.08	0.92	161.4	2.63	
MR3.2.2	1.70 – 1.80	83.15	15.35	1.5	169.54	2.56	
MR3.2.2	1.80 – 1.90	86.58	12.56	0.86	208.96	2.26	
MR3.2.2	1.90 – 2.00	81.31	16.62	2.08	207.28	2.27	
MR3.2.3	2.00 – 2.10	88.83	10.80	0.37	140.65	2.83	
MR3.2.3	2.10 – 2.20	85.76	13.21	1.02	135.88	2.88	
MR3.2.3	2.20 – 2.30	82.34	17.41	0.26	132.36	2.92	2.01
MR3.2.3	2.30 – 2.40	80.81	18.83	0.36	124.89	3.00	
MR3.2.3	2.40 – 2.50	77.13	20.90	1.97	121.11	3.05	
MR3.2.3	2.50 – 2.60	70.72	27.70	1.58	95.14	3.39	
MR3.2.3	2.60 – 2.70	76.23	22.53	1.24	116.6	3.10	
MR3.2.3	2.70 – 2.80	81.19	18.02	0.79	123.79	3.01	
MR3.2.3	2.80 – 2.90	84.23	15.61	0.17	142.81	2.81	
MR3.2.3	2.90 – 3.00	76.1	22.82	1.08	107.67	3.22	
MR3.2.4	3.00 – 3.10	77.96	21.50	0.54	104.4	3.26	
MR3.2.4	3.10 – 3.20	84.47	14.74	0.79	175.91	2.51	
MR3.2.4	3.20 – 3.30	91.2	8.16	0.64	327.02	1.61	
MR3.2.4	3.30 – 3.40	95.12	4.74	0.14	392.73	1.35	
MR3.2.4	3.40 – 3.50	96.21	3.59	0.20	415.33	1.27	
MR3.2.4	3.50 – 3.60	96.77	3.23	0.00	371.96	1.43	

g

Core	Depth (m)	Sand (%)	Silt (%)	Clay (%)	Mean (μm)	Sorting (ø)	Grains > 1500 μm (% weight)
MR3.3.1	0.00 – 0.10	91.18	8.82	0.00	142.67	2.81	
MR3.3.1	0.10 – 0.20	84.93	14.52	0.55	125.71	2.99	
MR3.3.1	0.20 – 0.30	87.02	12.97	0.01	129.44	2.95	
MR3.3.1	0.30 – 0.40	90.58	9.33	0.09	158.22	2.66	
MR3.3.1	0.40 – 0.50	76.98	22.34	0.68	103.74	3.27	
MR3.3.1	0.50 – 0.60	80.56	19.44	0.00	106.74	3.23	
MR3.3.1	0.60 – 0.70	80.96	18.69	0.35	126.36	2.98	
MR3.3.1	0.70 – 0.80	82.34	16.93	0.73	133.05	2.91	
MR3.3.1	0.80 – 0.90	84.25	15.33	0.42	130.96	2.93	
MR3.3.1	0.90 – 1.00	81.52	17.32	1.15	130.41	2.94	
MR3.3.2	1.00 – 1.10	87.51	12.08	0.41	139.45	2.84	
MR3.3.2	1.10 – 1.20	81.33	18.02	0.65	105.76	3.24	
MR3.3.2	1.20 – 1.30	83.35	16.51	0.15	110.37	3.18	
MR3.3.2	1.30 – 1.40	73.75	25.31	0.94	91.38	3.45	
MR3.3.2	1.40 – 1.50	80.16	19.77	0.06	110.35	3.18	
MR3.3.2	1.50 – 1.60	70.35	28.26	1.38	97.97	3.35	
MR3.3.2	1.60 – 1.70	82.17	17.02	0.81	123.04	3.02	
MR3.3.2	1.70 – 1.80	86.46	12.81	0.73	175.61	2.51	
MR3.3.2	1.80 – 1.90	76.93	21.67	1.4	127.02	2.98	
MR3.3.2	1.90 – 2.00	57.10	39.90	2.99	69.63	3.84	
MR3.3.3	2.00 – 2.10	77.74	20.60	1.66	115.00	3.12	
MR3.3.3	2.10 – 2.20	82.88	15.89	1.23	131.38	2.93	
MR3.3.3	2.20 – 2.30	84.28	14.56	1.15	131.45	2.93	
MR3.3.3	2.30 – 2.40	84.06	15.13	0.80	134.91	2.89	
MR3.3.3	2.40 – 2.50	86.82	12.20	0.99	176.58	2.5	
MR3.3.3	2.50 – 2.60	87.72	11.35	0.93	227.10	2.14	30.56
MR3.3.3	2.60 – 2.70	90.76	8.29	0.95	495.41	1.01	33.37
MR3.3.3	2.70 – 2.80	94.64	4.91	0.45	792.25	0.34	58.85
MR3.3.3	2.80 – 2.90	91.36	7.93	0.71	507.71	0.98	47.51
MR3.3.3	2.90 – 3.00	95.48	4.29	0.22	666.86	0.58	31.97